Interphase mass transfer in porous media

vorgelegt von
M.Sc.
Berken Agaoglu
geb. in Edirne/Türkei

von der Fakultät VI – Planen Bauen Umwelt
der Technischen Universität Berlin
zur Erlangung des akademischen Grades

Doktor der Ingenieurwissenschaften
– Dr.-Ing. –

genehmigte Dissertation

Promotionsausschuss:

Vorsitzender:	Prof. Dr. Uwe Tröger
Gutachter:	PD Dr. Traugott Scheytt
Gutachter:	Prof. Dr. –Ing. Reinhard Hinkelmann
Gutachter:	Prof. Dr. Nadim K. Copty

Tag der wissenschaftlichen Aussprache: 18. Mai 2015

Berlin 2015

Promotionausschuss:

Vorsitzender:

Berichter:

Tag der wissenschaftlichen Aussprache:

Abstract

Interphase mass transfer between fluids in porous media is an important part of transport phenomenon in nature and found distinct applications in different fields of science and technology such as oil extraction, Non-aqueous phase liquid (NAPL) remediation and CO_2 injection into deep saline aquifers. In this study different aspects of this process are investigated in terms of both experimental and computational work. The investigations incorporated also different couples of fluids to examine the impact of fundamental fluid properties on this process. Influence of characteristic fluid/porous medium properties and phase formations on this process constitutes a major point of focus.

Interphase mass transfer in porous media involves a number of complex processes mostly in relevance with the complexity of the flow in porous media. The interfacial domains being formed by multiphase flow processes cause further complications. The alteration of the fluid properties due to interactions occurring between different types of fluid couples is also a formidable subject as each fluid pair may entail unique interactions e.g., the different interactions between cosolvent containing aqueous solutions and organic phase compared to surfactant containing aqueous solutions and organic phase. Despite the association of diverse fields of science and the complexity appearing in this process, there is not an integral review of this topic in the literature. To address this absence part of this thesis is dedicated to review the numerous scientific articles committed to investigate interphase mass transfer. In this review, characteristic length scale of the existing literature and the flow configurations of the fluids in porous media served as a foundation to group studies with similar conditions. Apart from the experimental work also both analytical and numerical models were reviewed. This work provides a unified comprehension of interphase mass transfer in porous media where the cross interactions between different system parameters due to multiphase flow conditions are revealed.

The impact of pore scale mechanisms on interphase mass transfer is not a subject that is investigated in detail as the most of the investigations focusing on interphase mass transfer are conducted at meso-scale. To investigate the impact of pore scale mechanisms a pore scale numerical model is developed. The results of the numerical model demonstrated that the distribution of NAPL at the pore scale has a large impact on the developed meso-scale interphase mass transfer correlations. Especially the geometric allocations of interfacial area which makes up the actual domain for interphase mass transfer were shown to have considerable impact. The reason for that was observed to be the alteration of the concentration profile at pore scale. The results also showed that the interfacial area is not linearly correlated to interphase mass transfer rate due to this alteration. A particular result was that the same interfacial area can lead to an order of magnitude lower interphase mass transfer rate if the orientation with respect to flow direction is changed from orthogonal to parallel. The explicit mass transfer coefficients, which are derived by considering the impact of interfacial area separately, are supposed to consider this effect. It was pointed out that the existing correlations of mass transfer coefficient are mostly dependent on flow velocity of solvent phase and do not consider the impact of the spatial distribution of the interfacial area.

Several chemical agents have found significant use in different fields to enhance interphase mass transfer e.g., cosolvents and surfactants in petroleum and environmental engineering. Accordingly, the combination of ethanol as a chemical agent with water was examined with respect to its impact on the recovery of NAPL toluene from water saturated porous medium. The two recovery mechanisms, enhanced solubilization and mobilization, were inspected through column experiments. It was demonstrated that there is an interaction between these two mechanisms such that the sufficient reduction of interfacial tension (with use of intermediate ethanol contents in the flushing solution) leads to creation of preferential flow paths inducing a steep decrease in the interphase mass transfer rates. This was attributed to the existence of lower capillary pressure present at larger pore throats. It was demonstrated that solvent solutions applied at slow velocities may prevent the creation of such preferential flow paths and the reduced interphase mass transfer rates. Along with the column

experiments, an REV (Representative elementary volume) based multiphase multicomponent numerical model was also used to investigate if this condition is captured by the model. The only available numerical model that can simulate cosolvent use, UTCHEM, is employed for this purpose. It was shown that this pore scale condition cannot be simulated. In such numerical models these pore scale conditions are considered within the interphase mass transfer formulations (i.e., Sherwood formulations) adopted in the model. However in literature there is not a Sherwood formulation that is developed for the cases where such chemical agents are present.

Recently a long known Sherwood formulation found significant use in several multiphase numerical models. However no analysis of this Sherwood formulation exists and therefore its validity is dubious. To address this absence in literature a detailed analysis of this formulation is conducted. It was demonstrated that this particular Sherwood formulation involves a fundamental mathematical error that renders it unusable. Moreover, it was also demonstrated that the original data used by this Sherwood formulation incorporates a high level of uncertainty meaning that even the corrected version of this formulation is not eligible to be used in a numerical model. The implication of this error is the invalidity of the results presented in some recent publications that used this Sherwood formulation in a certain type of REV based numerical model.

The thesis in hand attests to the cross interactions between various parameters involved in interphase mass transfer in porous medium. As the predictive accuracy of interphase mass transfer dictates the consideration of these parameters and interactions fairly well, further research must set sight on the clear characterization of the system at various length scales. With that perspective potential areas for future research are also highlighted.

Zusammenfassung
Massentransfer zwischen mehreren Flüssigkeiten in porösen Medien ist ein wichtiger Bestandteil von Transport-Phänomenen in der Natur und hat eine große Bedeutung in unterschiedlichen Bereichen der Wissenschaft und Technologie wie Ölgewinnung, Grundwassersanierung und Injektion und Einlagerung von CO_2 in tiefen salinen Aquiferen. In der vorliegenden Studie werden verschiedene Aspekte dieses Prozesses mittels experimenteller und theoretischer Arbeiten untersucht. Die Untersuchungen beinhalten auch unterschiedliche Paare von Fluiden, um den Einfluss der grundlegenden Flüssigkeitseigenschaften auf diesen Prozess zu untersuchen. Der Einfluss der charakteristischen Eigenschaften von porösem Medium und von Phasenbildungen auf diesen Prozess stellen einen zentralen Punkt dar.

Der Massentransfer zwischen Flüssigkeiten in porösen Medien umfasst eine Reihe komplexer Prozesse hauptsächlich hinsichtlich der Komplexität der Strömung in porösen Medien. Die Tatsache, dass die Grenzfläche zwischen unterschiedlichen Phasen von Mehrphasen-Strömungsvorgängen gebildet wird, verursacht weitere Komplikationen. Die Veränderung der chemischen Eigenschaften zwischen verschiedenen Fluidpaaren stellt einen weiteren Aspekt dar, weil jedes Fluidpaar spezifische Interaktionen umfassen kann, z.B. Interaktionen zwischen Kosolventlösungen und organischen Phasen im Vergleich zu Interaktionen zwischen Tensidlösungen und organischen Phasen. Trotz der Beteiligung unterschiedlicher Forschungsrichtungen und der entsprechenden Komplexität gibt es keine integrierende Zusammenschau zu diesem Thema in der Literatur. Um diese Mängel anzugehen, ist eine Teil der Dissertation der Überprüfung der zahlreichen wissenschaftlichen Artikel, die diesen Prozess untersuchen, gewidmet. In diesem Review dienen die charakteristische Längenskala der vorhandenen Untersuchungen und die Strömungskonfigurationen der Flüssigkeiten in porösen Medien als Grundlage zur Gruppierung der Studien. Neben den vorhandenen experimentellen Arbeiten fanden auch auch analytische und numerische Modelle Berücksichtigung. Diese Arbeit bietet ein ganzheitliches Verständnis des Massentransfers zwischen unterschiedlichen Phasen in porösen Medien, wo die Wechselwirkungen zwischen den verschiedenen Systemparametern, die durch Mehrphasenströmungsverhältnisse auftreten, dargelegt werden.

Die Auswirkungen von Mechanismen auf der Porenskala auf dem Massenaustauch können entscheidend sein. Allerdings sind die meisten Untersuchungen auf der Mesoskala durgeführt worden. Hier wurden die Mechanismen der Porenskala durch ein numerisches Modell auf der Porenskala untersucht. Die Ergebnisse des numerischen Modells zeigen, dass die Verteilung des "non-aqueous phase liquid" (NAPL) auf der Porenskala erheblichen Einfluss auf die entwickelten mesoskaligen Massentransfer- Korrelationen hat. Besonders die geometrischen Zuordnungen der Grenzfläche, die die tatsächliche Domäne für Massentransfer darstellt, haben einen unmittelbaren Einfluss. Der Grund dafür ist die Änderung des Konzentrationsprofils auf der Porenskala. Die Ergebnisse zeigen auch, dass die Grenzfläche mit dem Massentransfer aufgrund dieser Änderung nicht linear korreliert. Ein besonderes Ergebnis war, dass die gleiche Grenzfläche zu einer Größenordnung geringeren Massenaustausch führen kann, wenn die Ausrichtung bezüglich der Fließrichtung von der senkrechten hin zu einer parallelen Fließrichtung geändert wird. Die expliziten Massentransferkoeffizienten sollen diesen Effekt berücksichtigen. Jedoch sind die bestehenden Korrelationen von Massentransferkoeffizienten meistens abhängig von der Strömungsgeschwindigkeit der Lösemittelphase und die Auswirkung der räumlichen Verteilung der Grenzfläche ist nicht berücksichtigt.

Mehrere chemische Substanzen wurden in unterschiedlichen Bereichen eingesetzt, um den Massenaustausch zu erhöhen, z.B. Kosolvent- und Tensidlösungen in der Erdöl- und Umwelttechnik. Dementsprechend wurde die Kombination von Ethanol als chemisches Mittel und Wasser im Hinblick auf ihre Auswirkungen auf die Gewinnung des NAPL Toluol aus wassergesättigten porösen Medien untersucht. Die beiden Gewinnungsmechanismen, vergrößerte Löslichkeit (enhanced solubilization) und Mobilisierung, wurden durch Säulenversuche bestimmt. Es wurde gezeigt, dass es eine

Wechselwirkung zwischen diesen beiden Mechanismen gibt, die zu einer Verringerung der Grenzflächenspannung führt (bei Verwendung von mittleren Ethanolgehalten in der Spüllösung). Dies wiederum führt zur Schaffung von präferentiellen Fließwegen, die eine steile Abnahme in der Massenaustausch bewirkt. Dieses wurde durch den niedrigeren Kapillardruck bei vorliegenden größeren Porenengstellen erklärt. Bedeutsam ist, dass bei langsamen Fließgeschwindigkeiten eine Entstehung dieser präferentiellen Fließwege vermieden werden kann und damit auch die negative Auswirkung auf dem Massenaustausch. Zusammen mit den Säulenversuchen wurde ein REV (Repräsentatives Elementarvolumen) basiertes numerisches Mehrphasen-Mehrkomponenten- Modell eingesetzt, um zu untersuchen, ob dieses Verhalten durch das Modell simuliert werden kann. Das einzig verfügbare numerische Modell, das den Einsatz von Kosolventen modellieren kann, UTCHEM, wurde für diesen Zweck verwendet. Es wurde festgestellt, dass die erwähnten Porenengstellen und präferentiellen Fließwege nicht zufriedenstellend simuliert werden können. In solchen numerischen Modellen werden die Zustände auf der Porenskala durch Massenaustausch-Gleichungen (d.h. Sherwood Gleichungen) repräsentiert. Dementsprechend wurde festgestellt, dass die besondere Wirkung dieser chemischen Substanzen auf die Grenzflächenspannung und Löslichkeit spezifische Massenaustausch-Korrelationen mit entsprechend angepassten Gleichungen erfordert. Allerdings gibt es in der Literatur bisher keine Sherwood Formulierung, die das Auftreten solcher chemischen Substanzen berücksichtigt.

Der letzte Teil der Untersuchungen beschäftigt sich mit der seit langem bekannten Sherwood Gleichung, die in mehreren numerischen Mehrphasenmodellen Verwendung findet. Allerdings ist keine analytische Untersuchung für diese Sherwood-Gleichung vorhanden, so dass die allgemeine Gültigkeit bezweifelt wird. Um dieser Frage nachzugehen, wurde eine detaillierte Analyse dieser Gleichung durchgeführt. Es zeigte sich, dass diese allgemein bekannte Sherwood-Gleichung einen grundlegenden mathematischen Fehler enthält. Dadurch ist die Gleichung unbrauchbar. Darüber hinaus wurde auch gezeigt, dass die ursprünglichen Daten, auf der die Sherwood-Gleichung beruht, einen hohen Unsicherheitsgrad enthalten und deswegen auch die korrigierte Version dieser Gleichung von zweifelhaftem Wert ist. Die Folge dieses Fehlers führt zu falschen Ergebnissen einigen aktuellen Veröffentlichungen, die diese Sherwood Gleichung in einer bestimmten Art von REV basierten numerischen Modellen verwenden.

Die vorliegende Arbeit beweist die Wechselwirkungen zwischen verschiedenen Parametern des Massentransfers zwischen mehrere Flüssigkeiten in porösen Medien. Da die Vorhersagegenauigkeit des Massenaustauschs durch die genaue Berücksichtigung dieser Parameter und der dazugehörigen Wechselwirkungen bestimmt wird, muss der Inhalt der zukünftigen Forschung die Charakterisierung des Systems auf verschiedenen Skalen zum Inhalt haben. Die Berücksichtigung der Porenskala und die daraus gewonnenen Erkenntnisse für die anderen Skalen dürften dabei von entscheidender Bedeutung sein.

Table of contents

1. Introduction 1

1.1. Fields of applications 1

1.2. Multiphase flow 2

1.2.1. Scale effect 3

1.3. Chemical Agents 4

1.4. Motivation 4

1.5. Outline of the thesis 5

1.6. References 7

2. Interphase Mass Transfer between Fluids in Subsurface Formations: A Review 11

2.1. Introduction 14

2.2. Fundamentals of interphase mass transfer 15

2.2.1. Ionic strength and temperature 19

2.2.2. Multi-component NAPLs and aging 20

2.2.3. Cosolvents and surfactants 20

2.3. Mechanics of interphase mass transfer 21

2.3.1. Pore scale 22

2.3.2. Meso scale 24

2.3.3. Field scale 26

2.3.4. Factors influencing interphase mass transfer 29

2.3.4.1. Interfacial area 29

2.3.4.2. Hysteresis 32

2.3.4.3. Entrapment 33

2.3.4.4. Wettability 35

2.3.4.5. Mean grain diameter 35

2.3.4.6. Pore size distribution 36

2.3.4.7. NAPL mobilization 37

2.3.4.8. Desorption 38

2.3.4.9. Density and viscosity 38

2.4. Modeling of interphase mass transfer 38

2.4.1. Analytical models 39

2.4.2. Pore scale numerical models 43

2.4.2.1. Pore network models 43

2.4.2.2. Other pore scale models 47

2.4.3. REV-based numerical models 48

2.4.3.1. Single phase models 48

2.4.3.2. Semi-multiphase models 49

2.4.3.3. Multiphase models 50

2.5. Summary and conclusion 55
2.6. References 58
3. Impact of NAPL architecture on interphase mass transfer: A pore network study 78
3.1. Introduction 80
3.2. Pore network 82
3.2.1. Implementation of pore scale numerical model 83
3.2.2. Validation of the numerical model 86
3.3. Computation of interphase mass transfer 87
3.4. Results and discussions 87
3.4.1. Saturation-interfacial area 87
3.4.2. NAPL spatial distribution 89
3.4.3. Mean grain diameter 90
3.4.4. Domain size 91
3.4.5. The use of explicit vs. modified Sherwood expression in REV-based models 92
3.5. Conclusion 94
3.6. References 96
4. Laboratory scale experiments and numerical modeling of cosolvent flushing of multi-component NAPLs in saturated porous media 99
4.1. Introduction 102
4.2. Experimental procedure 103
4.2.1. Batch experiments 103
4.2.2. Column experiments 104
4.3. Model development 105
4.4. Results and discussions 109
4.4.1. Batch experiments 109
4.4.2. Column experiments 111
4.4.3. Model results 115
4.5. Conclusions 122
4.6. References 124
5. The use of Pfannkuch Sherwood Number Correlation for the calculation of the interphase mass transfer in porous media 128
5.1. Introduction 130
5.2. Calculation of Sherwood expression by Pfannkuch [1984] 130
5.3. Reliability of corrected Sherwood numbers 134
5.4. Implications on the numerical models 134
5.5. References 135

6. Synthesis 137
6.1. Summary and the discussion the main findings 137
6.2. Potential areas for future research 139
7. List of figures 141
8. List of tables 143
9. Annexes 144
9.1. Angaben zum Eigenanteil (Outline of the author's contributions 145
9.2. Acknowledgements 146
9.3. Eidesstattliche Erklarung 147
9.4. Curriculum Vitae 148

1. Introduction

This cumulative dissertation comprises a collection of authors publications dedicated to advance our understanding on the interphase mass transfer between fluids in geologic porous media. The entire research was conducted between 2010 and 2014.

The chapter in hand is an introduction that provides an overview of this dissertation and the interrelations between conducted investigations. Specifically, section 1.1 presents the fields of applications that involve the interphase mass transfer in porous media whereas section 1.2 confers the complexity of this process due to its direct relevance to multiphase flow patterns that occur in porous medium and shed some light on some of the influential parameters. In section 1.3 the impact of chemical agents on interphase mass transfer is introduced while in section 1.4 the motivation and the purpose of the conducted studies are presented. An outline of the manuscripts is presented in section 1.5. Chapters 2, 3, 4 and 5 are reserved for each publication whereas Chapter 6 presents the synthesis of all the published/submitted manuscripts and potential areas for future research. The references are provided at the end of each chapter separately.

1.1. Fields of applications

Interphase mass transfer in porous media has been a subject of interest within various scientific fields. Applications involving interphase mass transfer include oil recovery, non-aqueous phase liquid (NAPL) contamination/remediation, CO_2 injection into deep saline aquifers, fuel cells, and numerous industrial applications involving drying of porous media such as coatings, food, paper, textile, wood, ceramics, building materials, granular materials, electronic devices and pharmaceuticals (Abriola, 1989; Joekar-Niasar and Hassanizadeh, 2012; Mercer and Cohen, 1990; Niessner and Hassanizadeh, 2009; Yiotis et al., 2001).

The initial investigations focusing on interphase mass transfer in porous media were conducted within chemical engineering field where the porous domain and the corresponding flow field was mostly unambiguous (e.g.,(Pfeffer and Happel, 1964)). In petroleum engineering field, research focused on interphase mass transfer between fluids in the geologic porous media which consists of a flow domain that has substantial level of uncertainty (e.g., Lake, 1989). Starting from the early 1980's a considerable amount of interest was shown within environmental engineering whereby the remediation of subsurface contaminated with NAPLs was at the center of the efforts (e.g., Miller et al., 1990; Nambi and Powers, 2003; Parker and Park, 2004; Powers et al., 1991; Saba and Illangasekare, 2000; Schnaar and Brusseau, 2005). Compared to petroleum engineering field, more accurate understanding of this process was required within environmental engineering as minor levels of NAPL contamination could have led to groundwater concentrations that exceeded the regulatory levels, hence unsuccessful remediation efforts (Abriola and Pinder, 1985).

Interphase mass transfer has been investigated under four different length scales: i) sub-pore scale ii) pore scale iii) meso-scale iv) field scale. Research conducted at sub-pore scale is very recent and mostly in computational sense as it is very difficult to obtain experimental observations at this scale (e.g., Zhao and Ioannidis, 2007). On the other hand pore-scale experimental observations are currently available and there is also a substantial amount of computational investigations (e.g., Dillard and Blunt, 2000; Held and Celia, 2001a; Jia et al., 1999). In literature most of the studies focusing on interphase mass transfer in porous media are conducted at meso-scale. Meso-scale is the length scale where the discrete porous medium properties are averaged over some porous medium volume. The characteristic length of these studies ranges from 1 to 5 cm (e.g., Miller et al., 1990; Pfannkuch, 1984;

Powers et al., 1994). Finally field scale is the case where the field properties such as macro scale heterogeneity is encountered within. Most of the investigations at this scale have been computational as observation of subsurface conditions at this scale is rather complicated and costly (e.g., (Christ et al., 2006; Maji and Sudicky, 2008; Parker and Park, 2004)).

The long term investigation of interphase mass transfer by various scientific fields attests to the complexity that this process incorporates. Primarily, this circumstance is a result of the link between interphase mass transfer and the multiphase flow in porous media which is actually the fact that multiphase flow patterns occurring in porous media establish the domain for interphase mass transfer. Consequently, a sound understanding of interphase mass transfer dictates a firm knowledge on multiphase flow in porous media.

1.2. Multiphase flow

Two phase flow in porous media is described as either imbibition or drainage depending on the wettability of the porous media (Held and Celia, 2001b). Drainage is the case where non-wetting fluid intrudes into wetting phase saturated porous media. There is substantial amount of experimental and computational investigations focusing on this process at pore scale (e.g., Chen et al., 2007; Hilpert and Miller, 2001; Lenordmand et al., 1988). Piston-type movement dominates the flow in drainage (Joekar-Niasar and Hassanizadeh, 2012). The flow behavior was shown to be related to pore size distribution of the porous media, viscosity difference of the fluids and the pressure of the advancing phase (Lenordmand et al., 1988). Stability of the movement of the front and therefore also the amount of the receding phase that is bypassed by the advancing phase is dependent on these parameters.

Imbibition is the case where the wetting fluid intrudes into the non-wetting phase saturated porous media. Imbibition was shown to be more complex than drainage (Hughes and Blunt, 2000) as also snap-off mechanism can occur in addition to piston-type movement during the intrusion of the wetting phase (Lenordmand et al., 1983). The pore size distribution, the aspect ratio, the contact angle between fluids, and the velocity of the advancing phase, which is related to pressure of the advancing phase, were shown to be very influential on this process (Blunt and Scher, 1995; Hughes and Blunt, 2000).

The above mentioned pore scale physical displacement mechanisms create the interfacial area and corresponding pore scale flow paths that will be of significance during the interphase mass transfer. Therefore, any prediction of the interphase mass transfer at larger scales have to incorporate accurate estimates of these parameters. This still proves to be a challenging subject. This is due to the fact that accurate estimates of these parameters at a scale larger than pore scale necessitates the knowledge on the average behavior of multiphase flow at that scale which is rather difficult to obtain as a result of the uncertainty that exists within the average porous media properties (e.g., wettability, spatial distribution of the pore bodies/throats).

A further complication that appears in multiphase flow is its link to its history which is known as “hysteresis”. It has been long acknowledged that relations existing between Capillary pressure-Relative permeability-saturation are not unique and subject to hysteresis (Culligan et al., 2006). The occurrence of hysteresis is a result of lumping of too many system parameters (Gray and Hassanizadeh, 1991; Hassanizadeh and Gray, 1993) e.g., the change of flow paths at drainage and imbibition (due to dominance of piston type movement in drainage compared to occurrence of snap-off mechanism together with piston-type movement in the imbibition). This phenomenon can be easily visualized at subsequent imbibitions and drainages (Chen et al., 2006). For example once the initial drainage is completed and subsequent imbibition starts the snap-off occurrence may change the path of

advancement for the wetting fluid hence the relation between Capillary pressure-Relative permeability-saturation for the porous domain under consideration (Lenordmand et al., 1983). Since the accurate estimates of interphase mass transfer necessitates the accurate interfacial areas and corresponding flow paths this condition should also be considered.

The flow properties of the solvent phase adjacent to the interfacial area is of specific importance. This is because the occurrence of stagnant solvent formations limit the interphase mass transfer by the diffusion coefficient of the dissolving solute. The above mentioned multiphase flow patterns determine whether the existing interfacial area is in a stagnant region or not. Moreover it is also possible to have some portions of the interfacial area adjacent to mobile solvent phase whereas other portions reside adjacent to stagnant regions. For example, the meniscus interfacial area occurring between a NAPL blob and aqueous phase in water wet porous media can be adjacent to a mobile water formation whereas the film area (i.e., the interfacial area between NAPL and film water formation that exist between NAPL and grain particle) can be adjacent to stagnant water formation (Bradford et al., 1999; Sahloul et al., 2002). This issue has considerable impact on interphase mass transfer. For example in NAPL wetting media, where the most of the existing interfacial area (both meniscus and film area) is likely to reside adjacent to mobile water formations, interphase mass transfer from NAPL to mobile aqueous phase has been observed to be greater compared to water wet porous media (Bradford et al., 1999).

In literature, interphase mass transfer was mostly investigated at meso-scale and the discrete pore scale information (e.g., interfacial area, pore throat/body sizes) and its impact on the interphase mass transfer was not explicitly discovered but roughly estimated by regression analyses (performed as correlating the interphase mass transfer coefficients to the system properties (i.e., fluid and characteristic porous medium properties) (e.g., Imhoff et al., 1994; Powers et al., 1992). As a result of these regression analyses mathematical formulations have been established that relate interphase mass transfer coefficient to these system properties. These mathematical formulations have been constructed in dimensionless form with use of Sherwood numbers. In literature there is a substantial number of Sherwood number formulations developed by various scientists (e.g.,Imhoff et al., 1994; Miller et al., 1990; Nambi and Powers, 2003; Pfannkuch, 1984; Powers et al., 1992). During the last two decades it has also been acknowledged these Sherwood number formulations return conflicting interphase mass transfer rates when they are applied on the same fluid/porous medium conditions (e.g.,Kokkinaki et al., 2013; Maji and Sudicky, 2008). One major reason is the fact that these Sherwood formulations are actually developed from distinct fluid/porous medium conditions at the pore scale yet their development through meso-scale observation prevented the comprehension/assessment of such distinctions accurately.

1.2.1. Scale effect

Interphase mass transfer between fluids in porous media can be observed at different length scales. The magnitude of the impact of different system parameters on interphase mass transfer are observed at different orders at different length scales. For example, the impact of density at the field scale can be observed relatively straightforward as lighter solvent phase will flow above the denser dissolving phase (i.e., stratification, Mackay et al., 1985). However the impact of stratification at pore scale is not easy to observe and in some cases even not possible due to ignorance of gravitational forces in the experimental methodology (e.g., 2D horizontal micro models, Jia et al., 1999).

The mathematical modeling of interphase mass transfer at different scales requires different methodologies even though the results at different scales are intrinsically related by the physics of flow/interphase mass transfer mechanisms. Pore scale investigations have been conducted to

investigate the impact of discrete pore space characteristics and lead to improvement of meso-scale results. Meso-scale investigations, on the other hand, led to improvement of field scale investigations. In accordance with the fields of applications associated with interphase mass transfer, the ultimate goal is to obtain accurate predictions of interphase mass transfer at the field scale and therefore such interconnectedness between different length scales attests to importance of pore scale accuracy for the field scale prediction efforts. Field scale predictions are also strictly dependent on the flow paths (i.e., bypass conditions) at macro-scale (i.e., due to macro-scale heterogeneity of the porous media). Any prediction effort based on erroneous permeability field (hence flawed bypassing conditions) will therefore return invalid results (Parker and Park, 2004).

Accurate predictions at the field scale should consider all the involved parameters considerably well. Such consideration is easier within REV (representative elementary volume) based numerical models compared to the analytical methods. The analytical methods are known for their ease for use, however, the simplification of subsurface conditions which lead to the reduced accuracy is a drawback (e.g., Zhu and Sykes, 2004). REV-based numerical models can be significantly complicated based on the type of flow that is modeled (e.g., oil extraction with surfactant solutions) yet they provide flexibility on the input parameters that influence the results and therefore deliver more accurate results (e.g., Maji and Sudicky, 2008). A particular issue for the simulation of interphase mass transfer with REV-based numerical models is the choice of grid block size. Since these models forces grid block size be equal to REV, the size of grid block should be chosen with care meaning that it should be compatible with the size of the experiments that the adopted Sherwood formulation is derived from. If this condition is not met, the delivered interphase mass transfer rates will be erroneous.

1.3. Chemical agents

Interphase mass transfer between two fluids in porous media can incorporate further complications if a chemical agent that alters the fundamental interactions between fluids is introduced into the system. Most prominent chemical agents that have been employed in both petroleum and environmental engineering fields are surfactants and cosolvents. The purpose of their use is to increase the recovery rate of the organic phase either with mobilization or enhanced solubilization or with both concurrently (Aydin et al., 2011). The term “enhanced solubilization” refers to interphase mass transfer where these agents are used.

The specific impacts of such chemicals are a reduction in the interfacial tension between the two fluids and an increase in the miscibility of the system (i.e., increase in equilibrium concentrations of species in counter phases, Liang and Falta, 2008). The alteration of these two parameters can have drastic impact on the multiphase flow behavior at various scales. At pore scale the impact of the decrease in interfacial tension on the flow conditions can be readily observed as the capillary force existing in a pore throat is a function of the interfacial tension and contact angle (Pennell et al., 1994). On the other hand, a field scale consequence is the increase in miscibility leading to a change in the fluid densities and also viscosities that may instigate unstable flow conditions or over-riding of the solvent phase (i.e., stratification) which would have significant impact on the interphase mass transfer (Palomino and Grubb, 2004).

1.4. Motivation

Apart from the topics briefly mentioned in this introduction, several other issues (e.g., desorption, mobilization of dissolving phase, ionic strength, aging, multicomponent organic phases, etc.) have considerable impact on interphase mass transfer. A detailed assessment of all these conditions on

interphase mass transfer in literature is missing. To address this absence a detailed review of interphase mass transfer between fluids in porous media is conducted as a part of this work. To evaluate the impact of pore scale configurations on meso-scale interphase mass transfer formulations a computational pore scale investigation of interphase mass transfer is also performed in another chapter of this dissertation. One other chapter deals with the impact of cosolvents on interphase mass transfer both in experimental and computational terms. Along with one dimensional dissolution experiments also REV-based multiphase multicomponent numerical simulator UTCHEM was employed for this purpose. In addition to these, a mathematical error conducted during the development of a particular Sherwood formulation, which has significant consequences on a number of recent publications by several authors, is also presented in the thesis.

1.5. Outline of the thesis

This cumulative dissertation consists of 4 manuscripts, one of which is already published in "Journal of Contaminant Hydrology". The other manuscripts are currently under review in "Advances in water resources" and "Water resources research".

1. **Agaoglu, B.,** Copty, N. K., Scheytt, T., Hinkelmann. R., (2015) Interphase mass transfer between fluids in subsurface formations: A review. Advances in Water Resources; 79, 162-194 (Chapter 2);

2. **Agaoglu, B.,** Scheytt, T., Copty, N. K., (Submitted) Impact of NAPL architecture on interphase mass transfer: A pore network study (Chapter 3);

3. **Agaoglu, B.,** Scheytt, T., Copty, N. K., (2012) Laboratory scale experiments and numerical modeling of cosolvent flushing of multicomponent NAPLs in saturated porous media. Journal of Contaminant Hydrology; 140, 80 – 94 (Chapter 4);

4. **Agaoglu, B.,** Scheytt, T., Copty, N. K., (Submitted) The use of Pfannkuch Sherwood Number Correlation for the calculation of the interphase mass transfer in porous media (Chapter 5).

The first article is a review on interphase mass transfer in porous media that attempts to shed light on the origins of this process in relation to complex nature of the multiphase flow in porous media. Characteristic length scale of observations/models was specifically discussed while the mathematical modeling of interphase mass transfer is also reviewed within this article. The second article focuses on the influence of sub-grid scale properties on interphase mass transfer through use of a two-dimensional pore network model. The third manuscript comprises of both experimental and numerical investigations focusing on the impact of cosolvents on the dissolution of multicomponent NAPLs through use of column experiments and multiphase multicomponent flow simulator UTCHEM. The fourth manuscript is a short paper on the use of a particular Sherwood formulation in a certain type of REV based numerical model.

Chapter 2: "Interphase mass transfer between fluids in subsurface formations: A review"
Interphase mass transfer between fluids in porous media is a complex process that involves many distinct physical and chemical processes within. To date there is not an integral examination of this process in literature that deals with the interactions existing between the parameters that affect this process. This work is an attempt to address this absence. More than 300 papers are cited and their indications are evaluated in correspondence to each other. Flow configurations that occur in porous

media between two fluids in relation to wettability and the mobility of phases were shown to specifically influence interfacial area that contributes to interphase mass transfer. Length scale of observation was particularly taken into consideration during assessment of the literature. Mathematical modeling of interphase mass transfer was also a major of point of focus. Finally, potential fields for future research were highlighted.

Chapter 3: "Impact of NAPL architecture on interphase mass transfer: A pore network study"
The simulation of interphase mass transfer in porous media is commonly conducted based on Sherwood number expressions that are developed in terms of fluid and porous medium properties averaged over a representative volume. In this work the influence of sub-grid scale properties on interphase mass transfer was investigated through use of a two-dimensional pore network model. It was shown that the variability of different properties at sub-grid scale has significant impact on the predicted interphase mass transfer. Interfacial area was shown to have a complex impact on interphase mass transfer in relation with the flow bypassing induced by the pore scale NAPL architecture and porous medium properties. It was also demonstrated that the domain size has impact on the interphase mass transfer.

Chapter 4: "Laboratory scale experiments and numerical modeling of cosolvent flushing of multicomponent NAPLs in saturated porous media"
In this study the impact of cosolvent use on interphase mass transfer was investigated. Enhanced NAPL dissolution was examined through column experiments whereby the flushing solution consists of water, and ethanol mixtures at different percentages. To investigate the appropriateness of the existing numerical models that are capable of simulating cosolvent flushing of NAPLs, multiphase multicomponent flow simulator UTCHEM was employed. It was demonstrated that the reduction in interfacial tension with intermediate amounts of cosolvent use, leads to occurrence of preferential flow paths in the porous medium. This results in substantial bypassing of the NAPL by the flushing solution and therefore a steep decrease in the interphase mas transfer rates. UTCHEM, which is the only numerical model that is capable of simulating cosolvent flushing of NAPLs, was shown to be incapable of simulating this phenomenon. This indicates the need for novel interphase mass transfer formulations that accounts for the effect the interfacial tension reduction and corresponding bypass conditions that may occur in case of chemical agent use.

Chapter 5: "The use of Pfannkuch Sherwood Number Correlation for the calculation of the interphase mass transfer in porous media"
Sherwood formulation developed by Pfannkuch (1984) has been used in numerous investigations that deal with interphase mass transfer in porous media. Among others Thermodynamics Model which took considerable attention in the last 5 years particularly relies on the use of this formulations. In this work, we have demonstrated that the formulation developed by Pfannkuch (1984) is clearly flawed due to some mathematical error made during its development. It was also shown that the uncertainty associated with the data used by Pfannkuch (1984) for the development of this model is significant which renders its use not possible. Consequently, the implications of using this flawed formulation in Thermodynamics model and the corresponding simulation results presented by the authors of Thermodynamics model were discussed.

1.6. References

Abriola, L.M., 1989. Modeling multiphase migration of organic chemicals in groundwater systems--a review and assessment. Environ. Health Perspect. 83, 117–43.

Abriola, L.M., Pinder, G.F., 1985. A multiphase approach to the modeling of porous-media contamination by organic-compounds .2. numerical-simulation. Water Resour. Res. 21, 19–26. doi:10.1029/WR021i001p00019

Aydin, G.A., Agaoglu, B., Kocasoy, G., Copty, N.K., 2011. Effect of temperature on cosolvent flooding for the enhanced solubilization and mobilization of NAPLs in porous media. J. Hazard. Mater. 186, 636–44. doi:10.1016/j.jhazmat.2010.11.046

Blunt, M.J., Scher, H., 1995. Pore-level modeling of Wetting. Phys. Rev. E 52, 6387–6403.

Bradford, S.A., Vendlinski, R.A., Abriola, L.M., 1999. The entrapment and long-term dissolution of tetrachloroethylene in fractional wettability porous media. Water Resour. Res. 35, 2955–2964. doi:10.1029/1999WR900178

Chen, D., Pyrak-Nolte, L.J., Griffin, J., Giordano, N.J., 2007. Measurement of interfacial area per volume for drainage and imbibition. Water Resour. Res.

Chen, L., Kibbey, T.C.G., Street, W.B., 2006. Measurement of Air - Water Interfacial Area for Multiple Hysteretic Drainage Curves in an Unsaturated Fine Sand 6874–6880. doi:10.1029/2004WR003278.(1)

Christ, J.A., Ramsburg, C.A., Pennell, K.D., Abriola, L.M., 2006. Estimating mass discharge from dense nonaqueous phase liquid source zones using upscaled mass transfer coefficients: An evaluation using multiphase numerical simulations. Water Resour. Res. 42, n/a–n/a. doi:10.1029/2006WR004886

Culligan, K.A., Wildenschild, D., Christensen, B.S.B., Gray, W.G., Rivers, M.L., 2006. Pore-scale characteristics of multiphase flow in porous media: A comparison of air–water and oil–water experiments. Adv. Water Resour. 29, 227–238. doi:10.1016/j.advwatres.2005.03.021

Dillard, L.A., Blunt, M.J., 2000. Development of a pore network simulation model to study nonaqueous phase liquid dissolution. Water Resour. Res. 36, 439–454.

Gray, W., Hassanizadeh, S., 1991. Unsaturated flow theory including interfacial phenomena. Water Resour. Res.

Hassanizadeh, S.M., Gray, W.G., 1993. Thermodynamic basis of capillary pressure in porous media. Water Resour. Res.

Held, R.J., Celia, M.A., 2001a. Pore-scale modeling and upscaling of nonaqueous phase liquid mass transfer. Water Resour. Res. 37, 539–549.

Held, R.J., Celia, M.A., 2001b. Modeling support of functional relationships between capillary pressure, saturation, interfacial area and common lines. Adv. Water Resour. 24, 325–343. doi:10.1016/S0309-1708(00)00060-9

Hilpert, M., Miller, C.T., 2001. Pore-morphology-based simulation of drainage in totally wetting porous media. Adv. Water Resour. 24, 243–255. doi:10.1016/S0309-1708(00)00056-7

Hoffmann, B., 1969. Über die ausbreitung gelöster kohlenwasserstoffe im grundwasserleiter. Inst. f. Wasserwirtschaft u. Landwirtschaftl. Wasserbau d. Techn. Univ.

Hughes, R.G., Blunt, M.J., 2000. Pore Scale Modeling of Rate Effects in Imbibition. Transp. porous media 40, 295–322.

Imhoff, P.T., Jaffé, P.R., Pinder, G.F., 1994. An experimental study of complete dissolution of a nonaqueous phase liquid in saturated porous media. Water Resour. Res. 30, 307–320.

Jia, C., Shing, K., Yortsos, Y.C., 1999. Visualization and simulation of non-aqueous phase liquids solubilization in pore networks. J. Contam. Hydrol. 35, 363–387. doi:10.1016/S0169-7722(98)00102-8

Joekar-Niasar, V., Hassanizadeh, S.M., 2012. Analysis of Fundamentals of Two-Phase Flow in Porous Media Using Dynamic Pore-Network Models: A Review. Crit. Rev. Environ. Sci. Technol. 42, 1895–1976. doi:10.1080/10643389.2011.574101

Kokkinaki, A., O'Carroll, D.M., Werth, C.J., Sleep, B.E., 2013. An evaluation of Sherwood-Gilland models for NAPL dissolution and their relationship to soil properties. J. Contam. Hydrol. 155, 87–98. doi:10.1016/j.jconhyd.2013.09.007

Lake, W.L., 1989. Enhanced oil recovery. Prentice-Hall, Englewood Cliffs, N.J.

Lenordmand, R., Toulboul, E., Zarcone, C., 1988. Numerical models and experiments on immiscible displacements in porous media. J. Fluid Mech. 189.

Lenordmand, R., Zarcone, C., Sarr, A., 1983. Mechanisms of the displacement of one fluid by another in a network of capillary ducts. J. Fluid Mech. 135, 337–353.

Liang, H., Falta, R.W., 2008. Modeling field-scale cosolvent flooding for DNAPL source zone remediation. J. Contam. Hydrol. 96, 1–16. doi:10.1016/j.jconhyd.2007.09.005

Mackay, D.M., Roberts, P. V, Cherry, J.A., 1985. Transport of organic contaminants in groundwater. Environ. Sci. Technol. 19, 384–92. doi:10.1021/es00135a001

Maji, R., Sudicky, E.A., 2008. Influence of mass transfer characteristics for DNAPL source depletion and contaminant flux in a highly characterized glaciofluvial aquifer. J. Contam. Hydrol. 102, 105–119. doi:10.1016/j.jconhyd.2008.08.005

Mercer, J., Cohen, R., 1990. A review of immiscible fluids in the subsurface: Properties, models, characterization and remediation. J. Contam. Hydrol. 6.

Miller, C.T., Poirier-McNeill, M.M., Mayer, A.S., 1990. Dissolution of trapped nonaqueous phase liquids: Mass transfer characteristics. Water Resour. Res. 26, 2783–2796.

Nambi, I.M., Powers, S.E., 2003. Mass transfer correlations for nonaqueous phase liquid dissolution from regions with high initial saturations. Water Resour. Res. 39, n/a–n/a. doi:10.1029/2001WR000667

Niessner, J., Hassanizadeh, S.M., 2009. Modeling kinetic interphase mass transfer for two-phase flow in porous media including fluid–fluid interfacial area. Transp. porous media 80, 329–344. doi:10.1007/s11242-009-9358-5

Palomino, A.M., Grubb, D.G., 2004. Recovery of dodecane, octane and toluene spills in sandpacks using ethanol. J. Hazard. Mater. 110, 39–51. doi:10.1016/j.jhazmat.2004.02.035

Parker, J.C., Park, E., 2004. Modeling field-scale dense nonaqueous phase liquid dissolution kinetics in heterogeneous aquifers. Water Resour. Res. 40, n/a–n/a. doi:10.1029/2003WR002807

Pennell, K., Jin, M., Abriola, L., Pope, G., 1994. Surfactant enhanced remediation of soil columns contaminated by residual tetrachloroethylene. J. Contam. Hydrol. 00.

Pfannkuch, H., 1984. Determination of the contaminant source strength from mass exchange processes at the petroleum-ground-water interface in shallow aquifer systems. Water Well Assoc. Am. Pet. Inst. Houston, Tex.

Pfeffer, R., Happel, J., 1964. An analytical study of heat and mass transfer in multiparticle systems at low Reynolds numbers. AIChE J. 10, 605–611.

Powers, S.E., Abriola, L.M., Weber, W.J., 1992. An experimental investigation of nonaqueous phase liquid dissolution in saturated subsurface systems: Steady state mass transfer rates. Water Resour. Res. 28, 2691–2705.

Powers, S.E., Abriola, L.M., Weber, W.J., 1994. An experimental investigation of nonaqueous phase liquid dissolution in saturated subsurface systems: Transient mass transfer rates. Water Resour. Res. 30, 321–332.

Powers, S.E., Loureiro, C.O., Abriola, L.M., Weber, W.J., 1991. Theoretical study of the significance of nonequilibrium dissolution of nonaqueous phase liquids in subsurface systems. Water Resour. Res. 27, 463–477. doi:10.1029/91WR00074

Saba, T., Illangasekare, T.H., 2000. Effect of groundwater flow dimensionality on mass transfer from entrapped nonaqueous phase liquid contaminants. Water Resour. Res. 36, 971–979. doi:10.1029/1999WR900322

Sahloul, N.A., Ioannidis, M.A., Chatzis, I., 2002. Dissolution of residual non-aqueous phase liquids in porous media: pore-scale mechanisms and mass transfer rates. Adv. Water Resour. 25, 33–49. doi:10.1016/S0309-1708(01)00025-2

Schnaar, G., Brusseau, M.L., 2005. Pore-scale characterization of organic immiscible-liquid morphology in natural porous media using synchrotron X-ray microtomography. Environ. Sci. Technol. 39, 8403–10.

Yiotis, A.G., Stubos, A.K., Boudouvis, A.G., Yortsos, Y.C., 2001. A 2-D pore-network model of the drying of single-component liquids in porous media. Adv. Water Resour. 24, 439–460. doi:10.1016/S0309-1708(00)00066-X

Zhao, W., Ioannidis, M.A., 2007. Convective mass transfer across fluid interfaces in straight angular pores. Transp. porous media 495–509. doi:10.1007/s11242-006-0025-9

Zhu, J., Sykes, J.F., 2004. Simple screening models of NAPL dissolution in the subsurface. J. Contam. Hydrol. 72, 245–58. doi:10.1016/j.jconhyd.2003.11.002

2. Interphase Mass Transfer between Fluids in Subsurface Formations: A Review

Berken Agaoglu[a,c], Nadim K Copty[b], Traugott Scheytt[a], Reinhard Hinkelmann[c]

[a] Institute of Applied Geosciences, Berlin Institute of Technology, Sekr. BH 3-2, Ernst-Reuter-Platz 1, 10587 Berlin, Germany

[b] Institute of Environmental Sciences, Bogazici University, 34342 Bebek, Istanbul, Turkey

[c] Chair of Water Resources Management and Modeling of Hydrosystems, Department of Civil Engineering, Berlin Institute of Technology, TIB 1-B14, Gustav-Meyer-Allee 25, 13355 Berlin, Germany

Citation:
Agaoglu, B., Copty K. N., Scheytt T., Hinkelmann R., "Interphase mass transfer between fluids in subsurface formations: A Review". Advances in Water Resources 79 (2015): 162-194

Abstract

This paper presents a review of the state-of-the-art on interphase mass transfer between immiscible fluids in porous media with focus on the factors that have significant influence on this process. In total close to 300 papers were reviewed focusing to a large extent on the literature relating to NAPL contamination of the subsurface. The large body of work available on this topic was organized according to the length scales of the conducted studies, namely the pore, meso and field scales. The interrelation of interphase mass transfer at these different scales is highlighted. To gain further insight into interphase mass transfer, published studies were discussed and evaluated in terms of the governing flow configurations defined in terms of the wettability and mobility of the different phases. Such organization of the existing literature enables the identification of the interfacial domains that would have a significant impact on interphase mass transfer. Available modeling approaches at the various length scales are discussed with regard to current knowledge on the physics of this process. Future research directions are also suggested.

Nomenclature

Roman Letters

A	Absolute interfacial area (L^2)
A_{ia}	The air-water interfacial area normalized by total porous medium volume (1/L)
A_{ij}	Cross section area of the pore throat between pore i and j (L^2)
A^*_{NW}	Interfacial area between wetting and non-wetting phase per unit pore volume (1/L)
$A_{na,i}$	Interfacial area in pore i (L^2)
A^*_{sN}	Interfacial area between solid and non-wetting phase per unit pore volume ($A^*_{sN} = 0\ if\ S_w = 1$) (1/L)
A_w	Cross sectional area in water filled pore throat (L^2)
a	Specific interfacial area (1/L)
α^{wn}	Effective specific interfacial area (meniscus interfacial area per unit volume of porous media (1/L)
C	Solute concentration (M/L^3)
C_a	Solute concentration at the center of each subdivision (M/L^3)
$C_{a,i}$	Solute concentration in pore i (M/L^3)
C_a^S	Solute equilibrium concentration (M/L^3)
C_b	Concentration in bulk phase (M/L^3)
C_{eq}	Equilibrium concentration of solute (M/L^3)
C_i	Solute concentration in pore i (M/L^3)
C_i^{in}	Solute concentration entering to pore i (M/L^3)
C_i^{out}	Solute concentration leaving pore i (M/L^3)
C_j^{in}	Solute concentration entering pore j (M/L^3)
C_{NW}	Constant of integration
C_{out}	Effluent concentration (M/L^3)
C_s	Solute equilibrium concentration (M/L^3)
$C_{(s)}$	Solute equilibrium concentration (M/L^3)
C_t^{in}	Solute concentration entering pore throat (M/L^3)
D	Molecular diffusion coefficient (L^2/T)
D_m	Molecular diffusion coefficient (L^2/T)
D_y	Dispersion coefficient in y direction (L^2/T)
d_s	Diameter of spherical blobs (L)
d_m	Grain diameter (L)
E	Interphase mass transfer rate divided by the interfacial area
E_d	Energy dissipation factor (eq. 10)
E_d	Normalized average effluent conc. (eq.25)
E_{wn}	Interfacial area production rate(1/LT)
e_i	Separation distance between nodes (L)
e_{wn}	Strength of change in specific interfacial area(1/L)
$F^{(j)}$	Force acting on postion x of component j (ML/T^2)
F_{ij}	Mass flux between pore i and j (M/L^2T)
$F(x_j - x_i, y_j - y_i, z_j - z_i)$	erfc type transport function (open format can be found in [221])
G_{ij}	Pore conductance between pore i and j (TL^4/M)
G_{jk}	Interaction strength parameter between component j and k (eq. 29)
GTP	Ganglia to pool ratio
I_i	Interphase mass transfer term
K_f	Ratio of NAPL density to the contaminant conc. in the flushing solution in stream tube i (eq. 19)
K_l	Mass transfer rate coefficient (i.e., Mass transfer coefficient lumped with interfacial area) (1/T)
$\overline{K_s}$	Average hydraulic conductivity of domain (L/T)
$k_{f1,2}$	Mass transfer coefficient (L/T)
l	Length of hypothetical film thickness (L)
l	Length of the pore throat (eq. 23) (L)
l_t	Length of the pore throat (L)
L	Length in x direction (L)
$M_{(t)}$	NAPL mass at time t (M)
M_i	Number of interfaces connected to pore i
M_0	Initial NAPL mass (M)
m	Parameter determined with respect to uniformity coefficient of the medium (eq. 7)
N	Number of subdivisons (eq.13, 14)
N	Number of adjacent pores to pore i (eq. 22)
N_i	Number of pores connected to pore i
N_i	Molar flux of component i (eq.30) (mol/L^2T)
n	Parameter determined with respect to uniformity coefficient of the medium (eq. 7)
P_{ij}	Pressure difference between pore i and j (M/LT^2)
P_c^{crit}	Critical disjoining pressure (M/LT^2)
Pe	Peclet number
Q_{ij}	Flow rate between pore i and j (L^3/T)
Q_{ij}^w	Flow rate of water between pore i and j (L^3/T)
Q_{ij}^α	Flow rate of phase α between pore i and j (L^3/T)
q	Superficial aqueous phase velocity (L/T)
$\bar{q}$	Average Darcy velocity (L/T)
Re	Reynolds number
R_i	Retardation factor of stream tube i
R_t	Pore throat radius (L)
SA	Specific surface area of the porous medium (L^2/M)
S_i^α	Local saturation of phase α in pore i
$\check{S}_i$	Trajectory average NAPL saturation of stream tube i
S_m	Monolayer saturation
S_w	Wetting phase saturation
s	Normalized surface area of the porous media
Sh	Sherwood number
Sh'	modified Sherwood number
t_i	Nonreactive travel time in stream tube I T
U	Velocity (L/T)
U_x	Velocity in x direction (L/T)
$V_{a,i}$	Volume of pore containing water (L^3)
V_i	Volume of pore I (L^3)
V_s	Volume of NAPL in shape of spherical blobs per unit volume of medium (eq. 12) (L^3)
V_s	Volume of site (pore i) (eq. 23) (L^3)
x	Geometric parameter related to pore wall curvature that is positive for convex shape (eq.28)
x, y, z	Lengths in x, y and z-directions (L)

Greek Letters

α	Parameter determined with respect to uniformity coefficient of the medium (eq. 7)
β	Mass depletion exponent
β_1	Velocity dependence parameter
β_2	Mass depletion exponent
κ_{eff}	Mass transfer rate coefficient (1/T)
κ_0	Parameter found by fitting the analytical solution to numerical results
Π^{max}	Maximum disjoining pressure (M/LT^2)
σ	Interfacial tension (M/T^2)
σ_{NW}	Interfacial tension between non-wetting and wetting phases (M/T^2)
τ_i	Reactive travel time in stream tube i (T)
ϕ	Porosity of the porous medium (eq. 10)
ϕ_{sNW}	Contact angle (O)
Φ_{NW}	Area under capillary pressure – saturation curve
$[\Phi_{NW}(S_w)]^{D,I,D^*}$	Area under capillary pressure – saturation curve for primary drainage, secondary and all subsequent imbibition, and main and all subsequent drainage conditions.
Ψ	Ratio of the effective to total specific interfacial area
$\Psi^{(j)}$	Effective mass given as a function of local density (eq.29)

1. Introduction

Multiphase flow in porous media is encountered in numerous natural and industrial systems. Water seepage through the vadose zone during precipitation events is just one example of the many natural systems involving the flow of multiple phases. Applications involving multiphase flow include fuel cells, oil recovery, non-aqueous phase liquid (NAPL) contamination/remediation, CO_2 injection into deep saline aquifers, and numerous industrial applications involving drying of porous media such as coatings, food, paper, textile, wood, ceramics, building materials, granular materials, electronic devices and pharmaceuticals [1–5]. A fundamental process that is common to all these multiphase systems is interphase mass transfer, which is the transfer of components across the interface separating the different phases.

Given the centrality of interphase mass transfer to many applications, significant efforts across a number of disciplines have been directed to characterize this process. Earlier efforts were mostly in relation to petroleum exploration and in the field of chemical engineering, dealing mostly with engineered packed bed systems [6,7]. Starting in the late twentieth century when NAPL contamination of the subsurface was recognized as one of the most challenging environmental problem, significant research was conducted to elucidate the factors influencing interphase mass transfer such as NAPL dissolution. Much of the advances of these research efforts consisted of meso-scale experiments that led to the definition of empirical expressions of interphase mass transfer (e.g., [8,9]). These expressions were mostly specific to the conditions present during the experiments and a unified interphase mass transfer theory was beyond reach. Major limitations have been the inability to define the spatial distribution of the multiphase system, including the distribution of the interfacial areas and the transient flow in the surrounding regions.

In the past two decades significant developments in experimental technologies such as non-invasive imaging techniques and pore scale modelling have meant that the multiphase system within the porous medium can be more accurately characterized. In this work we present a review of the state-of-the-art on interphase mass transfer in porous media with focus on the factors that have significant influence on that process. The molecular basis of interphase mass transfer is presented initially, followed by the mechanics of interphase mass transfer when multiple fluids exist in porous media. In the latter section the existing literature is grouped under different "fluid-porous medium" configurations. As interphase mass transfer is directly influenced by the contact area and the flow properties (velocity, path) of the solvent phase, such distinction between different two-phase flow conditions in porous media enables a comparative evaluation and further insight into this process. Table 1 presents 5 different flow configurations that can exist in two phase flow in porous media. These are; INtoMW: Mass transfer from the **I**mmobile **N**on-wetting phase to the **M**obile **W**etting phase; IWtoMN: Mass transfer from the **I**mmobile **W**etting phase to the **M**obile **N**on-wetting phase; MNtoIW: Mass transfer from the **M**obile **N**on-wetting phase to the **I**mmobile **W**etting phase; MWtoIN: Mass transfer from the **M**obile **W**etting phase to the **I**mmobile **No**n-wetting phase; CHEM: Mass transfer when miscibility-enhancing **CHEM**ical agents are present. Here after these flow configurations will be referred to with their acronym defined above and in Table 1.

Table 1: Classification of two phase flow in porous media for the evaluation of interphase mass transfer

Acronym	Dissolving Phase	Solvent Phase	Examples
INtoMW	**I**mmobile, **N**on-wetting	**M**obile, **W**etting	Non-wetting NAPL dissolution
IWtoMN	**I**mmobile, **W**etting	**M**obile, **N**on-wetting	Air Sparging
MNtoIW	**M**obile, **N**on-wetting	**I**mmobile, **W**etting	CO_2 Injection
MWtoIN	**M**obile, **W**etting	**I**mmobile, **N**on-wetting	Gas exsolution
CHEM	Mobility and wettability of phases is altered through the use of miscibility enhancing chemical agents		Enhanced NAPL remediation

"INtoMW" is encountered in applications such as NAPL dissolution in subsurface systems contaminated by non-wetting NAPLs whereas "IWtoMN" can be observed during remediation activities such as air sparging, NAPL dissolution of wetting NAPLs and applications involving drying of porous medium. "MNtoIW" appears in CO_2 injection into saline aquifers and "MWtoIN" is observed in, for example, gas exsolution applications. "CHEM" occurs in enhanced oil recovery and enhanced NAPL remediation activities. The advantages of the categorization adopted in this review paper are further discussed in Section 3.1. It should be mentioned that both "MNtoIW" and "MWtoIN" have been investigated only recently and as a results there are only a handful of reported studies on these configurations. Therefore they are mentioned only briefly in this review.

Although the research on interphase mass transfer relating to NAPL contamination of the subsurface constitutes the foundation of this review, the discussion of the physics of this process enables the transition of the findings to other applications with similar conditions. Within the environmental field, interphase mass transfer has been commonly investigated at three different scales; i) pore scale, ii) meso-scale, iii) field scale [2,10,11]. Pore scale is the scale where the flow properties at discrete pore bodies/throats can be observed. On the other hand the characteristic length of the meso-scale mostly ranges from 1 to 5 cm whereas field scale ranges from a decimeter to hundreds of meters where the influence of the large scale heterogeneity becomes significant. Although interphase mass transfer at these different scales is intrinsically related, the experimental and mathematical tools used for their investigation can be significantly different. Here we review the research on all three scales and attempt to shed light on the relationship between the different scales. For each of the scales, the discussion is also framed in terms of the different flow configurations defined above.

The rest of this paper is organized as follows: Section 2 presents basic definitions of mass transfer and its fundamentals including its basis in molecular chemistry. Section 3 discusses the mechanics of interphase mass transfer in porous media with an emphasis on scale issues. Mathematical models developed for the simulation of interphase mass transfer in porous media are presented in Section 4. All mathematical terms appearing in these models are defined in the nomenclature. Section 5 presents a critical assessment of the reviewed works and identifies areas for future research.

2. Fundamentals of interphase mass transfer

The partitioning of one type of molecule into a different phase environment is determined by the combined effect of the intermolecular forces namely: the London dispersive forces, dipole-dipole forces and dipole induced forces [12–16]. These forces are much weaker than the intramolecular forces such as covalent bonds [12]. The partitioning can be defined thermodynamically in terms of the chemical potential of the compound. If the chemical potentials of a compound in two adjacent systems

(in this case; phases) are the same, this means that equilibrium is present and no net interphase mass transfer of that compound would occur [16].

A commonly adopted approach to determine the interphase mass transfer rate is to define it as the product of a coefficient of interphase mass transfer that is unique for the system conditions and the concentration difference (or chemical potential) between the interface, where it is assumed to be at solubility, and the bulk solvent phase where sufficient mixing can be assumed to occur allowing for the definition of a representative concentration over some specific volume. Since the interphase mass transfer is function of the interfacial area across which the mass transfer is occurring, the interfacial area is also incorporated in this approach resulting in [8] :

$$\frac{\partial M}{\partial t} = k_{f1} A (C_s - C) \qquad (1)$$

Various theories have been developed to relate interphase mass transfer to system parameters based on the type of the boundary conditions that occur at the interface. These theories include the film theory, boundary layer theory, penetration theory and surface renewal theory [17–20]. These theories were mostly developed for an air-water interface which in nature often exhibits turbulence conditions especially at the air side. As a result the influence of turbulence on diffusivity is considered to be significant in the development of these theories. The film theory, which is based on bottleneck boundary conditions (i.e., abrupt decrease of diffusivity adjacent to an interface), assumes that a stagnant thin layer develops at the interface between the two phases where molecular diffusion is the governing mass transport process. Consequently the mathematical description of interphase mass transfer proposed by the film theory expresses the interphase mass transfer coefficient in terms of the diffusion coefficient and a hypothetical film thickness value l,

$$\frac{\partial M}{A \partial t} = \frac{D}{l} (C_s - C) \qquad (2)$$

The boundary layer theory on the other hand assumes a gradual decrease in diffusivity (i.e., the sum of molecular and turbulent diffusivities) with approach to the interface, while the interphase mass transfer coefficient is defined through Schmidt number [20]. Detailed description of these theories can be found in [13,21,22].

It has been well shown in the literature that one of the most influential parameters on interphase mass transfer is the velocity. The dependence of interphase mass transfer coefficient on the velocity of the solvent phase was first investigated by Frössling [23] and Ranz & Marshall [24]. Friedlander [25] derived an analytical solution for evaporation of a single droplet and cylinder whereas Dobry & Finn [26] conducted laboratory experiments to determine the impact of velocity on mass transfer. Kusik & Happel [27] developed an analytical solution for interphase mass transfer in particle beds. Williamson et al. [28] investigated the velocity dependence of the dissolution of benzoic acid spheres in a bed of particles flushed with water, which is analogous to dissolution from non-wetting fluid trapped in a packed bed to a flowing wetting fluid. These studies have consistently shown that the interphase mass transfer coefficient increases with velocity (e.g., the Ranz-Marshall equation). However, there is no agreement on a universal relationship as it is system dependent.

The influence of the system complexities arising from the porous structure of the medium, on particle to fluid interphase mass transfer was first examined by Pffefer & Happel [29] who focused on the influence of the void ratio of the porous media. Wilson & Geankoplis [30] showed the influence of axial mixing in packed beds on interphase mass transfer. Dwidedi & Upadhyay [6] reviewed the prior data on interphase mass transfer in packed beds and showed that it is inversely proportional to the void fraction of the medium. One of the earliest investigations focusing on NAPL contamination in porous media was conducted by van der Waarden et al. [31]. The authors showed that NAPL dissolution from

unsaturated porous media is a much more complex process than dissolution of solid particles such as benzoic acid spheres in porous media even though there are similarities between the two. The main reason for that difference is the complex mechanics of phase formation during multiphase flow in porous media, which are discussed in detail in Section 3 of this manuscript.

In natural porous medium tortuosity of the medium leads to occurrence of complex diffusion paths and moreover the complexity of multiphase flow leads to uncertainty in the distribution of flow/phases which in turn, renders the use of the physical theories (e.g., the determination of the film thickness for film theory) very difficult if not impossible. As a result the mass transfer coefficients have been usually fit to data with respect to known system properties that exist in flow in porous media (e.g., porosity, uniformity coefficient, density, average velocity etc.). The difficulty in observation of interfacial area in porous media has also led researchers to lump the k_{f1} and A into a single coefficient K_l (e.g., [32]).

Fig. 1 illustrates a typical NAPL contamination scenario. Fig. 1a schematically depicts an idealized condition where the NAPL blobs are entrapped uniformly in a uniform porous medium. The dissolved concentration with distance for two different flow velocities (low/high Peclet numbers) for this idealized case is presented in fig.1b and 1c. The dominant transport process in Fig. 1b (low Peclet number) is diffusion which results in a concentration equal to the aqueous solubility within the NAPL zone. In Fig. 3c (high Peclet number) the higher velocity means that the contact time between the flowing fluid and the NAPL is insufficient to yield concentrations equal to the solubility. As a result the effluent concentration is lower than the aqueous solubility at the end of the domain. However, the higher velocity condition leads to higher concentration gradients between the interface and bulk fluid, resulting an increase in the interphase mass transfer rate.

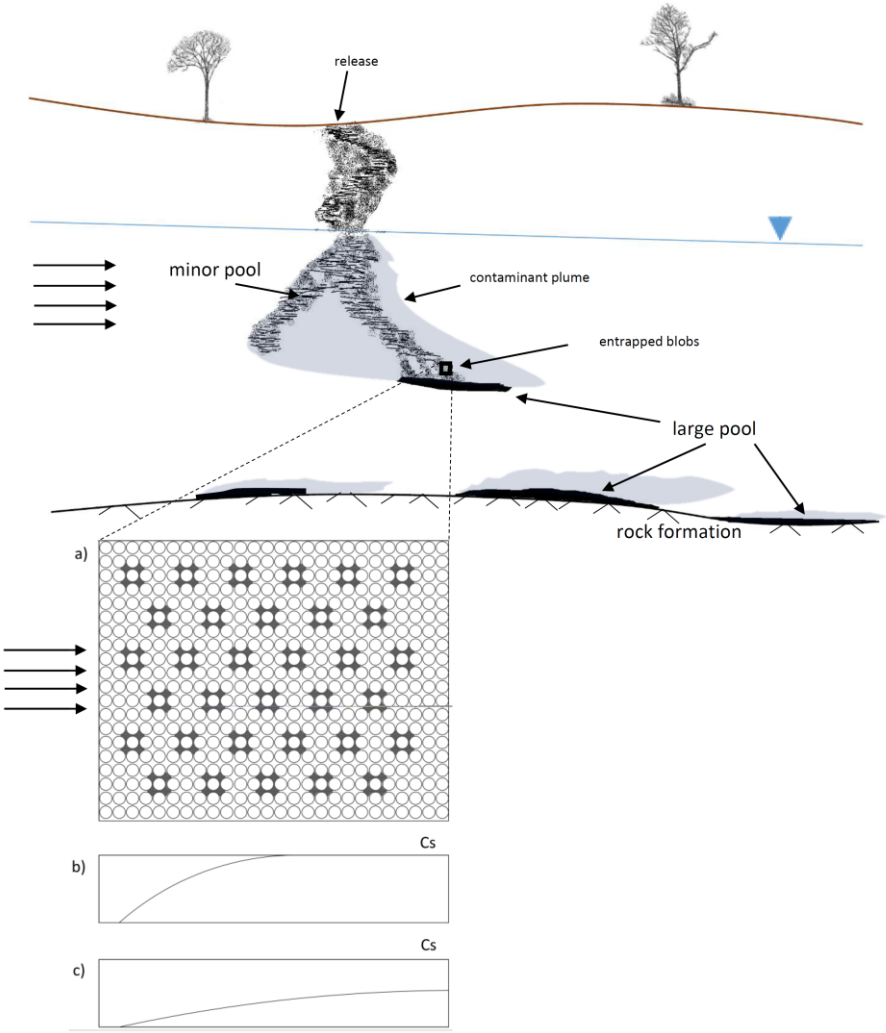

Fig. 1. Typical NAPL contamination; a)Schematic of a uniformly distributed NAPL blobs (shaded area), flow is from left to right; b) Concentration as a function of distance; for low Peclet number; c) Concentration as a function of distance; for high Peclet number.

Investigation of interphase mass transfer at different scales can be easily followed from Fig.1. The pore scale investigations focus on the discrete pore scale parameters that are presented idealistically in Fig.1a. Meso-scale investigations focus on the average dissolution behavior of some certain porous medium volume such as the whole domain presented in Fig.1a. The field scale investigations incorporate the large scale flow attributes such as permeability distribution in the field and corresponding bypass conditions.

Initial attempts to mathematically describe interphase mass transfer for NAPL dissolution in porous media were derived based on the steady state one-dimensional advection/dispersion equation coupled with a mass release term into the flowing water similar to equation 1. [8,33,34]. By further assuming that advection is the dominant solute transport process [9], the solute transport equation can be rewritten as:

$$q\frac{\partial C}{\partial x} = k_{f2}a(C_s - C) \qquad (3)$$

The above equation was first proposed to back calculate an interphase mass transfer coefficient from 1D experimental data observed at the meso-scale. Here "a" refers to the specific interfacial area

[L^2/L^3], or the interfacial area per unit porous medium whereas "A" in eq. 1 refers to the absolute interfacial area between the two phases [L^2]. In both of the approaches "C" refers to bulk concentration [M/L^3] in the aqueous phase which is a function of location x, and the interphase mass transfer is defined as first order rate limited via k_f's which are system unique interphase mass transfer coefficients and have units of [L/T]. The latter equation can be solved for "k_{f2}" analytically yielding;

$$k_{f2} = -\left(\frac{q}{La}\right)\ln\left(1 - \frac{C_{eff}}{C_s}\right) \qquad (4)$$

Here C_{eff} refers to the concentration at the downstream end of the NAPL zone (x=L). Although equation 4 has a number of simplifying assumptions, it has been used to calculate the interphase mass transfer coefficients from experimental data such as column experiments (e.g., [9,35–37]) and to develop upscaled mass transfer coefficients at the field scale [37]. On the other hand, the definition of the mass transfer given in equation 1, has rarely been used for the interpretation of experimental data (e.g., [32] with lumped approach) because it requires the estimates of the concentration distribution and interfacial areas which are generally not available. Equation 1 however can be used with data obtained from pore scale numerical models (e.g., pore network models; [38]) where the explicit concentration distribution in the domain, which can be used to determine to representative concentration, is available. Equation 4 might further suggest that k_{f2} is linear function of the velocity q; however, this is not the case because, as shown in Fig. 1b and 1c, increases in velocity may also decrease C_{eff}. The relationship between interphase mass transfer and velocity will be further discussed in section 3.

It is evident that interphase mass transfer is controlled by the thermodynamic driving force and the physics of advective and diffusive transport. The influence of the chemical properties of the existing phases (i.e., thermodynamic driving force) is further addressed below in this section where as the mechanics of phase formation and its influence on the physics is discussed under section 3.

2.1 Ionic strength and temperature

The mass transfer of organic compounds from the non-aqueous phase to the aqueous phase can be significantly reduced by the ionic strength of the aqueous solution. Setchenow [39] presented a simple equation to predict the solubility of organic compounds for different ionic strengths. This is particularly relevant to groundwater remediation activities especially since groundwater contaminated by organic compounds in the vicinity of landfills and industrial areas often has high ionic strengths. Lesage & Brown [40] showed that for certain multi-component NAPLs, the solubility of all components decreased by 2-3 folds with flushing of 1M NaCl aqueous solution. However it is also reported that salting-in effect may sometime occur for certain organic compounds ion combinations such as naphthols in sodium flouride solutions [41].

The temperature of the multiphase system can influence interphase mass transfer through different pathways. Increase in temperature will lead to increase in the solubility of organic species in aqueous solutions [42,43]. The diffusion coefficient of the organic species also increases with increasing temperature [44]. Consequently, the mass transfer coefficient of organic species from the non-aqueous phase to the aqueous phase would also increase with increasing temperature. Moreover, temperature has even further implications on mass transfer because high temperature gradients in the aqueous phase might cause convection and further mixing of the aqueous phase leading to an increase in the mass transfer rate. However this was reported to have insignificant influence within typical aquifer conditions [45]. Sorption onto the solid surface and interfacial tension between organic and aqueous phase which has direct impact on the mobilization of organic phase, are also affected by temperature change [42,46].

2.2 Multi-component NAPLs and aging

When multi-component NAPLs are present, the dissolution of individual organic compounds into the aqueous phase interfere with each other. These interactions occur both on the aqueous side and NAPL sides of the interface. The diffusion coefficient of an organic compound dissolved in the aqueous phase would depend on whether or not other compounds are also present in the aqueous solution. Pfannkuch [17] pointed out that for multi-component NAPLs, the more soluble organic compounds will impact the diffusivity of the less soluble ones and, consequently, its interphase mass transfer rate. Moreover, if the change of the composition at the interface with dissolution cannot be compensated with diffusion of the organic compounds from the bulk NAPL to the interface, the interphase mass transfer rates of each compound will change since the composition of NAPL at the interface will be different than the initial conditions [47]. Furthermore, multi-component complex NAPLs often behave as non-ideal liquids due to the non-equal attraction between different molecules and molecules of the same type. This non-ideal behavior which would lead to activity coefficients that are significantly different from unity further complicates the rate of interphase mass transfer [48,49].

Luthy et al. [50] investigated the effect of NAPL aging on interphase mass transfer and showed that a single coal tar droplet develops wrinkled, skin-like formation after as little as 3 days of direct water contact. This formation is likely to occur in case of multi-component NAPL comprising of high molecular weight organic compounds. For crude oil it was reported that these surface deformations are due to adsorption of high molecular weight polar molecules at the crude oil-water interface [51]. The interphase mass transfer rate of naphthalene from coal tar was shown to decrease after the occurrence of the skin [50].

2.3 Cosolvents and surfactants

Various chemical agents have often been considered for the enhanced recovery of NAPLs from the subsurface. The two primary recovery mechanisms are enhanced dissolution and/or mobilization of the NAPL mass. The most known agents in the literature are cosolvents and surfactants, and, to a lesser extent cyclodextrins and humic substances [52,53]. In this work we cover only the first two agents. Although both cosolvents and surfactants can enhance interphase mass transfer, the chemical processes that lead to enhancement of dissolution are different [54]. The majority of the studies cited in this section are based on batch tests and meso-scale column experiments.

Cosolvents are chemical compounds that exhibit both polar and non-polar behavior which eventually leads to increased miscibility of phases. Cosolvents can primarily partition into the aqueous phase (e.g., ethanol) or into the NAPL (e.g., methanol) and in both cases the dilute solution assumption does not hold for both of the existing phases. This partitioning influences the diffusion coefficients of each component in each phase [55] and there are few methods to predict the diffusion coefficients in ternary phase systems (e.g., [56]). The change in the diffusive flux, in turn, influences interphase mass transfer. Imhoff et al. [57] demonstrated the non-linear alteration of the mass transfer coefficients with increasing cosolvent mass fraction. The equilibrium compositions of the phases can be calculated from thermodynamic principles which are incorporated in the computer codes UNIQUAC and UNIFAC [58,59]. On the other hand, the Hand's method, which defines the phase equilibria as straight lines on a log-log plot, has been used in several multiphase multi-component models due its easier applicability [60–62]. The Hand's model input includes the constants that define the ternary phase diagram (i.e., height of the binodal curve, plait point) which can be acquired via batch experiments [63]. For multi-component NAPLs it was shown that the increase in ethanol content of the aqueous solution leads to enhanced solubility of each component but at different proportions [53]. A simple model to predict the equilibrium solubility of organic compounds in aqueous phase in the presence of cosolvents was also developed by Yalkowsky [64] whereby the enhanced solubility is proportional to the octanol-water partition coefficient of the organic compounds. In NAPL remediation the use of cosolvents also influences the interfacial tension, viscosity, density and microbial activity [65–67]. As will be discussed

in Section 3, alteration of these properties may also have a significant indirect impact on the interphase mass transfer process.

Surfactants are surface active materials that enhance the dissolution of organic compounds by encapsulating them in micelles which exhibit a polar outer and a non-polar inner surface [68,69]. Several mechanisms have been proposed to represent the miceller solubilization process such as: oil diffusion model; micelle diffusion-adsorption model; micelle disassociation-reformation model [70–72]. Unlike the log-normal dependency of solubility values of organic compounds to cosolvent amount as proposed by Yalkowsky [64], surfactant solubilization is linearly dependent on the surfactant amount. Moreover, the enhanced solubility does not exhibit any preferences between organic compounds from a multi-component NAPL whereas cosolvents dissolve the compounds with higher octanol-water partition coefficient at higher rates [53,54,71]. Similar to cosolvents the phase behavior of the multiphase system can be defined through ternary phase diagrams for surfactant solutions [73]. Surfactant micelles do not form unless a critical surfactant concentration is achieved (referred to as the critical micelle concentration, CMC). This means that the surfactant has minimal effect on the solubility below the CMC [74]. The addition of surfactant at concentrations below its CMC however yields substantial decline in interfacial tension [75].

It has also been shown that the interphase mass transfer coefficient decreases with increasing surfactant concentration above CMC [71,72,74,75]. Grimberg et al. [71] proposed that this is due to the retardation of the diffusion of solute saturated micelles from the NAPL-aqueous interface towards the bulk solution. This phenomenon was attributed to the accumulation of surfactants near the NAPL-aqueous phase interface retarding the diffusion of micelles containing organic compounds [76]. The partitioning of the surfactant micelles into NAPL has been also shown to influence the enhanced interphase mass flux [77,78]. However Lee et al. [79] proposed that the impact of partitioning into the NAPL be taken into account together with the solubilization capacity. Effect of pH and ionic strength on surfactant enhanced dissolution has also been investigated for certain surfactant, organic compound couples. For example Park [80] found that lower pH leads to higher solubilization of pentachlorophenol (PCP) due to the greater hydrophobicity of PCP, whereas increased ionic strength leads to a decrease in solubilization.

3. Mechanics of interphase mass transfer

In this section we review studies that investigated interphase mass transfer at the pore, meso and field scales. The discussion of each scale includes also the influence of different flow configurations, which were described in Table 1. Pore scale studies (e.g., micro-models, pore network models, [81,82]) have been used to understand the implications of key parameters at the meso-scale. This is because pore scale investigations enable the control of each parameter separately (e.g., individual pore throats, pore sizes, etc.). On the other hand interphase mass transfer studies at meso-scale have been used to evaluate the mass transfer at the field scale. The most common method for that has been to simulate field scale scenarios with use of REV-based numerical models where the interphase mass transfer formulations developed from meso-scale investigations are applied for each computational node (i.e., grid block) (e.g., [37,83]). Representative elementary volume (REV) is the volume over which a pore scale phenomena, in this case interphase mass transfer, is considered uniform. In practice the grid discretization of REV-based numerical models forces REV to be defined at the size of grid block. For example, it can range from a size of 1 cm^3 to model a 1 L column to a size of 10000 cm^3 to model 1000 m^3 field scale problem. Hence, an REV in one study may be even greater than the whole domain of another study. This is further elaborated in the following sections.

3.1 Pore scale

The investigation of interphase mass transfer at the pore scale requires information on the spatial distribution of the interfacial area and relevant flow paths within individual pores. Recent experimental techniques have identified three different domains of interfacial area when two phases are present in a porous domain: 1) capillary (or meniscus) area; 2) thin film area; 3) grain surface roughness area (Fig. 2) [84–86].The capillary area is the interface that forms at the meniscus of a pore whereas the film area is formed when the wetting phase covering the soil particle is surrounded by a non-wetting phase. A third domain forms, referred to as the grain surface roughness area, when the wetting phase saturation approaches zero such that the grain surfaces are covered with a very thin layer of wetting fluid that follows the roughness (troughs and ridges) present on surfaces. Interphase mass transfer can potentially occur through these domains in all of the flow configurations described in Table 1.

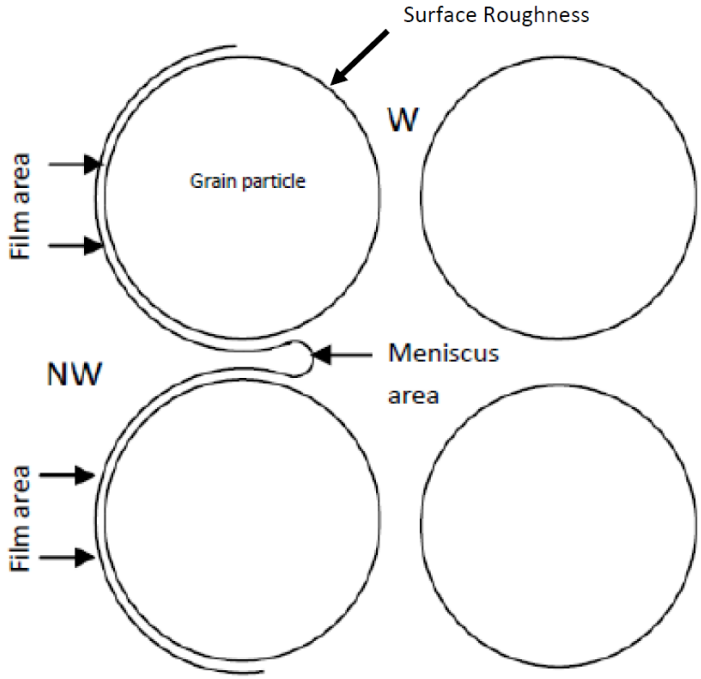

Fig. 2. Schematic of the meniscus and film area around grain particles. Electron-microscopy visualization of surface roughness can be found in [84].

Fig. 3 demonstrates the possible flow pathways that will lead to interphase mass transfer in two different cases of wettability. In the first case, where the mobile phase constitutes the wetting phase (Fig. 3a; "INtoMW"), both meniscus and film areas can contribute to interphase mass transfer. The impact of film interfacial area on total interphase mass transfer is proportional to the flow rate through the corner which is a function of the 4^{th} power of the corner equivalent radius (Poisuielle's flow). The reduction of the non-wetting blob via dissolution induces shrinking. As dissolution continues, the length of the corner diminishes. However, the equivalent radius of the corner is not significantly influenced by this shrinking because the non-wetting phase approaches a more stable spherical shape with on-going dissolution. Once the blob takes the shape of a sphere, further dissolution leads to the reduction of the equivalent radius of the corner (position 5 in Fig. 3a). This means that the flow velocity will increase in the film layer only after the blob takes a spherical shape and decreases in radius. To date there is no experimental study that has presented the flow velocities occurring through film layers due to experimental difficulties at this small scale. Even though Poisuielle's equation can provide an estimate of the flow velocity, the influence of surface roughness of grains on the flow cannot be accurately determined.

Fig. 3b depicts the case when the mobile phase constitutes the non-wetting phase (i.e., "IWtoMN"). Under these conditions, most of the interphase mass transfer occurs from the film area. As the mobile phase transports the dissolved solutes from the interfacial film area, this film area is depleted and the wetting phase residing in the meniscus region spreads itself to the film area. This leads eventually to the withdrawal of the meniscus (from position 3 to 1 in Fig. 3b) until the pressure of the mobile non-wetting phase overcomes the capillary pressure and breaks the wetting phase. At this instant the equivalent radius of the pore throat center (where the mobile phase starts to flow through) increases significantly because the wetting phase spreads itself over the grain surface to form a more thermodynamically suitable shape. The formations represented in Fig. 3 have been shown qualitatively in micro-model experiments conducted by Sahloul et. al. [81]. Zhao & Ioannidis [87] used pore network modeling to demonstrate that the continuity of the NAPL film, which is a function of the wettability of the medium, is the most influential factor on the interphase mass transfer rate for NAPL wet-media.

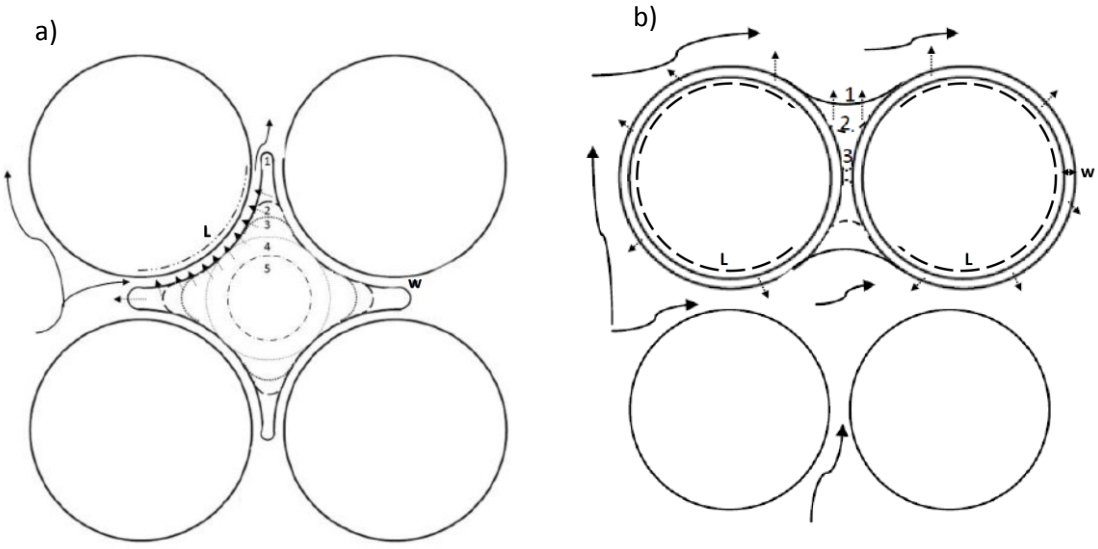

Fig. 3. Shrinking of a non-wetting blob (a) and wetting blob (b) via dissolution. Numbers represent the progression of dissolution in time. L and w are the film length and width respectively [81,88].

The benefit of defining the flow configurations as in Table 1 is clearly observed in the discussion presented above along with Fig. 3. For example in "IWtoMN" (i.e., Fig. 3b) the dominant interfacial domain in terms of interphase mass transfer is the film area in contact with mobile water regions whereas for "INtoMW" (i.e., Fig. 3a) mass transfer is mostly through the meniscus area as the flow rate in the film region is very low and therefore the contribution of these regions to interphase mass transfer is limited although some studies suggest that the film area may also contribute to the interphase mass transfer especially at high pressure gradients ([82,89]). It should be noted to date there is no quantitative data on the thickness of film layer presented in Fig. 3a for real porous media which is the parameter governing the flow rate within this film layer. However, x-ray microtomography images taken by Schnaar & Brusseau [36] showed that the film thickness appearing in "INtoMW" (i.e., Fig. 3a) is extremely small. Furthermore the curvature and surface roughness of the grain particles may even further impede the flow within the film layer. In accordance with these observations, Bradford et al. [88] experimentally showed that the interphase mass transfer in NAPL-wet media is much greater than the water-wet media providing further evidence that the flow configurations depicted in Fig. 3 can be useful in identifying which components of the interfacial areas contribute the most to the interfacial mass transfer

"MNtoIW" can be visualized from Fig. 3b if dissolution occurred from mobile phase to immobile wetting phase. "MNtoIW"" appears in high pressure CO_2 injection (i.e., supercritical phase)

applications [90,91]. “MWtoIN” can be observed also from Fig. 3a if the dissolution were to occur from the mobile phase to the immobile non-wetting blob. “MWtoIN” is investigated within gas exsolution applications where for example; the injected wetting phase (water) is super saturated with CO_2, leading to the expansion of the non-wetting CO_2 gas bubble (blob) with dissolution from the water phase to the gas phase [92,93]. In both of these applications mobile phase is the dissolving one. The implication of this condition is that now the velocity of the mobile phase is responsible for the magnitude of interphase mass transfer as it supplies the dissolving compounds to the interface. This is different than the first two configurations (“INtoMW” and “IWtoMN”) where the velocity of the solvent phase is responsible for the magnitude of interphase mass transfer. This is the reason why both “MNtoIW” and “MWtoIN” are categorized as new flow configurations even though they have the same influential interfacial domains with “INtoMW” and “IWtoMN” respectively. It must be noted that both “MNtoIW” and “MWtoIN” have not been studied in detail in terms of dissolution in porous media as these subjects are relatively new in the field. “CHEM” is observed in enhanced NAPL remediation/oil recovery applications and depending on the wettability of the system either Fig. 3a or Fig. 3b will appear. However at very high amounts of chemical agents the phases become fully miscible in both conditions.

In two-phase flow both components dissolve to some extent into the counter phases. However in most real applications one of the components is generally of significance and therefore the dissolution of the other component is ignored if it does not have significant impact on system behavior (e.g., the resistance of dissolving solutes in the dissolving phase is negligible due to very low amount of mutual dissolution; dilute solution). For example in NAPL remediation investigations, the dissolution of water molecules into NAPL is ignored in experimental studies as well as in numerical studies (e.g., pore network models, single phase REV models, semi-multiphase REV models) as it does not influence fate of organic compounds in the system. However, especially in enhanced NAPL remediation applications, even though the fate of a certain compound is sought (i.e., fate of organic compound), interphase mass transfer of all components into both phases should be considered as the composition of both phases may significantly change the system behavior in some instances [21,59,62].

3.2 Meso scale

Most of the data and observations on interphase mass transfer in porous media are derived from the column or tank experiments. The complexity of flow in porous media prevents the use of physical models such as film layer or boundary layer theory and as a result many of the experimental and numerical investigations developed correlations between interphase mass transfer coefficients and system parameters. The information gathered at this scale has been used in numerical models defined in terms of Representative Elementary Volumes (REV). Earlier investigations were based on derivation of interphase mass transfer coefficients from column and tank experiments with use of eq. 4 or similar approaches (e.g., [8,9,34,94]). As noted in Section 2, the unavailability of the interfacial area was compensated by lumping the area term into the mass transfer rate coefficient, K_l. Recent advances in non-invasive imaging technologies have in some instances led to relaxation of this assumption, enabling the direct use of eq. 4 (e.g., [36]). In addition investigations based on pore network models also permit the use of eq. 1 because these models can provide the concentration distribution within the porous media domain (e.g., [38]).

After the mass transfer coefficient is determined from experimental data, a Sherwood number ($Sh = {k_f d_m}/{D}$) is defined and correlated against the system properties such as porosity, velocity, and uniformity coefficient. The modified Sherwood number ($Sh' = {K_l {d_m}^2}/{D}$) has been used in cases when accurate estimates of the interfacial area are not available. Below are two examples of these Sherwood formulations developed by Pfannkuch [17] (eq. 5) and Nambi & Powers [35] (eq. 6).

$$Sh = 0.55 + 0.025Pe^{1.5} \qquad (5)$$

$$Sh' = 37.2{S_n}^{1.24}Re^{0.61} \qquad (6)$$

Pfannkuch developed the above Sherwood formulation (eq. 5) from the results of column experiments conducted by Hoffmann [95] and by using the Bowman's equation as a base. Hoffmann's experimental set up consists of a stagnant oil phase located in the upper half of a horizontal column filled with glass beads with water flowing horizontally along the flat contact area. Pfannkuch developed the Sherwood formulation of each experiment having different velocity with use of the equation; $Sh = \frac{E\, d_m}{C_s\, D}$. As E refers to interphase mass transfer rate divided by the interfacial area, (which is rather clearly defined in [95]), k_f is calculated, also by ignoring the concentration of solute in the column along the oil-water contact area due to lack of direct measurements, with; $k_f = \frac{\frac{\partial M}{\partial t}\frac{1}{A}}{C_s}$ (i.e., use of eq. 1 assuming *C*=0). Furthermore, in the original German text Hoffmann states that the solubility of domestic fuel oil in his experiments (i.e., Heiz Öl) is between 10^3 and 10^5 mg/m^3 and Pfannkuch assumed this value in his calculation to be 10^4 mg/m^3 which is another source of uncertainty to the calculated mass transfer coefficient. Nonetheless, the main advantage of this set up was that it allowed for the estimation of the oil-water contact area, whereas in other situations the interfacial area would be a complex function of fluid and porous media properties that is difficult to measure or estimate accurately. This feature of the Pfannkuch's Sherwood expression led to its use in several subsequent studies [96–98]. It is important to note that in real systems the complex NAPL distribution and complex flow fields may actually lead to different concentration profiles than those proposed for these idealized conditions. The influence of these factors on interphase mass transfer coefficient is discussed in Section 3.4.

The modified Sherwood formulation of Nambi & Powers [35] (eq. 6) was developed from the results of small 2D experiments using eq. 4, where the interphase mass transfer coefficient is lumped with interfacial area (i.e., mass transfer rate coefficient), and multiple regression analysis was used [9,35]. A number of studies have developed similar Sherwood formulations (e.g., [8,32,99–101]) from meso-scale experiments whereby the NAPL was mostly in the form of distributed blobs while Nambi and Powers [35] is the only study that was based on pool NAPL configuration. In recent years, several studies have also shown that the use of the modified Sherwood formulations may lead to contradicting results when used in numerical models even though they have the same input parameters [82,83,89,98,102–108]. This is mostly attributed to differences in the specific experimental conditions used in developing these models. The Sherwood formulations which consider interfacial area (e.g., Pfannkuch [17] eq. 5), are also subject to this consideration. For example Pfannkuch developed one other Sherwood formulation from the results of the experiments of Zilliox [109] which had median grain size of 2000 micrometer, compared to 500 micrometer for the Hofmann data. The calculated Sherwood numbers were found to be about 10 to 100 times greater than the Sherwood numbers calculated from Hoffmann's experiments for the same Peclet numbers. Moreover these Sherwood formulations (both $Sh'$and Sh; e.g., [8,17,105,110]) have been mostly developed from the results of column experiments. In many instances these formulations are used in numerical models with node (REV) sizes that are significantly different from the experimental scale that they have been developed which may also lead to erroneous results. This is a result of the fact that the parameters used to calculate mass transfer coefficients via eq. 1 and 4 change at different orders when system size changes. For example; a large grid block having a uniform NAPL blob distribution would lead to near equilibrium conditions even for high velocities whereas a small grid having the same type of NAPL distribution and flow velocity would result in rate limited behavior. If one chooses a Sherwood formulation developed from an experiment with similar size and conditions to the small grid block described above and uses it in a numerical model with larger grid sizes, this may result in under-estimation of interphase mass transfer. Furthermore, because the variability at the sub grid scale cannot be accounted for, the larger grid size would also result in a higher level of approximation. Because most of the Sherwood formulations are derived from column experiments with uniform NAPL blob distributions accurate REV based numerical simulations requires the compatibility with this condition in the grids that contain NAPL. If this condition is not met corresponding interfacial area and

flow paths will cause different results than the predicted one. Consequently, the adoption of Sherwood formulations to real applications should be done with caution.

3.3 Field Scale

The salient difference observed at the field scale compared to meso-scale experiments is the complexity of the NAPL spatial distribution and the groundwater flow field. In the subsurface NAPLs can be retained as either residual, pool or both. For NAPL-water system residual saturation of NAPL refers to the case where NAPL cannot further decrease in saturation with applied hydraulic pressure (e.g., [111]) and exist in the form of single or multi-pore blobs. In pool configuration the saturation is greater than the residual yet hydraulic pressure is not enough to initiate mobilization. Such configuration is especially observed when DNAPL accumulates over impermeable media after downward leakage or when LNAPL is formed over the water table. As in other subsurface applications (e.g., groundwater extraction) the most important factor that controls interphase mass transfer at the field scale is the permeability spatial distribution at the site [83]. It has been reported that poorly accessible NAPL mass is the primary reason for the long term mass fluxes observed at field [112].

Many studies have reported that the interphase mass flux from residual NAPLs is significantly higher than pool NAPLs (e.g., [113,114]). Anderson et al. [115] showed that flow through a residual DNAPL zone leads to equilibrium concentrations which decrease with reduction in NAPL saturation. In residual NAPL regions, the interphase mass transfer rate can also decrease due to dissolution fingering. Imhoff & Miller [116] reported that the non-uniform distribution of residual NAPL leading to variation in flow velocity between pores is the primary reason for this phenomenon. On the other hand it has been also shown that such fingers are limited in length due to transverse dispersion [117–119].

For pool NAPL configurations Brusseau et al. [120] demonstrated that dilution via clean water bypassing NAPL contaminated regions is a major reason for the reduced effluent concentrations. Spatial variability in intrinsic permeability is the primary reason for the flow diversion and dilution. Variations in the relative permeability of aqueous phase in the NAPL contaminated area can also cause flow diversion and low effluent concentrations. Nambi & Powers [121] showed that in case of pooled NAPL in a heterogeneous media water flow lines are diverged around the surface of the contaminated region, initially inducing slower interphase mass transfer rates. At later stages when the water starts to penetrate into the contaminated area due to increase in aqueous phase relative permeability the mass transfer rate increased substantially. Similar results were reported by Marble et al. [107] and Zhang et al. [122]. Page et al. [123] also showed that the reduction of effluent concentrations due to increased velocity is not significant compared to bypassing of NAPL. Brusseau et al. [112] reported that NAPL existing in poorly accessible porous media (i.e., lower hydraulic conductivity regions) regardless of being pool or residual leads to low effluent concentrations and long term mass fluxes. These observations were mostly obtained from tank experiments with localized NAPL pools and are discussed here because of the similarity of the initial localized NAPL configurations used in these studies with those typically observed in field applications. It is important to note that the method used for emplacing the entrapped NAPL within the porous medium is also of particular importance [9,32]. Mixing the sand with the contaminant phase which has been performed in a number of studies (such as [8,120,124]), rather than injecting the NAPL, might result in different dissolution patterns.

Estimates of interphase mass transfer at the field scale have been mostly obtained from modeling studies (e.g., [37]). As also observed in large scale tank experiments, these numerical models have shown that flow bypassing due to permeability and relative permeability differences is the major reason for low effluent concentrations. Using an REV-based numerical model for a domain size of 10 m x 10 m x 10 m Parker & Park [37] showed that the interphase mass transfer rate coefficients determined from field-scale applications (i.e., up-scaled mass transfer rate coefficients) tend to be much lower than those derived from meso-scale experiments. The difference is attributed mostly to the higher degree of bypassing of the NAPL zone at the field scale compared to meso-scale. The authors

also reported that reducing the domain size led to slight increase in the calculated interphase mass transfer coefficients.

Groundwater flow velocity is another factor influencing interphase mass transfer; however this dependency differs from the one observed at the meso-scale. Parker & Park [37] stated that the mass transfer coefficient of their field scale simulation is a function of velocity with a power of 1 whereas meso- scale studies reported a power of ~0.7 (e.g., [8,9]). These differences further shows that the formulations of interphase mass transfer coefficients are dependent on the system conditions (e.g., permeability distributions, saturation, etc.) that they are developed from.

The complex features of the field scale NAPL distributions are also influential on the field scale dissolution behavior. Zhu et al. [125] stated that early high concentrations are related to dissolution of residual NAPLs as they enable contact with the flow through the NAPL region. Following a steep decrease in effluent concentrations, once residual NAPLs are depleted, a period of low effluent concentrations initiates. The invalidity of interphase mass transfer expressions derived from meso-scale studies to field applications led some researches to develop analytical interphase mass transfer formulations that are specific for field scale NAPL dissolution problems (e.g., [11,37,125]). For example Christ et al. [11] proposed that ganglia NAPL mass to pool NAPL mass ratio can be used to predict effluent concentrations in field. The authors used the results of a field scale numerical model, whose three dimensional domain was 8 m x 8 m x 9 m, to develop such an analytical formulation. These formulations are discussed under section 4.

Because these analytical formulations are determined from the results of numerical models, their validity is directly related to the accuracy of the numerical simulations. A particularly relevant study is that of Maji & Sudicky [83] who simulated a field scale NAPL dissolution problem (domain size of 10 m x 16 m x 6.7 m with a grid block size of 0.25 m x 0.50 m x 0.10 m) with 10 different mass transfer formulations. It was demonstrated that the time needed for full depletion of NAPL mass varied from 562 days (local equilibrium approach) to 48085 days (formulation of Saba & Illangaskare [105]) between different mass transfer formulations. On the contrary park and Parker & Park [37] compared the depletion time of full NAPL mass for two formulations (local equilibrium and model of Miller et al. [8]) and stated that the difference is not significant and local equilibrium approach might be usable. In a related issue Nambi & Powers [35,121] showed that saturation above 35% would lead to local equilibrium conditions for their meso-scale NAPL dissolution experiments meaning that use of local equilibrium in a grid block of an REV based numerical model might be a viable option in such cases. Yet this threshold saturation value that results in equilibrium conditions in a grid block is variable for different sizes of grid blocks and different types of porous media and NAPL distribution topologies. Decreasing the grid block size would decrease this threshold provided the grid block size does not decrease below possible minimum REV size value. Yet no data were reported on the dependence of this threshold saturation on grid block sizes for different velocities, and porous medium properties. The accuracy of numerical models with different mass transfer formulations may be checked against small 3D dissolution experiments. However it should also be noted that discrepancies between observed and simulated NAPL dissolution is likely to increase at the field compared to smaller 3D laboratory experiments due to use of the larger grid block sizes and greater NAPL amount at the field.

In field applications many contaminated sites are decades old and therefore it is likely that the residual NAPL residing in accessible media is already depleted. Therefore, assuming that NAPL containing REV's are at pool conditions and they can be represented with local equilibrium assumption, seems to be in some instances viable. But the influence of dissolution once the saturation decreases below threshold NAPL saturation is subject to discussion. As the influence of residual NAPL in accessible media can be neglected and fast dissolution can be assumed it is also likely that in poorly accessible media the residual NAPL will lead to slow dissolution and tailing of effluent concentrations. The difference in dissolution behavior of residual NAPL in high and low hydraulic conductivity media is further discussed

under section 3.4.5. Finally it should be emphasized again that field scale NAPL dissolution, like other real subsurface applications, is strongly controlled by the permeability differences in subsurface and correct description of field characteristics is essential for any prediction effort.

Apart from the above discussion which pertains to “INtoMW", the use of surfactants and cosolvents or their mixtures for enhanced remediation purposes (i.e., “CHEM”) can drastically alter the original multiphase flow conditions at field scale. Application of cosolvents/surfactants may culminate into increased miscibility whereby the dilute solution assumption is not valid anymore [62]. The density alteration of the existing phases may lead to flow stratification which can lead to bypassing and reduced overall mass transfer [126,127]. The alteration of viscosity might also induce development of fingers and influence system stability which can also lead to bypassing [128–130]. Reduction of interfacial tension may also influence the system mobility which, as reported by Agaoglu et al. [53], can significantly impact interphase mass transfer rate. Zhong et al. [131] observed the occurrence of dissolution fingering during surfactant flushing. The authors also showed that once a finger reaches the effluent end, a substantial decrease of the interphase mass transfer develops, implying significant bypassing of NAPL by surfactant solution. This can significantly influence the performance of field scale enhanced remediation activities.

“IWtoMN” is encountered in the field as NAPL dissolution in NAPL-wet media or air sparging applications. In comparison to former, air sparging shows very unstable flow conditions due to high viscosity difference between the two phases. The injected air was shown to follow three different flow patterns namely; bubble flow, channel flow and chamber flow. In a tank of uniformly packed glass beads Brooks et al. [132] demonstrated that channel flow occurs within glass beads smaller than or equal to 1-2 mm size whereas bigger glass beads lead to bubble flow (e.g., flow of discrete bubbles). Peterson et al. [133] pointed to chamber flow which can be identified by a significant horizontal component in case of a porous media of very fine to fine sand (d_{50}<0.21 mm). Selker et al. [134] showed that a near injection region is formed after the injection of air where viscous forces dominate the buoyancy forces and lead to lateral expansion of the gas channels. Beyond this region, the injected air starts to move in a parabolic pathway upwards. The authors also observed direct vertical or near vertical movement of air bubbles in coarser sand and for typical injection pressures. The above literature focusing on the flow paths occuring in air sparging is retrieved from air-water system without NAPL existence in the medium. Heron et al. [135] showed that air sparging is not effective for pooled DNAPLs since both DNAPL pools and the air injection point typically reside at the bottom of the aquifer and horizontal movement of air channels is limited. Berkey et al. [136] reported substantial short circuiting of air channels in fine sand (silty sand). Thomson et al. [137] and Waduga et al. [138] reported that the prediction of accurate recovery rates necessitates the accurate topology of the air channels and NAPL. The reasons of unstable movement of air is discussed in more detail in section 3.4.3. A part from that air sparging can lead to decrease in relative permeability of the groundwater at the injection region in case of a moving contaminant plume [139]. The system under consideration in the above cited works relating to NAPL recovery was entrapped NAPL (in form of pools and entrapped blobs) in saturated porous medium meaning that the interphase mass transfer occurred from both air-water and air-NAPL interface.

Steam injection is another groundwater remediation application that falls under “IWtoMN”. Steam injection was first proposed by Hunt et al. [140] whereby the NAPL is vaporized during the flow of steam in the aquifer. Once the steam front reaches the NAPL zone, it instigates interphase mass transfer from the NAPL to the steam. Reverse mass transfer can occur in the form of re-condensation and accumulation of the vaporized NAPL at the steam front due to heat loss [141–143]. Several factors have been shown to impact NAPL mass transfer and recovery including, the presence of air with the steam [112], injection pressure [113] and field conditions such as soil type and well distance [144–146].

3.4 Factors influencing interphase mass transfer

The preceding section highlighted some of the main features of interphase mass transfer at the pore, meso and field scales. In this section, we review and discuss the influence of individual parameters on interphase mass transfer. The information presented here is mostly inferred from controlled pore and meso-scale experiments.

3.4.1 Interfacial area

Interfacial area is one of the most influential parameter on interphase mass transfer. As depicted in Fig. 1, there are three different domains that contribute to interphase mass transfer, namely: 1)capillary (or meniscus) area, 2)thin film area, 3)grain surface roughness area. Because the grain surface roughness area occurs when saturation of wetting phase approaches zero, it is relevant to the flow configuration "IWtoMN". The meniscus and thin film area dominate the flow configuration "INtoMW".

A substantial body of literature investigated the interfacial areas in two phase flow in porous media. The mostly used techniques to determine the interfacial domains have been interfacial tracers and non-invasive imaging technologies [84–86]. Because of the resolution limits of the latter which is on the order micrometers, the third domain (grain surface roughness), which is on the order of nanoscales, has only been studied with interfacial tracers [147,148]. Non-invasive technologies such as X-ray microtomography have been shown to be capable of distinguishing between the meniscus and film areas where as interfacial tracers provide a measure of the overall interfacial area. In addition it has been also demonstrated that the gaseous phase interfacial tracers have more accessibility to the interfaces that occur in porous media compared to aqueous tracers [85,149].

The interfacial area between water and air has been reported to increase with decreasing saturation of the wetting phase (aqueous phase) [150,151] and decreasing mean grain diameter [147,152]. The change of interfacial area was also shown to be greater for poorly sorted media [148]. It has been found that the data inferred from synchrotron x-ray micro-tomography exhibits a negative linear relationship between water saturation and interfacial area whereas interfacial tracer tests indicates a negative exponential relationship especially when the water saturation approaches zero. This was attributed to the inability of micro-tomography to measure the very thin layer of water forming on the surface roughness of grain particles [153,154]. Distinction between meniscus and thin film area made by non-invasive methods demonstrated that meniscus area diminishes to zero when wetting saturation decreases to a certain saturation depending on the type of porous medium [111,153]. Generic relationships between the interfacial area of different domains as a function of wetting phase saturation (during the first drainage) are presented in Fig. 4.

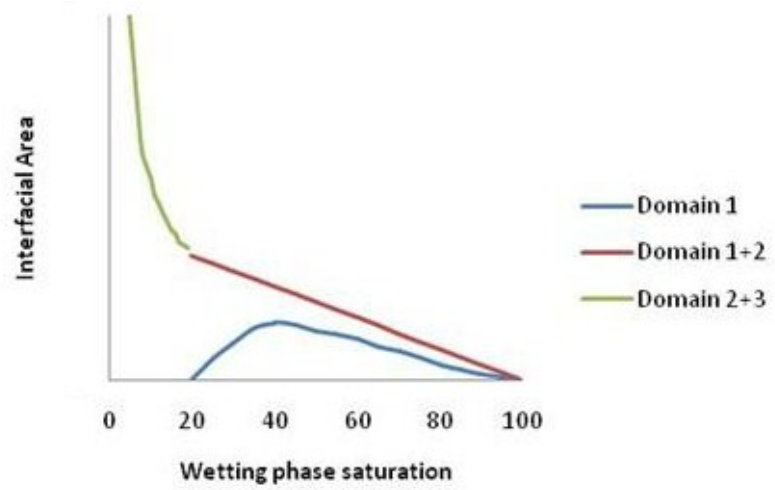

Fig. 4. Variation of different domains of the interfacial area with wetting phase saturation.

The interfacial area between air and water was also found to be influenced by the existence of surfactant molecules when present in the aqueous phase. It has been demonstrated that increase in surfactants content alter the interfacial tension between air and water which eventually affects the saturation profile of the system in a non-linear manner [154]. Interfacial area was also investigated in fractured media however it was reported that in fractured media there is no correlation between interfacial area, saturation and aperture/aperture ratio [155].

The evolution of interfacial area during the dissolution of residual NAPL was first demonstrated via MRI for a column filled with glass beads. It was shown that interfacial area decreases linearly with saturation along dissolution [156,157]. This was also shown to be the case for real porous media [36]. It also argued that the meniscus interfacial area is the principal domain for interphase mass transfer. However the ratio of meniscus interfacial area to film area (domain 1 to domain 2) increased as dissolution proceeded, reaching 50% once 95% of the NAPL is dissolved. The authors attributed this increase to conversion of film area to meniscus area as the dissolution shrinks the NAPL blobs. This is also depicted in Fig. 3a which shows that the ratio of the meniscus area increasing from position 1 to position 5.

Several studies attempted to develop functional relationships for the prediction of interfacial area for air-water system. Peng & Brusseau [148] used a Van Genuchten type equation to predict the total interfacial area (domain 1,2 and 3) normalized by the total porous medium volume:

$$A_{ia} = s\left[1 + \left(\alpha(S_w - S_m)\right)^n\right]^{-m} \qquad (7)$$

The authors found good agreement between the developed relationship and experimental data from a single study. Costanza-Robinson et al. [86] developed another functional relationship which focused on the prediction of interfacial area of domains 1 and 2 excluding domain 3. The authors reported that when the air-water interfacial area in a particular porous media is normalized by the geometric surface area of that medium, the relation between this normalized interfacial area and water saturation is independent of porous medium type:

$$A_{ia}(cm^{-1}) = SA[(-0.9112)S_w + 0.9031] \qquad (8)$$

Consequently, the developed relationship can be used to determine the air-water interfacial area if the water saturation of a sample and the mean grain diameter of the medium (to be used in the determination of the geometric surface area, *SA*) are known. It was reported that this predictive method resulted in good agreement for experiments conducted with glass bead media whereas for natural media some inconsistencies emerged.

Thermodynamics has been also used to investigate the interfacial area in porous media [158]. Morrow [159] presented a method for the estimation of interfacial areas through thermodynamic-based approach which can also be found in Bradford & Leij [160]. This method relates the external work applied on a closed system of porous medium comprising of two phases (which constitutes the area under Pc-Sw) to the existing interfacial area through a constant of integration (C_{NW}) which refers to the influence of existing NAPL blobs. C_{NW} is zero for the first drainage/imbibitions and nonzero after the formation of first residual saturation:

$$\Phi_{NW}(S_W^{NW}) + C_{NW} = \sigma_{NW} cos(\phi_{sNW}) A_{sN}^*(S_W^{NW}) + \sigma_{NW} A_{NW}^*(S_W^{NW}) \qquad (9)$$

Dalla et al. [161] adopted the pore scale model of Hilpert & Miller [162], where the domain comprised of spherical particles, to investigate the development of interfacial area and to compare the results against the thermodynamics-based predicted interfacial area developed by Bradford & Leij [160] and

interfacial area measured by Kim et al. [150] using aqueous tracer tests. The authors showed that the thermodynamics approach of Bradford & Leij [160] predicted larger interfacial area compared to the area attained through their pore network model and aqueous tracer tests conducted by Kim et al. [150]. The dissipation of the mechanical work applied to the system (i.e., conversion of only a portion of the mechanical energy into surface energy) which is not accounted for in Bradford's method [160], is stated to be the main reason for the higher interfacial area calculated by this method. Another reason for the low interfacial areas determined by the aqueous interfacial tracer test compared to results of Bradford & Leij [160] is reported to be the partial measuring of the interfacial areas by aqueous tracers because of the non-continuity of the aqueous phase especially at reduced water saturations. Dobson et al. [163] showed that the Bradford & Leij [160] method culminates into the prediction of lower interfacial areas compared to experimental ones measured by the aqueous tracer test on a NAPL–water system whereby the NAPL saturation was residual. It must be noted that in Dobson et al. [163] the aqueous phase was continuous, meaning that all interfacial areas are measured with aqueous interfacial tracers and therefore the method of Bradford & Leij [160] is expected to better fit the measured data. However the method of Bradford, along with a similar method developed by Oostrom et al. [164] produced smaller values compared to the measured ones which lead the authors to develop a modified version of this method that considers the area under the drainage curve minus the area under the imbibition curve. The authors found good agreement between the predicted and the measured interfacial areas for different type of porous medium having different median grain size.

Another predictive method derived from thermodynamics principles was developed by Grant & Gerhard [165] whereby the focus was on the meniscus interfacial area considering energy dissipation. Similar to the modified version of the Bradford method which is presented in Dobson et al. [163], this method also considers the areas under both the drainage and imbibitions curves. However, this method enables the prediction of the interfacial area along the saturation curve contrary to the Dobson et al. [163] who investigated only the residual saturation. Moreover, the Grant's method [165] accounts for the effect of hysteresis in the P_c – S relationship and therefore enables the prediction of interfacial area at subsequent drainages and imbibitions:

$$\alpha^{wn}\left(S_W^i\right) = \Psi\left(S_w^i\right).E_d.\phi.\frac{[\Phi_{NW}(S_W)]^{D,I,D^*}}{\sigma_{NW}} \qquad (10)$$

The authors also made the assumption that capillary (meniscus) interfacial area decreases linearly with reduction of non-wetting phase saturation induced by dissolution. This was tested in a semi-multiphase flow model in a companion paper [96]. It is interesting to note that the authors made the correct assumption independently of the study of Schnaar & Brusseau [36] who had presented the linear relationship between capillary (meniscus) interfacial area and saturation induced by dissolution via micro-tomography. Since thermodynamics approaches give information about the total interfacial area (e.i. domain 1 and 2) the authors used an equation, which is extracted from the results of the pore scale model of Dalla et al. [161], that gives the ratio of capillary (meniscus) interfacial area (referred to in this paper as specific interfacial area) to total interfacial area at different water saturations. However the influence of hysteresis on this ratio is not considered in this equation. The authors set the energy dissipation parameter (E_d) to 0.21 after testing it against the interfacial area measured by Brusseau et al. [166]. It is noteworthy that the single equation representing the ratio of capillary interfacial area to total interfacial area and single valued energy dissipation chosen by the authors (i.e., E_d=0.21) may be system dependent; further experimentation would be required to establish its general validity. The assumption that the dissolution occurs only through the capillary interfacial area is also subject to discussion which will be considered further in this review under the pore network modelling section.

Occurrence of interfaces in porous media between three fluid phases is an even more complex process involving spreading coefficients [167]. Consequently, there are only a handful of studies which attempted to investigate this problem, mostly through micro-models (e.g., [167,168]). Schaefer et al.

[151] measured the interfacial area between water and oil using interfacial tracers for a porous medium containing the three phases water, air and oil. The authors reported that the interfacial area between water and oil increased linearly with decreasing water saturation yet the measured values were half of the values that were measured for the two phase experiment (water – oil) at the same conditions. This result appears to contradict findings of earlier micro-model work [167,168].

3.4.2 Hysteresis

NAPL spatial distribution in the subsurface and, consequently the resulting interfacial area and flow paths have major implications on the interphase mass transfer as discussed above. The distribution of NAPL mass is typically represented in terms of constitutive relationships which express the capillary pressure and relative permeability of the phases in terms of fluid saturations. A complication that appears in porous media relating to these relationships is hysteresis. P_c-S relationship of the initial drainage was shown to be different than the following imbibition, as also subsequent drainages and imbibitions were shown to be distinct. This hysteric behavior is argued to be a result of lumping of too many system parameters [169]. Using micro tomography Cullingan et al. [111] also showed that the saturation – interfacial area (S-A_i) relationship exhibits hysteric behavior. As accurate interphase mass transfer predictions require accurate determination of NAPL spatial distribution and interfacial area, the hysteresis should also be adequately accounted for. Starting from thermodynamics principles and taking into account the forces acting on fluid interfaces, Hassanizadeh & Gray [169] proposed that the incorporation of interfacial areas in P_c-S relationship would likely reduce hysteresis. Early investigations of this hypothesis were based on pore network models due to the difficulty arising in experimental observation of the interfacial areas. Reeves & Celia [170] demonstrated that the hysteric behavior can be discarded when the P_c-S relation is extended to include the A_i existing between two phases and that the P_c-S-A_i surface is unique for a particular fluid/fluid/medium system. It should be noted that the pore network model did not include snap off mechanisms. Held & Celia [171] expanded this model to embody several snap off mechanisms providing further data supporting the hypothesis of Hassanizadeh & Gray [169]. Another pore network model which confers further evidence in support of this hypothesis was developed by Joekar-Niasar et al. [172]. The authors showed that the trapping assumptions incorporated in the pore network models significantly influence the P_c-S-A_i relationship. Moreover it was reported that the structure of the pore network is also influential on this relationship such that one of the pore network models used in that study (namely, the tube model) could not reproduce hysteresis in the P_c-S curve during imbibition. The first experimental confirmation of dependence of interfacial area on the P_c-S curve with use of micro model was presented by Cheng et al. [173] who showed that the P_c-S-A_i surface is unique. Chen et al. [174] presented further evidence that the P_c-S-A_i relationship is a unique surface and independent of whether it is acquired through imbibition or drainage scanning curves. In these pore network studies and micro model experiments the determined interfacial area comprises only of the capillary (meniscus) interfacial area (domain 1) excluding the film area (domain 2). The inclusion of film area leads to linear dependence of interfacial area on saturation which prevents the generation of a unique P_c-S-A_i surface as was the case observed in Chen et al. [175] who determined the interfacial area with interfacial tracer tests which give information about the two interfacial domains (1 and 2) jointly. Joekar-Niasar et al. [176] developed an unstructured pore network model that resembles the topology of the micromodel used by Cheng et al. [173] to simulate their experiments. In addition to good agreement between the P_c-S-A_i surface attained from pore network model and from experiments, the authors also showed that the obtained surfaces were independent of whether they are obtained from drainage or imbibitions curves as has been demonstrated earlier by Chen et al. [174].

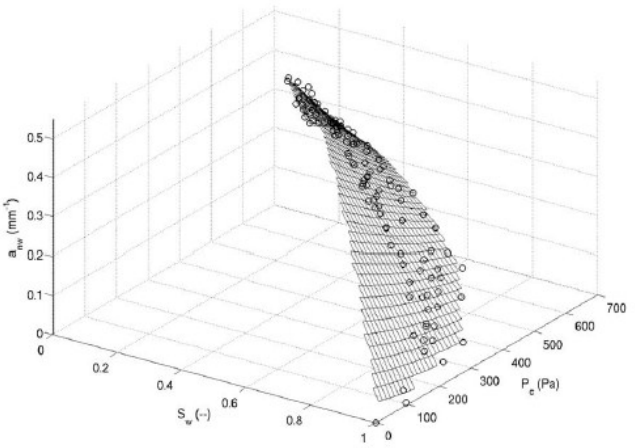

Fig. 5. P_c-S-A_i relationship obtained from LB model; from [177].

Porter et al. [177] confirmed the hypothesis put forward by Hassanizadeh & Gray [169] using the Lattice Boltzmann (LB) method for multiphase flow (Shan and Chen type) within a glass bead domain that simulates the experiments conducted by Culigan et al. [111] (Fig. 4). The relatively minor discrepancy between the interfacial areas determined via the LB method and Culligan et al.'s experiment was attributed to the unphysical spreading of the wetting phase during imbibition leading to increased film flow within the LB method. Porter et al. [178] demonstrated the unique surface of P_c-S-A_i with micro-tomography and also showed that this surface can be estimated from thermodynamics method based on the area under the P_c – S curve developed by Grant & Gerhard [165].

3.4.3 Entrapment

Entrapment is one of key parameters influencing the spatial distribution of phases in the porous media and the interfacial area which in turn have significant impact on interphase mass transfer. Entrapment of a fluid phase in porous media is directly related to pore scale movement of the intruding phase in the media which is directly related to the wettability of the media. In drainage the intrusion of non-wetting fluid is determined by an invasion process and piston-type motion prevails [179]. In imbibition the wetting phase moves also through the crevices and snap-off mechanisms occur together with piston-type motion [180]. In this case the flow is less predictable as both mechanisms also rely on the surrounding topology of the phases.

At the meso-scale the P_c – S curve in a porous domain provides information on the entrapped portion of the receding phase against the applied pressure on the advancing phase (i.e., the injection pressure of the advancing phase) while the pressure of receding phase is kept constant. The residual saturation represents the lowest saturation of the receding phase that can be attained.

For NAPLs in water-wet media Anderson et al. [115] reported that the residual saturation will increase as the median grain size decreases. Using MRI Zhang et al. [181] showed that finer media will lead to greater residual saturation given the same wettability and grain size variance. A physical explanation for the occurrence of higher residual saturation is the increase in capillary force with decrease in grain size, and subsequently, pore throat, leading to entrapment of more NAPL blobs. Schnaar & Brusseau [36] showed that as the uniformity index (U_i=d_{60}/d_{10}) increases, the residual saturation of NAPL (TCE) decreases for the same median grain size and wettability. Different correlations between residual saturation and porous medium properties (i.e., median grain size, wettability, pore size distribution) have been proposed by different authors. For example the residual saturations measured by Powers et al. [9] do not have the same relationship with medium properties as Bradford et al. [88] or Schnaar & Brusseau [36] presented. One reason for these variations is that the meso-scale experiments present the impact of system parameters on entrapment jointly. Micro model experiments and pore network models provide a better picture of this process.

Imbibition starts with piston type movement but in cases where the topology does not enable piston type movement snap-off would occur due to decrease in capillary pressure [180]. The two movement mechanisms have been shown to lead to different types of displacement patterns (i.e., flat-frontal; self-affine growth; bond percolation; compact cluster growth etc.) [182]. Capillary number and contact angle have been demonstrated to have influence on these flow regimes [183]. It was also demonstrated that decreasing the aspect ratio suppresses snap-off hence residual saturation and very low aspect ratio with high porosity may even lead to zero snap-off and residual saturation [176,182,183].

In drainage the only flow mechanism is piston type motion and therefore pore size variance is responsible for entrapment of receding phase [179,184]. Slight occurrence of snap-off at the front of non-wetting phase is reported yet it does not have influence as it gets connected to non-wetting phase with ongoing invasion at the front [4]. In drainage the viscosity ratio of the fluids has significant impact on entrapment of phases at different pressure levels. Lenordmand et al. [179] demonstrated that higher viscosity of the invading fluid relative to the receding fluid induces less entrapment via pore network modeling. Fig. 6 demonstrates the different types of entrapment with respect to the capillary number and the viscosity ratio proposed by the pore network model of [179]. It was demonstrated that for unfavorable viscosity ratios (i.e., lower viscosity of the invading fluid) pore size variance has pronounced effect on the flow regime [184]. One implication of this phenomenon is that pore scale capillary forces dominate the development of the fingers in air sparging (Fig. 6).

DNAPL entrapment in water-wet media resembles residual non-wetting phase occurrence during imbibition as water imbibes into a DNAPL region from above during downward leakage of DNAPL. On the other hand DNAPL entrapment in NAPL-wet media resembles residual wetting phase occurrence during drainage as water drains into a DNAPL region from above during downward leakage of DNAPL. For both of the cases the intrusion velocity of water into a DNAPL region impacts amount of entrapped NAPL and several authors proposed several relationships departing from the results of the pore network simulations [179,182,183]. In addition to velocity, the other parameters discussed in this section (such as contact angle, viscosities, pore size distributions, aspect ratio) determine the interfacial area at the pore scale which influence the interphase mass transfer at the meso-scale. This area is a subject of further research.

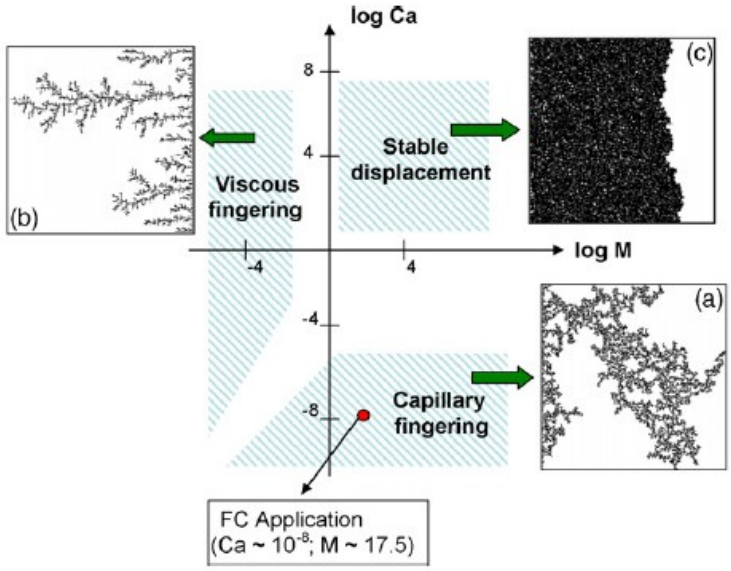

Fig. 6. Emergence of fingering as a function capillary number and viscosity ratio based on Lenordmand et al.[179]; from [185].

3.4.4 Wettability

Wettability describes the tendency of a fluid to spread over a solid surface in the presence of another fluid. The configuration of fluids on the solid surface is affected by aqueous chemistry, solid phase mineralogy, organic matter distribution, surface roughness and charge, and contaminant aging [119]. Generally aquifer solids are accepted as water wet however non-water wetting or partially NAPL-wetting media can also be found [186]. Moreover, the wettability of a porous media can be altered through interaction with molecules of one of the phases. For example, in petroleum engineering it was reported that the adsorption of high molecular weight polar compounds existing in organic phase may lead to alteration of wettability [187]. Powers et al. [186] demonstrated that neat NAPLs such as toluene, TCE and isooctane do not alter the wettability of a quartz surface whereas complex petroleum and coal derived NAPLs can. The authors reported that creosote and coal tar makes a distinct alteration of the quartz surface causing it to become fully oil wet whereas crude oil and its derivations (e.g., gasoline, fuel oil, etc.) lead to a partially oil wet surface. The alteration of surface also has impact on the P_c – S curve whereby flushing of the NAPL contaminated area by water does not culminate into imbibition but drainage. However, during a DNAPL spill event the aquifer is already water saturated and the direct contact of the wettability-altering fluid with grain surface is limited [188]. The relative permeability of the water has also been shown to increase when the soil becomes more NAPL wetting [189,190].

Partially NAPL-wet media, which is likely to occur in cases where NAPLs have been in contact with the media longer than months [188], further complicates the formation of phases. Bradford et al. [88] confirmed this phenomenon on fractional wettable media which is a mixture of water-wet and NAPL-wet media. The authors showed that in water-wet media residual NAPL exists as single or multi-pore blobs. However, in fractional wettable media a NAPL film exist around the NAPL wet soil particles in addition to blobs. It was also reported that in fine porous media, which contains a small amount of NAPL-wet media (10%), NAPL residual saturation is lower compared to fully water wet media. This is attributed to the formation of NAPL films around NAPL wet grains which enable the movement of some of the NAPL globules through those NAPL wet pores. It was also found that further increase in the fraction of NAPL-wet media (>50%) leads to increase of residual saturation which was attributed to formation of NAPL film on many soil particles. A similar trend exists in coarse porous media which contains a small amount of NAPL-wet media (10%) such that NAPL residual saturation is lower compared to fully water-wet media. However when the fraction of the NAPL wet media increases (>50%) in coarse medium, the residual saturation does not increase further as it does in finer media. The authors also conducted dissolution experiments which demonstrated that in all types of porous media considered, increase in the NAPL wet fraction of the media leads to higher interphase mass transfer rate which was attributed to NAPL films around soil particles having a much larger interfacial area compared to non-wetting blobs retained in the pores. The authors also showed that within high fraction of NAPL-wet media (>75%), grain size is not influential on the interphase mass transfer rate, whereas for low fraction NAPL-wet media (10%), decreasing the median grain size leads to lower mass transfer rates. In addition Seyedabbasi et al. [119] showed that the dissolution fingering reduces when the medium becomes more NAPL-wet.

3.4.5 Mean grain diameter

For “INtoMW”, Mayer & Miller [191] showed that the median grain size and median NAPL blob size at residual NAPL saturation are positively correlated. Schnaar & Brusseau [192] reported that the ratio of the two values is between 1 and 2 for different types of porous media. Zhang et al. [181] also showed that the number of blobs in finer media is greater than the coarser one. Intuitively, greater mass transfer coefficients may be expected to occur in finer media (smaller median grain size) due to the existence of greater residual saturation and larger number of blobs, leading to more contact area between the flowing aqueous phase and entrapped NAPL. However, the mass transfer coefficients were found to be proportional to the median grain size in different studies such as [9,32,110,181]. One explanation of this apparent phenomenon is presented in Zhang et al. [181] which relates to the

geometry of the entrapped NAPL. It was reported that the blobs occurring in coarser media are mostly spherical singlet blobs whereas in finer media they are distributed among singlet, doublet, triplet and multipore NAPL blobs. These multipore NAPL blobs induce stagnant water formations adjacent to NAPL-water interface, and as a result the flowing water tends to follow preferential flow paths without contacting the interface. In coarser media, on the other hand, the occurrence of singlets does not create stagnant water formations and the aqueous phase flows in a more distributed manner leading to more contact with the NAPL. The aforementioned flow field condition was also demonstrated using pore scale modeling (Lattice-Boltzmann) by Knutson et al. [193] and in etched network experiments by Chomsurin & Werth [194]. The implication of this phenomenon on field scale is the retention of residual NAPL formations in less accessible media leading to further tailing of effluent concentrations.

In air sparging the mean grain size influences the flow paths of the mobile phase. The radius of influence of the air sparging cone was shown to be influenced by the mean grain size. Reddy & Adams [195] showed that the radius of influence is greater for finer sand. On the other hand Peterson et al. [196] showed that sand with Average Modal Grain diameter (AMG, defined as is the average grain size of sediment retained in the ASTM sieve with the largest volume yield) smaller than 1.3 mm leads to discrete air channels whereas AMG greater than 1,84mm leads to a pervasive occurrence of air channels distributed as a symmetrical cone around the injection point. Between the two values a mixture of both flow types occur. Braida & Ong [197] and Rogers & Ong [198] showed that in sandy material the recovery rate decreases with decreasing mean grain diameter for the case where recovery is through volatilization of the solutes through the water-air interface (i.e., not directly from NAPL-air interface). The decrease is attributed to increased distance between the air-water interface and the NAPL-water interface owing to the greater tortuosity of the finer sand. However their experimental set up is based on a tank which had custom made wide air channels, meaning that the results may not directly apply to air sparging.

3.4.6 Pore size distribution

For “INtoMW”, Mayer & Miller [191] showed that the pore size distribution of a porous media influences the formation of residual NAPL blobs whose size distribution can be defined in terms of a Van-Genuchten type equation. The authors did not quantify the relation between blobs and pore size distributions because all the tested porous media had overlapping pore size distributions. However, it was shown that the variance of the blob size distribution is greater than the variance of the pore size distribution. Schnaar & Brusseau [36,192] investigated this relation for residual NAPL (TCE) blobs using synchrotron x-ray micro-tomography. The authors showed that when the variance of the pore size distribution (defined through a uniformity index) increases, the variance of the NAPL blob size distribution increases. The number of blobs created in the non-uniform media is also found to be higher than the uniform one. One possible explanation for that can be found in Brooks et al. [132] who stated that when the grain size distribution becomes wider, the larger pores created by big grain particles are filled with small grain particles leading to the formation of smaller pore bodies. Under such conditions, the pore space will be governed by the small grain particles as observed in the x-ray images presented by [192]. Schnaar & Brusseau [36] also showed that the number of blobs with relatively higher volumes is greater in uniform media compared to non-uniform media. As discussed under the section “median grain size”, smaller pore bodies might lead to higher number of NAPL blobs and multi-pore blobs which eventually induce NAPL bypassing and stagnant zones [193], [181]. Consequently, high uniformity coefficient media may lead to smaller pore bodies and, therefore, a decrease in the mass transfer coefficients. In accordance with this argument Chomsurin & Werth [194] demonstrated on an etched network that less uniform media leads to a smaller mass transfer coefficient at the same Peclet number. Russo et al. [199] also showed that non-uniform media (hayhook soil U_i=16, d_{50}=0.26mm) leads to 10 times smaller mass transfer coefficient than uniform media (Accusand 45/50, U_i =1, d_{50}=0.35). However in both studies the more non-uniform media is also the one with smaller median grain size which might be one other possible reason for the difference in mass transfer of these two media. Schnaar & Brusseau [36] on the other hand reported greater mass

transfer coefficients for non-uniform sand in comparison to uniform sand having the same median grain size. However, greater flushing velocity was used in their dissolution experiment with the more non-uniform sand which may have also contributed to the greater mass transfer coefficient with the more non-uniform porous media. The impact of non-uniformness of the soil on the interphase mass transfer was also investigated by Powers et al. [9]. The authors conducted column experiments using 6 different sand types whose uniformity index varied between 1 and 3. From their dissolution experiments the authors developed a Sherwood number formulation as function of the uniformity index with a power of 0.41 implying that the more non-uniform media would lead to higher mass transfer coefficients. Even though the dissolution results comply with findings of Schnaar & Brusseau [36] it must be noted that the mean grain diameter is not the same among the sands used in Powers et al. [9] which makes a direct comparison not possible.

In general it is reasonable to presume that non-uniform media will have smaller pore bodies due to filling of big pores with smaller grain particles in comparison with uniform media. However this might not always be the case. The development of a correlation between grain size distribution (i.e., uniformity coefficient) and pore size distribution for natural porous media would contribute substantially to the prediction of phase occurrences.

Pore size distribution is also known to increase fingering when the viscosity ratio of the advancing phase to the receding phase is very low [184]. Hence, the flow paths that occur during air drainage into water saturated media (e.g., during air sparging) are significantly influenced by the pore size distribution. In case of water imbibition into a NAPL pool in NAPL-wet media, pore size distribution has minor influence due to much smaller viscosity ratio between the NAPL and water.

3.4.7 NAPL mobilization

NAPL mobilization in the subsurface is expected to occur when the exerted hydraulic pressure and gravitational force exceed the capillary pressure at the widest pore throat [200]. Observation of the main drainage and imbibition capillary pressure-saturation curve of a two-phase system indicates that mobilization stops when the residual saturation is reached. Mobilization is at maximum for a saturation value between the residual saturations of the two phases depending on the multiphase system [201]. DNAPL mobilization is mostly encountered either during the initial leakage period when gravitational forces induce fast downward movement or at a slower rate after the leakage and pooling over an inclined deep impermeable barrier. LNAPL mobilization on the other hand occurs mostly due to inclined water table level, exerted hydraulic gradient or changes in the water table level [200,202,203]. In an MRI study Johns & Gladden [157] showed that the velocity of the water during the leakage of the NAPL not only influences the entrapped NAPL amount, but also the average ganglion volume which decreases with higher water velocities. This was attributed to the higher pressured exerted on larger size ganglions due to their higher cross sectional area orthogonal to the flow direction. It must be noted that the diameters of the chosen glass beads ranged between 1 and 5 mm whereas the aqueous superficial flow velocity was very high compared to typical groundwater velocities. The influence of the velocity on average ganglion volume would likely be less significant at typical groundwater velocities. Recently Schnaar & Brusseau [36] reported that a formerly trapped NAPL blob can be mobilized due induced blob diameter reduction induced by dissolution. The mutual mobilization of the two phases is likely to increase the mass transfer coefficient due to mechanical mixing occurring during flow of the two phases in porous media; however, no experimental observation of the alteration of the mass transfer coefficient has been reported in the literature.

Mobilization becomes significant especially when remedial agents such as cosolvents and surfactants (i.e., “CHEM”) are used. Both types of chemical agents can significantly decrease the interfacial tension between NAPL and aqueous phase which may lead to mobilization if the capillary force is overcome at the pore throat. Aydin et al. [46] demonstrated that mobilization is enhanced with increasing temperature due to reduced interfacial tension whereas Agaoglu et al. [53] showed that the use of

intermediate levels of ethanol content in the flushing solution may lead to the development of preferential flow paths and the decrease of interphase mass transfer.

3.4.8 Desorption

Zhu & Sykes [125] proposed that dissolution of entrapped NAPL blobs (i.e., residual) be defined through three stages. The first stage is defined by equilibrium or near equilibrium concentrations. The second stage is characterized by a rapid drop in effluent concentrations by three orders of magnitude. The third stages appears as tailing of the effluent concentrations which is associated with about 0.5% initial NAPL mass remaining in the aquifer. Imhoff et al. [204] stated that this last stage tailing may occur due to desorption or dissolution of isolated NAPL blobs. Gradual desorption of organic contaminants from aquifer solids can significantly increase the time of remediation [205]. Especially the slow diffusion of desorbed contaminants from the stagnant regions of porous media (i.e., low permeability zones) or other mechanisms of kinetically slow desorption can cause long-term slow rates of solute flux which indicates that distinguishing between desorption and interphase mass transfer may be difficult in some cases. The processes and the modeling associated with desorption is, however beyond the scope of this work, and we refer the interested reader to [206–208].

3.4.9 Density and Viscosity

Interphase mass transfer is influenced by the interfacial area which is also controlled by the stability of the interface during mobilization. Stability has been shown to be a function of density and viscosity differences [209]. Density difference in aquifer fluids leads to stratification of the multiphase system. Mackay et al. [210] reported that stratification forms when the density difference exceeds 1%. The impact of density is easily observed in various applications such as the use of remedial agents for groundwater remediation, air sparging activities and CO_2 injection applications. The density of the remedial solution (i.e., "CHEM") strongly influences the formation of over- or under-riding of the flushing solution, and, consequently, the contact of fluids which has a crucial impact on the interphase mass transfer. Jawitz et al. [126] showed that the cosolvent solution which is comprised of 20% ethanol+ 80% water, moves upwards during flushing due to density contrast against pure water (i.e., density difference of 2.7%) whereas the subsequent water flushing of the cosolvent solution leads to under-riding of water and trapping of cosolvent solution in capillary fringe. Furthermore, when the cosolvent solution comes in contact with NAPL, it drives the NAPL either upwards or downwards depending on its density further advancing stratification which decreases the field scale interphase mass transfer. In case of remediation of LNAPLs with densities higher than ethanol (e.g., toluene, benzene) the stratification and its negative effect on recovery can be overcome with the use of water ethanol mixtures which would decrease the density contrast that leads to stratification [211]. Grubb & Sitar [212,213] showed the occurrence of stratification when pure ethanol was flushed through DNAPL source zone.

Another influence of density on interphase mass transfer is observed in high pressure CO_2 injection into brine aquifer. The dissolution of the CO_2 into brine aquifer at the CO_2-brine interface at great amounts (due to its very high pressure) leads to density driven convection of CO_2 enriched brine and collapsing of the boundary layer and, consequently, enhancing the interphase mass transfer [214,215].

4. Modeling of interphase mass transfer

A large number of mathematical models have been developed in the past several decades that focus on interphase mass transfer in porous media, particularly in relation to the dissolution of NAPLs into the surrounding flow. These models have generally included other fate and transport processes, such as advection and diffusion, because of the dependence of interphase mass transfer on these processes. These models have mostly been used in predictive models to estimate contaminant concentrations in the vicinity of NAPL zones as well as in inverse mode to quantify the impact of different operational

parameters and to back calculate interphase mass transfer parameters based on observed experimental data.

In reviewing this body of work we have broadly classified the developed models as analytical or numerical. Analytical solutions are generally easier to apply and are in many instances used for screening purposes since they don't require detailed information about the subsurface conditions; however, their drawback is the oversimplification of the subsurface multiphase system The scale that these models are developed for ranges from field scale applications with NAPL zones that can be on the order of 10s of meters to meso-scale- experiments with NAPL zones on the order of a few cm.

Numerical models on the other hand generally provide more flexibility by relaxing some of the limiting assumptions incorporated in analytic models, yet they require more information about subsurface properties and the NAPL distribution and substantially larger effort to simulate the multiphase system. Numerical models that incorporate interphase mass transfer can be broadly divided into pore scale models and REV-based models. Pore scale models which focus on the interaction of interphase mass transfer and other multiphase flow processes at the pore scale mostly based on pore network models, are used to quantify interphase mass transfer at the meso-scale. Two other types of pore-scale models namely, Lattice Boltzmann and Volume of fluid method have also been proposed for modeling interphase mass transfer at pore scale. REV-based models represent the interphase mass transfer at the continuum scale, and hence can be used to simulate interphase mass transfer at the field scales. Three different types of REV based models can be identified as: single phase models, multiphase models and an intermediate category, referred to in this review as semi-multiphase models which simulate the flow of a single phase that is influenced by the existence of the other phase.

4.1 Analytical models

The first models that focused on interphase mass transfer in porous media were developed to simulate NAPL dissolution (e.g., "INtoMW"). These models consisted of analytical solutions of the partial differential equation (PDE) describing solute transport in porous media that is the advection-dispersion equation. The connection of the solute transport equation to interphase mass transfer is accomplished through a prescribed concentration equal to the solubility at the NAPL-water interface [33].

Hunt et al. [200] was one of the first papers that specifically considered dissolution from different NAPL configurations entrapped in porous media. For pool NAPLs oriented parallel to the flow direction, the steady- state concentration as a function of vertical distance from the pool is:

$$C(L,y) = C_{(s)} erfc\left(\frac{y}{2\left(\frac{D_y L}{U_x}\right)^{1/2}}\right) \qquad (11)$$

For a region of uniformly distributed spherical NAPL blobs, Hunt et al. [200] derived the following PDE to describe the transient state NAPL dissolution:

$$\frac{\partial C(x,t)}{\partial x} = \frac{k_f(d_s)}{U}\left[\frac{6V_s(x.t)}{d_s(x.t)}\right][C_s - C(x.t)] \qquad (12)$$

The above equation expresses the dissolved contaminant concentration gradient as a function of interfacial area, the difference between the concentration at solubility and initial concentration, and the mass transfer coefficient which is expressed as a function of the NAPL blob diameter. The authors reduced the above PDE to an ordinary differential equation (ODE) by solving it for a particular point in time knowing the volume of NAPL (V_s; assumed to be in shape of spherical blobs) and diameter of spherical blobs (d_s). The above equations are applicable at meso-scale as they require continuous NAPL

formation whereas the authors applied them to a larger scale with NAPL length of 10 m referring to field scale. However, in such lengths the field scale permeability distribution and in relevance in-continuous NAPL distribution have significant impact on the interphase mass transfer which are not accounted for in the above formulations. Hunt et al. [200] also derived expressions for the transient mass transfer coefficient based on blob mass balance consideration. Both of the equations are based on the idealized assumption that NAPL is continuous in the space either as a pool or spherical blobs along the flow direction.

While the above equations can be used to predict dissolved hydrocarbon concentrations near NAPL zones, a number of studies have used similar equations in an inverse mode to estimate the mass transfer coefficient of conducted meso-scale experiments [8,9,36]. These studies have also attempted to relate the estimated mass transfer coefficient to the experimental operational parameters such as flow velocity, saturation, and viscosity (eq. 1,2,3,4). Similar approaches had been developed by Williamson et al. [28] and Wilson & Geankoplis [30] to determine the mass transfer coefficients of benzoic acid sphere dissolution in packed beds.

Anderson et al. [115] used a Laplace approach to solve the governing PDE for both residual and pool NAPL dissolution at the field scale. This approach ignores the impact of field scale permeability (e.g., flow bypassing) on interphase mass transfer. The authors showed that the orthogonal position of a vertical NAPL finger (whereby the aqueous phase flowing through residual NAPL region is assumed to be at solubility) with respect to groundwater flow leads to the occurrence of high concentrations at the down gradient of the finger due to advection of dissolved contaminants. On the other hand, a NAPL pool oriented parallel to groundwater flow induces lower concentrations because advection occurs parallel to the pool and dispersion is the only mechanism for the orthogonal spreading of the dissolved contaminant. Experimental observations that support these findings were discussed above in section two of this review. In some instances water might penetrate the pool NAPL depending on the saturation as shown by Nambi & Powers [121].

Hatfield & Stauffer [216] developed one dimensional analytical model for residual NAPL dissolution at the meso-scale that incorporates the mobile and immobile regions of water (due to clogging of a pore by NAPL) into the transport equation which also includes the sorption of solutes on solid surfaces. The acquired partial differential equations for mobile and immobile regions were solved using a Laplace transform approach. Soerens et al. [217] also divided the porous media into two domains at the meso-scale namely: a NAPL region which represents flow paths that are in contact with NAPL and a clean region which represents flow paths that bypass the NAPL. Unlike the Hatfield model, Soerens et al. [217] assumed flow through the NAPL region. The total effluent concentration is defined as the sum of the concentration of the NAPL region multiplied by the fraction of flow through that region and the concentration of the clean region multiplied by the fraction of flow through that region. The effluent concentrations in both regions were determined through eq. 4 whereby the interfacial area is lumped into mass transfer rate coefficient. The authors demonstrated the dependence of effluent concentrations on interphase mass transfer coefficients and other operational parameters (e.g., fraction of flow) by investigating three different scenarios through which i) the clean region concentration was set to 0 when interphase mass transfer in the NAPL region is assumed to be rate limited, ii) the clean region is set to rate limited interphase mass transfer when the NAPL region is assumed to be at equilibrium conditions or iii) both regions are set as rate limited interphase mass transfer with NAPL region having a mass transfer coefficient 100 times greater than that of the clean region.

Chrysikopoulos et al. [218,219] computed the dissolution of a DNAPL pool residing beneath the aquifer in 2-dimensional and 3-dimensional spaces respectively. Holman & Javandel [220] solved for the dissolution of an LNAPL pool residing on top of water table. The solutions presented in these studies were derived by solving the governing differential equation using a Laplace transformation approach.

An analytical model referred to as multiple analytical source superposition technique (MASST) which enables the solution for multiple NAPL sources was presented by Sale & McWhorter [221]. The model is based on the analytical solution derived by Hunt [222] for the solute transport equation incorporating one dimensional advection, three-dimensional dispersion and a source term which refers to instantaneous occurrence of solute due to interphase mass transfer. The source term was defined through a first order mass transfer term, $M = k(C_s - C_a)$. With this term the solution considers the influence of existing concentration (C_a) on source term. The authors expanded the methodology to multiple NAPL source zones. For that; a domain (here named subzone) is defined as a summation of subdivisions and the concentration at the centroid of each subdivision is found with respect to other subdivisions and their respective existing concentrations which are unknown. Writing this summation equation for each subdivision leads to N number of equations with N number of unknowns (C_a; the concentrations at the center of each subdivision) with the mass transfer coefficient of each subdivision defined by the user (eq. 13) [221]. Since this methodology does not incorporate the impact of field scale heterogeneity and the corresponding issues on interphase mass transfer, it is suitable for meso-scale investigations. Accordingly the authors applied it to a meso-scale domain.

$$C_a(x_j, y_j, z_j) = \sum_{i=1}^{N} K_l\big(C_s - C_a(x_i, y_i, z_i)\big) \cdot F\big(x_j - x_i, y_j - y_i, z_j - z_i\big) \qquad (13)$$

where;

$$i, j = 1,2,3, \ldots., N. \qquad (14)$$

This procedure enables MAAST to define the initial and boundary conditions in a more detailed manner including discontinuous NAPL formations a condition often encountered in the field. .

Parker & Park [37] developed an analytical approach to estimate the effluent concentrations at the field scale (with a domain size of 10m) based on the ODE defining the concentration change with respect to location (eq. 4). The authors assumed that the exponential solution of the governing ODE can be approximated by a linear function when the mass transfer coefficient is very small (k<<1) which is often the case in the field:

$$\frac{C_{out}}{C_{eq}} \approx \frac{\kappa_{eff} L}{\bar{q}} \qquad (15)$$

$$for\ \frac{\kappa_{eff} L}{\bar{q}} \ll 1 \qquad (16)$$

The authors coupled this equation with the change of NAPL mass in the domain with time by correlating the mass transfer coefficient to change of mass with a power beta (i.e., $\left(\frac{M_{(t)}}{M_0}\right)^{\beta_2}$).

$$\frac{C_{out}}{C_{eq}} = \frac{\kappa_0 L}{\bar{q}} \left(\frac{\bar{q}}{\overline{K_s}}\right)^{\beta_1} \left(\frac{M_{(t)}}{M_0}\right)^{\beta_2} \qquad (17)$$

The power beta, β_2, is an empirical parameter (also named “mass depletion exponent”) which is reported to be a function of field conditions and was obtained through fitting the analytical solution to measured data.

Zhu & Sykes [125] presented a NAPL dissolution model whereby the effluent concentration is either a linear (L-model) or non-linear (N1-model; N2-model) function of the change of NAPL mass in the domain. The constant parameters are chosen by fitting the analytical solution to experimental results.

Similar approaches were presented by Falta et al. [223]. Christ et al. [11] investigated the relation between the mass depletion exponent and aquifer contamination conditions in the field. The authors proposed that ganglia to pool ratio (GTP, the saturation of NAPL ganglia formations to saturation of pool NAPL formations in the domain) which has been investigated by Lemke et al. [224] is a better predictor of NAPL mass dissolution characteristics. Therefore, the authors suggested that the "mass depletion exponent" be estimated from the GTP:

$$\beta = 1.5 \cdot GTP^{-0.26} \qquad (18)$$

Christ et al. [225] improved the estimation of the mass depletion exponent by considering whether the mass flux is from a NAPL pool or a ganglia region. The authors note that when residual NAPL exists together with pool NAPL, the time evolution of effluent concentrations shows two distinct trends: an initial high concentrations stage attributed to residual NAPL dissolution followed by a stage of lower concentrations resulting from pool NAPL dissolution. The authors stated that for pool formations the mass depletion exponent can be assumed to be 0.5 until the mass is almost depleted in this region whereas in regions with residual NAPL the exponent is given by the formulation proposed by Christ et al. [11] (eq. 18). In addition to the GTP, the flux contributions of each region are also input parameters in this approach, which are difficult to estimate in the field.

The ratio of the solute mass flux reduction to NAPL mass reduction has also been considered at the field scale as a possible parameter for estimating the duration of remediation activities [226]. Brusseau et al. [112] showed that pool NAPL formations lead to approximately 1 to 1 flux reduction against mass reduction which can be represented by the GTP approach [11] fairly well whereas uniformly distributed residual NAPL leads to the occurrence of high effluent concentrations until 80% of NAPL mass is depleted. Hence, the use of GTP approach does not cover this behavior. Similar results were also reported by Difilippo et al. [227].

Stream tube analysis, which is based on a stochastic advective transport approach was also used to investigate the relationship between mass flux reduction and mass reduction in the field [228,229]. Jawitz et al. [228] showed that the increase in variance of the reactive travel time, τ distribution between streamlines, which is a function of the hydraulic conductivity variance coupled with the variance of spatial distribution of NAPL leads to faster decrease of the effluent concentration:

$$\tau_i = t_i R_i = t_i + t_i K_f \check{S}_i \qquad (19)$$

The required parameters of this method such as moments of reactive and non-reactive travel times can be deduced from tracer tests. It should be noted that the stream tube analysis is based on the conditions where the NAPL saturation is around or less than residual saturation such that the decrease in NAPL saturation (via dissolution) does not lead to the occurrence of new stream lines.

Zhang et al. [108] used different analytical approaches including MASST and the stream tube approach to model four different 3D flow cell experiments each with different NAPL saturation and hydraulic conductivity fields. The authors showed that none of the models were able to capture all the change in effluent concentration with time. Chen et al. [230] evaluated the feasibility of the equilibrium stream tube approach for cosolvent/surfactant flushing applications (CHEM) over a 2D flow chamber where the average NAPL saturations are low (0.007-0.039). The occurrence of mobilization would prevent the use of stream tube analysis due to the change of NAPL configuration that was defined apriori through reactive tracer tests, however the authors observed no mobilization during flushing. Wood et al. [231] on the other hand did not consider this phenomenon for predictions of cosolvent flushing with cosolvent content as high as 72% which likely initiates mobilization and changes the NAPL configuration defined earlier for the use of stream tube model.

Braida & Ong [232] developed a simple model to predict vapour phase concentrations in air sparging applications based on the air-water interfacial area determined from the number and characteristics of air channels, the diffusive mass transfer zone (MTZ) in the aqueous phase around the gas channels and a user-defined rate limited volatilization parameter. The basis of the MTZ concept had been presented earlier by Chao et al. [233].

4.2 Pore scale numerical models

4.2.1 Pore network models

Flow in porous media can be represented as flow in a network of pore throats and pore bodies which is the founding aspect of pore network models [179]. In pore network models the flow is defined through Poisuielle's law due to the laminar structure of flow in porous media if the domain chosen in the pore network model has a cylindrical cross section [179]. In case of rectangular shapes adapted versions of Poisuielle's flow can be used by determining an equivalent pore radius [82,234]. Pore network models can be divided into two categories i) quasi static models and ii) dynamic models [235]. Dynamic models can simulate the transient behavior of the flow when the viscous forces are comparable to capillary forces [4,236]:

$$V_i \frac{\partial S_i^{\alpha}}{\partial t} + \sum_{j=1}^{N_i} Q_{ij}^{\alpha} = 0 \qquad (20)$$

However, the pore network models used to investigate interphase mass transfer processes are quasi static models which simulate the equilibrium states of drainage and imbibition processes when capillary forces dominate the flow which is the case in typical oil/water flow (e.g., for capillary number in the order of 10^{-7}) [237]:

$$Q_{ij} = G_{ij} \Delta P_{ij} \qquad (21)$$

$$\sum_j Q_{ij} = 0 \qquad j = 1,2, \dots \dots N \qquad (22)$$

Another common feature of the pore network models investigating interphase mass transfer is that they assume the dissolving phase to be immobile, trapped in the pore throats/bodies. Therefore, displacement processes are not covered. Reviews of pore network models are presented by [4,235,238].

One of the first efforts to use pore network models for simulating NAPL dissolution was presented by Jia et al. [234]. The exact locations of NAPL blobs were obtained from visual observation of a micro model and incorporated into the pore network model. The time evolution of the NAPL constituents in the aqueous phase at the nodes which do not neighbour any NAPL-water interface was determined using the following equation with the flow velocity determined using Poisuielle's law.

$$V_s \frac{\Delta C_i}{\Delta t} = \sum_j D A_{ij} \frac{\Delta C_{ij}}{l} + \sum_j \left[\frac{G_{ij} \Delta P_{ij}}{l} C_{ij} \right] \qquad (23)$$

For nodes neighbouring the NAPL-water interface it was assumed that the interface in the pore throat resembles either a flat or a cavity like shape. The equation describing the time evolution of NAPL constituents in these neighbouring nodes contains an extra first order mass transfer term with a mass transfer coefficient that is determined from the assumed interface shape (i.e., flat or cavity). The authors demonstrated that when the mass transfer process in the nodes neighbouring the NAPL-water

interface is well described, the results of the pore network model match quite well with the experimental results.

Dillard & Blunt [82] used a pore network model to simulate the NAPL dissolution experiments conducted by Powers et al. [9]. The authors used the invasion percolation method, developed by Wilkinson & Willemsen [239], to generate the fluid distributions. The pore size distribution of the network model was created by conditioning the simulated P_c-S curve to the experimental data of Powers by adjusting the size of pore throats. In the pore network model solute transport occurs through advection and diffusion with possible corner flow of the aqueous phase when the NAPL is trapped in a pore body or pore throat:

$$F_{ij} = Q_{ij}^{w} C_t^{in} + D_m A_w \left(\frac{C_i^{out} - C_j^{in}}{l_t} \right) \qquad (24)$$

The interphase mass transfer was assumed to occur only during the corner flow of the aqueous phase (see Fig. 7) with a first order term (in this work named as "E_d") is determined from the analytical approach presented by Lake [7] which is based on the solution of the advective-diffusive transport equation for flat fluid-fluid surface conditions. For a NAPL filled chamber i, solute concentration leaving the chamber through corner flow is given with respect to mass transfer coefficient:

$$C_i^{out} = C_i^{in} + E_d \left(C_s - C_i^{in} \right) \qquad (25)$$

Unlike the work of Jia et al. [234], Dillard & Blunt [82] excluded NAPL dissolution into the aqueous phase through diffusion from the NAPL-water interface which resides at the pore body or throats facing NAPL-free pore body/throat. The authors demonstrated that the dependence of effluent concentrations to the Peclet number agrees well with experimental data for a constant NAPL volume assumption. In another pore network model the authors generated the time evolution data of effluent concentrations as the NAPL volume decreased with dissolution. However, slight discrepancy was observed between simulated and experimental data which was attributed to the complex nature of interphase mass transfer. A salient property of the difference between simulated and experimental effluent concentrations is the tailing which occurred in simulation but was not observed in the experimental data. This may be attributed to the fact that the size reduction of NAPL blobs due to dissolution instigated the mobilization of these blobs in the column experiment whereas in pore network model the NAPL blobs were set to be trapped permanently during dissolution.

The column experiments conducted by Powers et al. [9] were also simulated by Zhou et al. [100] using a physics-based model which represents the porous media as bundle of parallel pores. It was shown that this model structure is capable of representing the interphase mass transfer in porous media. The number of pores in a pore bundle was not found to be important as the geometry itself enables a realistic representation of the corner diffusion, the pore diffusion (i.e., the dissolution from the NAPL interface orthogonal to flow direction) and mixing of stream lines. The model was suitable to simulate column experiments which represent one-dimensional flow with relatively small cross-sectional area (e.g., Powers et al. [9] column diameter 5.5 cm) because at each incremental distance from the inlet the flow can be assumed to be mixed as can be represented with the connection of pore bundles. This assumption however may not be valid for larger scale flows when flow diversion or low transverse dispersivity conditions are present, and might limit the use of this approach at larger scales. The authors also modelled interphase mass transfer in NAPL wet media to compare the results with the column experiments conducted by Parker et al. [240]. In this case the NAPL was assumed to be residing adjacent to the pore walls enabling aqueous flow through the center of the pores. Corner diffusion was assumed to be the only pattern for interphase mass transfer (however in this case from corner to center). The fraction of corner flow, β which is necessary for this model, is difficult to estimate in practice since it is a function of many properties which may preclude the use of this model in a

predictive way. By matching model results to the experimental results, the authors were able to develop a relation between mass transfer coefficient and Peclet number.

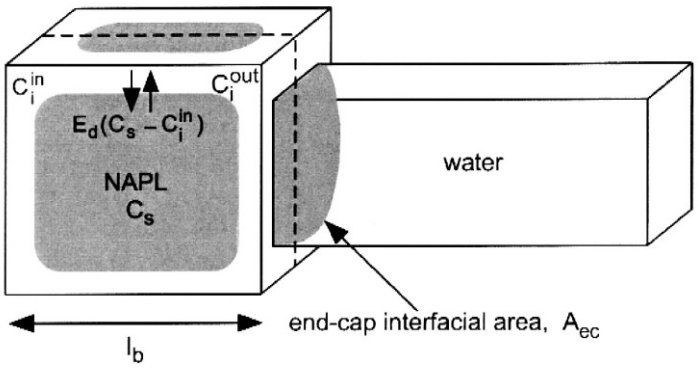

Fig. 7. Schematic of NAPL formation in a chamber in pore network model of Dillard et al. [89].

Dillard et al. [89] used the same pore network model presented by [82] to investigate the mass transfer rate coefficient, $K_l$of an REV based numerical model with respect to NAPL saturation and Peclet number. The authors also simulated DNAPL dissolution using an REV based numerical model that incorporated the mass transfer formulation developed from their pore network model. For comparison the authors used the same REV based numerical model with local equilibrium approach and with the mass transfer formulation developed by Powers et al. [9]. It was reported that the results were similar for all three simulations which was attributed to low velocities used in the simulations (about 1m/d). The pore scale interphase mass transfer coefficient developed from the analytical solution presented in Lake [7], which was employed in the pore network models of [82,89,100], was also investigated by Sahloul et al. [81]. The authors solved the transport equation numerically in a corner with adequate boundary conditions to determine the relationship between mass transfer coefficient and flow conditions in that corner and showed that the analytical solution presented in Lake [7] underestimates the interphase mass transfer. It was reported that the discrepancy was caused by the chosen boundary conditions and the non-uniform velocity distribution assumed to exist in their corner model.

Held & Celia [38] used the pore network model of Reeves & Celia [170] to generate NAPL distributions in a network whose pore structure was defined based on the properties of the porous medium used in the column experiments of Imhoff et al. [32] with incorporation of the reported pore size distributions. The generated fluid distributions were used to create the aqueous flow field in the network which was then used to simulate transport of dissolved constituents. No diffusive transport of solutes was incorporated in the model; only the diffusive flux appearing in the interphase mass transfer term was accounted for. Advective transport was modelled by tracking the dissolved mass explicitly in time (i.e., no matrix is solved due to discretization):

$$V_{a,i}\frac{\Delta C_{a,i}}{\Delta t} + \sum_{j\in N_i}\left[Q_{ij}C_{a,j}\right] = \sum_{j\in M_i}\left[J_j A_{na,j}\right] \qquad (26)$$

where;

$$\sum_i \left[J_i A_{na,i}\right] = \sum_i \left[A_{na,i}\frac{D_m}{l_i}\left(C_a^S - C_{a,i}\right)\right] \qquad (27)$$

Full depletion of NAPL in a pore body due to dissolution was followed by generation of the new aqueous velocity field. The authors excluded corner diffusion and the only pattern of interphase mass

transfer was defined through mass flux from the NAPL into adjacent NAPL-free pore body via diffusion along the stagnant aqueous phase residing in the pore throat between. The authors reported excellent agreement with results reported by [32].

Yiotis et al. [2] focused on the drying of liquid phase in a porous domain which is closed from all sides except one where a fracture allowed gas phase to be purged through. The authors excluded the film formation in their pore network model and the mass flux from liquid to the gas phase at a pore containing a gas-liquid interface was determined with the stagnant gas phase assumption in that pore (i.e., a function of the molecular diffusion of liquid molecules in the gas phase and stagnant boundary layer length). In case of a liquid filled pore, that is adjacent to a fracture which has flowing gas phase, the mass flux was expressed in terms of the velocity of the gas phase in the fracture. The authors pointed to the influence of trapped wetting phase islands on interphase mass transfer. However, the exclusion of film formation, which is shown by Sahloul et al. [81] to be a dominant process in case of non-wetting phase intrusion, may have influenced the results significantly. Zhao & Ioannidis [87] investigated the same phenomena for a NAPL-wet domain with the wetting NAPL phase trapped in the middle of the domain with the non-wetting water phase flowing through the surrounding pores. The authors represented interphase mass transfer from the NAPL filled pore/throat to the water filled pore/throat with stagnant layer assumption and from the NAPL film residing at the corner to the water residing at the center of the pore/throat with a first order mass transfer coefficient which was determined with the formulation developed by Sahloul et al. [81]. The authors also incorporated the NAPL dissolution behavior in the NAPL wet domain that was investigated by [81] via micro model experiments. The NAPL filled chambers feeding the NAPL films eventually ceased as these films dissolve into the aqueous phase. The disconnection of films and the chambers was represented by assigning a critical value of capillary pressure at which NAPL connection is broken. This critical value was defined in the model as part of the input. The authors showed that the disconnection of NAPL filled chambers from anterior NAPL films lead to a sharp decrease in interphase mass transfer rates. This was attributed to the vanishing of NAPL film interfacial areas once the disconnected NAPL film depletes. Zhao & Ioannidis [241] expanded this model by determining the critical value of capillary pressure in terms of the pore radius:

$$P_c^{crit} = \Pi^{max} - x\sigma/R_t \qquad (28)$$

Zhao & Ioannidis [242] investigated the corner interphase mass transfer coefficient in a 3D corner geometry whereby the fluid-fluid interface (i.e., one side of the corner) is assumed to be at solubility and compared the results with the results presented by [81,82,100]. The authors considered both slip and no-slip conditions and found that representing the corner diffusion (E_d) via the 2D analytical solution of Lake [7] leads to erroneous predictions because in reality the corner is a 3D geometry which results in distinct velocity distributions that are not accounted in the 2D approach. The relation between E_d and dimensionless residence time of wetting phase in a 3D corner developed by Zhao & Ioannidis [242] was further used in a pore network model developed by Zhao & Ioannidis [92] (see Fig. 8) to investigate the CO_2-gas exsolution processes (i.e., supersaturated CO_2 concentration in aqueous phase dissolving into gaseous phase of CO_2). In this model the commencement of gas bubbles was assigned to arbitrarily chosen sites. The authors demonstrated that the mass transfer characteristic is significantly influenced by the initiation of gas bubbles.

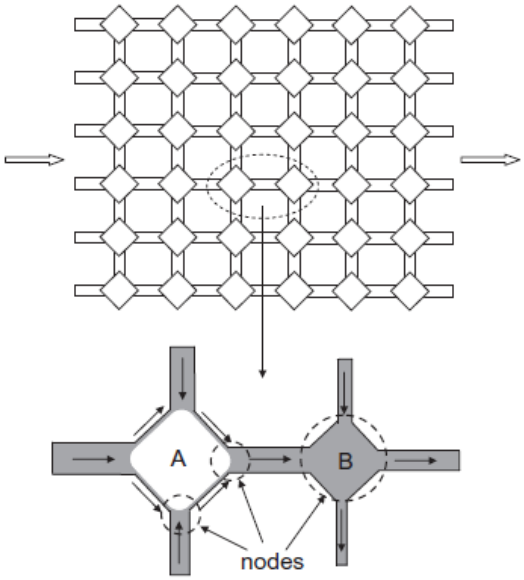

Fig. 8. Schematic of pore network model with water flowing around a bubble.

4.2.2 Other pore scale models

Pore scale multiphase multi-component flow can also be simulated by Shan-Chen type Lattice Boltzmann (LB) model [243]. In this approach the forces acting on a node due to interaction with other nodes of other type components is added to the LB equation. This methodology accounts for the diffusion in the LB equation. The interaction force is determined as a function of the user-defined interaction strength parameter, G, and the separation distance between the corresponding nodes, e. The force acting at position x of component j due to interaction between component j and k (G_{jk}) for a multi-component system is given by:

$$F^{(j)}(x,t) = -\Psi^{(j)}(x,t)\sum_{k=1}^{k=C}\sum_{i} G_{jk}(|e_i|)\Psi_{(k)}(x+e_i)e_i \qquad (29)$$

Small values of G induce considerable amounts of diffusion which also means high miscibility whereas larger values lead to occurrence of purer phases. An alternative approach can be found in Swift et al. [244]. Most of the SC-LB implementations in porous media presented in this work have been conducted to investigate fluid-fluid interfaces or saturation-capillary pressure relations (e.g., [177,245,246]). Meakin & Tartakovsky [247] reported that the poor numerical stability of LB models in case of large density and viscosity contrasts prevents their use in geologically important systems (e.g., water-air flow in vadose zone) whereas incorporation of moderate density or viscosity ratios for the sake of stability leads to unrealistically high diffusion rates. Very recently new formulations of interaction force have also been presented that is suitable for use of higher density ratios [248,249]. It is important to note that LB models have very high computational costs in comparison to pore network models. However, the structure of the model enables easy parallelization [246,250].

The Volume of Fluid method has also been used to simulate multiphase flow at pore scale. Raeini et al. [251,252] further developed the openFOAM two phase flow simulator to account for the sub-pore scale forces emerging in flow through porous medium. However solute transport and interphase mass transfer have not been yet considered in this approach.

4.3 REV-based numerical models

4.3.1 Single phase models

Single phase numerical models are based on the solution of the solute transport equation in the aqueous phase while NAPL zone is assumed to be immobile. The effect of saturation on the relative permeability of the aqueous phase is also ignored. In single phase numerical models an interphase mass transfer term (e.g., first order mass transfer) is introduced into the transport equation for NAPL containing nodes. Powers et al. [34] simulated a typical NAPL (TCE) dissolution scenario (i.e., "INtoMW") through which the interphase mass transfer is defined as "$M = k(C_s - C)$". Depletion of the NAPL mass is accounted for by deducting the total mass of the dissolved contaminants from the remaining NAPL mass at each grid block and at each time step. Interphase mass transfer coefficients were obtained from different formulations developed by Pfannkuch; Wilson & Geankoplis; Williamson et al.; Friedlander [17,25,28,30] that relate the mass transfer coefficient to system parameters such as flow rate, viscosity, density, porosity and saturation. The authors showed that predictions of the various formulations can vary significantly especially at high flow rates and low NAPL saturations. Borden [48] used a similar approach for multi-component NAPL (gasoline) dissolution using both equilibrium and a rate limited mass transfer approach with a mass transfer coefficient determined by matching experimental effluent concentrations. Powers et al. [94,110] developed "theta" and "sphere" models for the prediction of interphase mass transfer coefficients which were subsequently incorporated into single phase dissolution model. The sphere model incorporates the interfacial area between NAPL and aqueous phase while maintaining the Sherwood number as a function of Reynolds number only; that is, it ignores the impact of saturation, uniformity coefficient and other parameters. In theta model, the Sherwood number is a function of all parameters with the interfacial area lumped in it. The authors showed that the sphere model can simulate the effluent concentrations accurately provided the calibration parameter, F is known apriori.

Baldwin & Gladden [102] solved the transport equation in the aqueous phase by defining the aqueous phase as "1-Saturation of NAPL". This allowed the use of the NAPL saturation data that were determined using MRI data from column experiments. The authors also considered interphase mass transfer with a linear mass transfer model, a shrinking-core model and a pore-diffusion model for comparison. Significant deviations from the measured saturations were predicted by all three models. Johns & Gladden [156] improved the linear dissolution model of Baldwin & Gladden [102] by correlating the interfacial area to saturation. The NAPL saturation data used in the model were determined experimentally using MRI. The mass transfer coefficients were subsequently determined by fitting the numerical results to the experimental data.

Kim & Chrysikopoulos [253] and Chrysikopoulos & Kim [101] simulated solute transport due to NAPL dissolution assuming that solute concentrations in NAPL-containing nodes of the domain were equal to the solubility value. The contributions of the sub REV parameters on the interphase mass transfer flux in the NAPL containing nodes such as flow field, saturations, interfacial area were not accounted for. Bradford et al. [104] modified the framework developed by Powers by including sorption and discretizing the PDE using finite difference. The authors showed that the mass transfer formulations developed by [32,42,110] cannot simulate interphase mass transfer for different wettable media. Consequently, the authors developed a revised formulation for interphase mass transfer coefficient that considers the wettability of the media using data obtained from column experiments by Bradford et al. [88]. The developed model does not consider interfacial area separately but lumps it into the interphase mass transfer rate coefficient.

Abriola et al. [74], Mayer et al. [76] and Schaerlaekens et al. [254] simulated the dissolution of residual NAPL using a surfactant solution (i.e., "CHEM") by incorporating the increased solubility value obtained from batch experiments in the mass transfer term. Formulations for the mass transfer coefficients

were determined by fitting the numerical results to experimental data. Ji & Brusseau [255] presented a similar approach for enhanced dissolution by different chemical agents.

4.3.2 Semi-multiphase models

Semi multiphase models consider the flow of only one phase that is influenced by the saturation of the other phase. For example, in case of "INtoMW" saturation of immobile phase has impact on the flow of the mobile aqueous phase by changing its relative permeability. Although the solute transport equation applied to the aqueous phase transport equation is mathematically similar to the single phase models, the incorporation of relative permeability in the model can fundamentally alter the flow field by causing NAPL-bypassing conditions which in turn can have significant impact on transport simulations. Geller & Hunt [256] used this methodology to simulate multi-component NAPL dissolution. The authors used the Wyllie function to estimate the relative permeability of the aqueous phase based on the saturation and updated the interfacial area at each time step with respect to the depleted NAPL mass. The authors excluded dispersion because it is already accounted for in the mass transfer coefficient which is adopted from Hunt et al. [200]. This however also means that no dispersion is accounted at nodes containing no NAPL. Imhoff et al. [116,117] used a similar approach but included the dispersion term and used the mass transfer formulations of Powers et al., Imhoff et al. and Miller et al. [8,32,110] for comparison. The authors reported that the two formulations [32,110] predicted similar results but deviated from the experimentally measured results at later dissolution times.

Powers et al. [257] used the flow and transport simulators, MODFLOW (Waterloo Hydrogeologic) and MT3D (Waterloo Hydrogeologic) in a sequential procedure to approximate NAPL dissolution. The relative permeability was defined through the Corey function [258] and used in MODFLOW to determine the velocity field which was subsequently used as an input for MT3D to simulate the solute transport. The change in saturation due to interphase mass transfer was represented as a decrease in saturation at each time step. The comparison of simulation and experimental results for high NAPL saturations (0.71 in coarse medium) demonstrated that the model is capable of capturing the main trend of the experimental data, although significant difference between the two was observed. This was attributed to the use of the local equilibrium assumption in the transport model. Frind et al. [124] followed a similar approach whereby the groundwater flow was simulated numerically to determine the hydraulic head distribution which was then used in the transport model to simulate contaminant transport. Unlike Powers et al. [257] the authors incorporated rate limited mass transfer in their model with the mass transfer coefficient determined with a new formulation developed by the authors. Saba & Illangaskare [105] also used MODFLOW and MT3D to simulate NAPL dissolution. The hydraulic conductivity of the medium in MODFLOW was defined equal to the relative permeability (estimated by Wyllie function) times the intrinsic permeability. The authors conducted a tank experiment and developed a new mass transfer formulation by regression analysis performed between effluent concentrations attained from experiment and MT3D model. For verification the authors performed another tank experiment that had slightly more complex contamination area and simulated this experiment with MT3D that is revised to include the mass transfer formulations of Powers et al. and Imhoff et al. [32,110] and the one developed from the tank experiment. The authors reported that the latter formulation predicted the observed contaminant plume better. The authors reported that the difference between the new mass transfer formulation and the previous ones is because the new formulation is developed from two-dimensional dissolution experiment whereas other formulations [32,110] are developed from 1D column dissolution experiments. The significance of the dimensionality of the experiments was also evaluated by Brusseau et al. [259] who used a mass transfer formulation developed from 1D experiments to simulate 2D dissolution experiments. Contrary to Saba & Illangaskare [105], Brusseau et al. [259] stated that the simulations gave good agreement with experimental results even though the mass transfer coefficient is derived from 1D experiments.

Imhoff et al. [118] used the numerical algorithm presented by Miller et al. [260] to investigate the dissolution fingering in two dimensional flow where the relative permeability was determined from the Wyllie expression whereas the rate limited mass transfer was determined from the formulation developed by Powers et al. [110]. The authors showed that increasing the variance of hydraulic conductivity leads to greater fingering, whereas increasing the transverse dispersivity lead to the suppression of fingering. Parker & Park [37] used a percolation model to generate a DNAPL saturation profile as the DNAPL leaks downward. The percolation model was followed by the MODFLOW and MT3D model to simulate the interphase mass transfer. The authors stated that modeling NAPL dissolution with this approach enables the use of very fine mesh (one million nodes for a 10 m^3 domain) and time steps.

Marble et al. [107] used the model presented by Brusseau et al. [259] with a new mass transfer formulation which is independent from the experimental conditions that the mass transfer coefficient is derived from. Seyedabbasi et al. [119] improved the model of [260] to account for the influence of wettability of the medium (i.e., different flow configurations) by incorporating: i) the Modified Mualem's approach [190] which relates the relative permeability to the wettability of the media and ii) the interphase mass transfer formulation developed by Bradford et al. [104].

Mason & Kueper [261] simulated surfactant enhanced dissolution of pooled DNAPL ("CHEM") using a revised semi multiphase approach whereby both saturation and interfacial tension control the relative permeability of the flushing solution. The DNAPL saturation distribution along the pool is calculated separately based on the capillary pressure at each location along the pool. The authors used two different approaches for the determination of interphase mass transfer. In the first approach the parameters that are required for the interphase mass transfer coefficients were determined by fitting the numerical results to experimental data. In the second approach the solubility value (C_s) appearing in the linear mass transfer term is defined as a function of time. The authors simulated the column experiments that they had conducted and reported that the second approach resulted in better predictions. Rathfelder et al. [262] modelled surfactant enhanced NAPL dissolution experiments using a modified version of the MISER model [263] whereby the use of surfactants do not reduce the interfacial tension to such level that mobilization is initiated. Apart from the rate limited mass transfer formulation which is obtained from Taylor et al. [264], the authors also considered the influence of density and viscosity alteration due to the use of surfactants on contaminant transport. The authors reported good agreement with the experimental results.

4.3.3 Multiphase models

Prior to their use for environmental applications, multiphase models were mostly developed within the field of petroleum engineering. Here we specifically focus on how interphase mass transfer processes are implemented into multiphase models. For brevity we exclude the equations describing multiphase flow which have been presented in comprehensive reviews by Abriola [1] and Miller et al. [10].

The first multiphase model developed for environmental applications is the compositional model of Abriola & Pinder [265] which assumed equilibrium partitioning of the constituents between phases. Apart from Abriola & Pinder, early multiphase modelling efforts were based on immiscible flow of liquids whereby each fluid is assumed to be comprised of only one constituent (e.g., aqueous phase comprising only water) without interphase mass transfer [266–268]. Sleep & Sykes [269] presented a compositional model, solved with both the fully implicit and IMPES schemes, through which interphase mass transfer was determined according to local equilibrium assumption. White et al. [270] developed another local equilibrium compositional model "STOMP" using the multiphase formulations of the Richards equations [271]. Unger et al. [103] developed a three phase compositional model which allows for the interphase mass transfer to be defined as rate limited or at equilibrium. Adapted versions of mass transfer formulations developed by Mayer & Miller [99] and Guiger & Frind [272]

were incorporated in the model. Application of these mass transfer formulations to 20 different NAPL contamination scenarios, each with a different hydraulic conductivity field but having the same variance, showed that the uncertainty of the time required for the dissolution of all NAPL mass is greatest for the formulation of [99] whereas the equilibrium partitioning assumption induced the lowest uncertainty. The authors also conducted a set of simulations where they scaled the relative permeability - saturation curve of each node with respect to the permeability of that node. It was demonstrated that the uncertainty of the time required for the dissolution of all the NAPL mass decreased with this scaling procedure which also induced more lateral spreading of the NAPL. No scaling was performed on the capillary pressure – saturation curve. It was also reported that decreasing the variance of the permeability field leads to a reduction of the uncertainty of the time required for the complete dissolution of the NAPL mass. Dekker & Abriola [273] modified an IMPES type model (VALOR) by scaling the capillary pressure-saturation curve and residual saturation of each node with the permeability of that node to investigate the impact of these parameters on DNAPL spill geometry. Residual saturations were determined as a log-linear function of permeability whereas the P_c-S curve was scaled by changing the "α" parameter of the Van-Genuchten formulation with respect to permeability. The authors demonstrated that increasing the vertical correlation length of the permeability increased the penetration depth and decreased the spread and maximum NAPL saturations. The horizontal correlation lengths on the other hand did not have a significant impact. Hinkelmann et al. [274,275] further developed the MUFTE-UG model [276] to include two phase (gas-liquid) three component (methane-water-air) conditions. This was achieved without an additional mass transfer term in the mass balance but by coupling the mole fraction of methane in the water phase to its gaseous mole fraction using Henry's law which is essentially an equilibrium condition [277].

Falta [278] modified the T2VOC code [279] with a dual-domain approach. The author defined two distinct zones whereby the first zone contains the NAPL and the aqueous phase which is assumed to be at equilibrium. The other zone contains only the aqueous phase and acquires the dissolved solute concentration from the surface of the first zone. The mass flux from this surface is determined with the integral of the analytical solution presented by Hunt et al. [200] which encompasses transverse dispersivity and the length of the NAPL containing zone. The NAPL pool is assumed to be immobile. The main advantage of this modelling approach is the possibility of using coarser grid cells and the reduction of computation times.

Grant & Gerhard [96] used the DNAPL3D code (which solves the immiscible multiphase flow equation for a water-NAPL system) and MT3D sequentially to simulate NAPL dissolution experiments by first simulating DNAPL migration over a time step followed by contaminant transport over the same time step. The authors used three different approaches to simulate interphase mass transfer: i) a local equilibrium approach, ii) a rate-limited mass transfer approach that explicitly accounted for the interfacial area, and iii) a rate-limited mass transfer approach without interfacial area (e.g., a lumped mass transfer approach). In the case of approach ii), the authors determined the interfacial area using the thermodynamics-based approach developed by Grant & Gerhard [165] which considers the area under the P_c-S curve. The mass transfer coefficient was determined from the Peclet number as proposed by Pfannkuch [17]. In the case of lumped rate-limited mass transfer, the mass transfer rate coefficient was determined using the formulation developed by Saba & Illangaskare [105]. The authors reported that the rate-limited mass transfer approach that explicitly accounted for the interfacial area produced the best agreement with the experimental data. It must be noted that this kind of modeling of interphase mass transfer necessitates the choice of an interphase mass transfer coefficient that is independent of the interfacial area. The authors have chosen the formulation of Pfannkuch [17] which is actually adopted from the work of Hoffmann [95]. In this work the dependence of interphase mass transfer coefficient to velocity is only determined for a specific NAPL-water interfacial area meaning that the relationship between interphase mass transfer coefficient and Peclet number is only valid for the particular interfacial area used in the experiment of [95]. Furthermore, in approach ii) the mass transfer rate always increases with interfacial area. However, this assumption is not always true as the

mass transfer depends on the geometry of the entrapped NAPL and the flow field around it. Hence, greater interfacial area in some instances might lead to smaller mass transfer (see section mean grain diameter). Moreover, this method accounts for the meniscus interfacial area only, ignoring the contribution of film interfacial area to interphase mass transfer. Especially in "IWtoMN" interfacial area has been shown to be the dominant contributor of interphase mass transfer (see [81]). Kokkinaki et al. [97] followed a similar methodology and incorporated the interfacial area that is calculated by Grant's method [165] into model developed by Sleep & Sykes [269] to model interphase mass transfer that explicitly accounts for interfacial area. The authors also compared different interphase mass transfer formulations to 3D NAPL dissolution experiment conducted by Zhang et al. [108]. In relevance Kokinnaki et al. [98] developed simplified thermodynamic model and power law model for non-hysteric case by comparing the Grant' s method of interfacial area calculation to saturation parameter that appears as a surrogate for interfacial area in simple Sherwood formulation.

Basu et al. [280] used the UTCHEM code to simulate DNAPL leakage and to conduct tracer tests to be used in their stream tube model. The DNAPL was flushed with water to compare the interphase mass transfer pattern with the stream tube model predictions. UTCHEM enables the use of local equilibrium or a rate limited mass transfer approach with the mass transfer coefficient determined from the formulation developed by Miller et al. [8]. The authors stated that even at high velocities, the use of local equilibrium assumption and the rate limited approach both yielded the same average effluent concentrations. This was attributed to the fact that NAPL architecture is the predominant factor of the non-equilibrium conditions. Basu et al. [281] employed the T2VOC model to investigate how the first and second moments of the flux distribution on a control plane down gradient of the source zone changes with NAPL mass reduction. The mean and standard deviation of the flux distribution was found to decrease with source mass depletion by dissolution. Maji & Sudicky [83] used the Compflow model to simulate DNAPL dissolution using the hydrogeological data set of a real site in Tübingen/Germany whose parameters such as permeability, effective porosity, grain size, mineralogy and sorption coefficients were determined with high resolution. The authors generated 20 realizations of the hydraulic conductivity field using a transition probability/Markov chain (TP/MC) method that uses the Tubingen data for conditioning. 10 different mass transfer formulations were incorporated in the model to determine the interphase mass transfer coefficient (including the formulations of Miller et al., Powers et al., Imhoff et al, Saba & Illangasekare, Geller & Hunt, Nambi & Powers [8,32,105,110,121,256] and 4 other S_n-based models with differing parameters). The authors reported that the model of Saba & Illangasekare and Nambi & Powers [105,121] deviated from others in terms of time required for the dissolution of all the NAPL mass whereas the other formulations culminated in dissolution times similar to the local equilibrium approach. The authors also showed that even after significant NAPL mass reduction (99.99%), the concentrations at a plane located at 10m down-gradient of the source can exceed regulatory targets (i.e., maximum concentration level; MCL). It was also demonstrated that the mass flux / mass reduction relationships emanating from the different realizations may vary vastly which also depends on the mass transfer formulation used. O'Carroll & Sleep [282] simulated hot water flushing of NAPL with the compositional model developed by [269] which assumed local equilibrium conditions. It was demonstrated that increased temperature has significant impact on NAPL mass recovery due to alteration of viscosity yet uncontrolled NAPL downward migration might pose a greater risk at elevated temperatures.

Reitsma & Kueper [62,283] developed the first fully implicit two-phase three-component (cosolvent-water-NAPL) compositional model that simulates cosolvent flushing of PCE (CHEM). The model assumes the fluids to be non-ideal whereby diffusion of one type of molecule is calculated with "Maxwell-Stefan Diffusivity" as a function of the composition of the multi-component fluid. The detailed derivation of the mass flux concept and its relation to the diffusion coefficient is presented in Taylor & Krishna [55]. The phase behavior was determined by Hand's method, which states that equilibrium phase concentrations are straight lines on a log-log plot, because of its practicality. This approach had been also integrated into UTCHEM for surfactants [61]. Interphase mass transfer flux

was defined through the two-film model and the diffusion coefficient in the boundary layer was assumed to be a constant. The interphase mass transfer rate was set to equal to the molar flux times the specific interfacial area:

$$I_i = N_i a \qquad (30)$$

Interfacial area is determined with respect to the saturation of that specific node with use of an equation that ignores the effect of hysteresis, developed from a pore network model [284]. The alteration of interfacial tension with respect to cosolvent content was determined based on the expression proposed by Li & Fu [285] which is also used to scale the relative permeability. The authors fit their simulation to experimental data to determine the film thickness appearing in film model. As mentioned in Section 2, the film model with a hypothetical film thickness does not apply directly to interphase mass transfer in porous media and, therefore, the determined film thickness is only valid for that particular experiment.

Roeder & Falta [286] modified the UTCHEM code for cosolvent-enhanced NAPL recovery and demonstrated that fine meshed heterogeneous 3D domains can simulate unstable flow conditions which may occur during cosolvent flushing of DNAPLs. Fluid viscosities were determined with method of Grunberg whereas interfacial tension alteration as a function of cosolvent content was determined with the Li & Fu method [285]. Liang & Falta [287] used UTCHEM to simulate NAPL dissolution with very high cosolvent content in the flushing solution (% 95 ethanol+ % 5 water) and demonstrated that the rate limited interphase mass transfer behavior vanishes at such high cosolvent contents. Kaye et al. [288] used the same model to investigate the occurrence of over- and under-riding of the NAPL mass for different flushing solutions. Agaoglu et al. [53] simulated cosolvent flushing of multicomponent NAPL using UTCHEM and demonstrated that bypassing of the NAPL mass at intermediate cosolvent contents, which was observed in laboratory experiments conducted by the authors, could not be fully captured by the model. The development of preferential paths and NAPL bypassing was attributed to the mobilization of the NAPL mass residing within the larger pores due to the cosolvent-induced low interfacial tensions even for relatively homogeneous systems. Use of finer 3D meshes did not improve the simulation results because of the difficulty of accurately representing pore scale heterogeneity in the model.

Lingieni & Dhir [289] simulated air sparging of NAPL contaminated soil (“IWtoMN”) by first solving the immiscible multiphase flow equations to determine gas velocity which was then used to simulate the transport of the volatilized contaminant. Interphase mass transfer from NAPL to gas modelled with both equilibrium and a rate limited approach, with the mass transfer coefficient related to the Reynolds and Schmidt numbers. Comparison of model simulations to column experimental results showed that better agreement was obtained with the rate limited approach. Lundegrad & Andersen [145] investigated the radius of influence and air flow path distribution during air sparging with a multiphase flow model initially developed for petroleum reservoir simulations (TETRAD). The development of radius of influence was also investigated by McCray & Falta [146] and Hein et al. [290] using the T2VOC code. These studies focusing on radius of influence were based on air-water system excluding NAPL.

Mclure & Sleep [291] employed the compositional model developed by Sleep & Sykes [269] to investigate the bio-venting of soils to promote contaminant (toluene in this case) biodegradation. The parameters that have significant impact on this type of bio-remedial activity, namely: oxygen distribution in aqueous phase from the injected air, contaminant partitioning into the aqueous phase from the NAPL, contaminant evaporation and extraction through the injected air, were all modelled using a local equilibrium approach. The authors pointed to the difficulty of estimating the interphase mass transfer coefficients and stated that if equilibrium conditions do not exist, contaminant removal would be reduced.

Unger et al. [292] used the Compflow model to simulate air sparging of soil contaminated with a DNAPL. It was reported that at early stages recovery is high due to direct contact of NAPL with air flow-paths and direct vaporization. However, after this initial stage the recovery decreases and is controlled by the NAPL dissolution rate into the aqueous phase because contaminants must first dissolve into the aqueous phase and subsequently must travel to the air flow-paths for eventual recovery. Thomson & Johnson [137] showed that multiphase flow models may not be capable of accurately predicting mass recovery estimates from air sparging activities due to the emergence of discrete capillaries leading to the formation of channels which are not accounted for in continuum-based models unless a very fine discretized grid is used which in practice is not possible. The presence of these channels is attributed to the formation of viscous fingering when air flows in a water-saturated medium and its sensitivity to pore scale heterogeneity. Yoon et al. [293] incorporated the rate limited mass transfer formulation of Miller et al. [8] to the STOMP model to investigate the impact of non-equilibrium conditions on soil vapour extraction applications. Jang & Aral [139] also used rate limited mass transfer approach in a multiphase flow model to investigate the impact of different design parameters of air sparging such as injection rate, under various site conditions.

Xu et al. [294] considered the simulation of CO_2 into a deep sandstone aquifer and its immobilization through carbonate precipitation. In this flow configuration the CO_2 is the mobile non-wetting phase that dissolves into the groundwater (i.e., "MNtoIW"). The model was based on the computer code TOUGHREACT which is a part of the TOUGH2 suite of programs [295]. TOUGHREACT first solves the multiphase flow equation to determine phase velocities and uses this information in the reactive transport equation. The TOUGHREACT code assumes equilibrium partitioning of constituents between phases. To date non-equilibrium interphase mass transfer has not been used in CO_2 simulations.

CO_2 injection in the subsurface involves high pressures and concentrations gradients resulting in significant convective mixing. Thiebeau & Dutin [296] used the computer code Eclipse to investigate the impact of convective mixing on a large field scale study (i.e., on the orders of kilometres). The computational grid used in this study was 10 m in the vertical direction. The authors stated that convective mixing (which is a result of density difference between two locations) and its influence on interphase mass transfer cannot be captured when such relatively large computational grids are employed. The authors attempted to overcome this problem by upscaling the diffusion coefficient of CO_2 in aqueous phase to represent convective mixing.

Enouy et al. [93] used the Compflow model to simulate column experiments involving injection of aqueous phase supersaturated with CO_2 (i.e., "MWtoIN"). Injection of aqueous phase supersaturated with CO_2 has been recently investigated as a potential surrogate to air sparging activities to extract NAPL within exsolution gas or to promote biodegradation if oxygen is chosen as injected solute. The potential of this procedure was stated to lie in the more distributed gas formation in comparison to air sparging at least in the gas exsolution region because the flow paths in air sparging are highly dependent on the pore scale capillary pressure heterogeneity. The authors modelled the partitioning of CO_2 from the supersaturated aqueous solution to the gas phase which emerges as nucleation, based on the mass transfer coefficient adopted from the formulations of Nambi & Powers and Unger et al. [35,103].

Recently Niessner & Hassanizadeh [3,297] modeled the multiphase flow approach presented by Hassanizadeh & Gray [169,298] that also incorporates the mass balance of specific interfacial area. The time evolution of the interfacial area was set equal to the interfacial area production rate, E_{WN}, minus the advective transport of interfacial area. This latter term is set equal to the interfacial area permeability times the gradient of interfacial area which is related to the gradient of Gibbs free energy. The parameter "E_{WN}" was determined from:

$$E_{wn}(S_w, P_c) = e_{wn}(S_w, P_c) \cdot \frac{\partial S_w}{\partial t} \qquad (31)$$

e_{wn} is the strength of change in specific interfacial area determined by linear interpolation between its two limits which is determined based on the assumption that those limits occur at the beginning and end of drainage.

The authors simulated a case where the non-wetting phase was injected into the porous media saturated with the wetting phase (e.g., drainage). Interphase mass transfer between the wetting and non-wetting phases was also incorporated in the model. The interphase mass flux was expressed in terms of the mole fractions with the interphase mass transfer coefficient derived based on the film layer theory. However, this approach is not suitable for an REV based model as film thickness (in this work named as diffusion length) is not a known parameter for a computational node of REV based model. It is a function of the various properties of the porous media as has been described in this Section 2 and 3. As a result the authors defined this parameter as a fit parameter. The constitutive function between capillary pressure – saturation – interfacial area incorporated in the model was the one developed from the pore network model of Joeker-Niasar et al. [172]. The dissolution from the immobile wetting phase into the non-wetting phase (i.e., "IWtoMN") occurs mainly from film interfacial area as reported by [81,87,241]. However this pore network model did not account for the film interfacial area.

Recently multiscale modeling of multiphase flow in porous media was presented by Jackson et al. [299] which formulates the mass, momentum and energy balances over the volumes, interfacial areas and common curves with constraints arising from entropy inequality, the second law of thermodynamics and other equilibrium thermodynamics relations [300]. The multiphase system considered in this approach is immiscible [301].

5. Summary and conclusions

This review paper examines the factors influencing interphase mass transfer in porous media and the mathematical models developed to analyze this process. The large volume of studies reviewed in this manuscript attests to the significance of interphase mass transfer in porous media in various applications and the challenges encountered in characterizing this process. Because of the significance of scales on the apparent interphase mass transfer, we have framed this review according to the length scales of the reviewed studies, namely: the pore-scale, meso, and field scales. The characteristics of the multiphase flow regime in porous media is another important factor that influences interphase mass transfer. Hence, to gain further insight, published studies were also discussed in terms of five flow configurations defined based on the mobility and wettability of the phases (Table 1). The review also surveys various mathematical models that have been developed for the analysis and simulation of interphase mass transfer in porous media, particularly those relating to the dissolution of NAPLs into the surrounding flow.

Published studies have shown that the interphase mass transfer is influenced by a number of key parameters in a complex manner. Identifying these relationships is essential for further improvement in our understanding of and ability to model mass transfer. Foremost among these parameters is the interfacial area separating the interphases within the porous media. Recent technological advances in non-invasive imaging are promising in identifying the pore space geometry and phase distributions within. Such accurate determination of the interfacial area can potentially be incorporated into REV-based models and other modelling efforts where the lack of precise control on the interfacial area and how it varies with time is cited as a key factor contributing to uncertainties in model prediction. However, reported data clearly indicates that the relationship between the interfacial area and mass transfer rate is quite complex. For example; in case of residual NAPL, the porous medium with smaller

median grain size generally leads to greater specific interfacial area. However, the generation of multi-pore blobs within finer medium induces stagnant regions around the interfacial domains, bringing about smaller mass transfer rates in comparison to coarser media where the specific interfacial area is smaller but with less stagnation regions.

In a related issue no REV-based model to date has attempted to incorporate separately the film and meniscus area data into the mass transfer term. The main reason for that is the difficulty in determining the distribution of the flow rates of the mobile phase within the film and meniscus areas of discrete pore throats. One promising avenue for future research is pore network modelling which can be used to efficiently evaluate the impact of different trapped phase configurations on interphase mass transfer for different realizations of pore sizes.

The pore space and the variance between pore sizes/throats have been shown to have a significant impact on interphase mass flux through their influence on different parameters and mechanisms such as interfacial areas, entrapment, and flow field. Some authors have used the uniformity coefficient to account for the impact of pore size distribution in phenomenological models. However using the uniformity coefficient as a surrogate for the pore size distribution might not always be correct, as in some situations big pores may be filled with smaller grains meaning that pore space is mostly determined by the smaller grains. Non-invasive techniques for the observation of porous media with different uniformity coefficients and pore space may shed further light on the correlation between uniformity coefficients and pore size distribution.

Wettability of the porous medium is another important parameter influencing interphase mass transfer as it has significant implications on a number of parameters, most notably the flow paths and interfacial domains. The impact of wettability on the pore-scale phase distribution especially in partially oil-wet media is still lacking. Moreover, the potential alteration of wettability with the factors influencing this mechanism needs further investigation, especially in relation to NAPL remediation activities. Most models ignore the impact of wettability because of the lack of reliable information on its influence even though the significance of wettability on multiphase flow and interphase mass flux is acknowledged. Besides wettability, the impact of aging, ionic strength and temperature are mostly ignored in existing models even though they may have significant impact on mass transfer.

Flow instability is another important parameter that can have major implication on interphase mass transfer. The formation of instabilities has direct influence on interphase mass flux through their influence on interfacial areas and flow paths. Modeling efforts have shown that REV-based multiphase flow models are generally unable to simulate discrete capillaries that arise in viscous fingering due to the variance in pore sizes. The incorporation of spatially variable parameters defined on three-dimensional, fine computational grids can partially address this issue but at a large computational cost and up to a limited extent because discrete pore throats are much smaller than the smallest possible mesh.

There is suggestion in the literature that the mobilization of NAPL entrapped in porous media may also influence the mass transfer characteristics. Recently mobilization of the trapped blobs which are reduced in size due to dissolution has been depicted by non-invasive methods. Micro-models may be used to capture this process and to provide some data to quantify this mass transfer mechanism. In groundwater remediation applications miscibility-enhancing agents can be used at intermediate contents whereby the interfacial tension is sufficiently reduced to cause some of the entrapped NAPL, particularly entrapped in larger pores, to be mobilized and lead to development preferential flow paths similar to dissolution fingering. Most efforts to predict enhanced NAPL recovery have relied on equilibrium assumptions or have used mass transfer expressions that are originally developed for water-NAPL interphases. More broadly, there is a need to develop specific studies that address interphase mass transfer during enhanced NAPL recovery

In this review we referred to a large number of phenomenological models that have attempted to relate the interphase mass transfer to key operational parameters. These models are generally deduced from meso-scale based experiments with limited information on pore scale processes. Although these models provide insight into the factors influencing interphase mass transfer and are useful as a predictive tool, it is important to note that the predictions of these different models are in some instances inconsistent with each other even when the same input parameters are used (see; [82,83,89,98,102–108]). This is mostly attributed to differences in the specific experimental conditions used in developing these models. Further detailed studies that can isolate the impacts of each parameter are needed to develop more generally applicable interphase mass transfer correlations. In particular, the combination of meso-scale studies along with accurate pore-scale characterization of the porous media and the multiphase system via non-invasive methods and pore scale models may be an optimal avenue for further progress in the effort towards the development of generalized, accurate and robust Sherwood formulations that can be incorporated in REV-based models. Pore network models are especially useful in providing detailed information of the porous medium and flow that can be incorporated into these expressions, while non-invasive characterization techniques can provide testing of the assumptions used to develop pore network model. Attempts to incorporate more physics-based processes into Sherwood formulations, which have been mostly derived from empirical data, is one promising avenue for future research.

A salient feature of field scale applications is the complex spatial structure of the permeability field and the NAPL distribution and, due to limited data, the lack of complete knowledge of these properties. The challenges observed at the field has led in some instances to the use of REV based numerical models to investigate field scale NAPL dissolution behavior. In a recent study it has been shown that the use of different mass transfer formulations for a well characterized aquifer results in different NAPL depletion times [83] whereas others stated that the difference is insignificant [37]. In many field cases, NAPL contamination are several decades old and to a large extent, the accessible residual NAPLs have already been depleted, with the remaining NAPL existing mostly in the form of pools. In modeling of such conditions, the use of local equilibrium in a grid block of an REV based model that contain NAPL may be viable as they are likely to contain more NAPL than the threshold saturation that leads to achievement of solubility. However, further work is needed to evaluate the impact of dissolution of the inaccessible NAPLs on overall field scale dissolution performance, once they reduce below residual levels. The development of more precise mass transfer formulations that can be used in REV based numerical models specifically applied to field applications will allow for the more accurate evaluation and prediction of NAPL behavior in the field.

In summary, it is evident that interphase mass transfer in porous media is a result of the complex, dynamic multiphase flow occurring within porous media. It is equally evident that significant progress has been achieved in recent decades to better understand this critical process. This review shows that interphase mass transfer is governed by both pore scale characteristics of the multiphase system, such as wettability and pore size distributions, as well as large scale flow attributes such as NAPL bypassing due to porous media heterogeneities at the field scale. Interphase mass transfer is the results of interplay of all these factors. Therefore, further work must set sights on the characterization of the pore scale system and how it relates to the interphase mass transfer. Equally important, research efforts must also attempt to develop robust means of representing the larger scale dynamic nature of multiphase flow field within the porous medium and its influence on the interfacial fluid contact and mass transfer.

References

[1] Abriola LM. Modeling multiphase migration of organic chemicals in groundwater systems--a review and assessment. Environ Health Perspect 1989;83:117–43.

[2] Yiotis AG, Stubos AK, Boudouvis AG, Yortsos YC. A 2-D pore-network model of the drying of single-component liquids in porous media. Adv Water Resour 2001;24:439–60. doi:10.1016/S0309-1708(00)00066-X.

[3] Niessner J, Hassanizadeh SM. Modeling kinetic interphase mass transfer for two-phase flow in porous media including fluid–fluid interfacial area. Transp Porous Media 2009;80:329–44. doi:10.1007/s11242-009-9358-5.

[4] Joekar-Niasar V, Hassanizadeh SM. Analysis of Fundamentals of Two-Phase Flow in Porous Media Using Dynamic Pore-Network Models: A Review. Crit Rev Environ Sci Technol 2012;42:1895–976. doi:10.1080/10643389.2011.574101.

[5] Mercer J, Cohen R. A review of immiscible fluids in the subsurface: Properties, models, characterization and remediation. J Contam Hydrol 1990;6.

[6] Dwivedi PN, Upadhyay SN. Particle-fluid mass transfer in fixed and fluidized beds. Ind Eng Chem … 1977;16:157–65.

[7] Lake WL. Enhanced oil recovery. Prentice-Hall, Englewood Cliffs, NJ 1989.

[8] Miller CT, Poirier-McNeill MM, Mayer AS. Dissolution of trapped nonaqueous phase liquids: Mass transfer characteristics. Water Resour Res 1990;26:2783–96.

[9] Powers SE, Abriola LM, Weber WJ. An experimental investigation of nonaqueous phase liquid dissolution in saturated subsurface systems: Steady state mass transfer rates. Water Resour Res 1992;28:2691–705.

[10] Miller CT, Christakos G, Imhoff PT, McBride JF, Pedit JA, Trangenstein JA. Multiphase flow and transport modeling in heterogeneous porous media: challenges and approaches. Adv Water Resour 1998;21:77–120. doi:10.1016/S0309-1708(96)00036-X.

[11] Christ JA, Ramsburg CA, Pennell KD, Abriola LM. Estimating mass discharge from dense nonaqueous phase liquid source zones using upscaled mass transfer coefficients: An evaluation using multiphase numerical simulations. Water Resour Res 2006;42:n/a–n/a. doi:10.1029/2006WR004886.

[12] Anslyn E V. Physical organic chemistry. Univ Sci Books 2006.

[13] Schwarzenbach RP, Gschwend PM, Imboden DM. Environmental organic chemistry. John Wiley Sons 2005.

[14] Israelachvilli J. Intermolecular and Surface Forces. ForcesAcademic Press Inc" San Diego 1992.

[15] Zumdahl SS, J DD. Chemical principles. Chem Princ Cengage Learn 2011.

[16] Weber WJ, McGinley PM, Katz LE. Sorption phenomena in subsurface systems: Concepts, models and effects on contaminant fate and transport. Water Res 1991;25:499–528.

[17] Pfannkuch H. Determination of the contaminant source strength from mass exchange processes at the petroleum-ground-water interface in shallow aquifer systems. Water Well Assoc Am Pet Inst Houston, Tex 1984.

[18] Baehr HD, Stephan K. Heat and Mass Transfer. Berlin, Heidelberg: Springer Berlin Heidelberg; 2006. doi:10.1007/3-540-29527-5.

[19] Whitman W. Gas transfer to and across an airtwater interface. Chem Metall Eng 1923;29:146–8.

[20] Deacon E. L. Gas transfer to and across an airtwater interface. Tellus 1977;29:363–84.

[21] Cussler EL. Diffusion: mass transfer in fluid systems. Cambridge university press; 2009.

[22] Clark MM. Transport Modeling for Environmental Engineers and Scientists. Wiley Interscience; 1996.

[23] Frössling N. Über die Verdunstung fallender Tropfen. Gerlands Beitrage Zur Geophys 1938.

[24] Ranz W, Marshall W. Evaporation from drops. Chem Eng Prog 1952.

[25] Friedlander SK. Mass and heat transfer to single spheres and cylinders at low Reynolds numbers. AIChE J 1957;3:43–8. doi:10.1002/aic.690030109.

[26] Dobry R, Finn RK. Mass transfer to a cylinder at low Reynolds numbers. Ind Eng Chem 1956:540–3.

[27] Kusik CL, Happel J. Boundary Layer Mass Transport with Heterogeneous Catalysis. Ind Eng Chem Fundam 1962;1:163–72. doi:10.1021/i160003a002.

[28] Williamson JE, Bazaire KE, Geankoplis CJ. Liquid-phase mass transfer at low Reynolds numbers. Ind Eng Chem Fundam 1963;249:0–3.

[29] Pfeffer R, Happel J. An analytical study of heat and mass transfer in multiparticle systems at low Reynolds numbers. AIChE J 1964;10:605–11.

[30] Wilson EJ, Geankoplis CJ. Liquid Mass Transfer at Very Low Reynolds Numbers in Packed Beds. Ind Eng Chem Fundam 1966;5:9–14. doi:10.1021/i160017a002.

[31] Van der Waarden M, Bridie ALAM, Groenewoud WM. Transport of mineral oil components to groundwater—I. Water Res 1971;5:213–26. doi:10.1016/0043-1354(71)90054-6.

[32] Imhoff PT, Jaffé PR, Pinder GF. An experimental study of complete dissolution of a nonaqueous phase liquid in saturated porous media. Water Resour Res 1994;30:307–20.

[33] Genuchten M Van, Alves W. Analytical solutions of the one-dimensional convective-dispersive solute transport equation 1982.

[34] Powers SE, Loureiro CO, Abriola LM, Weber WJ. Theoretical study of the significance of nonequilibrium dissolution of nonaqueous phase liquids in subsurface systems. Water Resour Res 1991;27:463–77. doi:10.1029/91WR00074.

[35] Nambi IM, Powers SE. Mass transfer correlations for nonaqueous phase liquid dissolution from regions with high initial saturations. Water Resour Res 2003;39:n/a–n/a. doi:10.1029/2001WR000667.

[36] Schnaar G, Brusseau ML. Characterizing pore-scale dissolution of organic immiscible liquid in natural porous media using synchrotron X-ray microtomography. Environ Sci Technol 2006;40:6622–9.

[37] Parker JC, Park E. Modeling field-scale dense nonaqueous phase liquid dissolution kinetics in heterogeneous aquifers. Water Resour Res 2004;40:n/a–n/a. doi:10.1029/2003WR002807.

[38] Held RJ, Celia MA. Pore-scale modeling and upscaling of nonaqueous phase liquid mass transfer. Water Resour Res 2001;37:539–49.

[39] Setchenow M. Action de l'acide carbonique sur les solutions des sels a acides forts. Ann Chim Phys 1892;25.

[40] Lesage S, Brown S. Observation of the dissolution of NAPL mixtures. J Contam Hydrol 1994;15:57–71.

[41] Almeida MB, Alvarez AM, Miguel EMD, Hoyo ESD. Setchenow coefficients for naphthols by distribution method. Can J Chem 1983;61:244–8. doi:10.1139/v83-043.

[42] Imhoff PT, Frizzell A, Miller CT. Evaluation of thermal effects on the dissolution of a nonaqueous phase liquid in porous media. Environ Sci Technol 1997;31:1615–22.

[43] Horvath AL. Halogenated hydrocarbons: solubility-miscibility with water. CRC Press 1982.

[44] Tyn MT, Calus WF. Diffusion coefficients in dilute binary liquid mixtures. J Chem Eng Data 1975;20:106–9. doi:10.1021/je60064a006.

[45] Javaheri M, Abedi J, Hassanzadeh H. Linear Stability Analysis of Double-Diffusive Convection in Porous Media, with Application to Geological Storage of CO2. Transp Porous Media 2009;84:441–56. doi:10.1007/s11242-009-9513-z.

[46] Aydin GA, Agaoglu B, Kocasoy G, Copty NK. Effect of temperature on cosolvent flooding for the enhanced solubilization and mobilization of NAPLs in porous media. J Hazard Mater 2011;186:636–44. doi:10.1016/j.jhazmat.2010.11.046.

[47] Conrad SH, Wilson JL, Mason WR, Peplinski WJ. Visualization of residual organic liquid trapped in aquifers. Water Resour Res 1992;28:467–78. doi:10.1029/91WR02054.

[48] Borden RC, Piwoni MD. Hydrocarbon dissolution and transport: A comparison of equilibrium and kinetic models. J Contam Hydrol 1992;10:309–23.

[49] Mukherji S, Peters CA, Weber WJ. Mass Transfer of Polynuclear Aromatic Hydrocarbons from Complex DNAPL Mixtures. Environ Sci Technol 1997;31:416–23. doi:10.1021/es960227n.

[50] Luthy RG, Ramaswami A, Ghoshai S, Merkel W. Interfacial films in coal tar nonaqueous-phase liquid-water systems. Environ Sci Technol 1993:2914–8.

[51] Denekas MO, Carlson FT, Moore JW, Dodd CG. Materials Adsorbed at Crude Petroleum-Water Interfaces. Isolation and Analysis of Normal Paraffins of High Molecular Weight. Ind Eng Chem 1951;43:1165–9.

[52] Oostrom M, Dane JH, Wietsma TW. A Review of Multidimensional, Multifluid Intermediate-Scale Experiments. Vadose Zo J 2006;5:570. doi:10.2136/vzj2005.0125.

[53] Agaoglu B, Scheytt T, Copty NK. Laboratory-scale experiments and numerical modeling of cosolvent flushing of multi-component NAPLs in saturated porous media. J Contam Hydrol 2012.

[54] Jawitz JW, Dai D, Rao PSC, Annable MD, Rhue RD. Rate-limited solubilization of multicomponent nonaqueous-phase liquids by flushing with cosolvents and surfactants: modeling data from laboratory and field experiments. Environ Sci Technol 2003;37:1983–91.

[55] Taylor R, Krishna R. Multicomponent mass transfer. New York: Wiley; 1993.

[56] Kooijman H, Taylor R. Estimation of diffusion coefficients in multicomponent liquid systems. Ind Eng Chem Res 1991;30:1217–22.

[57] Imhoff PT, Gleyzer SN, Mcbride JF, Vancho LA, Okuda I, Miller CT. Cosolvent-enhanced remediation of residual dense nonaqueous phase liquids: Experimental investigation. Environ Sci Technol 1995;29:1966–76.

[58] Abrams DS, Prausnitz JM. Statistical Thermodynamics of Liquid Mixtures: A New Expression for the Excess Gibbs Energy of Partly or Completely Miscible Systems. AIChE J 1975;21:116–28.

[59] Lee KY, Peters CA. UNIFAC Modeling of Cosolvent Phase Partitioning in Nonaqueous Phase Liquid-Water Systems. J Environ Eng 2004;130:478–83.

[60] Hand D. Dineric distribution. J Phys Chem 1930.

[61] Delshad M. UTCHEM Version 6. 1 technical documentation. Austin, Texas Cent Pet Geosys-Tems Eng Univ Texas Austin 1997.

[62] Reitsma S, Kueper BH. Non-equilibrium alcohol flooding model for immiscible phase remediation: 1. Equation development. Adv Water Resour 1998;21:649–62.

[63] Chang YC, Moulton RW. Quternary Liquid Systems with Two Immiscible Liquid Pairs. Ind Eng Chem 1953:2350–61.

[64] Yalkowsky SH. Solubility and solubilization in aqueous media. Oxford Univ Press 1999.

[65] Brandes D, Farley KJ. Importance of phase behavior on the removal of residual DNAPLs from porous media by alcohol flooding. Water Environ Res 1993;65:869–78.

[66] Hayden NJ, Van der Hoven E. Alcohol flushing for enhanced removal of coal tar from contaminated soils. Water Environ Res 1996;68:1165–71.

[67] Ramakrishnan V, Ogram A V, Lindner AS. Impacts of co-solvent flushing on microbial populations capable of degrading trichloroethylene. Environ Health Perspect 2005;113:55–61. doi:10.1289/ehp.6937.

[68] Abdul AS, Gibson TL, Devi NR. Selection of surfactants for the removal of petroleum products from shallow sandy aquifers. Ground Water 1990;28:920–6.

[69] Fortin J, Jury WA, Anderson MA. Enhanced removal of trapped non-aqueous phase liquids from saturated soil using surfactant solutions. J Contam Hydrol 1997;24:247–67.

[70] Carroll BJ. The kinetics of solubilization of nonpolar oils by nonionic surfactant solutions. J Colloid Interface Sci 1981;79:126–135.

[71] Grimberg SJ, Nagel J, Aitken MD. Kinetics of phenanthrene dissolution into water in the presence of nonionic surfactants. Environ Sci Technol 1995;29:1480–7.

[72] Zhong L, Mayer AS, Pope GA. The effects of surfactant formulation on nonequilibrium NAPL solubilization. J Contam Hydrol 2003;60:55–75.

[73] St-Pierre C, Martel R, Gabriel U, Lefebvre R, Robert T, Hawari J. TCE recovery mechanisms using micellar and alcohol solutions: phase diagrams and sand column experiments. J Contam Hydrol 2004;71:155–92. doi:10.1016/j.jconhyd.2003.09.010.

[74] Abriola LM, Dekker TJ, Pennell KD. Surfactant-enhanced solubilization of residual dodecane in soil columns. 2. mathematical modeling. Environ Sci Technol 1993;27:2332–40.

[75] Johnson JC, Sun S, Jaffe PR. Surfactant enhanced perchloroethylene dissolution in porous media: The effect on mass transfer rate coefficients. Environ Sci Technol 1999;33:1286–92.

[76] Mayer AS, Zhong LR, Pope GA. Measurement of mass-transfer rates for surfactant-enhanced solubilization of nonaqueous phase liquids. Environ Sci Technol 1999;33:2965–72.

[77] Zimmerman JB, Kibbey TCG, Cowell MA, Hayes KF. Partitioning of Ethoxylated Nonionic Surfactants into Nonaqueous-Phase Organic Liquids: Influence on Solubilization Behavior. Environ Sci Technol 1999;33:169–76.

[78] Sharmin R, Ioannidis MA, Legge RL. Effect of nonionic surfactant partitioning on the dissolution kinetics of residual perchloroethylene in a model porous medium. J Contam Hydrol 2006;82:145–64. doi:10.1016/j.jconhyd.2005.10.001.

[79] Lee DH, Cody RD, Hoyle EL. Laboratory evaluation of the use of surfactants for ground water remediation and the potential for recycling them. Ground Water Monit Remediat 2001.

[80] Park S-K, Bielefeldt AR. Equilibrium partitioning of a non-ionic surfactant and pentachlorophenol between water and a non-aqueous phase liquid. Water Res 2003;37:3412–20. doi:10.1016/S0043-1354(03)00237-9.

[81] Sahloul NA, Ioannidis MA, Chatzis I. Dissolution of residual non-aqueous phase liquids in porous media: pore-scale mechanisms and mass transfer rates. Adv Water Resour 2002;25:33–49. doi:10.1016/S0309-1708(01)00025-2.

[82] Dillard LA, Blunt MJ. Development of a pore network simulation model to study nonaqueous phase liquid dissolution. Water Resour Res 2000;36:439–54.

[83] Maji R, Sudicky EA. Influence of mass transfer characteristics for DNAPL source depletion and contaminant flux in a highly characterized glaciofluvial aquifer. J Contam Hydrol 2008;102:105–19. doi:10.1016/j.jconhyd.2008.08.005.

[84] Kim H, Rao PSC, Annable MD. Gaseous tracer technique for estimating air–water interfacial areas and interface mobility. Soil Sci Soc . 1999:1554–60.

[85] Costanza-Robinson MS, Brusseau ML. Air-water interfacial areas in unsaturated soils: Evaluation of interfacial domains. Water Resour Res 2002;38:13–1–13–7. doi:10.1029/2001WR000738.

[86] Costanza-Robinson MS, Harrold KH, Lieb-Lappen RM. X-ray microtomography determination of air− water interfacial area− water saturation relationships in sandy porous media. Environ Sci Technol 2008:2949–56.

[87] Zhao W, Ioannidis MA. Pore network simulation of the dissolution of a single-component wetting nonaqueous phase liquid. Water Resour Res 2003;39:n/a–n/a. doi:10.1029/2002WR001861.

[88] Bradford SA, Vendlinski RA, Abriola LM. The entrapment and long-term dissolution of tetrachloroethylene in fractional wettability porous media. Water Resour Res 1999;35:2955–64. doi:10.1029/1999WR900178.

[89] Dillard LA, Essaid HI, Blunt MJ. A functional relation for field-scale nonaqueous phase liquid dissolution developed using a pore network model. J Contam Hydrol 2001;48:89–119.

[90] Leonenko Y, Keith DW. Reservoir engineering to accelerate the dissolution of CO2 stored in aquifers. Environ Sci Technol 2008;42:2742–7.

[91] Taku Ide S, Jessen K, Orr FM. Storage of CO2 in saline aquifers: Effects of gravity, viscous, and capillary forces on amount and timing of trapping. Int J Greenh Gas Control 2007;1:481–91. doi:10.1016/S1750-5836(07)00091-6.

[92] Zhao W, Ioannidis MA. Gas exsolution and flow during supersaturated water injection in porous media: I. Pore network modeling. Adv Water Resour 2011;34:2–14. doi:10.1016/j.advwatres.2010.09.010.

[93] Enouy R, Li M, Ioannidis MA, Unger AJ a. Gas exsolution and flow during supersaturated water injection in porous media: II. Column experiments and continuum modeling. Adv Water Resour 2011;34:15–25. doi:10.1016/j.advwatres.2010.09.013.

[94] Powers SE, Abriola LM, Dunkin JS, Weber WJ. Phenomenological models for transient NAPL-water mass-transfer processes. J Contam Hydrol 1994;16:1–33.

[95] Hoffmann B. Über die ausbreitung gelöster kohlenwasserstoffe im grundwasserleiter. Inst F Wasserwirtschaft U Landwirtschaftl Wasserbau D Techn Univ 1969.

[96] Grant GP, Gerhard JI. Simulating the dissolution of a complex dense nonaqueous phase liquid source zone: 2. Experimental validation of an interfacial area-based mass transfer model. Water Resour Res 2007;43:n/a–n/a. doi:10.1029/2007WR006039.

[97] Kokkinaki A, O'Carroll DM, Werth CJ, Sleep BE. Coupled simulation of DNAPL infiltration and dissolution in three-dimensional heterogeneous domains: Process model validation. Water Resour Res 2013;49:7023–36. doi:10.1002/wrcr.20503.

[98] Kokkinaki A, O'Carroll DM, Werth CJ, Sleep BE. An evaluation of Sherwood-Gilland models for NAPL dissolution and their relationship to soil properties. J Contam Hydrol 2013;155:87–98. doi:10.1016/j.jconhyd.2013.09.007.

[99] Mayer AS, Miller CT. The influence of mass transfer characteristics and porous media heterogeneity on nonaqueous phase dissolution. Water Resour Res 1996;32:1551–67. doi:10.1029/96WR00291.

[100] Zhou D, Dillard LA, Blunt MJ. A physically based model of dissolution of nonaqueous phase liquids in the saturated zone. Transp Porous Media 2000:227–55.

[101] Chrysikopoulos C V, Kim TJ. Local mass transfer correlations for nonaqueous phase liquid pool dissolution in saturated porous media. Transp Porous Media 2000:167–87.

[102] Baldwin CA, Gladden LF. NMR Imaging of nonaqueous-phase liquid dissolution in a porous medium. AIChE J 1996;42:1341–9. doi:10.1002/aic.690420514.

[103] Unger AJ., Forsyth P., Sudicky E. Influence of alternative dissolution models and subsurface heterogeneity on DNAPL disappearance times. J Contam Hydrol 1998;30:217–42. doi:10.1016/S0169-7722(97)00041-7.

[104] Bradford SA, Phelan TJ, Abriola LM. Dissolution of residual tetrachloroethylene in fractional wettability porous media: correlation development and application. J Contam Hydrol 2000;45:35–61. doi:10.1016/S0169-7722(00)00118-2.

[105] Saba T, Illangasekare TH. Effect of groundwater flow dimensionality on mass transfer from entrapped nonaqueous phase liquid contaminants. Water Resour Res 2000;36:971–9. doi:10.1029/1999WR900322.

[106] Zhu J, Sykes J. The influence of NAPL dissolution characteristics on field-scale contaminant transport in subsurface. J Contam Hydrol 2000;41:133–54. doi:10.1016/S0169-7722(99)00064-9.

[107] Marble JC, DiFilippo EL, Zhang Z. Application of a lumped-process mathematical model to dissolution of non-uniformly distributed immiscible liquid in heterogeneous porous media. J Contam Hydrol 2008;100:1–10. doi:10.1016/j.jconhyd.2008.04.003.

[108] Zhang C, Yoon H, Werth CJ, Valocchi AJ, Basu NB, Jawitz JW. Evaluation of simplified mass transfer models to simulate the impacts of source zone architecture on nonaqueous phase liquid dissolution in heterogeneous porous. J Contam Hydrol 2008;102:49–60. doi:10.1016/j.jconhyd.2008.05.007.

[109] Zilliox L, Muntzer P, Menanteau J. Probleme de l'echange entre un produit petrolier immobile et l'eau en mouvement dans un milieu poreux. Rev IFP 1973;28:185–200.

[110] Powers SE, Abriola LM, Weber WJ. An experimental investigation of nonaqueous phase liquid dissolution in saturated subsurface systems: Transient mass transfer rates. Water Resour Res 1994;30:321–32.

[111] Culligan KA, Wildenschild D, Christensen BSB, Gray WG, Rivers ML. Pore-scale characteristics of multiphase flow in porous media: A comparison of air–water and oil–water experiments. Adv Water Resour 2006;29:227–38. doi:10.1016/j.advwatres.2005.03.021.

[112] Brusseau ML, DiFilippo EL, Marble JC, Oostrom M. Mass-removal and mass-flux-reduction behavior for idealized source zones with hydraulically poorly-accessible immiscible liquid. Chemosphere 2008;71:1511–21. doi:10.1016/j.chemosphere.2007.11.064.

[113] Voudrias EA, Yeh MF. Dissolution of a toluene pool under constant and variable hydraulic gradients with implications for aquifer remediation. Ground Water 1994.

[114] Whelan MP, Voudrias EA, Pearce A. DNAPL pool dissolution in saturated porous media: procedure development and preliminary results. J Contam Hydrol 1994;15:223–37. doi:10.1016/0169-7722(94)90026-4.

[115] Anderson M, RL J, Pankow J. Dissolution of dense chlorinated solvents into groundwater. 3. Modeling contaminant plumes from fingers and pools of solvent. Environ Sci Technol 1992.

[116] Imhoff PT, Miller CT. Dissolution Fingering During the Solubilization of Nonaqueous Phase Liquids in Saturated Porous Media: 1. Model Predictions. Water Resour Res 1996;32:1919–28. doi:10.1029/96WR00602.

[117] Imhoff PT, Thyrum GP, Miller CT. Dissolution Fingering During the Solubilization of Nonaqueous Phase Liquids in Saturated Porous Media: 2. Experimental Observations. Water Resour Res 1996;32:1929–42. doi:10.1029/96WR00601.

[118] Imhoff PT, Farthing MW, Gleyzer SN, Miller CT. Evolving interface between clean and nonaqueous phase liquid (NAPL)-contaminated regions in two-dimensional porous media. Water Resour Res 2002;38.

[119] Seyedabbasi MA, Farthing MW, Imhoff PT, Miller CS. The influence of wettability on NAPL dissolution fingering. Adv Water Resour 2008;31:1687–96. doi:10.1016/j.advwatres.2008.08.003.

[120] Brusseau ML, Nelson NT, Oostrom M, Zhang Z, Johnson GR, Wietsma TW. Influence of heterogeneity and sampling method on aqueous concentrations associated with NAPL dissolution. Environ Sci Technol 2000:3657–64.

[121] Nambi IM, Powers SE. NAPL dissolution in heterogeneous systems: an experimental investigation in a simple heterogeneous system. J Contam Hydrol 2000;44:161–84. doi:10.1016/S0169-7722(00)00095-4.

[122] Zhang C, Werth CJ, Webb AG. Characterization of NAPL Source Zone Architecture and Dissolution Kinetics in Heterogeneous Porous Media Using Magnetic Resonance Imaging. Environ Sci Technol 2007;41:3672–8.

[123] Page JWE, Soga K, Illangasekare T. The significance of heterogeneity on mass flux from DNAPL source zones: an experimental investigation. J Contam Hydrol 2007;94:215–34. doi:10.1016/j.jconhyd.2007.06.004.

[124] Frind EO, Molson JW, Schirmer M, Guiger N. Dissolution and mass transfer of multiple organics under field conditions: The Borden emplaced source. Water Resour Res 1999;35:683–94.

[125] Zhu J, Sykes JF. Simple screening models of NAPL dissolution in the subsurface. J Contam Hydrol 2004;72:245–58. doi:10.1016/j.jconhyd.2003.11.002.

[126] Jawitz JW, Annable MD, Rao PS. Miscible fluid displacement stability in unconfined porous media: J Contam Hydrol 1998;31:211–30.

[127] Ramsburg CA, Pennell KD. Density-modified displacement for DNAPL source zone remediation: density conversion and recovery in heterogeneous aquifer cells. Environ Sci Technol 2002;36:3176–87.

[128] Lunn SRD, Kueper BH. Manipulation of density and viscosity for the optimization of DNAPL recovery by alcohol flooding. J Contam Hydrol 1999;38:427–45.

[129] Martel R, Gelinas PJ, Desnoyers JE. Aquifer washing by micellar solutions: 1 Optimization of alcohol-surfactant-solvent solutions. J Contam Hydrol 1998;29:319–46.

[130] Van Valkenburg ME, Annable MD. Mobilization and entry of DNAPL pools into finer sand media by cosolvents: two-dimensional chamber studies. J Contam Hydrol 2002;59:211–30.

[131] Zhong L, Mayer A, Glass RJ. Visualization of surfactant-enhanced nonaqueous phase liquid mobilization and solubilization in a two-dimensional micromodel. Water Resour Res 2001;37:523.

[132] Brooks MC, Wise WR, Annable MD. Fundamental changes in in situ air sparging how patterns. Ground Water Monit Remediat 1999.

[133] Peteron JW, Murray KS, Tulu YI, Peuler BD, Wilkens DA. Air-flow geometry in air sparging of fine-grained sands. Hydrogeol J 2001;9:168–76. doi:10.1007/s100400000104.

[134] Selker JS, Niemet M, Mcduffie NG, Gorelick SM, Parlange J-Y. The Local Geometry of Gas Injection into Saturated Homogeneous Porous Media. Transp Porous Media 2006;68:107–27. doi:10.1007/s11242-006-0005-0.

[135] Heron G, Gierke JS, Faulkner B, Mravik S, Wood L, Enfield CG. Pulsed air sparging in aquifers contaminated with dense nonaqueous phase liquids. Ground Water Monit Remediat 2002.

[136] Berkey JS, Lachmar TE, Doucette WJ, Ryan Dupont R. Tracer studies for evaluation of in situ air sparging and in-well aeration system performance at a gasoline-contaminated site. J Hazard Mater 2003;98:127–44.

[137] Thomson NR, Johnson RL. Air distribution during in situ air sparging: an overview of mathematical modeling. J Hazard Mater 2000;72:265–82.

[138] Waduge WAP, Soga K, Kawabata J. Effect of NAPL entrapment conditions on air sparging remediation efficiency. J Hazard Mater 2004;110:173–83. doi:10.1016/j.jhazmat.2004.02.050.

[139] Jang W, Aral MM. Multiphase Flow Fields in In-situ Air Sparging and its Effect on Remediation. Transp Porous Media 2008;76:99–119. doi:10.1007/s11242-008-9238-4.

[140] Hunt JR, Sitar N, Udell KS. Nonaqueous phase liquid transport and cleanup: 2. Experimental studies. Water Resour Res 1988;24:1259–69. doi:10.1029/WR024i008p01259.

[141] Schmidt R, Betz C, Faerber A. LNAPL and DNAPL behaviour during steam injection into the unsaturated zone. IAHS Publ Assoc Hydrol Sci 1998:111–7.

[142] She HY, Sleep BE. Removal of perchloroethylene from a layered soil system by steam flushing. Ground Water Monit Remediat 1999;19:70–7.

[143] Kaslusky SF, Udell KS. A theoretical model of air and steam co-injection to prevent the downward migration of DNAPLs during steam-enhanced extraction. J Contam Hydrol 2002;55:213–32.

[144] Ji W, Dahmani A, Ahlfeld DP, Lin JD, Hill E. Laboratory study of air sparging: Air flow visualization. Groundw Monit Remediat 1993;13:115–36.

[145] Lundegard PD, Andersen G. Multiphase numerical simulation of air sparging performance. Groundwater 1996.

[146] McCray JE, Falta RW. Defining the air sparging radius of influence for groundwater remediation. J Contam Hydrol 1996;24:25–52.

[147] Faisal Anwar AHM, Bettahar M, Matsubayashi U. A method for determining air–water interfacial area in variably saturated porous media. J Contam Hydrol 2000;43:129–46. doi:10.1016/S0169-7722(99)00103-5.

[148] Peng S, Brusseau ML. Impact of soil texture on air-water interfacial areas in unsaturated sandy porous media. Water Resour Res 2005;41:n/a–n/a. doi:10.1029/2004WR003233.

[149] Rao PSC, Annable MD, Kim H. NAPL source zone characterization and remediation technology performance assessment: recent developments and applications of tracer techniques. J Contam Hydrol 2000;45:63–78. doi:10.1016/S0169-7722(00)00119-4.

[150] Kim H, Rao PSC, Annable MD. Determination of effective air-water interfacial area in partially saturated porous media using surfactant adsorption. Water Resour Res 1997;33:2705–11.

[151] Schaefer CE, DiCarlo DA, Blunt MJ. Determination of Water-Oil Interfacial Area during 3-Phase Gravity Drainage in Porous Media. J Colloid Interface Sci 2000;221:308–12. doi:10.1006/jcis.1999.6604.

[152] Cho J, Annable MD. Characterization of pore scale NAPL morphology in homogeneous sands as a function of grain size and NAPL dissolution. Chemosphere 2005;61:899–908. doi:10.1016/j.chemosphere.2005.04.042.

[153] Brusseau ML, Peng S, Schnaar G, Murao A. Measuring air-water interfacial areas with X-ray microtomography and interfacial partitioning tracer tests. Environ Sci Technol 2007;41:1956–61.

[154] Kim H, Choi K-M, Moon J-W, Annable MD. Changes in air saturation and air-water interfacial area during surfactant-enhanced air sparging in saturated sand. J Contam Hydrol 2006;88:23–35. doi:10.1016/j.jconhyd.2006.05.009.

[155] Schaefer CE, Callaghan A V, King JD, Mccray JE. Dense nonaqueous phase liquid architecture and dissolution in discretely fractured sandstone blocks. Environ Sci Technol 2009;43:1877–83.

[156] Johns ML, Gladden LF. Magnetic Resonance Imaging Study of the Dissolution Kinetics of Octanol in Porous Media. J Colloid Interface Sci 1999;210:261–70. doi:10.1006/jcis.1998.5950.

[157] Johns ML, Gladden LF. Probing Ganglia Dissolution and Mobilization in a Water-Saturated Porous Medium using MRI. J Colloid Interface Sci 2000;225:119–27. doi:10.1006/jcis.2000.6742.

[158] Leverett MC. Capillary behaviour in porous solids. Trans AIME 1941:152– 170.

[159] Morrow NR. Physics and thermodynamics of capillary action in porous media. Ind Eng Chem Res, 1970;62:32–56.

[160] Bradford SA, Leij FJ. Estimating interfacial areas for multi-fluid soil systems. J Contam Hydrol 1997;27:83–105. doi:10.1016/S0169-7722(96)00048-4.

[161] Dalla E, Hilpert M, Miller CT. Computation of the interfacial area for two-fluid porous medium systems. J Contam Hydrol 2002;56:25–48.

[162] Hilpert M, Miller CT. Pore-morphology-based simulation of drainage in totally wetting porous media. Adv Water Resour 2001;24:243–55. doi:10.1016/S0309-1708(00)00056-7.

[163] Dobson R, Schroth MH, Oostrom M, Zeyer J. Determination of NAPL-water interfacial areas in well-characterized porous media. Environ Sci Technol 2006;40:815–22.

[164] Oostrom M, White MD, Brusseau ML. Theoretical estimation of free and entrapped nonwetting–wetting fluid interfacial areas in porous media. Adv Water Resour 2001;24.

[165] Grant GP, Gerhard JI. Simulating the dissolution of a complex dense nonaqueous phase liquid source zone: 1. Model to predict interfacial area. Water Resour Res 2007;43:n/a–n/a. doi:10.1029/2007WR006038.

[166] Brusseau ML, Peng S, Schnaar G, Costanza-Robinson MS. Relationships among air-water interfacial area, capillary pressure, and water saturation for a sandy porous medium. Water Resour Res 2006;42:n/a–n/a. doi:10.1029/2005WR004058.

[167] Fenwick DH, Blunt MJ. Three-dimensional modeling of three phase imbibition and drainage. Adv Water Resour 1998;21:121–43. doi:10.1016/S0309-1708(96)00037-1.

[168] Keller AA, Blunt MJ, Roberts AP V. Micromodel observation of the role of oil layers in three-phase flow. Transp Porous Media 1997:277–97.

[169] Hassanizadeh SM, Gray WG. Thermodynamic basis of capillary pressure in porous media. Water Resour Res 1993.

[170] Reeves PC, Celia MA. A functional relationship between capillary pressure, saturation, and interfacial area as revealed by a pore-scale network model. Water Resour Res 1996;32:2345–58.

[171] Held RJ, Celia MA. Modeling support of functional relationships between capillary pressure, saturation, interfacial area and common lines. Adv Water Resour 2001;24:325–43. doi:10.1016/S0309-1708(00)00060-9.

[172] Joekar-Niasar V, Hassanizdeh SM, Leijnse A. Insights into the relationships among capillary pressure, saturation, interfacial area and relative permeability using pore-network modeling. Transp Porous Media 2008;74:201–19. doi:10.1007/s11242-007-9191-7.

[173] Cheng JT, Pyrak-Nolte LJ, Nolte DD, Giordano NJ. Linking pressure and saturation through interfacial areas in porous media. Geophys Res Lett 2004;31.

[174] Chen D, Pyrak-Nolte LJ, Griffin J, Giordano NJ. Measurement of interfacial area per volume for drainage and imbibition. Water Resour Res 2007.

[175] Chen L, Kibbey TCG, Street WB. Measurement of Air - Water Interfacial Area for Multiple Hysteretic Drainage Curves in an Unsaturated Fine Sand 2006:6874–80. doi:10.1029/2004WR003278.(1).

[176] Joekar-Niasar V, Hassanizadeh SM, Pyrak-Nolte LJ, Berentsen C. Simulating drainage and imbibition experiments in a high-porosity micromodel using an unstructured pore network model. Water Resour Res 2009;45:1–15. doi:10.1029/2007WR006641.

[177] Porter ML, Schaap MG, Wildenschild D. Lattice-Boltzmann simulations of the capillary pressure–saturation–interfacial area relationship for porous media. Adv Water Resour 2009. doi:10.1016/j.advwatres.2009.08.009.

[178] Porter ML, Wildenschild D, Grant G, Gerhard JI. Measurement and prediction of the relationship between capillary pressure, saturation, and interfacial area in a NAPL-water-glass bead system. Water Resour Res 2010;46:1–10. doi:10.1029/2009WR007786.

[179] Lenordmand R, Toulboul E, Zarcone C. Numerical models and experiments on immiscible displacements in porous media. J Fluid Mech 1988;189.

[180] Lenordmand R, Zarcone C, Sarr A. Mechanisms of the displacement of one fluid by another in a network of capillary ducts. J Fluid Mech 1983;135:337–53.

[181] Zhang C, Werth CJ, Webb AG. A magnetic resonance imaging study of dense nonaqueous phase liquid dissolution from angular porous media. Environ Sci Technol 2002;36:3310–7.

[182] Blunt MJ, Scher H. Pore-level modeling of Wetting. Phys Rev E 1995;52:6387–403.

[183] Hughes RG, Blunt MJ. Pore Scale Modeling of Rate Effects in Imbibition. Transp Porous Media 2000;40:295–322.

[184] Chen JD, Wilkinson D. Pore-scale viscous fingering in porous media. Phys Rev Lett 1985;55.

[185] Sinha PK, Wang C. Pore-network modeling of liquid water transport in gas diffusion layer of a polymer electrolyte fuel cell. Electrochim Acta 2007;52:7936–45.

[186] Powers SE, Anckner WH, Seacord TF. Wettability of NAPL-contaminated sands. J Environ Eng 1996:889–96.

[187] Kovscek AR, Wong H, Radke CJ. a pore level scenario for the development of mixed-wettability in oil reservoirs. US Dep Energy 1992.

[188] Valvatne PH, Blunt MJ. Predictive pore-scale modeling of two-phase flow in mixed wet media. Water Resour Res 2004;40:n/a–n/a. doi:10.1029/2003WR002627.

[189] Bradford SA, Abriola LM, Leij FJ. Wettability effects on two- and three-fluid relative permeabilities. J Contam Hydrol 1997;28:171–91. doi:10.1016/S0169-7722(97)00024-7.

[190] Hwang S Il, Lee KP, Lee DS, Powers SE. Effects of fractional wettability on capillary pressure–saturation–relative permeability relations of two-fluid systems. Adv Water Resour 2006;29:212–26. doi:10.1016/j.advwatres.2005.03.020.

[191] Mayer AS, Miller CT. The influence of porous medium characteristics and measurement scale on pore-scale distributions of residual nonaqueous-phase liquids. J Contam Hydrol 1992;11.

[192] Schnaar G, Brusseau ML. Pore-scale characterization of organic immiscible-liquid morphology in natural porous media using synchrotron X-ray microtomography. Environ Sci Technol 2005;39:8403–10.

[193] Knutson CE, Werth CJ, Valocchi AJ. Pore-scale modeling of dissolution from variably distributed nonaqueous phase liquid blobs. Water Resour Res 2001;37:2951–63.

[194] Chomsurin C, Werth CJ. Analysis of pore-scale nonaqueous phase liquid dissolution in etched silicon pore networks. Water Resour Res 2003;39:n/a–n/a. doi:10.1029/2002WR001643.

[195] Reddy KR, Adams JA. Effects of soil heterogeneity on airflow patterns and hydrocarbon removal during in situ air sparging. J Geotech … 2001:234–47.

[196] Peterson JW, Lepczyk PA, Lake KL. Effect of sediment size on area of influence during groundwater remediation by air sparging: A laboratory approach. Environ Geol 1999;38:1–6.

[197] Braida W, Ong SK. Influence of porous media and airflow rate on the fate of NAPLs under air sparging. Transp Porous Media 2000:29–42.

[198] Rogers SW, Ong SK. Influence of Porous Media, Airflow Rate, and Air Channel Spacing on Benzene NAPL Removal during Air Sparging. Environ Sci Technol 2000;34:764–70. doi:10.1021/es9901112.

[199] Russo AE, Narter M, Brusseau ML. Characterizing pore-scale dissolution of organic immiscible liquid in a poorly-sorted natural porous medium. Environ Sci Technol 2009:5671–8.

[200] Hunt JR, Sitar N, Udell KS. Nonaqueous phase liquid transport and cleanup: 1. Analysis of mechanisms. Water Resour Res 1988;24:1247–58. doi:10.1029/WR024i008p01247.

[201] Lenormand R, Zarcone C, Sarr A. Mechanisms of the displacement of one fluid by another in a network of capillary ducts. J Fluid … 1983.

[202] Schwille F. Petroleum contamination of the subsoil--A hydrological problem, in The Joint Problems of the Oil and Water Industries, Proceedingso f a Symposiume, dited by P. Hepple. Inst Pet London 1967.

[203] Illangasekare TH, Armbruster III EJ, Yates DN. Non-aqueous-phase fluids in heterogeneous aquifers-experimental study. J Environ Eng 1995.

[204] Imhoff PT, Arthur MH, Miller CT. Complete Dissolution of Trichloroethylene in Saturated Porous Media. Environ Sci Technol 1998;32:2417–24. doi:10.1021/es970965r.

[205] Mackay DM, Cherry JA. Groundwater contamination: Pump-and-treat remediation. Environ Sci Technol 1989.

[206] Ball WP, Roberts P V. “Diffusive Rate Limitations in the Sorption of Organic Chemicals,” Chapter 13,. In: Baker R., editor. Org. Subst. Sediments Water Vol. 2, Process. Anal., Lewis Publishers, Inc., Chelsea, MI,; 1991, p. pp. 273–310.

[207] Luthy RG, Aiken GR, Brusseau ML, Cunningham SD, Gschwend PM, Pignatello JJ, et al. Sequestration of Hydrophobic Organic Contaminants by Geosorbents. Environ Sci Technol 1997:3341 – 3347.

[208] Grathwohl P. Diffusion in Natural Porous Media: Contaminant Transport, Sorption/Desorption and Dissolution Kinetics. Kluwer Academic Publishers; 19998.

[209] Kueper BH, Frind EO. An overview of immiscible fingering in porous media. J Contam Hydrol 1988;2:95–110.

[210] Mackay DM, Roberts P V, Cherry JA. Transport of organic contaminants in groundwater. Environ Sci Technol 1985;19:384–92. doi:10.1021/es00135a001.

[211] Palomino AM, Grubb DG. Recovery of dodecane, octane and toluene spills in sandpacks using ethanol. J Hazard Mater 2004;110:39–51. doi:10.1016/j.jhazmat.2004.02.035.

[212] Grubb DG, Sitar N. Mobilization of trichloroethene (TCE) during ethanol flooding in uniform and layered sand packs under confined conditions. Water Resour Res 1999;35:3275–89. doi:10.1029/1999WR900222.

[213] Grubb DG, Sitar N. Horizontal ethanol floods in clean, uniform, and layered sand packs under confined conditions. Water Resour Res 1999;35:3291–302. doi:10.1029/1999WR900223.

[214] Xu X, Chen S, Zhang D. Convective stability analysis of the long-term storage of carbon dioxide in deep saline aquifers. Adv Water Resour 2006;29:397–407. doi:10.1016/j.advwatres.2005.05.008.

[215] Kneafsey TJ, Pruess K. Laboratory Flow Experiments for Visualizing Carbon Dioxide-Induced, Density-Driven Brine Convection. Transp Porous Media 2009;82:123–39. doi:10.1007/s11242-009-9482-2.

[216] Hatfield K, Stauffer TB. Transport in porous media containing residual hydrocarbon. I: model. J Environ Eng 1993;119:540–58.

[217] Soerens TS, Sabatini DA, Harwell JH. Effects of flow bypassing and nonuniform NAPL distribution on the mass transfer characteristics of NAPL dissolution. Water Resour Res 1998;34:1657–73.

[218] Chrysikopoulos C V., Voudrias EA, Fyrillas MM. Modeling of contaminant transport resulting from dissolution of nonaqueous phase liquid pools in saturated porous media. Transp Porous Media 1994;16:125–45. doi:10.1007/BF00617548.

[219] Chrysikopoulos C V. Three-Dimensional Analytical Models of Contaminant Transport From Nonaqueous Phase Liquid Pool Dissolution in Saturated Subsurface Formations. Water Resour Res 1995;31:1137–45.

[220] Holman HYN, Javandel I. Evaluation of Transient Dissolution of Slightly Water-Soluble Compounds From a Light Nonaqueous Phase Liquid Pool. Water Resour Res 1996;32:915–23.

[221] Sale TC, McWhorter DB. Steady state mass transfer from single-component dense nonaqueous phase liquids in uniform flow fields. Water Resour Res 2001;37:393–404.

[222] Hunt B. Dispersion sources in uniform groundwater flow. 1 Hydraul Div Am Soc Civ Eng 1960;104:75–85.

[223] Falta RW, Suresh Rao P, Basu N. Assessing the impacts of partial mass depletion in DNAPL source zones I. Analytical modeling of source strength functions and plume response. J Contam Hydrol 2005;78:259–80. doi:10.1016/j.jconhyd.2005.05.010.

[224] Lemke LD, Abriola LM, Lang JR. Influence of hydraulic property correlation on predicted dense nonaqueous phase liquid source zone architecture, mass recovery and contaminant flux. Water Resour Res 2004;40:n/a–n/a. doi:10.1029/2004WR003061.

[225] Christ JA, Ramsburg CA, Pennell KD, Abriola LM. Predicting DNAPL mass discharge from pool-dominated source zones. J Contam Hydrol 2010;114:18–34. doi:10.1016/j.jconhyd.2010.02.005.

[226] Rao PSC, Jawitz JW, Enfield CG, Falta RW, Annable MD, Wood AL. Technology integration for contaminated site remediation: clean-up goals and performance criteria. Groundw Qual . 2001:571–8.

[227] DiFilippo EL, Carroll KC, Brusseau ML. Impact of organic-liquid distribution and flow-field heterogeneity on reductions in mass flux. J Contam Hydrol 2010;115:14–25. doi:10.1016/j.jconhyd.2010.03.002.

[228] Jawitz JW, Fure AD, Demmy GG, Berglund S, Rao PSC. Groundwater contaminant flux reduction resulting from nonaqueous phase liquid mass reduction. Water Resour Res 2005;41:n/a–n/a. doi:10.1029/2004WR003825.

[229] Fure AD, Jawitz JW, Annable MD. DNAPL source depletion: linking architecture and flux response. J Contam Hydrol 2006;85:118–40. doi:10.1016/j.jconhyd.2006.01.002.

[230] Chen X, Jawitz JW. Reactive tracer tests to predict dense nonaqueous phase liquid dissolution dynamics in laboratory flow chambers. Environ Sci Technol 2008;42:5285–91.

[231] Wood AL, Enfield CG, Espinoza FP, Annable M, Brooks MC, Rao PSC, et al. Design of aquifer remediation systems: (2) estimating site-specific performance and benefits of partial source removal. J Contam Hydrol 2005;81:148–66. doi:10.1016/j.conhyd.2005.08.004.

[232] Braida W, Ong SK. Modeling of air sparging of VOC-contaminated soil columns. J Contam Hydrol 2000;41:385–402. doi:10.1016/S0169-7722(99)00075-3.

[233] Chao KP, Ong SK, Protopapas A. Water-to-air mass transfer of VOCs: laboratory-scale air sparging system. J Environ Eng 1998.

[234] Jia C, Shing K, Yortsos YC. Visualization and simulation of non-aqueous phase liquids solubilization in pore networks. J Contam Hydrol 1999;35:363–87. doi:10.1016/S0169-7722(98)00102-8.

[235] Celia MA, Reeves PC, Ferrand LA. Recent advances in pore scale models for multiphase flow in porous media. Rev Geophys 1995:1049–57.

[236] Joekar-Niasar V, Prodanović M, Wildenshild D, Hassanizadeh SM. Network model investigation of interfacial area, capillary pressure and saturation relationships in granular porous media. Water Resour Res 2010;46:1–18. doi:10.1029/2009WR008585.

[237] Al-Gharbi M, Blunt MJ. Dynamic network modeling of two-phase drainage in porous media. Phys Rev E 2005;71:016308. doi:10.1103/PhysRevE.71.016308.

[238] Blunt MJ. Flow in porous media—pore-network models and multiphase flow. Curr Opin Colloid Interface Sci 2001.

[239] Wilkinson D, Willemsen JF. Invasion percolation: a new form of percolation theory. J Phys A Math Gen 1983;16:3365–76. doi:10.1088/0305-4470/16/14/028.

[240] Parker JC, Katyal AK, Kaluarachchi JJ, Lenhard RJ, Johnson TJ, Jayaraman K, et al. Modeling multiphase organic chemical transport in soils and ground water. EPA/600/2-91/042, US Environ Prot Agency, Washington, DC 1991.

[241] Zhao W, Ioannidis MA. Effect of NAPL film stability on the dissolution of residual wetting NAPL in porous media: A pore-scale modeling study. Adv Water Resour 2007;30:171–81. doi:10.1016/j.advwatres.2005.03.025.

[242] Zhao W, Ioannidis MA. Convective mass transfer across fluid interfaces in straight angular pores. Transp Porous Media 2007:495–509. doi:10.1007/s11242-006-0025-9.

[243] Martys NS, Chen H. Simulation of multicomponent fluids in complex three-dimensional geometries by the lattice Boltzmann method. Phys Rev E 1996;53.

[244] Swift MR, Orlandini E, Osborn WR, Yeomans JM. Lattice Boltzmann simulations of liquid-gas and binary fluid systems. Phys Rev E Stat Phys Plasmas Fluids Relat Interdiscip Topics 1996;54:5041–52.

[245] Pan C, Hilpert M, Miller CT. Lattice-Boltzmann simulation of two-phase flow in porous media. Water Resour Res 2004;40:n/a–n/a. doi:10.1029/2003WR002120.

[246] Schaap MG, Porter ML. Comparison of pressure-saturation characteristics derived from computed tomography and lattice Boltzmann simulations. Water Resour Res 2007;43:1–15. doi:10.1029/2006WR005730.

[247] Meakin P, Tartakovsky AM. Modeling and simulation of pore-scale multiphase fluid flow and reactive transport in fractured and porous media. Rev Geophys 2009:1–47. doi:10.1029/2008RG000263.1.INTRODUCTION.

[248] Yuan P, Schaefer L. Equations of state in a lattice Boltzmann model. Phys Fluids 2006;18:042101. doi:10.1063/1.2187070.

[249] Bao J, Schaefer L. Lattice Boltzmann equation model for multi-component multi-phase flow with high density ratios. Appl Math Model 2013;37:1860–71. doi:10.1016/j.apm.2012.04.048.

[250] Blunt MJ, Bijeljic B, Dong H, Gharbi O, Iglauer S, Mostaghimi P, et al. Advances in Water Resources Pore-scale imaging and modelling. Adv Water Resour 2013;51:197–216.

[251] Raeini AQ, Blunt MJ, Bijeljic B. Modelling two-phase flow in porous media at the pore scale using the volume-of-fluid method. J Comput Phys 2012;231:5653–68. doi:10.1016/j.jcp.2012.04.011.

[252] Raeini AQ. Modelling multiphase flow through micro-CT images of the pore space 2013:1–152.

[253] Kim TJ, Chrysikopoulos C V. Mass transfer correlations for nonaqueous phase liquid pool dissolution in saturated porous media. Water Resour Res 1999;35:449–59.

[254] Schaerlaekens J, Vanderborght J, Merckx R, Feyen J. Surfactant enhanced solubilization of residual trichloroethene: an experimental and numerical analysis. J Contam Hydrol 2000;46:1–16.

[255] Ji W, Brusseau ML. A general mathematical model for chemical-enhanced flushing of soil contaminated by organic compounds. Water Resour Res 1998;34:1635.

[256] Geller JT, Hunt JR. Mass transfer from nonaqueous phase organic liquids in water-saturated porous media. Water Resour Res 1993;29:833–45.

[257] Powers SE, Nambi IM, Curry GW. Non–aqueous phase liquid dissolution in heterogeneous systems: Mechanisms and a local equilibrium modeling approach. Water Resour Res 1998;34:3293–302.

[258] Corey AT. The interrelation between gas and oil relative permeabilities. Prod Mon 1954;19:38–41.

[259] Brusseau ML, Zhang Z, Nelson NT, Cain RB, Tick GR, Oostrom M. Dissolution of nonuniformly distributed immiscible liquid: intermediate-scale experiments and mathematical modeling. Environ Sci Technol 2002;36:1033–41.

[260] Miller CT, Gleyzer SN, Imhoff PT. Numerical modeling of NAPL dissolution fingering in porous media, in Physical Nonequilibrium in Soils: Modeling and Application, edited by H. M. Selim and L. Ma,. Ann Arbor Press Ann Arbor, Mich 1998:389– 415.

[261] Mason AR, Kueper BH. Numerical simulation of surfactant-enhanced solubilization of pooled DNAPL. Environ Sci Technol 1996;30:3205–15.

[262] Rathfelder KM, Abriola LM, Taylor TP, Pennell KD. Surfactant enhanced recovery of tetrachloroethylene from a porous medium containing low permeability lenses. 2. Numerical simulation. J Contam Hydrol 2001;48:351–74.

[263] Abriola LM, Lang JR, Rathfelder KM. Michigan Soil Vapor Extraction Remediation MISER. Model: a computer program to model soil vapor extraction and bioventing of organic chemicals in unsaturated geologic materials. US Environ Prot Agency, EPAr600rR-97r099, Natl Risk Manag Res Lab Ada, OK 1997.

[264] Taylor TP, Pennell KD, Abriola LM, Dane JH. Surfactant enhanced recovery of tetrachloroethylene from a porous medium containing low permeability lenses. 1. Experimental studies. J Contam Hydrol 2001;48:325–50.

[265] Abriola LM, Pinder GF. A multiphase approach to the modeling of porous media contamination by organic compounds: 1. Equation development. Water Resour Res 1985;21:11–8.

[266] Kueper BH, Frind EO. Two-phase flow in heterogeneous porous media: 1. Model development. Water Resour Res 1991;27:1049–57.

[267] Faust CR. Transport of immiscible fluids within and below the unsaturated zone: A numerical model. Water Resour Res 1985;21:587–96.

[268] Osborne M, Sykes J. Numerical modeling of immiscible organic transport at the Hyde Park landfill. Water Resour Res 1986;22:25–33.

[269] Sleep BE, Sykes JF. Compositional simulation of groundwater contamination by organic compounds: 1. Model development and verification. Water Resour Res 1993;29:1697–708.

[270] White MD, Oostrom M, Imhard J. Modeling fluid flow and transport in variably saturated porous media with the STOMP simulator. 1 . Nonvolatile three-phase model description. Adv Water Resour 1995;18:353–64.

[271] Rathfelder K, Abriola LM. Mass conservative numerical solutions of the head-based Richards equation. Water Resour Res 1994;30:2579–86.

[272] Guiguer N, Frind EO. Dissolution and mass transfer processes for residual organics in the saturated groundwater zone. Dracos, Stauffer Eds., Transp React Process Aquifers Balkema, Rotterdam, 475–480 1994:475–80.

[273] Dekker TJ, Abriola LM. The influence of field-scale heterogeneity on the infiltration and entrapment of dense nonaqueous phase liquids in saturated formations. J Contam Hydrol 2000;42:187–218. doi:10.1016/S0169-7722(99)00092-3.

[274] Hinkelmann R, Breiting TR, Helmig R. Modeling of Hydrosystems with MUFTE-UG: Multiphase Flow and Transport Processes in the Subsurface.". Fourth Int Conf Hydroinformatics, Iowa, USA 2000.

[275] Hinkelmann R, Sheta H, Class H, Sauter EJ, Helmig R, Schlüter M. Numerical simulation of freshwater, salt water and methane interaction processes in a coastal aquifer.". Resour Recover Confin Remediat Environ Hazards (pp 263-281) Springer New York 2002.

[276] Helmig R, Class H, Huber R, Sheta H, Ewing R, Hinkelmann R., et al. Architecture of the modular program system MUFTE-UG for simulating multiphase flow and transport processes in heterogeneous porous media. Math Geol 1998;64:123–31.

[277] Hinkelmann R. Efficient numerical methods and information-processing techniques for modeling hydro-and environmental systems. Berlin: Springer 2005;21.

[278] Falta RW. Modeling sub-grid-block-scale dense nonaqueous phase liquid (DNAPL) pool dissolution using a dual-domain approach. Water Resour Res 2003;39:n/a–n/a. doi:10.1029/2003WR002351.

[279] Falta RW, Pruess K, Finsterle S, Battistelli A. T2VOC user's guide. Rep LBL-36400, Lawrence Berkeley Natl Lab, Berkeley, Calif, March 1995.

[280] Basu NB, Fure AD, Jawitz JW. Predicting dense nonaqueous phase liquid dissolution using a simplified source depletion model parameterized with partitioning tracers. Water Resour Res 2008;44:1–13. doi:10.1029/2007WR006008.

[281] Basu N, Rao P, Falta R, Annable M, Jawitz J, Hatfield K. Temporal evolution of DNAPL source and contaminant flux distribution: Impacts of source mass depletion. J Contam Hydrol 2008;95:93–109. doi:10.1016/j.jconhyd.2007.08.001.

[282] O'Carroll DM, Sleep BE. Role of NAPL Thermal Properties in the Effectiveness of Hot Water Flooding. Transp Porous Media 2009;79:393–405. doi:10.1007/s11242-008-9329-2.

[283] Reitsma S, Kueper BH. Non-equilibrium alcohol flooding model for immiscible phase remediation: 2. Model development and application. Adv Water Resour 1998;21:663–78.

[284] Gray WG, Celia MA, Reeves PC. Incorporation of interfacial areas in models of two-phase flow. Int Keamey Found Soil Sci Conf Vadose Zo Hydrol - Cut Across Discip Univ California, Davis, Sept 6-8 1995.

[285] Li B, Fu J. Interfacial tensions of two-liquid-phase ternary systems. J Chem Eng Data 1992;37:172–4.

[286] Roeder E, Falta RW. Modeling unstable alcohol flooding of DNAPL-contaminated columns. Adv Water Resour 2001;24.

[287] Liang H, Falta RW. Modeling field-scale cosolvent flooding for DNAPL source zone remediation. J Contam Hydrol 2008;96:1–16. doi:10.1016/j.jconhyd.2007.09.005.

[288] Kaye AJ, Cho J, Basu NB, Chen X. Laboratory investigation of flux reduction from dense non-aqueous phase liquid (DNAPL) partial source zone remediation by enhanced dissolution. J Contam Hydrol 2008;102:17–28. doi:10.1016/j.jconhyd.2008.01.006.

[289] Lingineni S, Dhir VK. Controlling transport processes during NAPL removal by soil venting. Adv Water Resour 1997;20:157–69. doi:10.1016/S0309-1708(96)00028-0.

[290] Hein GL, Gierke JS, Hutzler NJ, Falta RW. Three-Dimensional Experimental Testing of a Two-Phase Flow-Modeling Approach for Air Sparging. Ground Water Monit Remediat 1997.

[291] McClure PD, Sleep BE. Simulation of bioventing for soil and ground-water remediation. J Environ Eng 1996:1003–12.

[292] Unger AJA, Sudicky EA, Forsyth PA. Mechanisms controlling vacuum extraction coupled with air sparging for remediation of heterogeneous formations contaminated by dense nonaqueous phase liquids. Water Resour Res 1995;31:1913–25.

[293] Yoon H, Werth CJ, Valocchi AJ, Oostrom M. Impact of nonaqueous phase liquid (NAPL) source zone architecture on mass removal mechanisms in strongly layered heterogeneous porous media during soil vapor extraction. J Contam Hydrol 2008;100:58–71. doi:10.1016/j.jconhyd.2008.05.006.

[294] Xu T, Apps JA, Pruess K. Mineral sequestration of carbon dioxide in a sandstone–shale system. Chem Geol 2005.

[295] Xu T, Sonnenthal E, Spycher N, Pruess K. TOUGHREACT User's Guide: A Simulation Program for Non-isothermal Multiphase Reactive Geochemical Transport in Variably Saturated Geologic Media, V1. 2008.

[296] Thibeau S, Dutin A. Large scale CO2 storage in unstructured aquifers: Modeling study of the ultimate CO2 migration distance. Energy Procedia 2011;4:4230–7. doi:10.1016/j.egypro.2011.02.371.

[297] Niessner J, Hassanizadeh SM. A model for two-phase flow in porous media including fluid-fluid interfacial area. Water Resour Res 2008.

[298] Hassanizadeh SM, Gray WG. Mechanics and thermodynamics of multiphase flow in porous media including interphase boundaries. Adv Water Resour 1990.

[299] Jackson AS, Miller CT, Gray WG. Thermodynamically constrained averaging theory approach for modeling flow and transport phenomena in porous medium systems: 6. Two-fluid-phase flow. Adv Water Resour 2009;32:779–95. doi:10.1016/j.advwatres.2008.11.010.

[300] Miller CT, Dawson CN, Farthing MW, Hou TY, Huang J, Kees CE, et al. Numerical simulation of water resources problems: Models, methods, and trends. Adv Water Resour 2013;51:405–37. doi:10.1016/j.advwatres.2012.05.008.

[301] Jackson ABS. Multiscale Modeling of Multiphase Flow in Porous Media Using the Thermodynamically Constrained Averaging Theory Approach. PhD Diss, Univ NORTH CAROLINA CHAPEL HILL 2011.

3. Impact of NAPL architecture on interphase mass transfer: A pore network study

Berken Agaoglu[a], Traugott Scheytt[a], Nadim K. Copty[b],

[a] Institute of Applied Geosciences, Berlin Institute of Technology, Sekr. BH 3-2, Ernst-Reuter-Platz 1, 10587 Berlin, Germany

[b] Institute of Environmental Sciences, Bogazici University, 34342 Bebek, Istanbul, Turkey

Citation:
Agaoglu, B., Scheytt T., Copty K.N. Impact of NAPL architecture on interphase mass transfer: A pore network study. Submitted to Water resources research

Abstract

The simulation of interphase mass transfer in porous media is commonly conducted based on Sherwood number expressions that are developed in terms of fluid and porous medium properties averaged over a representative volume. In this work the influence of sub-grid scale properties on interphase mass transfer was investigated through use of a two-dimensional pore network model. The focus was on assessing the impact of pore-scale variability of (i) NAPL saturation, (ii) interfacial area (iii) NAPL spatial distribution, (iv) grain size distribution and (v) domain size on interphase mass transfer. Variability of both the mass transfer coefficient that explicitly accounts for the interfacial area and the mass transfer coefficient that lumps the interfacial area was examined. It was shown that the orientation of the NAPL mass at the pore scale relative to the flow direction has a significant impact on flow bypassing and the interphase mass transfer coefficient. As a result, the relationship between interfacial area and the interphase mass transfer rate is not linear. Furthermore, different values of mass transfer coefficients would be valid not only for different but also same amount of interfacial area meaning that explicitly accounting for the interfacial area does not eliminate the variability of mass transfer coefficient. It was also shown that for a given NAPL mass/interfacial area, the domain size has direct impact on the interphase mass transfer where by, even for explicitly defined flow patterns, changing the domain size influences the extent of NAPL bypassing and consequently the interphase mass transfer.

1. Introduction

Interphase mass transfer between fluids in porous media occurs in numerous industrial and natural applications [Abriola, 1989; Miller et al., 1998]. Significant work has been conducted in recent years especially in the field of NAPL remediation to elucidate the factors that affect this process (e.g., [Imhoff et al., 1994; Kokkinaki et al., 2013a; Nambi and Powers, 2003; Pan et al., 2007; Powers et al., 1991; Saba and Illangasekare, 2000]). The characteristic lengths of the conducted studies range from the pore scale to the meso-scale and field scale. Pore scale studies provide information and insight on the impact of pore scale conditions-- such as grain size and the pore scale distribution of the interfacial area-- on the interphase mass transfer (e.g.,[Joekar-Niasar and Hassanizadeh, 2011; Sahloul et al., 2002; Schnaar and Brusseau, 2006; Dillard and Blunt 2000]). Meso-scale investigations of interphase mass transfer have been mostly conducted through column experiments at a length scale of 1-5 cm (e.g., [Powers et al. 1991]). The field scale characterization of interphase mass transfer has been mostly conducted with use of numerical models based on the representative elementary volume (REV) (e.g., [Park and Parker, 2004). In this case, the magnitude of the interphase mass transfer in a single computational node is often obtained from meso-scale interphase transfer correlation incorporated in the numerical model. Differences between field conditions and the experimental conditions, from which the mass transfer correlations were initially developed, are cited as one of the main reasons for the limited accuracy of model predictions at the field scale [Basu et al., 2008; Fure et al., 2006; Jawitz et al., 2003; Zhang et al., 2008; Grant and Gerhard 2007a, 2007b]. Numerous studies have shown that, as a result of soil heterogeneity and the non-uniform spatial distribution of the NAPL mass, NAPL bypassing by the incoming solute-free water can occur at all these length scales resulting in complex relations between interphase mass transfer and flow and porous media properties [Agaoglu et al., 2012; Dillard and Blunt, 2000; Held and Celia, 2001a; Maji and Sudicky 2008; Marble et al., 2008; Unger et al., 1998; Zhang et al., 2002].

Interphase mass transfer rate is commonly defined in terms of the thermodynamic driving force, the interfacial area between fluids and a mass transfer coefficient [Powers et al., 1994a; Whitman, 1923]:

$$\frac{\partial M}{\partial t} = k_f A(C_s - C) \qquad (1)$$

where *M* is mass transferred between phases, *t* is time, k_f is interphase mass transfer coefficient, *A* is the interfacial area, C_s is solubility and C is the existing concentration in the solvent phase. The influence of fluid and pore scale porous medium characteristics on interphase mass transfer are incorporated within the mass transfer coefficient, k_f. In the literature the relation of mass transfer coefficient to system properties is often accomplished via Sherwood number correlations which incorporate the mass transfer coefficient, the diffusion coefficient of the dissolving solute, D, and a characteristic system length defined in this case as the mean grain diameter of the porous medium, d_m:

$$Sh = {k_f d_m}/{D} \qquad (2)$$

The inability to accurately determine the interfacial area in porous media has also led to the introduction of a lumped mass transfer coefficient, K_l, which incorporates the mass transfer coefficient and interfacial area, *A*, per unit porous medium volume, *V*:

$$K_l = {k_f A}/{V} \qquad (3)$$

The correlations developed between the lumped mass transfer coefficient and system properties have been commonly expressed in terms of a “modified Sherwood number” defined as:

$$Sh' = {K_l d_m^2}/{D} \qquad (4)$$

Hereafter, the Sherwood number that is defined through the mass transfer coefficient, k_f, (i.e., Eq. 2) will be referred to as the "explicit Sherwood number" to prevent any confusion with the "modified Sherwood number".

Numerous Sherwood formulations can be found in the literature relating the interphase mass transfer coefficient at the meso scale to system configurations. A detailed analysis of the interphase mass transfer in porous media and the existing Sherwood formulations can be found in a recent review by the authors (Agaoglu et al., 2015). Below are two such correlations of the explicit and modified Sherwood numbers developed by Powers et al., [1994a] and Imhoff et al., [1994], respectively:

$$Sh = 36.8Re^{0.654} \qquad (5)$$

$$Sh' = 340\theta_n^{0.87} Re^{0.71} \left({x}/{d_m}\right)^{-0.31} \qquad (6)$$

where Re is the Reynolds number, $\theta_n$is the NAPL saturation, and *x* refers to the distance into residual NAPL region from the inlet.

Modified Sherwood formulations lump the interfacial area within whereas explicit Sherwood number formulations are defined independent of the interfacial area as they are typically developed for some assumed contact area. There are only two explicit Sherwood formulations developed for NAPL dissolution in literature: the Pfannkuch [1984] correlation and the Powers et al., [1994a] correlation. Recently it was also demonstrated that the correlation of Pfannkuch involves some fundamental mathematical errors and uncertainty in the data which render the correlation unusable (Agaoglu et al., (under review in WRR))

It has been shown that the use of different Sherwood formulations in REV based numerical models can lead to different results even though they are used with the same input values [Kokkinaki et al., 2013b; Maji and Sudicky, 2008]. This is in part a result of the fact that these Sherwood formulations are actually derived for different pore scale system conditions which cannot be identically established at the REV-scale. Most existing Sherwood number formulations which are derived from column experiments with continuous, uniformly distributed NAPL saturations (e.g., [Imhoff et al., 1994; Powers et al., 1994a, 1992; Schnaar and Brusseau, 2006]), are used in the REV-based numerical models, assuming that the same type of NAPL formation occurs within a computational node. However, in reality the pore scale NAPL architecture may be significantly more complex than the continuous uniformly distributed form assumed in these models leading to important discrepancies between the real mass transfer and the one predicted by the REV-based model. The complex NAPL spatial distribution is to a large extent the result of the pore scale heterogeneity of the porous media leading to preferential flow paths during both NAPL intrusion into domain and subsequently during NAPL dissolution.

Rate limited dissolution leading to effluent concentrations lower than solubility are generally attributed to water bypassing the NAPL region and to dilution of the contaminant plume with adjacent clean water streamlines. In reality bypassing and dilution of the contaminant plume are intrinsically related as they are both the result of non-uniformity of the NAPL and flow distributions within the NAPL zone. Such small scale variability is generally not accounted for in meso-scale laboratory experiments from which most Sherwood correlations are developed. Therefore, in this work we investigate the impact of pore scale NAPL architecture and its contribution to flow bypassing (and with that respect also to dilution) on meso-scale interphase mass transfer using a pore network model. The key components of the pore network model and how it is implemented in this study are presented in Sections 2 and 3. The results of the numerical study are presented and discussed in Section 4.

2. Pore network

Flow in porous media can be represented as flow in connected pipes using Poiseuille's law [Jia et al., 1999] . Use of pore scale models to investigate interphase mass transfer were first considered by Jia et al., [1999] who simulated flow of the aqueous phase with the NAPL is placed in selected pores. Dissolution was assumed to occur only at the pore throats located between aqueous phase pores and NAPL-filled pores. Dillard and Blunt [2000, 2001] developed a pore scale model that considered flow of the aqueous phase along the edges of NAPL-filled pores (referred to as corner flow). Therefore, interphase mass transfer was assumed to occur only due to corner flow of aqueous phase ignoring interphase mass transfer occurring at the pore throats. Yiotis et al. [2001] on the other hand ignored corner flow and considered the dissolution occurring at the pore throat as the only pattern for dissolution. Held and Celia [2001] followed a similar approach assuming the dissolution at the pore throat as the only mechanism and achieved excellent agreement against the experimental data of Imhoff et al., [1994]. Zhao and Ioannidis [2003, 2007] considered both diffusion during corner flow and diffusion at the pore throat.

In the current study, dissolution due to flow through this thin layer (i.e., corner flow) was neglected as several authors have reported accurate dissolution predictions with pore network models without corner flow [Held and Celia, 2001a; Jia et al., 2001; Yiotis et al., 2000].

The pore network system considered in this analysis consisted of two dimensional square domains. Similar to the pore scale model of Jia et al., [1999], the developed model simulates a mobile aqueous phase with the NAPL placed in selected pore bodies at the beginning of each simulation. No aqueous flow is assumed to occur in NAPL-containing pores. The conservation of mass equation for the aqueous phase is first solved to determine the pressure at each node for some prescribed boundary conditions. The solute transport equation is then solved for the computed aqueous phase velocity field assuming that interphase mass transfer occurs along pore throats due to diffusion. A brief description of the equations used in the pore network model is presented below. The detailed description can be found elsewhere (e.g., [Dillard and Blunt, 2000]).

$$\sum_{j}^{N} Q_{ij} = 0 \qquad (8)$$

where Q_{ij} is the flow rate of water between chamber *i* and chamber *j*. *N* is the number of chambers adjacent to chamber *i*.

Poiseuille's law which is used to define the aqueous phase flow in the network can be written as.

$$Q_w = g_w \Delta P \qquad (7)$$

where *P* is the pressure of the pores and g_w refers to the conductance of chambers and tubes, which is defined as:

$$g_w = \frac{\pi r_{eq}^4}{8\mu_w l} \qquad (9)$$

where $\mu_w$is the viscosity of water and l is the length of the tube/chamber. The tubes and chambers are assumed to have square cross sectional area. Since Poiseuille's law is valid for circular pipes the conductance is adapted to square cross sections. This is achieved by defining an equivalent radius of the tube or chamber, denoted r_{eq}, which is given by:

$$r_{eq} = \frac{1}{2}(r + r_v) \qquad (10)$$

For a tube, *r* is equal to the average of the inscribed radius (i.e., width of the tube) and the volume radius r_v is the radius of a cylinder that gives the same volume of the tube, $\mu r_v^2 l_t$. The same analogy accounts for chambers.

The conductance between chambers *i* and *j* (i.e., g_{ij}^w) is found akin to capacitors in series:

$$\frac{1}{g_{ij}^w} = \frac{1}{g_t^w} + \left(\frac{1}{g_i^w} + \frac{1}{g_j^w}\right) \qquad (11)$$

where, g_i^w is the conductance of pore i, g_j^w is the conductance of pore j and g_t^w is the conductance of the tube between pores *i* and *j*. For all simulations conducted in this study, a pair of constant pressure boundary conditions were defined along with a pair of no flow boundaries.

Once the aqueous phase steady-state flow is simulated, solute transport is simulated using the two-dimensional advection diffusion equation:

$$V_s \frac{C_i^{t+1} - C_i^t}{\Delta t} = \sum_j^N \{Q_{ij} C_{ij}^t\} + \sum_j^N \left\{ DA_{ij} \frac{\Delta C_{ij}^t}{l} \right\} + \sum_j^K \left\{ DA_{ij} \frac{C_s - C_j^t}{l} \right\} \qquad (12)$$

where Q_{ij} is the flow rate from chamber *j* to chamber *i* (*N* is the number of water filled adjacent chambers to chamber *i*), C_{ij}^t is the difference of concentration between chamber *i* and *j*. A_{ij} is the pore throat area between chamber *i* and *j*. C_i^{t+1} is the concentration of chamber *i* at the next time step and V_s is the volume of chamber i. The third term accounts for the dissolution and is only applied if the chamber *i* is adjacent to NAPL-occupied chambers (*K* is the number of NAPL filled adjacent chambers to chamber *i*). The NAPL dissolution term is based on the stagnant layer assumption in the tube. The above system of equations accounts for both advection and diffusion of solutes within the pore network. Complete mixing of the solutes in chambers is assumed [Dillard and Blunt, 2000]. The transport model is solved explicitly in time until the change of solute concentration in each node ceases, meaning that the system has achieved steady state conditions. In this model, the NAPL dissolution is simulated for the particular NAPL configuration in each simulation ignoring the transient change of the NAPL size with dissolution and its effect on interphase mass transfer. The above equations are coded in MATLAB 2013R.

2.1. Implementation of pore scale numerical model

The pore network used in the simulations is shown in Figure 1. Figure 1a presents the packed sphere system (light blue spheres) and its representation as a network of chambers (purple) and tubes (dark blue). To show the correspondence between the two, Figure 1b shows the pore network superimposed over the packed sphere system. The cross sectional area of a chamber was assumed as four times the area of a tube. Furthermore, the chambers were assumed to be in cubic form whereas tubes had square cross sectional area and a length that is half of the tube width. This set up exhibits a pore chamber volume that is only 7% greater than the pore body volume of the packed sphere system as presented in Figure 1a (i.e., a coordination number of 6).

a)

b)

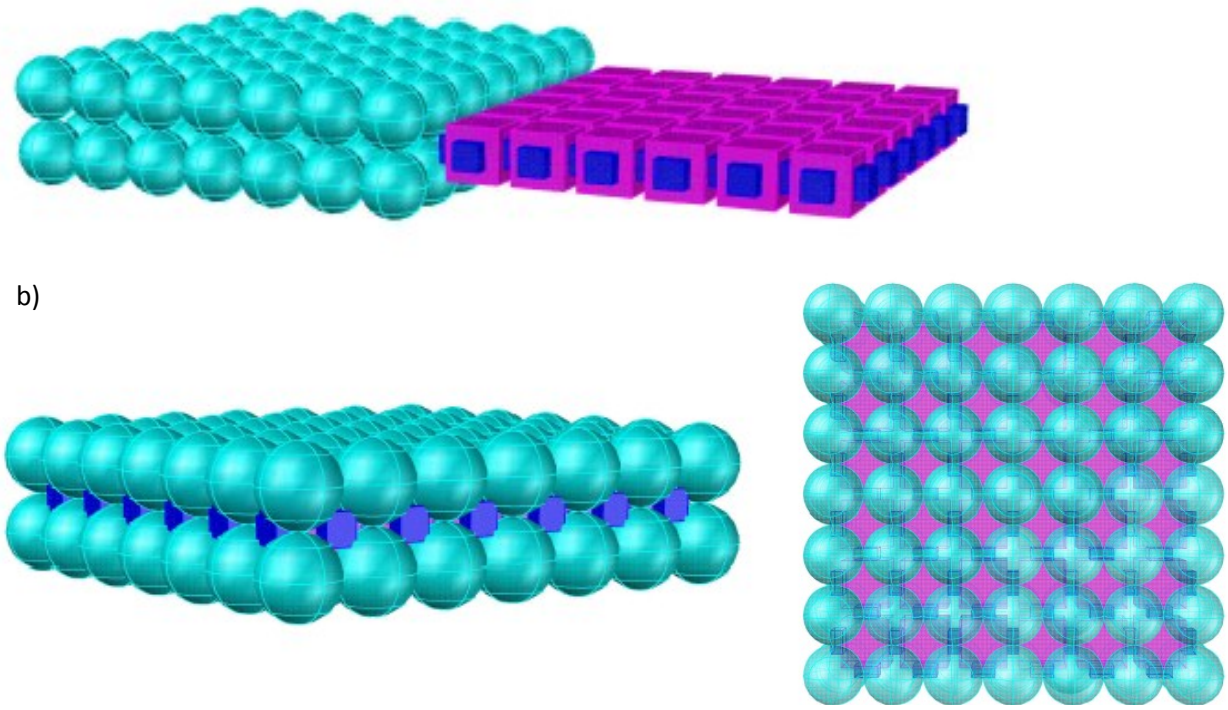

Figure 1. a) The packed sphere system (light blue) and its representation as a pore network consisting of chambers (purple) and tubes (dark blue) b) Perspective and plan view of the pore network model superimposed over the pores of packed spheres for comparison

For the sake of demonstration, toluene was chosen as the dissolving NAPL. This was needed for the definition of the NAPL properties; however, other NAPLs could have been equally selected. The diffusion coefficient and solubility of toluene are 8.6×10^{-10} m^2/s and 565 mg/L respectively. A list of the pore network simulations conducted in this study is presented in Table 1. In total 13 sets of simulations were conducted. Each simulation set was repeated for 14 different velocities ranging between 0.01 m/d to 28 m/d to reveal the effect of velocity in relation to other variables. The simulation variables include the saturation, mean grain diameter, domain size, effective specific interfacial area (i.e., total meniscus interfacial area divided by the total volume of the domain), and geometric allocation of the NAPL mass. The considered saturations ranged between 0.025 and 0.3. Greater saturations were not considered as it was noted that for saturations of 0.35 or greater, effluent concentrations would normally be close to solubility for the range of velocities that are encountered in the subsurface [Nambi and Powers, 2003, 2000] indicating that for such conditions rate limited mass transfer expressions would not be necessary.

Table 1. List of conducted pore-network simulations

Simulation Name	Saturation	Mean grain diameter (micrometer)	Chamber size (width, depth, length) (micrometer)	Tube size (width, depth, length) (micrometer)	Domain size	Effective specific interfacial area (1/m)	Geometric allocation of NAPL
Set 1	0.05	500	400, 400, 400	200, 200, 100	20X20X1	9.6	Side-parallel
Set 2	0.3	500	400, 400, 400	200, 200, 100	20X20X1	17.6	Side-parallel
Set 3	0.05	500	400, 400, 400	200, 200, 100	20X20X1	9.6	Orthogonal
Set 4	0.3	500	400, 400, 400	200, 200, 100	20X20X1	17.6	Orthogonal
Set 5	0.05	250	200, 200, 200	100, 100, 50	40X40X1	9.6	Side-parallel
Set 6	0.05	250	200, 200, 200	100, 100, 50	40X40X1	9.6	Orthogonal
Set 7	0.05	500	400, 400, 400	200, 200, 100	30X30X1	6.4	Side-parallel
Set 8	0.08	500	400, 400, 400	200, 200, 100	30X30X1	9.6	Side-parallel
Set 9	0.3	500	400, 400, 400	200, 200, 100	20X20X1	123.2	Distributed-orthogonal
Set 10	0.05	500	400, 400, 400	200, 200, 100	20X20X1	32	Distributed-orthogonal
Set 11	0.05	500	400, 400, 400	200, 200, 100	30X30X1	32	Distributed-parallel
Set 12	0.025	500	400, 400, 400	200, 200, 100	30X30X1	16	Distributed-orthogonal
Set 13	0.025	500	400, 400, 400	200, 200, 100	20X20X1	16	Distributed-parallel

The geometric allocation of NAPL, defined as side-parallel, orthogonal or distributed, refers to whether the NAPL is oriented in the direction of flow or orthogonal to flow or whether the NAPL is distributed within the domain. These configurations are presented graphically in Figure 2. Although in reality numerous geometric allocations can occur, only side-parallel, orthogonal and distributed have been considered in this analysis because these geometric settings are seen to bracket more complex NAPL distributions observed in real porous media in terms of their impact on interphase mass transfer. For the side-parallel and distributed-parallel configurations NAPL zone is mostly bypassed by flowing aqueous phase whereas in orthogonal and distributed-orthogonal cases most of the incoming solute free water contact NAPL zone leading to less bypassing.

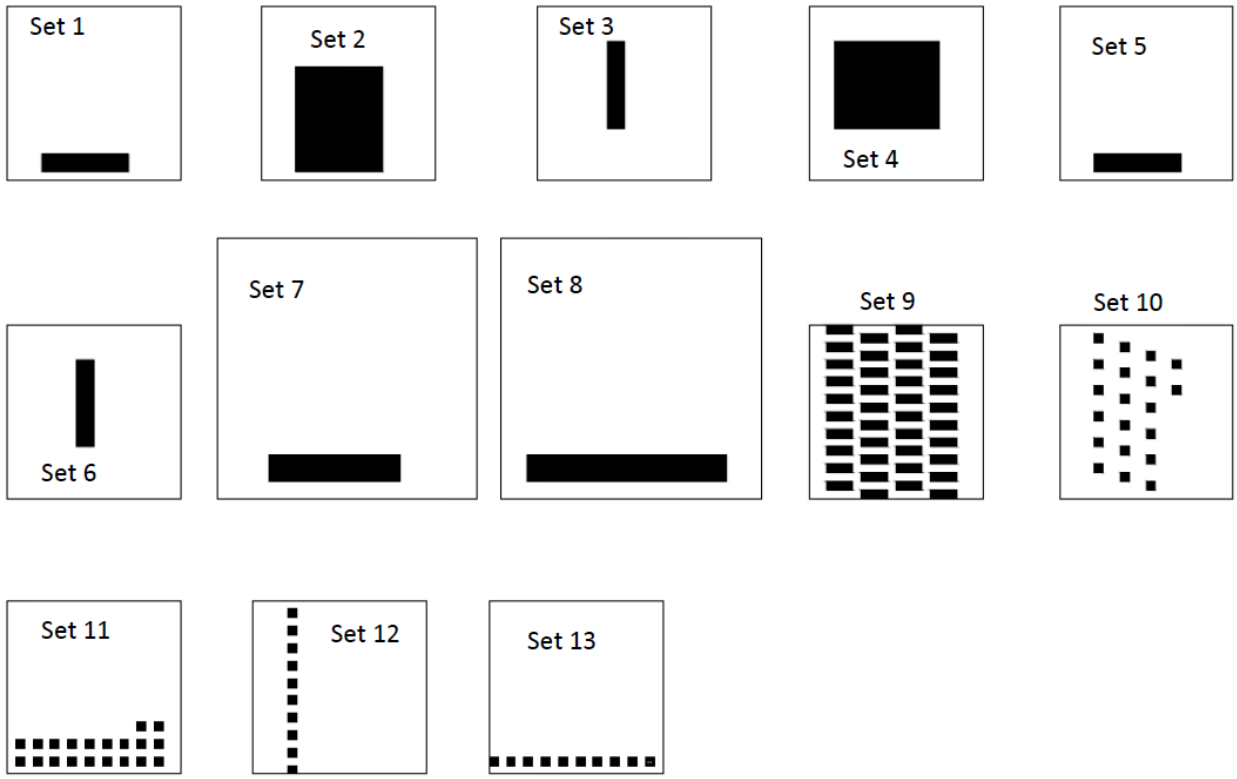

Figure 2. NAPL distributions (in black) within the pore network model considered in this analysis. Flow direction is from left to right.

2.2. Validation of the numerical model

A series of tests were conducted to validate the flow and transport components of the developed pore scale model. The aqueous phase mass balance which is used to calculate the pressure distribution in the domain was found to be conserved for each node. The solute mass balance transport equation checked to confirm that the solute mass balance is indeed conserved. To check the overall validity of the model, the two-dimensional pool NAPL dissolution experiment of Nambi and Powers [2000] was also simulated. The validated experiment (i.e., experiment no. 6 in Nambi and Powers [2000]) involves o-toluidine dissolution from a 3 cm x 5 cm rectangular pooled NAPL formation within a 10 cm x 17.8 cm rectangular porous domain with a mean grain diameter of 1500 micrometers. The solubility and diffusion coefficient of o-toluidine were 16.500 g/L and 7.5 x 10^{-10} m^2/s, respectively. In the numerical model the aqueous phase was assumed to be at residual saturation (immobile) which is consistent with the experimental conditions at the beginning of the experiment as described by Nambi and Powers [2000]. Therefore, the simulated effluent concentrations correspond to initial stage of the experiments where the NAPL is intact and no aqueous flow through NAPL region is present. The domain size for this validation simulation was defined as 70 x 125 x 1. The representation of the porous media with use of pore chambers and tubes were conducted with the same analogy presented in Section 2.1. The resulting pore chamber and tube dimensions were: 1100 µm x 1100 µm x 1100 µm and 600 µm x 600 µm x 300 µm, respectively. The numerical model predicted an average effluent concentration that is 10 % of solubility whereas in the experiment it was reported to be 8 %. The good agreement between model and experimental results provides further validation of the developed pore network model. Finally, through all simulations, water and solute mass balance over individual pores as well as along different sections of the domain was also checked to verify that indeed mass is being conserved.

3. Computation of interphase mass transfer coefficient

The interphase mass transfer coefficient defined at the meso-scale (i.e., derived from column experiments), is commonly calculated with the formulation presented by Powers et al., [1994a], which is based on the solution of the steady state transport equation neglecting the influence of diffusion:

$$k_f = -\left(\frac{q}{La}\right)\ln\left(1-\frac{C_{eff}}{C_s}\right) \qquad (14)$$

where C_{eff} is the effluent concentration, L is the length of the column, q is the velocity of aqueous phase and a is the specific interfacial area. This equation is based on one-dimensional flow assuming uniform NAPL saturation over the length *L*. A more appropriate approach for the analysis of the NAPL dissolution in the pore network model is described below.

For an infinitesimal area, *A*, the mass transfer coefficient can be determined directly from Eq. 1:

$$k_f = \left(\frac{\partial M}{\partial t}\right)\left(\frac{1}{A}\right)\left(\frac{1}{C_s - C}\right) \qquad (15)$$

For the pore network considered in this study, which can be also viewed as a single node in an REV-based numerical model, a representative interphase mass transfer coefficient k_f was computed from Eq. 15 using the entire interfacial area existing in the pore network and a representative concentration, *C*, of the entire domain. The area A in this case is the area that contributes to interphase mass transfer which is the total meniscus interfacial area in the pore network model. The concentration, *C*, was defined as the concentration of the aqueous phase averaged over the model domain. Using an average concentration is consistent with REV based numerical models which consider the concentration in a computational node to be representative of that node. In the pore network model the average concentration of the aqueous phase, *C*, can be computed numerically from the simulated pore network concentrations. This approach was also used by Held and Celia, [2001]. The NAPL dissolution rate into the aqueous phase ($\frac{\partial M}{\partial t}$) is the solute mass leaving the pore network domain at steady state, which is determined by summing the solute mass rate leaving the model domain (i.e., the column of pores at the end of the domain). The solute mass rate leaving a pore is determined by multiplying the flow rate of that pore with the concentration of that same pore.

Once the interphase mass transfer coefficient k_f is determined, the lumped interphase mass transfer coefficient K_l is calculated according to Eq. 3. Finally the explicit and modified Sherwood numbers are calculated from Eq. 2 and 4, respectively.

4. Results and Discussions

For each of the simulations listed in Table 1, the impact of pore-scale variability of the NAPL spatial distribution on interphase mass transfer was evaluated by comparing, for selected runs, the explicit and modified Sherwood numbers, expressed as a function velocity. Specifically, the simulations were used to evaluate the impact of five pore-scale factors on interphase mass transfer, namely: (i) NAPL saturation, (ii) Interfacial area (iii) NAPL spatial distribution, (iv) grain size distribution and (v) pore network domain size. Each of these factors is discussed in the following subsections.

4.1. Saturation-Interfacial area

The influence of NAPL saturation on interphase mass transfer can be evaluated by comparing simulation sets 1 to 2 (Table1). In both cases the NAPL has a side-parallel configuration. However, in the latter the NAPL blocks a larger fraction of the area, resulting in more contact of the inflowing water and less bypassing of the NAPL mass. Figure 3 shows the corresponding modified Sherwood numbers as a function of velocity.

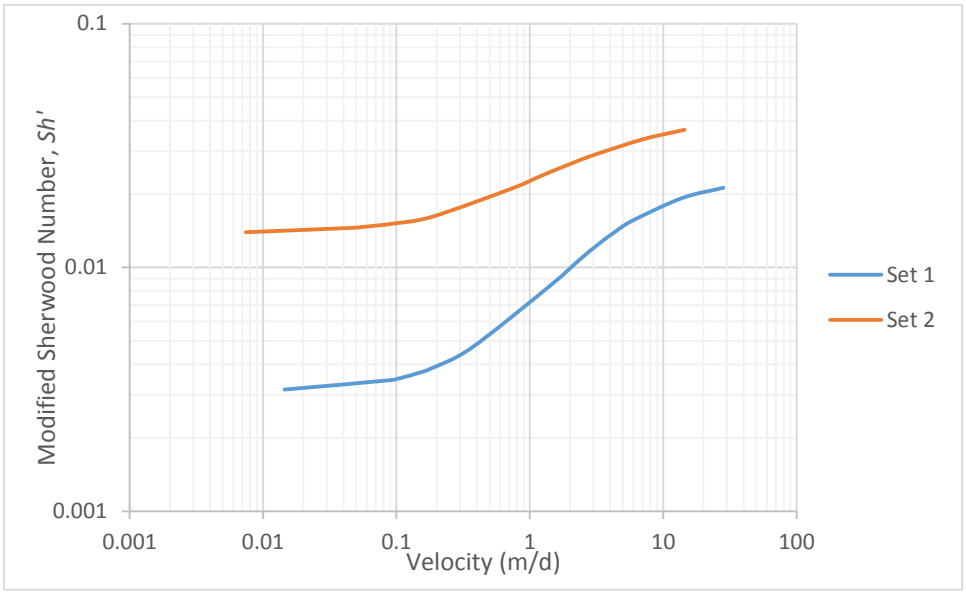

Figure 3. Impact of saturation on the modified Sherwood number

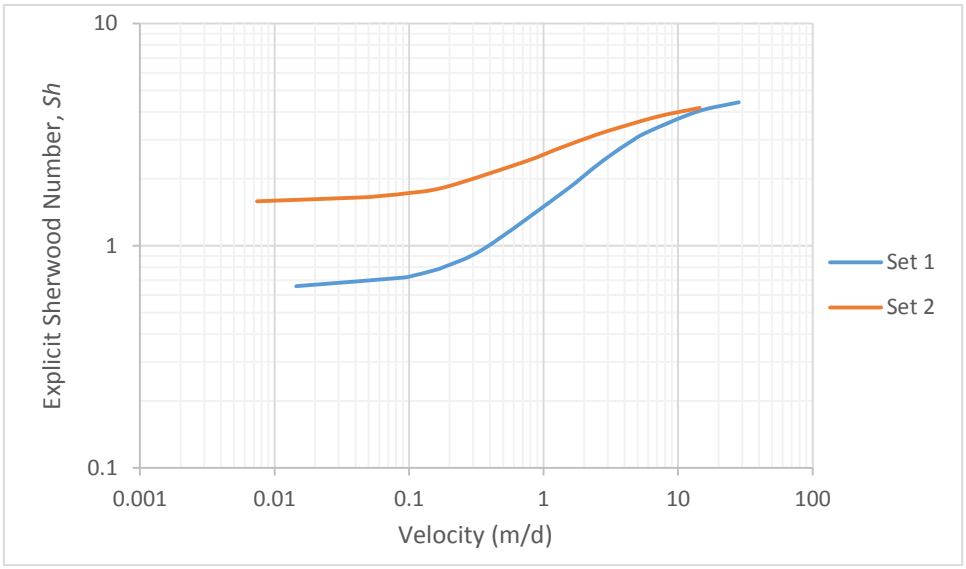

Figure 4. Impact of saturation on the explicit Sherwood number

Figure 3 demonstrates that Set 2 results in a greater modified Sherwood number for the range of velocities considered. Experimental results have also shown that increase in saturation increases the modified Sherwood number [Nambi and Powers, 2003; Powers et al., 1994a, 1994b, 1991; Saba and Illangasekare, 2000]. Similar to the modified Sherwood number results, the explicit Sherwood number increases with increase in velocity (Figure 4). Even though the interfacial area is independently accounted for in the computation of the interphase mass transfer coefficient in (Eq. 15) the explicit Sherwood numbers are different for the two cases. In other words, although the exact interfacial areas are independently accounted for in both sets of simulations, the distribution of the NAPL mass and its contact area do influence the concentration gradient (driving force) at the NAPL-water interface which, in turn, influences the dissolution rate ($\frac{\partial M}{\partial t}$) and the computed Sherwood number. This indicates that while interphase mass transfer at an infinitesimal scale is proportional to the area (Eq. 1), at the REV-scale which is equivalent to the pore network domain considered here, the impact of the interfacial area is not a simple linear relationship as suggested by Eq. 15.

4.2. NAPL spatial distribution

The influence of NAPL distribution and its contribution to NAPL bypassing by the aqueous phase is investigated by comparing Set 1 to Set 3 which have the same saturation and effective specific interfacial area (Table 1). However, the NAPL is located in the direction of flow in Set 1 whereas in the latter, the NAPL is located orthogonal to the flow direction. Figure 5 shows the explicit Sherwood numbers of both simulation sets as a function of velocity.

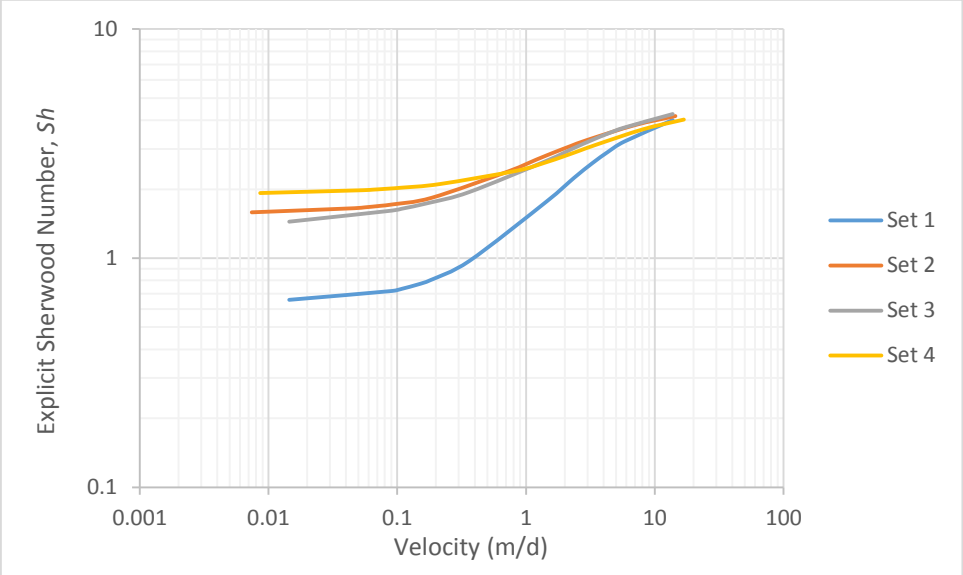

Figure 5. Impact of NAPL spatial distribution on the explicit Sherwood number.

As the NAPL is located orthogonal to the flow direction in Set 3, high contact between the incoming water and the NAPL surface (i.e., low bypassing) results in greater NAPL dissolution rate. In contrast, the NAPL mass located parallel to the flow direction in Set 1 is leading to more NAPL bypassing and lower average effluent concentrations. Therefore, the explicit Sherwood number of the orthogonal case is greater than the parallel case for the same velocities. This result further indicates that solely knowing the amount of interfacial area and velocity is not sufficient to estimate the interphase mass transfer coefficient. This synthetic example of two different NAPL mass distributions highlights the need to account for NAPL bypassing in both explicit and modified Sherwood number formulations. The orthogonal or parallel to flow configuration considered here bracket the more realistic cases observed in real systems. In practice it is not possible to know the exact spatial distribution of the NAPL. However, structural parameters of real porous medium such as mean grain diameters or pore size distribution/uniformity coefficient may be used to indirectly estimate a representative level of bypassing in real media. Such parameters have not been incorporated to existing explicit Sherwood number formulations.

The above simulations with parallel and orthogonal NAPL orientations were repeated for NAPL saturation of 0.3 (Sets 2 and 4). As observed in Figure 5 the difference between the explicit Sherwood numbers of the orthogonal and parallel cases for 0.3 saturation is smaller than the difference for 0.05 saturation. This is a result of the fact that the extent of bypassing becomes similar for both NAPL configurations at higher NAPL saturations because even in the most unfavorable situation (i.e., NAPL is oriented parallel to the flow direction) the NAPL covers a large area of the domain which decreases the potential for the flowing water to bypass the NAPL mass.

It is also observed from Figure 5 that at higher velocities the level of bypassing becomes closer to each other and as a result explicit Sherwood numbers approach each other. The reason for that lies in the description of dissolution in the pore network model. The dissolution of solutes from a NAPL blob residing in a pore chamber to an adjacent NAPL-free pore chamber is defined according to the stagnant

layer assumption given in Eq.13. At high velocities the level of dissolution between these two pores is dependent on the diffusion coefficient, the interfacial area and the tube length (Eq. 13) but to a lesser extent on the concentration in adjacent pore chamber (C_i) which remains substantially lower compared to the aqueous solubility due to the high aqueous phase velocities in any type of geometric settling. In reality the stagnant layer thickness would diminish at high velocities and the corner flow of aqueous phase within the NAPL pore may become significant. Therefore, the interphase mass transfer rate and coefficient would be different for different NAPL settlings at these high velocities. However, this phenomenon is only observed at high velocities, which are unlikely to occur under typical field conditions.

4.3. Mean grain diameter

To evaluate the influence of grain diameter size on mass transfer for both parallel and orthogonal NAPL orientations, Set 1 and 3 can be compared to Set 5 and Set 6, respectively. The decrease in grain size is achieved in the simulations by decreasing the chamber and tube sizes as given in Table 1. To facilitate the comparison the saturation and the effective specific interfacial area of Set 5 and Set 6 were maintained same in these sets. There is some suggestion in the literature that the interphase mass transfer coefficient decreases as the median grain size decreases for the same velocities [Zhang et al., 2002]. This was attributed to the fact that in media with small median grain size, NAPL blobs exist in the form of multi-pore blobs inducing stagnant water formations around them. This eventually leads to smaller interphase mass transfer coefficients. In our set up the geometric formation of NAPL blobs are the same (either parallel or orthogonal) for both high and low median grain size media. Therefore, the interphase mass transfer coefficient of Set 1 would be expected to be similar to Set 5 whereas Set 3 should be similar to Set 6. Because the Sherwood number definitions include the mean grain diameter (Eq. 2 and Eq. 4) which tends to complicate the comparison, the results are depicted instead in terms of the mass transfer coefficient, k_f, against velocity as shown in Figure 6.

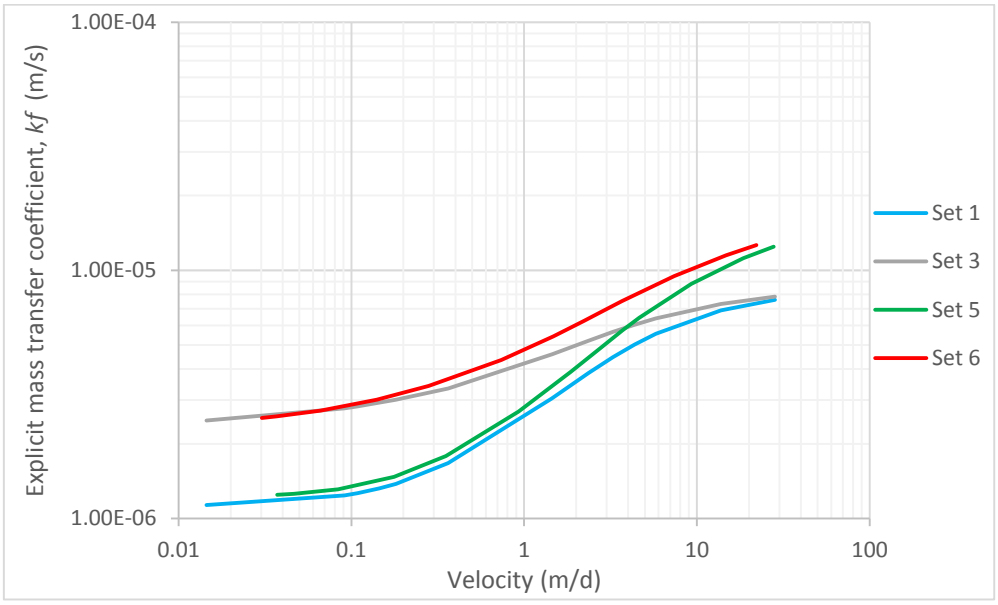

Figure 6. Impact of mean grain diameter on the interphase mass transfer coefficient.

Figure 6 shows that at low to medium velocities, k_f is almost identical for different median grain diameter both for the parallel and orthogonal cases. This results from having the same interfacial area and saturation. However, at high velocities some differences between the mass transfer coefficients is observed and this is attributed to the structure of the pore network model as explained at the end of Section 4.2. At high velocities the concentration of an adjacent-NAPL free chamber (C_i) approaches zero, and thus the dissolved amount becomes dependent on the diffusion coefficient, the interfacial area and tube length. The difference between high and low median grain diameter simulations also results in a difference in the tube length which is one of the terms appearing in Eq. 13. Therefore, at

high velocities, and as the concentrations in aqueous phase become closer to zero, the media with low median grain size is expected to have twice the interphase mass transfer appearing in high median grain size media, leading to the deviance observed at high velocities between Sets 1 and 5 on one hand and Sets 3 and 6 on the other.

It is important to also note that the pore network model presented here is based on a packed sphere system that has a coordination number of 6 and therefore a decrease in the grain diameter did not induce a decrease in total length of pore throats (tubes) in the domain (i.e., in both low and high median size media the total length of the domain is 1 cm in both x and y directions). However, a coordination number of 8 would be more representative of real porous media and, in such cases, a decrease in the mean grain diameter will also lead to increase in total length of tubes due to tortuosity which would mean a reduction in the diffusive transport (Eq. 12) and therefore in interphase mass transfer.

4.4. Domain size

The impact of domain size on the explicit Sherwood number was investigated while maintaining the same saturation and effective specific interfacial area. Therefore, Set 7 is a repeat of simulation set 1, which has a domain size of 20 x 20 (i.e., 1 cm x 1 cm), but with a domain size of 30 x 30 (i.e., 1.5 cm x 1.5 cm) while maintaining a saturation value of 0.05. The number of NAPL-filled chambers is increased from 20 to 45 to maintain the same saturation. However, the interfacial area does not increase at the same order of saturation for the parallel NAPL configuration of Sets 1 and 7 (Figure 1). Therefore, the effective specific interfacial area is smaller in Set 7. To investigate the effect of domain size on the explicit Sherwood number for the same effective specific interfacial area, an additional simulation with the domain size of 30 x 30 is conducted (i.e., Set 8) but with the same specific interfacial area as Set 1. To achieve the same effective specific interfacial area while maintaining the same NAPL configuration (i.e., parallel to flow direction) the saturation was increased to 0.08. Figure 7 shows the corresponding explicit Sherwood number relations as a function of velocity for Sets 1, 7 and 8.

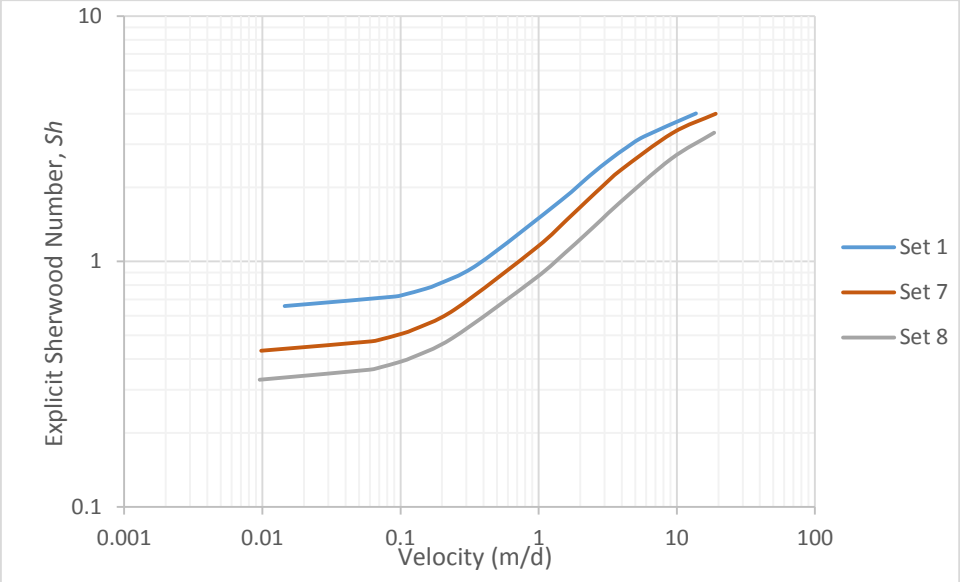

Figure 7. Impact of domain size on the interphase mass transfer coefficient.

The change of domain size from 1 cm x 1 cm to 1.5 cm x 1.5 cm while maintaining the same saturation or same effective specific interfacial area induced a change in the explicit Sherwood number, indicating that the explicit Sherwood formulations are also dependent on the domain sizes that they are developed for and this should be taken into account when Sherwood formulations are used in REV-based numerical models. This further highlights the significance of the grid size of REV-based models on predictions. It is also important to note that as the grid size of REV-based models increase further,

larger scale heterogeneities will be averaged out further reducing the reliability of the predictions of these model.

4.5. The use of the explicit vs. modified Sherwood Expressions in REV-based models

It is broadly acknowledged in the literature that the use of modified Sherwood formulations and the corresponding mass transfer coefficients K_l in REV-based numerical models, are associated with a high level of uncertainty as the impact of the interfacial area is not explicitly accounted. The use of the mass transfer coefficient, k_f on the other hand requires the independent definition of the interfacial area. However, the simulations and ensuing discussion presented in this paper have demonstrated that the explicit Sherwood formulations (and hence the mass transfer coefficient, k_f) also exhibit uncertainty due to NAPL spatial variability at the pore scale even though the interfacial area is accounted for in their development. Results of the pore network model can be further used to evaluate the range of possible values in both of the mass transfer coefficients; K_l and k_f.

The highest/lowest k_f value for a fixed interfacial area and pore network domain size is obtained when the least/most amount of NAPL bypassing by the aqueous phase occurs, respectively. These two extreme cases of bypassing refer to configurations where the NAPL oriented orthogonal and parallel to the flow direction, respectively.

For the lumped mass transfer coefficient K_l, the occurrence of highest and lowest values should be determined while the saturation is kept constant. Since K_l incorporates interfacial area, the highest value of K_l for a certain saturation is likely to occur when the interfacial area is maximum and bypassing is at its lowest. For example for a NAPL saturation of 0.05, the highest K_l is likely to occur when the NAPL is distributed along the domain as single blobs (i.e., the highest amount of interfacial area for that saturation) and also when these distributed NAPL blobs are emplaced orthogonal to flow direction (i.e. least bypassing) which refers to Set 10 in Table 1. On the other hand the lowest K_l for a certain saturation value is likely to occur when the interfacial area is minimum and bypassing is greatest meaning that most of the incoming solute free water leaves the domain without coming in contact with NAPL surface. For a NAPL saturation of 0.05, that refers to Set 1 (Table 1).

Below we compare the possible range of K_l's for two saturation (0.05 and 0.3) by considering extreme cases of bypassing and interfacial area.

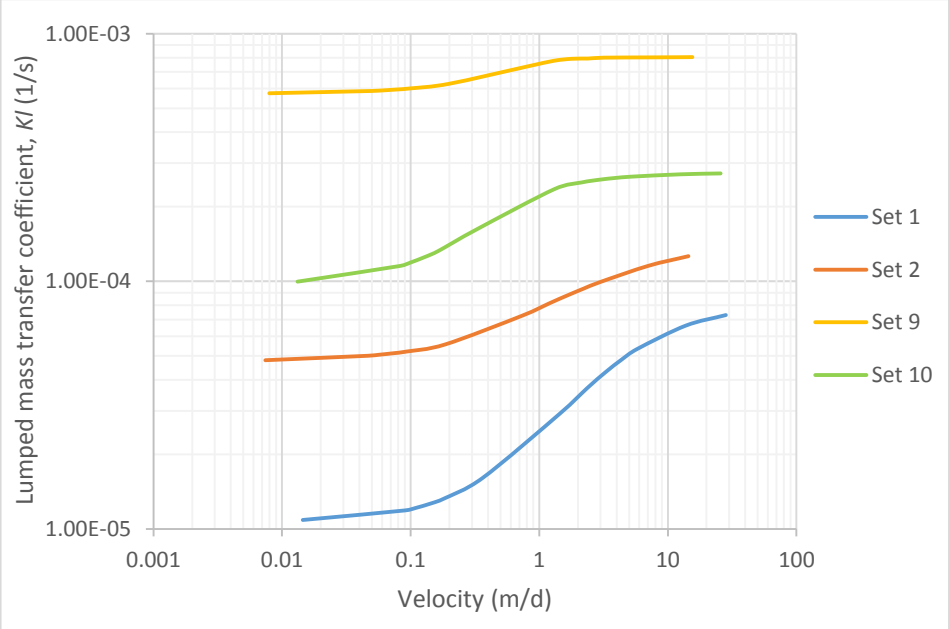

Figure 8. Variability of lumped mass transfer coefficient for a NAPL saturation of 0.05 (i.e., Set 1, 10) and 0.3 (i.e., Set 2, 9)

Figure 8 shows that for a NAPL saturation of 0.05, the highest K_l is given by Set 10 whereas the lowest K_l for the same saturation corresponds to Set 1. For a NAPL saturation of 0.03 the highest K_l is demonstrated by set 9, which has the highest interfacial area at that saturation and lowest bypassing (i.e., orthogonal), whereas Set 2 yields the lowest K_l as it incorporates the lowest interfacial area for that saturation and highest bypassing (i.e., parallel).

The level of uncertainty in mass transfer coefficient k_f, is also investigated for two values of specific interfacial area 16 m^{-1} (Set 12, 13) and 32 m^{-1} (Set 10, 11). At both interfacial areas the lowest and highest bypassing conditions were considered (i.e., orthogonal and parallel to flow direction).

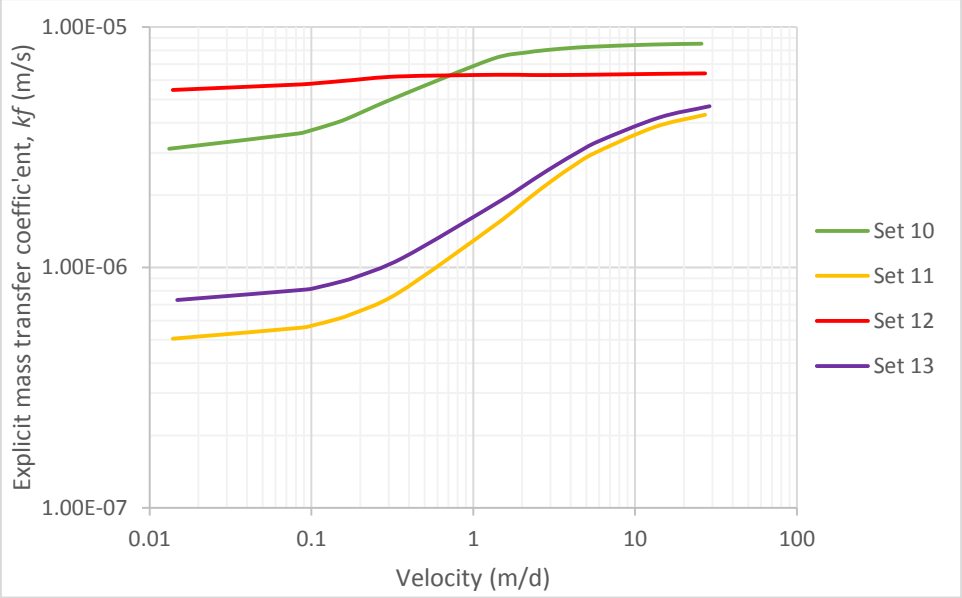

Figure 9. Variability of explicit mass transfer coefficient for an interfacial area of 16 m^{-1} (Set 12, 13) and 32 m^{-1} (Set 10, 11)

Comparison of Set 10 with Set 11 and Set 12 with Set 13 indicates that the lowest bypassing conditions (i.e., orthogonal) yields the highest k_f for the range of velocities for both amounts of interfacial area (Figure 9). For the specific conditions chosen in this exercise the variability of K_l and k_f can reach to an order of magnitude and possibly more due to pore scale NAPL architecture and interfacial area variability. It is important to note that the results presented in Figures 8 and 9 are specific for the assumptions and idealized conditions incorporated in the pore network model. Nonetheless they do provide some indication on the influence of NAPL architecture at the pore scale on interphase mass transfer.

The existing modified Sherwood number formulations (e.g., [Imhoff et al., 1994; Miller et al., 1990; Nambi and Powers, 2003; Powers et al., 1994a]) incorporate different system parameters along with saturation (e.g., uniformity coefficient, porosity etc.) and to some extent these parameters account for the uncertainty discussed above. This is because these parameters are determined from multiple regression analysis and in real porous media the interfacial area and the level of bypassing (which are the sources of the uncertainty demonstrated above) are result of the multiphase flow pattern conditions which are dependent on the pore scale characteristics of the porous medium. However as expressed before the existing explicit Sherwood formulations do not incorporate porous medium properties and this results in not accounting for the possible different bypassing conditions that can occur at sub-grid scale.

5. Conclusion

In this work we investigated the impact of pore scale NAPL architecture on interphase mass transfer using a two dimensional pore network model. This subject is of particular importance as the REV based numerical models rely on Sherwood formulations derived from laboratory- in many cases one-dimensional column- experiments which commonly assume that the NAPL mass is uniformly distributed. In reality, NAPL distributions are almost always spatially variable, even under the most controlled conditions. Their complex patterns of spatial variability stems from the heterogeneity of the porous media from the pore scale to the field scale. This means that the actual NAPL distributions would differ from the idealized conditions assumed in the development of the Sherwood formulations, resulting in significant discrepancies between simulated effluent concentrations and the observed ones.

It is demonstrated that even though the interfacial area is independently accounted for in the interphase mass transfer expressions, the representative mass transfer coefficient k_f of the system (also explicit Sherwood number) is not independent of the interfacial area. This is because the interfacial area does not influence the mass transfer coefficient k_f solely in linear terms but also has indirect influence on the concentration profile and dissolved mass due to pore scale flow patterns.

The pore network model was also used to evaluate the impact of the orientation of the NAPL mass relative to the flow direction. The NAPL configurations considered are NAPL mass oriented parallel to the flow and perpendicular to the flow which bracket the more realistic configurations that may exist in subsurface. The results of the pore scale numerical model demonstrated that different bypassing conditions may exist for the same interfacial area due to pore scale NAPL architecture and flow paths which can have a significant impact on the representative mass transfer coefficient k_f of the system.

The pore network model also shows Sherwood formulations are representative of the domain size that they are developed from and this should also be considered when these formulations are used in REV-based numerical models. It is commonly recognized that small scale variability in the flow parameters are averaged out when larger grid size are used in numerical models. The results shown in this study also demonstrate that even for explicitly defined flow patterns, changing the domain size influences the extent of NAPL bypassing and consequently the interphase mass transfer.

NAPL bypassing is recognized in the literature as an important parameter influencing interphase mass transfer. Some attempts have been made in the literature to quantify the impact of bypassing on interphase mass transfer by developing modified Sherwood formulations that incorporate fluid and porous medium parameters. Similar efforts have not considered with the explicit Sherwood formulations. The use of pore scale structural parameters such as mean grain diameter, pore size distribution, uniformity coefficient may be helpful in this regard. Similar efforts to incorporate fluid and porous media properties in explicit Sherwood formulations are lacking in the literature.

Finally it is important to note that this numerical investigation is not a substitute to detailed experimental investigations to elucidate and quantify the impact of various parameters on interphase mass transfer. However we identified some of the important pore-scale mechanisms and assumptions made during the determination of interphase mass transfer coefficients and their impacts on interphase mass transfer predictions. Along with detailed experimental research, also detailed three dimensional pore network models, developed in conjunction with the latest experimental techniques such as X-ray micro-tomography imaging, can potentially provide high quality data for the development of interphase mass transfer correlations. One of the advantages of pore network models lies in the fact that it provides flow properties in the discrete pores and throats and this information can provide detailed understanding of the transient NAPL dissolution processes in future research.

Notation

A	Interfacial area [L^2]
A_{ij}	Interfacial area between chamber *i* and *j* [L^2]
a	Specific interfacial area [L^{-1}]
C	Concentration [$M\ L^{-3}$]
C_{eff}	Effluent concentration [$M\ L^{-3}$]
C_s	Solubility [$M\ L^{-3}$]
C_{ij}^t	Concentration between chamber *i* and *j* at time step *t* (i.e., equal to concentration of chamber *j* if flow is in the direction of chamber *i* otherwise opposite) [$M\ L^{-3}$]
ΔC_{ij}^t	Concentration gradient between chamber *i* and *j* at time step *t*
D	Diffusion coefficient [$L^2\ T^{-1}$]
d_m	Mean grain diameter [L]
g_w	Conductance [$T\ L^4\ M^{-1}$]
g_i^w	Conductance of chamber *i* [$T\ L^4\ M^{-1}$]
g_t^w	Conductance of tube [$T\ L^4\ M^{-1}$]
g_{ij}^w	Conductance between chamber *i* and *j* [$T\ L^4\ M^{-1}$]
k_f	Explicit mass transfer coefficient [$L\ T^{-1}$]
K_l	Lumped mass transfer coefficient [T^{-1}]
L, l	Length [L]
l_t	Tube length [L]
M	Mass [M]
m_d	Mass transfer term [$M\ T^{-1}$]
P	Pressure [$M\ L^{-1}\ T^{-2}$]
Re	Reynolds number
r_{eq}	Equivalent radius [L]
r	Inscribed radius [L]
r_v	Volume radius [L]
Sh	Explicit Sherwood number
Sh'	Modified Sherwood number
Q_{ij}	Flow rate from between chamber *i* and *j* [$L^3\ T^{-1}$]
Q_w	Flow rate [$L^3\ T^{-1}$]
q	Velocity of aqueous phase [$L\ T^{-1}$]
t	Time [T]
V	Volume [L^3]
V_s	Chamber volume [L^3]
x	Distance into residual NAPL region from the inlet [L]

μ_w	Water viscosity [$M\ L^{-1}\ T^{-1}$]
θ_n	NAPL saturation

References

Abriola, L.M., (1989), Modeling multiphase migration of organic chemicals in groundwater systems--a review and assessment, Environ. Health Perspect. 83, 117–43.

Agaoglu, B.,T., Scheytt, and N.K., Copty, (2012), Laboratory-scale experiments and numerical modeling of cosolvent flushing of multi-component NAPLs in saturated porous media. J. Contam. Hydrol.140, 80-94

Agaoglu, B., Copty, K.N., Scheytt, T., and R., Hinkelmann (2015), Interphase mass transfer between fluids in subsurface formations: A Review., Adv. Water Resour. 79, 162-194.

Agaoglu, B., Scheytt, T., and Copty, K.N. (in review in WRR), The use of Pfannkuch Sherwood Number Correlation for the calculation of the interphase mass transfer in porous media

Basu, N., P, Rao, R., Falta, M., Annable, J., Jawitz, and K., Hatfield, (2008), Temporal evolution of DNAPL source and contaminant flux distribution: Impacts of source mass depletion. J. Contam. Hydrol. 95, 93–109. doi:10.1016/j.jconhyd.2007.08.001

Dillard, L.A., and M. J. Blunt (2000), Development of a pore network simulation model to study nonaqueous phase liquid dissolution, Water Resour. Res. 36, 439–454.

Dillard, L.A., H.I., Essaid, M.J., Blunt, (2001), A functional relation for field-scale nonaqueous phase liquid dissolution developed using a pore network model. J. Contam. Hydrol. 48, 89–119.

Fure, A.D., J.W. Jawitz, M.D., Annable, (2006), DNAPL source depletion: linking architecture and flux response. J. Contam. Hydrol. 85, 118–40. doi:10.1016/j.jconhyd.2006.01.002

Grant, G.P., and J.I., Gerhard, (2007a). Simulating the dissolution of a complex dense nonaqueous phase liquid source zone: 2. Experimental validation of an interfacial area-based mass transfer model. Water Resour. Res. 43, n/a–n/a. doi:10.1029/2007WR006039

Grant, G.P., and J.I., Gerhard, (2007b), Simulating the dissolution of a complex dense nonaqueous phase liquid source zone: 1. Model to predict interfacial area. Water Resour. Res. 43, n/a–n/a. doi:10.1029/2007WR006038

Held, R.J., and M. A. Celia (2001), Pore-scale modeling and upscaling of nonaqueous phase liquid mass transfer, Water Resour. Res. 37, 539–549.

Imhoff, P.T., P. R. Jaffé, and G. F. Pinder (1994), An experimental study of complete dissolution of a nonaqueous phase liquid in saturated porous media, Water Resour. Res. 30, 307–320.

Jawitz, J.W., D., Dai, P.S.C., Rao, M.D., Annable, and R.D., Rhue, (2003), Rate-limited solubilization of multicomponent nonaqueous-phase liquids by flushing with cosolvents and surfactants: modeling data from laboratory and field experiments. Environ. Sci. Technol. 37, 1983–1991.

Jia, C., K. Shing, and Y. C. Yortsos (1999), Visualization and simulation of non-aqueous phase liquids solubilization in pore networks, J. Contam. Hydrol. 35, 363–387. doi:10.1016/S0169-7722(98)00102-8

Joekar-Niasar, V., and S.M., Hassanizadeh, (2012), Analysis of Fundamentals of Two-Phase Flow in Porous Media Using Dynamic Pore-Network Models: A Review. Crit. Rev. Environ. Sci. Technol. 42, 1895–1976. doi:10.1080/10643389.2011.574101

Kokkinaki, A., D. M. O'Carroll, C. J. Werth, and B. E. Sleep (2013a), Coupled simulation of DNAPL infiltration and dissolution in three-dimensional heterogeneous domains: Process model validation, Water Resour. Res. 49, 7023–7036. doi:10.1002/wrcr.20503

Kokkinaki, A., D. M. O'Carroll, C. J. Werth, and B E. Sleep (2013b), An evaluation of Sherwood-Gilland models for NAPL dissolution and their relationship to soil properties, J. Contam. Hydrol. 155, 87–98. doi:10.1016/j.jconhyd.2013.09.007

Maji, R., and E. A. Sudicky (2008), Influence of mass transfer characteristics for DNAPL source depletion and contaminant flux in a highly characterized glaciofluvial aquifer, J. Contam. Hydrol. 102, 105–119. doi:10.1016/j.jconhyd.2008.08.005

Marble, J.C., E. L. DiFilippo, and Z. Zhang (2008), Application of a lumped-process mathematical model to dissolution of non-uniformly distributed immiscible liquid in heterogeneous porous media, J. Contam. Hydrol. 100, 1–10. doi:10.1016/j.jconhyd.2008.04.003

Miller, C.T., G. Christakos, P. T. Imhoff, J. F. McBride, J. A. Pedit, and J. A. Trangenstein (1998), Multiphase flow and transport modeling in heterogeneous porous media: challenges and approaches, Adv. Water Resour. 21, 77–120. doi:10.1016/S0309-1708(96)00036-X

Miller, C.T., M. M. Poirier-McNeill, and A. S. Mayer (1990), Dissolution of trapped nonaqueous phase liquids: Mass transfer characteristics, Water Resour. Res. 26, 2783–2796.

Nambi, I.M., and S. E. Powers, (2000), NAPL dissolution in heterogeneous systems: an experimental investigation in a simple heterogeneous system, J. Contam. Hydrol. 44, 161–184. doi:10.1016/S0169-7722(00)00095-4

Nambi, I.M., and S. E. Powers, (2003), Mass transfer correlations for nonaqueous phase liquid dissolution from regions with high initial saturations, Water Resour. Res. 39, n/a–n/a. doi:10.1029/2001WR000667

Pan, C., E. Dalla, D. Franzosi, and C. T. Miller (2007), Pore-scale simulation of entrapped non-aqueous phase liquid dissolution, Adv. Water Resour. 30, 623–640. doi:10.1016/j.advwatres.2006.03.009

Parker, J.C., and E., Park, (2004), Modeling field-scale dense nonaqueous phase liquid dissolution kinetics in heterogeneous aquifers. Water Resour. Res. 40, n/a–n/a. doi:10.1029/2003WR002807

Pfannkuch, H., (1984), Determination of the contaminant source strength from mass exchange processes at the petroleum-ground-water interface in shallow aquifer systems, Water Well Assoc. Am. Pet. Inst. Houston, Tex.

Powers, S.E.,L. M. Abriola, and J. S. Dunkin, and W. J. Weber (1994a), Phenomenological models for transient NAPL-water mass-transfer processes, J. Contam. Hydrol. 16, 1–33.

Powers, S.E., L. M. Abriola, and W. J. Weber (1992), An experimental investigation of nonaqueous phase liquid dissolution in saturated subsurface systems: Steady state mass transfer rates, Water Resour. Res. 28, 2691–2705.

Powers, S.E., L. M. Abriola and W. J. Weber (1994b), An experimental investigation of nonaqueous phase liquid dissolution in saturated subsurface systems: Transient mass transfer rates, Water Resour. Res. 30, 321–332.

Powers, S.E., C. O. Loureiro, L. M. Abriola, and W. J. Weber (1991), Theoretical study of the significance of nonequilibrium dissolution of nonaqueous phase liquids in subsurface systems, Water Resour. Res. 27, 463–477. doi:10.1029/91WR00074

Saba, T., and T. H. Illangasekare (2000), Effect of groundwater flow dimensionality on mass transfer from entrapped nonaqueous phase liquid contaminants, Water Resour. Res. 36, 971–979. doi:10.1029/1999WR900322

Sahloul, N. A., M. A. Ioannidis, and I. Chatzis. (2002), Dissolution of residual non-aqueous phase liquids in porous media: pore-scale mechanisms and mass transfer rates." Adv. Water Resour. 25, 33-49.

Schnaar, G., and M. L. Brusseau (2006), Characterizing pore-scale dissolution of organic immiscible liquid in natural porous media using synchrotron X-ray microtomography, Environ. Sci. Technol. 40, 6622–6629.

Unger, A.J., P., Forsyth, and E., Sudicky, (1998), Influence of alternative dissolution models and subsurface heterogeneity on DNAPL disappearance times. J. Contam. Hydrol. 30, 217–242. doi:10.1016/S0169-7722(97)00041-7

Whitman, W., (1923), Gas transfer to and across an airtwater interface, Chem. Metall. Eng. 29, 146–148.

Yiotis, A.G., A.K., Stubos, A.G., Boudouvis, and Y.C., Yortsos, (2001) A 2-D pore-network model of the drying of single-component liquids in porous media. Adv. Water Resour. 24, 439–460. doi:10.1016/S0309-1708(00)00066-

Zhang, C., C. J. Werth, and A. G. Webb (2002), A magnetic resonance imaging study of dense nonaqueous phase liquid dissolution from angular porous media, Environ. Sci. Technol. 36, 3310–7.

Zhang, C., H., Yoon, C.J., Werth, A.J., Valocchi, N.B., Basu, and J.W., Jawitz, (2008), Evaluation of simplified mass transfer models to simulate the impacts of source zone architecture on nonaqueous phase liquid dissolution in heterogeneous porous. J. Contam. Hydrol. 102, 49–60. doi:10.1016/j.jconhyd.2008.05.007

Zhao, W., and M.A. Ioannidis, (2003), Pore network simulation of the dissolution of a single-component wetting nonaqueous phase liquid. Water Resour. Res. 39, n/a–n/a. doi:10.1029/2002WR001861

Zhao, W., and M.A., Ioannidis, (2007), Effect of NAPL film stability on the dissolution of residual wetting NAPL in porous media: A pore-scale modeling study. Adv. Water Resour. 30, 171–181. doi:10.1016/j.advwatres.2005.03.025

Zhou, D., L. A. Dillard, and M. J. Blunt (2000) A physically based model of dissolution of nonaqueous phase liquids in the saturated zone, Transp. Porous Media 227–255.

4. Laboratory Scale Experiments and Numerical Modeling of Cosolvent flushing of Multi-component NAPLs in Saturated Porous Media

Berken Agaoglu[a], Traugott Scheytt[a], and Nadim K Copty[b]

[a] Institute of Applied Geosciences, Berlin Institute of Technology, Sekr. BH 3-2, Ernst-Reuter-Platz 1, 10587 Berlin, Germany

[b] Institute of Environmental Sciences, Bogazici University, 34342 Bebek, Istanbul, Turkey

Citation:

Agaoglu, Berken, Traugott Scheytt, and Nadim K. Copty. "Laboratory-scale experiments and numerical modeling of cosolvent flushing of multi-component NAPLs in saturated porous media." *Journal of contaminant hydrology* 140 (2012): 80-94.

Abstract

This study examines the mechanistic processes governing multiphase flow of a water cosolvent-NAPL system in saturated porous media. Laboratory batch and column flushing experiments were conducted to determine the equilibrium properties of pure NAPL and synthetically prepared NAPL mixtures as well as NAPL recovery mechanisms for different water-ethanol contents. The effect of contact time was investigated by considering different steady and intermittent flow velocities. A modified version of multiphase flow simulator (UTCHEM) was used to compare the multiphase model simulations with the column experiment results. The effect of employing different grid geometries (1D, 2D, 3D), heterogeneity and different initial NAPL saturation configurations were also examined in the model. It is shown that the change in velocity affects the mass transfer rate between phases as well as the ultimate NAPL recovery percentage. The experiments with low flow rate flushing of pure NAPL and the 3D UTCHEM simulations gave similar effluent concentrations and NAPL cumulative recoveries. Model simulations over-estimated NAPL recovery for high specific discharges and rate-limited mass transfer suggesting a constant mass transfer coefficient for the entire flushing experiment may not be valid. When multi-component NAPLs are present, the dissolution rate of individual organic compounds (namely Toluene and Benzene) into the ethanol-water flushing solution is found not to correlate with their equilibrium solubility values.

NOMENCLATURE

B: Empirical parameter(for symmetric bi-nodal curve=-1)
C_n^w: Concentration of water in NAPl phase (v/v)
C_w^n: Concentration of organic species in water phase (v/v)
C_p^c: Concentration of cosolvent in cosolvent poor phase (v/v)
C_{kl}^{eq}: Equilibrium concentration of component k in phase l (v/v)
C_{k2}^{oo}: Concentration of component k in NAPL phase (v/v)
C_{23N}: Equilibrium concentration of NAPL phase in aqueous phase (value attained from Ternary phase diagram) (v/v)
C_{min}: The minimum concentration of cosolvent at which HAND's method becomes effective (v/v)
C_k^{ow}: Equilibrium concentration of component k in pure water phase (v/v)
$C_{3_{max}}$: Intercept of maximum height of the Bi-nodal curve (associated with cosolvent at zero salinity) (v/v)
C_{2p}: Concentration of NAPL at plait point (v/v)
C_{kl}: Concentration of species k in phase l (v/v)
g: Gravitational force
$\vec{\vec{k}}$: Intrinsic permeability tensor
k: Intrinsic permeability
k_{rl}^o: Endpoint of relative permeability for phase l
$k_{rl}^{o^{low}}$: Endpoint of relative permeability for phase l at low capillary number
$k_{rl}^{o^{high}}$: Endpoint of relative permeability for phase l at high capillary number
k_{rl}: Relative permeability of phase l
$k_{li\&fu}$: Exponent for interfacial tension function
M_k: Mass transfer coefficient for component k
n_l^{low}: Exponent of relative permeability at low capillary number
n_l^{high}: Exponent of relative permeability at high capillary number
n_p: Number of phases
n_o: Number of organic species
N_{T_l}: Trapping number for phase l
N_{C_l}: Capillary number for phase *l*
N_{B_l}: Bond number for phase *l*
P_{bl}: Bubbling pressure for phase *l* (kP)
$P_{cll'}$: Capillary pressure between phase *l* and *l'* (kP)
S_{nl}: Normalized saturation of phase *l* (v/v)
S_{lr}: Residual saturation of phase *l* (v/v)
S_l: Saturation of phase *l* (v/v)
S_{lr}^{low}: Residual saturation of phase *l* at low capillary number (v/v)
S_{lr}^{high}: Residual saturation of phase *l* at high capillary number
T_l: Desaturation parameter for phase *l*

σ_0: Interfacial tension between water and NAPL phase (dyne/cm)
$\sigma_{ll'}$: Interfacial tension between phase l and l'(dyne/cm)
$\vec{\nabla}\phi_{l'}$: Gradient of flow potential
λ : Pore size distribution index
μ_3: Viscosity of cosolvent+NAPL+water mixture phase (cp)
μ_w: Viscosity of pure water phase (cp)
μ_N: Viscosity of pure NAPL phase (cp)
α_n: Input parameter for viscosity term, n=1,2,..,5
ρ_l: density of phase l (g/cm^3)

Indices refer to:
1= pure water phase
2= pure NAPL phase
3= cosolvent+water phase

1. Introduction

Contamination of the subsurface by hydrocarbons is one of the most challenging environmental problems. Petroleum products (such as benzene, toluene, ethylbenzene, xylene) and chlorinated solvents are among the most commonly encountered contaminants resulting from industrial activities (Wang et al., 1996). Because of their low aqueous solubility due to their non-polar molecular structure, these compounds are often present in the subsurface in the form of non-aqueous phase liquids (NAPL) (Pankow and Cherry, 1996). According to Environmental Protection Agency (EPA) there are about 200,000 NAPL-contaminated sites in the USA alone (U.S. EPA, 1997).

When leaked into the groundwater, NAPLs tend to stay immobile either as a pool or continuous ganglia (residual). The low mobility, solubility and volatility of many NAPLs lead to continuous contamination of the groundwater for decades and perhaps centuries after a spill occurs. Their persistence in the subsurface environment also means that remediation through classical pump & treat would be highly ineffective and that novel technologies are needed to address this problem. In the last two decades there has been substantial research focused on developing effective NAPL remediation technologies (see for example recent review by Henry et al. 2003; Soga et al., 2004; Oostrom et al., 2006). Soil vapor extraction, surfactant flushing and cosolvent flushing are among the most promising technologies for NAPL zone remediation (Oostrom et al., 2006). The use of thermal technologies to improve the remediation efficiency was also a subject of a number of studies (e.g., Davis E.L. 1995, Davis E.L. 1997, O'Caroll D.M. and Sleep B.E. 2005). Recently, the synergistic coupling of different remediation methods was also proposed by various authors. For example, Ramakrishnan et. al. (2005) focused on the effect of cosolvent on TCE biodegradation. Ramsburg et. al. (2004) conducted a field study which coupled the surfactant flooding with microbial reductive dechlorination. Akgoze Aydin et al. (2011) examined the effect of temperature manipulation on the cosolvent flushing efficiency of NAPLs.

In-situ flushing entails the injection of remedial agents into groundwater to enhance the dissolution of NAPL or to mobilize it by reducing its interfacial tension against the aqueous phase (Pennell et al., 1993, Lowe et al., 1999; Kostarelos et al., 1998; Lunn and Kueper, 1999, Jawitz et al., 2000, Wood et al., 2005). Most considered cosolvents in in-situ flushing applications and bench scale experiments are low molecular-weight alcohols such as ethanol, methanol, 1-propanol and 2-propanol (Oostrom et al., 2006). Flushing solutions containing alcohols in small ratios (<20%) are applied to enhance the dissolution mechanism, whereas higher alcohol ratios may also induce mobilization of the NAPL due to significant reduction of the interfacial tension (Imhoff et al., 1995). Under idealized conditions, the latter may propagate full recovery of NAPL within 1-2 pore volumes of flushing, whereas enhanced dissolution may require much larger flushing volumes and longer periods (Lunn and Kueper, 1997). The triggering of mobilization however, may end up with unwanted adverse effects such as downward migration and further spreading of NAPLs which are denser than water (DNAPL) (Grubb et al., 1999; Lunn and Kueper, 1997; Pennell et al., 1996). A large number of studies have focused on the manipulations of system properties (e.g. density, viscosity) to alleviate this problem (Lunn and Kueper, 1997; Brandes and Farley, 1993, Roeder et al., 2001; Van Valkenburg and Annable 2002, Boyd et al., 2006).

Evaluation of in-situ remediation technologies are mostly based on laboratory-scale experiments and, to a lesser extent, on pilot or field scale demonstrations (Oostrom et al., 2006). The number of modeling studies is substantially less due to the complexity of multiphase flow and the uncertainty in the mathematical representation of the governing processes. This is particularly true for multiphase systems that include surfactants/cosolvents in addition to the aqueous and NAPL components (Liang and Falta, 2008). Existing codes that can simulate multiphase flow developed by universities/companies either as open source or commercial include Eclipse, (Schlumberger Eclipse, 2005), UTCHEM (Delshad et al., 1996), T2VOC (Falta et al., 1995) and MUFTE-UG (Hinkelmann, 2005)

and the one developed by Reitsma and Kueper (1998a, 1998b). However among these multiphase programs only Eclipse and UTCHEM have the capability to model surfactant flushing and only the programs developed by Reitsma and Kueper (1998a, 1998b) and UTCHEM are capable of simulating cosolvent flushing.

Considerable efforts have been invested in the past two decades to understand the recovery mechanisms encountered during cosolvent flushing of NAPLs and their interactions. However, relatively few papers that considered both experimentation and numerical simulation of cosolvent flushing of NAPLs can be found in the literature. The more relevant works to the current study are briefly reviewed here. Reitsma and Kueper (1998a, 1998b) were one of the first published works that considered modeling cosolvent flushing of NAPLs. The multiphase model using a two-film model for mass transfer calculations was applied to alcohol flooding column experiments. Roeder and Falta (2001) modified the UTCHEM code, which was originally developed by Pope and Nelson in 1978 to simulate the enhanced recovery of oil using surfactant and polymer processes (Pope and Nelson 1978), to model unstable conditions which may occur during cosolvent flushing of DNAPLs. Roeder and Falta (2001) reported that adjusting the dispersion coefficients or application of a finer grid may be helpful to model the unstable flushings. Jawitz et al., (2003) considered immobile multicomponent NAPL dissolution into a mobile flushing solution by modeling the dissolution process as desorption. More recently, Kaye et al., (2007) modeled the over- and under-ride of cosolvent solution during DNAPL cosolvent flushing. Liang and Falta (2008) used UTCHEM to model the remediation of a field scale DNAPL contamination using cosolvent flushing with high ethanol content (95%). Liang and Falta (2008) also evaluated the influence of initial distribution of NAPL on model simulations.

The purpose of this study is to perform controlled laboratory-scale NAPL cosolvent flushing experiments involving enhanced solubilization and/or mobilization, and to assess to what extent state of the art modeling is capable of simulating these processes. Both pure and multi-component NAPLs are considered. We also investigated the impact of flushing solution velocity along with cosolvent content on the recovery mechanisms, and how the modeling of these mechanisms is influenced by the computational grid used in the model. In support of these transport experiments, batch experiments for the characterization of multi-component solubilization, interfacial tension (IFT) measurements, and ternary phase behavior with different contaminants and flushing solution compositions were conducted. A modified version of the multiphase flow code UTCHEM (Liang and Falta, 2008) was used to compare the column transport results with model simulations. To our knowledge, similar studies involving controlled experimentation (dissolution and mobilization) of cosolvent flushing of multi-component NAPL and its comparison to numerical simulation have not been published previously in the literature. The NAPLs considered in this work are benzene and toluene, and synthetically prepared mixtures of these two NAPLs. The flushing solutions consist of ethanol-water mixtures with ethanol contents ranging from 20% to 100 % by mass. Different flushing velocities were considered to examine the effect of both equilibrium and non-equilibrium flushing conditions. To investigate the impact of grid geometry on model predictions, model simulations were performed using one-, two-, and three-dimensional grids. The impact of soil heterogeneity on the simulated NAPL recovery was also examined.

2. Experimental Procedure

2.1. Batch Experiments

Batch experiments were performed to acquire the equilibrium properties of the ethanol–NAPL–water system. The interfacial tension (IFT) between the NAPL and aqueous phase was measured with a KSV 703 Digital Tensiometer using the Du Nouy Ring method. The NAPL phase was either pure NAPL (benzene or toluene) or a multi-component NAPL consisting of benzene and toluene at a mass ratio of 50% each. The measurements were conducted at 20 °C and for ethanol contents in the aqueous

phase ranging from 0 to 35% (by mass). For ethanol contents greater than 35%, reliable measurements were not attained due to the miscibility of the multiphase system. For quality control, all IFT measurements were performed in triplicates.

Batch experiments were performed to measure the solubility of pure benzene, pure toluene and a benzene/toluene mixture (consisting of 50% of each by mass) into the flushing solution. The ethanol contents considered in the solubility experiments ranged from 0 to 50% by mass. For larger ethanol contents, the two fluids become miscible. In order to attain equilibrium conditions, contact between the two phases was maintained for 24 hours. Samples from the aqueous phase were then extracted by a gas tight syringe and analyzed using a Hewlett-Packard 5890 Gas Chromatography equipped with flame ionization detector (detection limit = 2 mg/L). All solubility experiments were conducted at 20 °C. To evaluate the reliability of the solubility measurements, experiments were done in duplicates.

Ternary phase diagrams (TPD), describing the dissolution potential of the components within the various phases present in the system, were developed for toluene, benzene and NAPL mixtures. The data inferred from the TPD measurements form an essential part of the input to the multiphase flow simulator UTCHEM. A titration procedure was used to determine the turnover points between the one and two-phase regions which define the location of the miscibility curve on the ternary phase diagrams (Martel et al., 1998, St-Pierre et al. 2004). A solution with a known composition was placed in a glass vial capped with a Teflon mini-valve to minimize evaporation. TPD components (NAPL, water and ethanol) were then gradually added to the solution using a gas tight macro-syringe. After each addition, the amount of chemical added to solution was weighted. The turning point was observed directly from the change in transparency. The titration method was performed at 20 °C.

2.2. Column Experiments

Flushing experiments were conducted with a vertically oriented Chromaflex glass column that enables visual detection of NAPL movement. The column (inner diameter: 4.8 cm, length: 30 cm) was closed at both ends using a perforated Teflon® cap and a stainless steel screen was placed inside the caps to prevent the loss of fines. The column was connected to a peristaltic pump with tubing and packed with homogeneous sand with mean grain diameter of 0.2 mm. The sand consisted of 98.6% SiO_2 with no clay or silt and negligible organic content. To obtain uniform packing of the porous media in the column, the sand was placed and consistently compacted in two-cm increments. The resultant porosity of the sand column was approximately 0.36. The column was then saturated from the bottom by distilled water at a slow flow rate of 1 mL/min for 24 hours, which corresponds to more than 8 pore volumes of water flushing prior to the NAPL injection and ethanol flushing.

A list of the column experiments is presented in Table 1. Experiments were conducted with flushing solutions containing 20%, 50% and 100% ethanol by mass. The organic phase comprised of pure benzene, pure toluene or a mixture of these compounds at a mass ratio of 50% each (all Merck, Gas Chromatography grade). The organic contaminants were dyed with oil-red with a concentration of 4x10-4 M for visual detection. Two flow rates were considered in these experiments: 1 and 3.1 mL/min, which correspond to specific discharges of 0.92 $x10^{-5}$ and $2.8x10^{-5}$ m/s, respectively. One flushing experiment was also conducted with intermittent flow that involves repetitive cycles of flushing at 3.1 mL/min for 30 minutes followed by no flow for 15 minutes. Ten grams of the contaminant was introduced into the column via tubing from the bottom end of the column. It was visually observed that the organic phase distribution was limited to approximately the lower most 5 cm of the column. For each experiment, 4 pore volumes of flushing solution were injected upwards into the column. The effluent samples were analyzed promptly using a Hewlett-Packard 5890 Gas Chromatography equipped with flame ionization detector (detection limit = 2 mg/L).

Table 1: List of column experiments

NAPL	Ethanol Content	Flow Rate[1]
Toluene	100 %	High
Toluene	50 %	High
Benzene	50 %	High
Mixture	50 %	High
Mixture	50 %	Intermittent
Mixture	50 %	Low
Mixture	20 %	High
Mixture	20 %	Low

[1]"High" and "low" flow rates correspond to specific discharges of 2.85×10^{-5} and 0.92×10^{-5} m/s where as intermittent flow involves repetitive cycles of flushing at 2.85×10^{-5} m/s for 30 minutes followed by no flow for 15 minutes.

A tracer experiment was also conducted using CaCl (input concentration corresponding to a conductivity of 1170 mS and flow rate of 3.1 mL/min) to estimate the dispersivity of the sand column.

3. Model Development

A modified version of the multiphase flow simulator UTCHEM-9.0 was used in the numerical investigation. Since its first development by Pope and Nelson (1978), the UTCHEM code has undergone numerous revisions and extensions (Delshad et al., 1996, Roeder and Falta 2001). The model version that is used in the present study is equipped with the interfacial tension calculation method developed by Li and Fu (1992). This IFT calculation method enhances UTCHEM's capability to simulate cosolvent flooding of NAPLs. The modifications on the codes were performed by Liang and Falta (2008).

The main components of the multiphase model as used in the current simulations and how they relate to the parameters obtained from the batch experiments are described in the following sections.

Relative Permeability

The Brooks-Corey formulation (Brooks and Corey 1966) was used to compute the relative permeability of each phase. The relative permeability-saturation curves are scaled by the interfacial tension computed as follows:

$$\sigma = \sigma_0 \left(\frac{X}{X_0}\right)^{k_{li\&fu}} \quad (1)$$

where

$$X = \log\left(C_n^w + C_w^n + C_p^c\right), \quad (2)$$

$$X_0 = X \text{ when } C_p^c = 0 \quad (3)$$

The interfacial tension value obtained from Li and Fu's method, which depends on the phase concentrations of components in the relevant node, is first used to define the trapping number (Delshad et al., 1996):

$$N_{T_l} = \left|N_{C_l} + N_{B_l}\right| \quad (4)$$

where

$$N_{C_l} = \frac{\left|\vec{\bar{k}} * \vec{\nabla}\phi_{l'}\right|}{\sigma_{ll'}} \quad (5)$$

$$N_{B_l} = \frac{kg(\rho_l - \rho_{l'})}{\sigma_{ll'}} \quad \text{for } l = 1, \ldots, n_p \quad (6)$$

Once the trapping number is defined, the residual saturation value at that node and that moment in time is computed according to

$$S_{lr} = min\left(S_l\ , S_l^{high} + \frac{S_{lr}^{low} - S_{lr}^{high}}{1 + T_l N_{T_l}}\right) \quad \text{for } l = 1, \dots, n_p \tag{7}$$

Ultimately this residual saturation value is used to scale the endpoint and exponent relative permeability values which are used in the relative permeability function:

$$k_{rl}^o = k_{rl}^{o^{low}} + \frac{S_{lr}^{low} - S_{lr}}{S_{lr}^{low} - S_{lr}^{high}}\left(k_{rl}^{o^{high}} - k_{rl}^{o^{low}}\right), \tag{8}$$

$$n_l = n_l^{low} + \frac{S_{lr}^{low} - S_{lr}}{S_{lr}^{low} - S_{lr}^{high}}\left(n_l^{high} - n_l^{low}\right) \text{ for } l = 1, \dots, n_p \tag{9}$$

Where the super scripts "low" and "high" refer to low and high capillary numbers.

The relative permeability-saturation equation is defined according to the Brooks-Corey formulation. During a NAPL spill event, two phases (organic and water) are assumed to be present and the relative permeabilities of the water and organic phases are, respectively:

$$k_{r1} = k_{r1}^o (S_{n1})^{n1} \tag{10}$$

$$k_{r2} = k_{r2}^o (1 - S_{n1})^{n2} \tag{11}$$

with the normalized saturation of the water phase given by: $S_{n1} = \frac{S_1 - S_{r1}}{1 - S_{r1}}$

On the other hand, during remediation, up to three phases may be present (organic, water and cosolvent). The relative permeability of each phase is expressed as a function of normalized saturation of that phase:

$$k_{rl} = k_{rl}^o (S_{nl})^{n_l} \quad \text{for } l\text{=1,2 or 3} \tag{12}$$

where the normalized saturation of each phase is: $S_{nl} = \frac{S_l - S_{lr}}{1 - (S_{1r} + S_{2r} + S_{3r})}$ for *l*=1,2 or 3

Capillary Pressure

The capillary pressure was also calculated by the Brooks-Corey method:

$$\left(\frac{P_{bl}}{P_{cll'}}\right)^{\lambda} = 1 - \mathrm{S}_{nl'} \tag{13}$$

The flushing solution injection process is assumed to be in the imbibition direction for the entire injection period (Deshad et al., 1996). The capillary pressure function is scaled with respect to interfacial tension, porosity and permeability of the relevant node (Brooks and Corey 1966, Leverett 1941). The entry pressure for benzene, toluene and their mixture is determined using the Young-Laplace equation with a contact angle of 20 degree (highly hydrophilic medium). The computed entry pressure of 5.032 kP showed good agreement with the literature (Eichel et al., 2005). The pore size distribution index was taken as 2, which is typical for porous media similar to the fine sand used in our experiments (Corey 1994, Reitsma and Kueper 1998a).

Ternary phase diagrams (TPD)

UTCHEM uses TPD to define the dissolution potential of various phases within each other. The equilibrium solubility of NAPL in ethanol-water mixtures is calculated from the compositions acquired from TPD (Delshad et al., 1996). UTCHEM constructs the TPD using the Hand's method (Equations 14

and 15), which states that the equilibrium phase concentration ratios are straight lines on log-log scale (Hand 1939):

$$\frac{C_{3l}}{C_{2l}} = A\left(\frac{C_{3l}}{C_{1l}}\right)^{B} \quad l = 1{,}2 \; or \; 3 \tag{14}$$

$$A = \left(\frac{2C_{3max}}{1- C_{3_{max}}}\right)^{2} \tag{15}$$

The constructed TPD is symmetric. One important input parameter required to create TPD and used in Hand's method is the intercept of maximum height of the Bi-nodal curve (associated with cosolvent at zero salinity), C_{3max}. This input parameter was experimentally measured and used in model.

The UTCHEM model also requires the definition of the tie lines which are lines joining the composition of the equilibrium phases. In the UTCHEM model the tie lines are computed from plait points of the NAPL-water –cosolvent ternary system (Delshad et al., 1996);

$$\frac{C_{3l}}{C_{2l}} = E\left(\frac{C_{33}}{C_{13}}\right), l = 1{,}2 \; or \; 3 \tag{16}$$

$$\text{where; } E = \frac{1-\mathrm{C_{2p}}-\frac{1}{2}\left[-\mathrm{AC_{2p}}+\sqrt{\left(\mathrm{AC_{2p}}\right)^{2}+4\mathrm{AC_{2p}}\left(1-\mathrm{C_{2p}}\right)}\right]}{\mathrm{C_{2p}}} \tag{17}$$

Viscosity

The viscosity of cosolvent+water+NAPL mixture was calculated in terms of the viscosity of the pure phases (water and NAPL):

$$\mu_3 = C_{13}\mu_w e^{(\alpha_1(C_{23}+C_{33}))} + C_{23}\mu_N e^{(\alpha_2(C_{13}+C_{33}))} + C_{33}\alpha_3 e^{(\alpha_4 C_{13}+\alpha_5 C_{33})} \tag{18}$$

The alpha parameters in the above equation were chosen such that the calculated values match the measured viscosity data by Lee and Peters (2004) for a toluene-water-ethanol system.

Non-equilibrium Dissolution

Dissolution of pure compounds into the flushing solutions was defined in this study either as a local equilibrium or a non-equilibrium process. For non-equilibrium mass transfer, a linear driving force rate, as proposed by Powers et al. (1992) is used:

$$\text{Dissolution rate} = M_k\left(C_{k3}^{eq} - C_{k3}\right) \tag{19}$$

Thus the equilibrium solubility of each organic compound is an input parameter (Delshad et al., 1996). When the NAPL is dissolved into the cosolvent+water phase, Hand's equation is used to find the equilibrium solubility value used in the rate-limited mass transfer term.

The dissolution of individual components from a multi-component NAPL into flushing solutions can also be defined as either local equilibrium or non-equilibrium process. In both equilibrium and non-equilibrium conditions dissolution is defined as the summation of dissolution of NAPL into pure water (in the flushing solution) and into flushing solution itself (due to its cosolvent content):

$$C_{k3}^{eq} = C_{k2}^{oo} C_{23N}\left(1 - \sum_{k=1}^{n_o} C_k^{ow} - C_{min}\right) + C_k^{ow} \quad k = 1{,}2, \ldots, n_o \tag{20}$$

The individual dissolution of each organic compound into the cosolvent+water phase is also calculated with respect to the volume percentage of that organic compound in the NAPL phase in the relevant node. For non-equilibrium dissolution process a single mass transfer coefficient is assumed for every organic compound.

Model Discretization

To simulate the NAPL flushing experiments, the column length was discretized using 50 equally spaced nodes (0.6 cm in length). The horizontal discretization of the model was gradually increased to assess the impact of model dimensionality on model simulations. For two- and three-dimensional simulations, the cross-sectional area of the column was divided into 5 and 5 by 5 cells, respectively. The time step needed to produce a stable solution was defined internally by the model.

Initial and Boundary Conditions

For all simulations, the column was assumed to be initially fully saturated with water. Ten grams of NAPL were then injected into the center cell of the most bottom layer. This definition is similar to the setup used in the column experiments. The created NAPL distribution by the model at the end of the injection phase, which was later used as initial NAPL saturation in remediation simulations, was found to be limited to the bottom 5 cm of the column. Visual inspection of the column experiments indicated that the experimental and simulated NAPL distributions were consistent with each other.

No-flow conditions were imposed along the sides of the model column. Similar to the NAPL injection, the injection of the flushing solution was also assumed to be in the center cell of the bottom most layer. At the upper boundary a prescribed flow condition equal to the influent flow volume was imposed, with the composition of the effluent determined by the model.

Heterogeneity

To investigate the influence of heterogeneity on model simulations, a series of model simulations were performed assuming that the permeability is modeled as random spatial variable (Dagan, 1989, Rubin, 2003). The specific purpose of these simulations is to provide an order of magnitude assessment of the impact of potential non-uniformness of the sand material and its compactness on effluent concentrations and NAPL recovery. The mean of the permeability field was assumed to be 500 mD. The log transform of the permeability is assumed to have a multivariate Gaussian distribution. Its spatial structure is defined in terms of an exponential semi-variogram with a variance of 1 and an integral scale of 5 cm in the vertical direction and 1 cm in the transverse direction. Multiple fields of the permeability were generated using the turning bands method (Mantoglou et al., 1982) and then used as input in the UTCHEM model.

Table 2 summarizes the key parameter values used in the simulations along with the source of the data.

Table 2: List of key parameters used in the model simulations

Porosity: 0.36

Intrinsic Permeability: 500 mD

Longitudinal dispersivity: 2.5 mm[a]

Transverse dispersivity: 0.8 mm[a]

Hand's Paramaters:

for Toluene C_{3max}=0.615 (v/v)[b], C_{2p}=0.555 (v/v) [c], Cmin=0.01 (v/v) , B=-1

for Benzene C_{3max}=0.589 (v/v)[b], C_{2p}=0.505 (v/v) [c], Cmin=0.01 (v/v) , B=-1

for Mixture C_{3max}=0.601 (v/v)[b], C_{2p}=0.530 (v/v) [c], Cmin=0.01 (v/v), B=-1

Interfacial Tension:

for Toluene ρ_0=34 Dyne/cm, $k_{li\&fu}$=2 [d], X_0=-2.98

for Benzene ρ_0=34 Dyne/cm, $k_{li\&fu}$=2 [d], X_0=-2.54

for Mixture ρ_0=34 Dyne/cm, $k_{li\&fu}$=2 [d], X_0=-2.63

Viscosity parameters: α_1= 4 [e], α_2= 0.65 [e], α_3= 1.2 [e], α_4= 1 [e], α_5= 1 [e]

Capillary pressure parameters: λ=2 [f], $P_{bl} = 5.032kP$

Residual Saturations at low capillary number: S_1^{low}=0.20 [g], S_2^{low}=0.20 [g], S_3^{low}=0.20 [g],

Residual Saturations at high capillary number: S_1^{high}=0.05, S_2^{high}=0.05, S_3^{high}=0.05,

Relative permeability parameters at low capillary number:

$k_{r1}^{o^{low}}$ =0.46 [h], $k_{r2}^{o^{low}}$ =0.46 [h], $k_{r3}^{o^{low}}$=0.46 [h], n_1^{low}=4 [h], n_2^{low}=4 [h], n_3^{low}=4 [h],

Relative permeability parameters at high capillary number:

$k_{r1}^{o^{high}}$=1 [i], $k_{r2}^{o^{high}}$=1 [i], $k_{r3}^{o^{high}}$ =1 [i], n_1^{high}=1 [i] , n_2^{high}=1 [i] , n_3^{high}=1 [i]

[a]: Value found from tracer test.

[b]: Value found from TPD experiments.

[c]: Based on, Chang et al., 1953; Mondain-Monval et al., 1940.

[d]: Based on Li and Fu 1992; Reitsma and Kueper 1998a

[e]: Based on Lee and Peters 2004

[f]: Based on Corey 1994.

[g]: Based on Shah et al., 1995; Fortin et al., 1997

[h]: Based on Corey 1994

[i]: Value taken as "1" in order to make the relative permeability only a function of saturation when the capillary number is high.

4. Results and Discussion

4.1. Batch Experiments

Fig. 1 shows the measured IFT as a function of ethanol content for the three NAPLs considered in this study: pure toluene, pure benzene and an idealized NAPL mixture consisting of benzene and toluene each at 50 % by mass. The 3 NAPL systems showed near identical responses with increasing amount of ethanol in the aqueous phase. The IFT between the three NAPLs and aqueous phase progressively decreases with increase in ethanol content. This implies that the capillary forces between the NAPL phase and the flushing solution would be similar for the 3 NAPLs. Ternary phase diagrams which depict the phase behavior of these three NAPLs in the presence of ethanol are shown in Fig. 2. Toluene having the minor solubility has the greatest peak point at TPD confirming that NAPL toluene needs slightly more ethanol to become fully miscible with the aqueous phase than the benzene and mixture NAPLs.

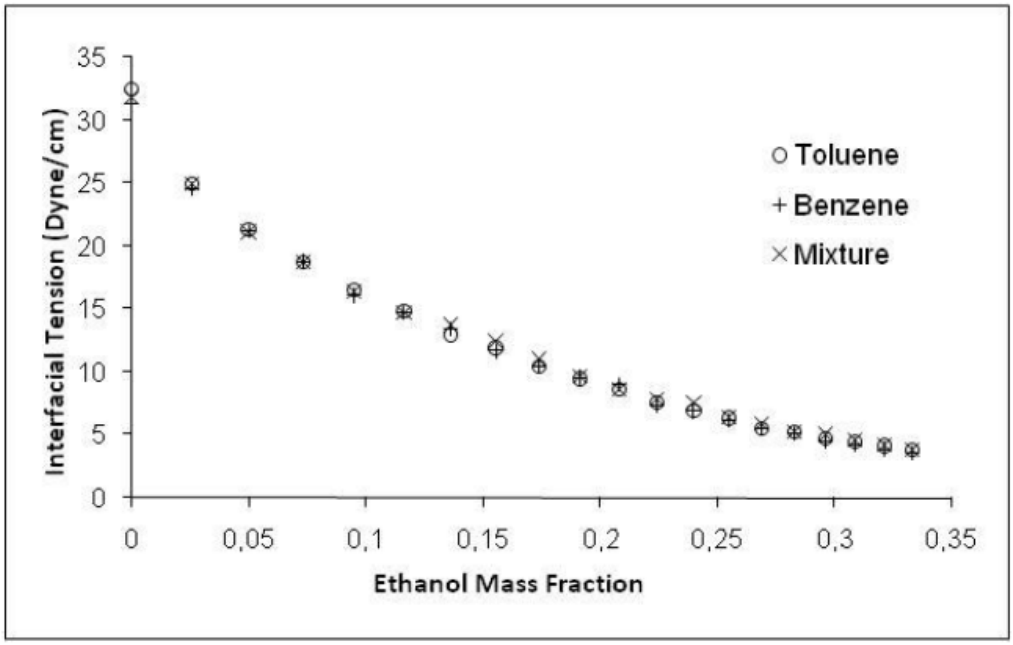

Fig.1 Interfacial tension as a function of ethanol mass fraction in aqueous phase

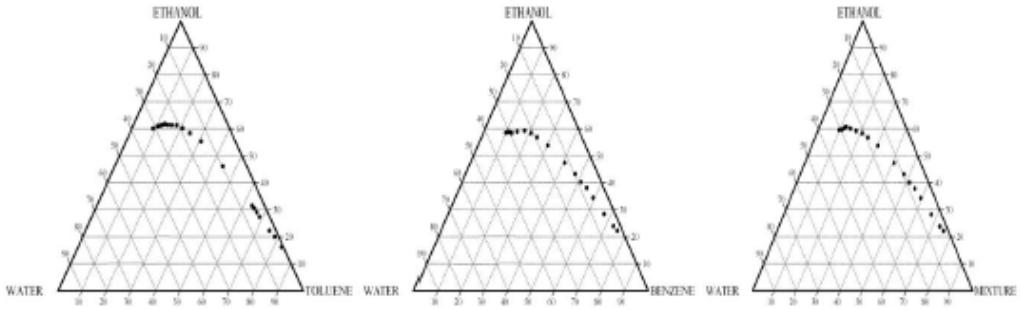

Fig.2 Ternary phase diagrams for a) toluene-ethanol-water b) benzene-ethanol-water c) NAPL mixture-ethanol-water

The solubility of these compounds in an ethanol-water solution can be further analyzed with the help of solubility data attained from batch solubility experiments. Fig. 3 shows the solubility values of different compounds either from pure or multicomponent NAPL.

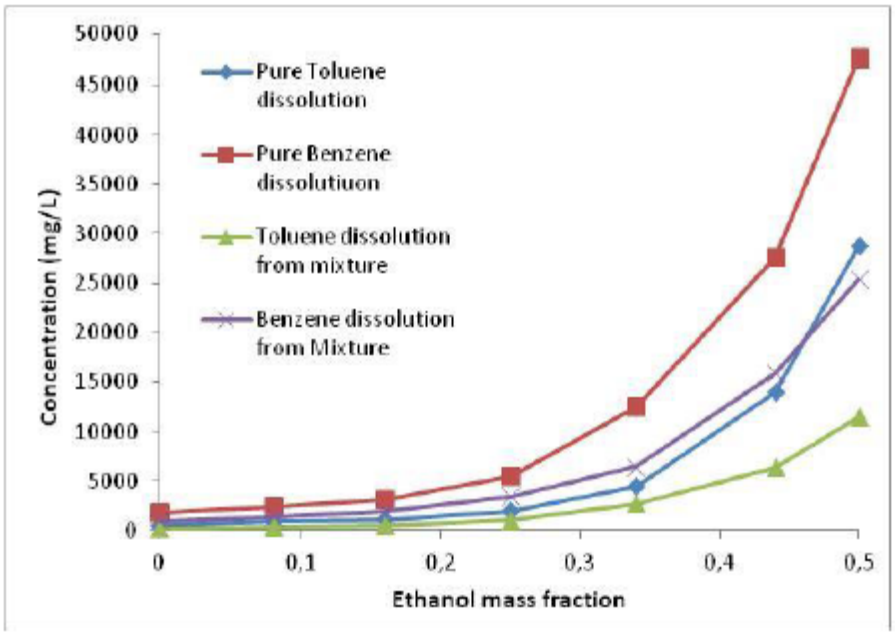

Fig.3 Solubility values attained from batch experiments as a function of ethanol mass fraction in the aqueous phase.
*Data for toluene in figures 1,2 and 3 is taken from Akgöze Aydin et al., 2011

In summary, the IFT data indicate that the potential mobilization of pure toluene, pure benzene and their mixtures using an ethanol-water flushing solution would be near identical. Any differences in the recovered toluene and benzene are likely to be due variations in their relative solubilities. The solubility data show that the benzene solubility is up to 3 times larger than that of toluene, depending on the ethanol content.

4.2. Column Experiments

Column flushing experiments were performed to assess the contribution of enhanced solubilization and mobilization to NAPL recovery. A list of the experiments is given in Table 1. The results of the experiments are presented and discussed in this section. The results of the modeling effort are presented in the following section.

Fig. 4 shows the effluent toluene concentration as a function of pore volume. The NAPL in this case was pure toluene while the specific discharge of the injected flushing solution was 2.8×10^{-5} m/s. Because of the high ethanol content of the flushing solution, near complete toluene recovery was observed. The peak toluene concentration occurred at the end of the first pore volume which indicates that mobilization of NAPL took place at the front edge of flushing solution (e.g., Falta 1998). Photos taken during the experiment also confirmed the presence of two phases in the effluent. Even though the ternary system is fully miscible at equilibrium conditions, the decrease in the IFT of the system to near zero values causes the NAPL to advance as a separate phase before full equilibrium conditions are achieved. It is anticipated that the NAPL would fully dissolve into the flushing solution if the column were long enough.

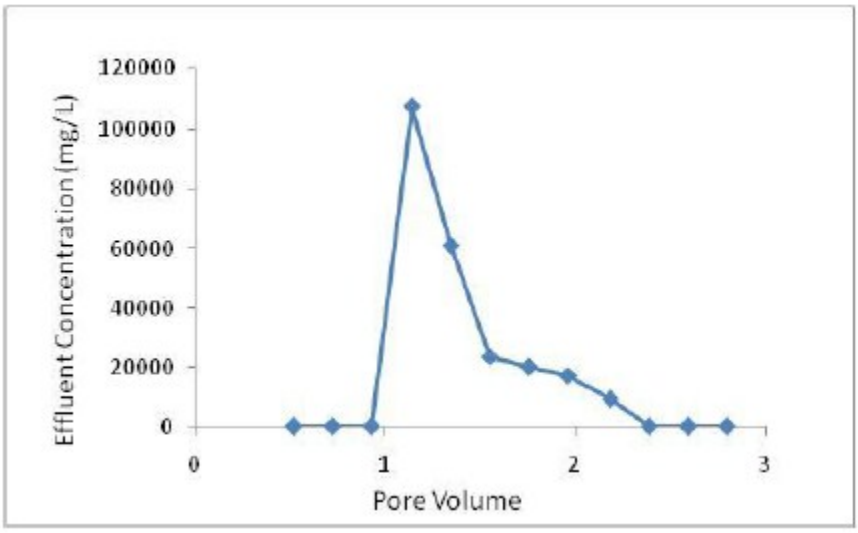

Fig.4 Toluene effluent concentration for the case of pure toluene NAPL and 100% ethanol content in the flushing solution

The next flushing experiments were conducted with pure NAPL (either benzene or toluene) and an ethanol-water mixture containing ethanol at a mass ratio of 50%. The flow rate was maintained uniform at 2.8×10^{-5} m/s (high flow rate). The observed effluent concentrations attained from these 2 column experiments are depicted in Fig. 5. The ultimate recovery for benzene and toluene was 80% and 60%, respectively, with little amount of free phase NAPL observed in the effluent. Although the equilibrium solubility of toluene and benzene in a 50% ethanol- water solution was found to be about 28000 mg/L and 47000 mg/L, dissolution after 4 pore volumes of flushing was significantly lower (<1000 mg/L) for both compounds even though free phase NAPL remained in the column. This is attributed to the presence of non-equilibrium conditions in the column due to the relatively large flow rate used and the shrinking NAPL volume within the porous media leading to less contact with the flushing solution.

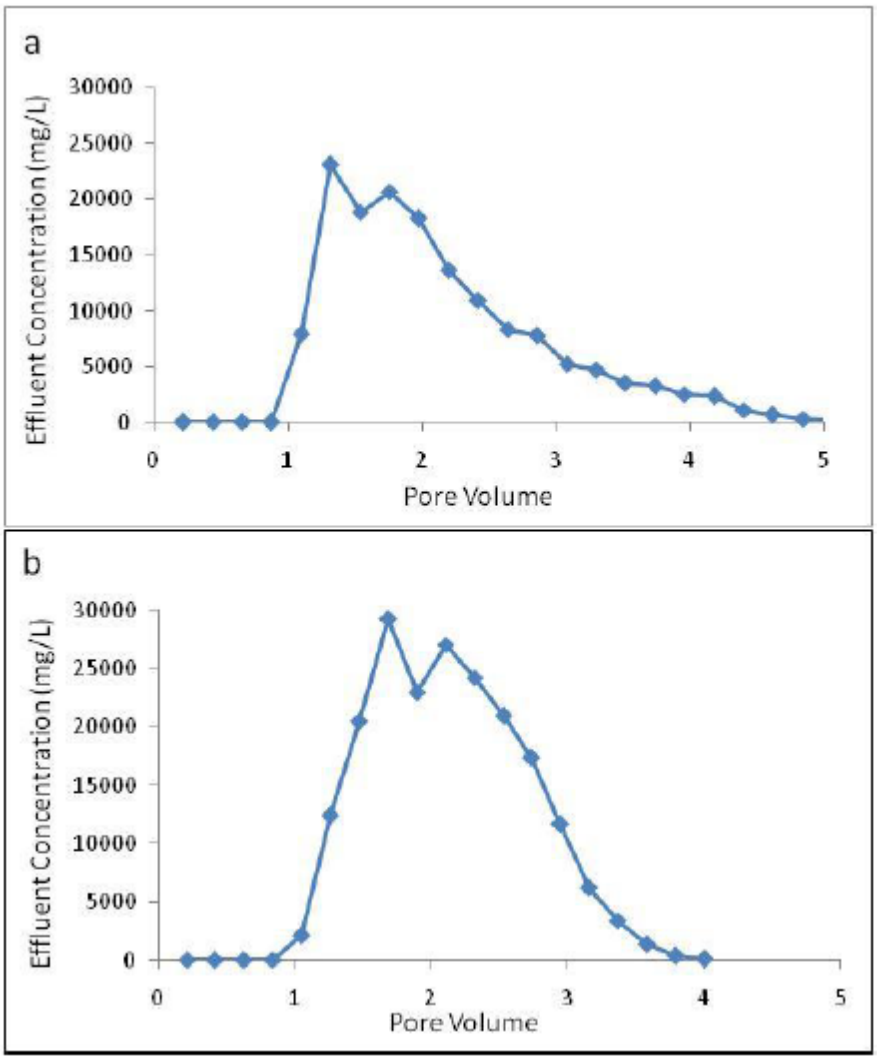

Fig.5 Effluent concentration for the case of (a) pure toluene NAPL and (b) pure benzene NAPL with 50% ethanol content in the flushing solution

The 50% ethanol solution was also used to flush a multi-component NAPL (50% toluene, 50% benzene by mass). To assess the impact of the velocity on mass recovery, the flushing experiments were conducted at two specific discharges: 2.85×10^{-5} and 0.92×10^{-5} m/s. The corresponding effluent concentrations of benzene and toluene are shown in Fig. 6 (a and b), respectively. The total NAPL recovery at the higher flow rate was about 71% which is consistent with the NAPL recovery obtained from the 50% ethanol solutions and pure NAPL experiments. The NAPL recovery at the lower flow rate was about 95%. The reduced recovery at the higher flow rate suggests that the fast flow rate induces preferential flow paths and as a result the NAPL was partially bypassed by the flushing solution. The capillary force between the 50% ethanol-water solution and the NAPL forces the flushing solution to go through the pores which do not exhibit any capillary force. Thus, once NAPL-free flow paths are created at the fast flow, the flushing solution tends to follow these paths. However this behavior did not occur with 100% ethanol flushing because pure ethanol and NAPL are fully miscible and hence the capillary force between these two fluids is zero due to zero interfacial tension between the ethanol and the NAPL.

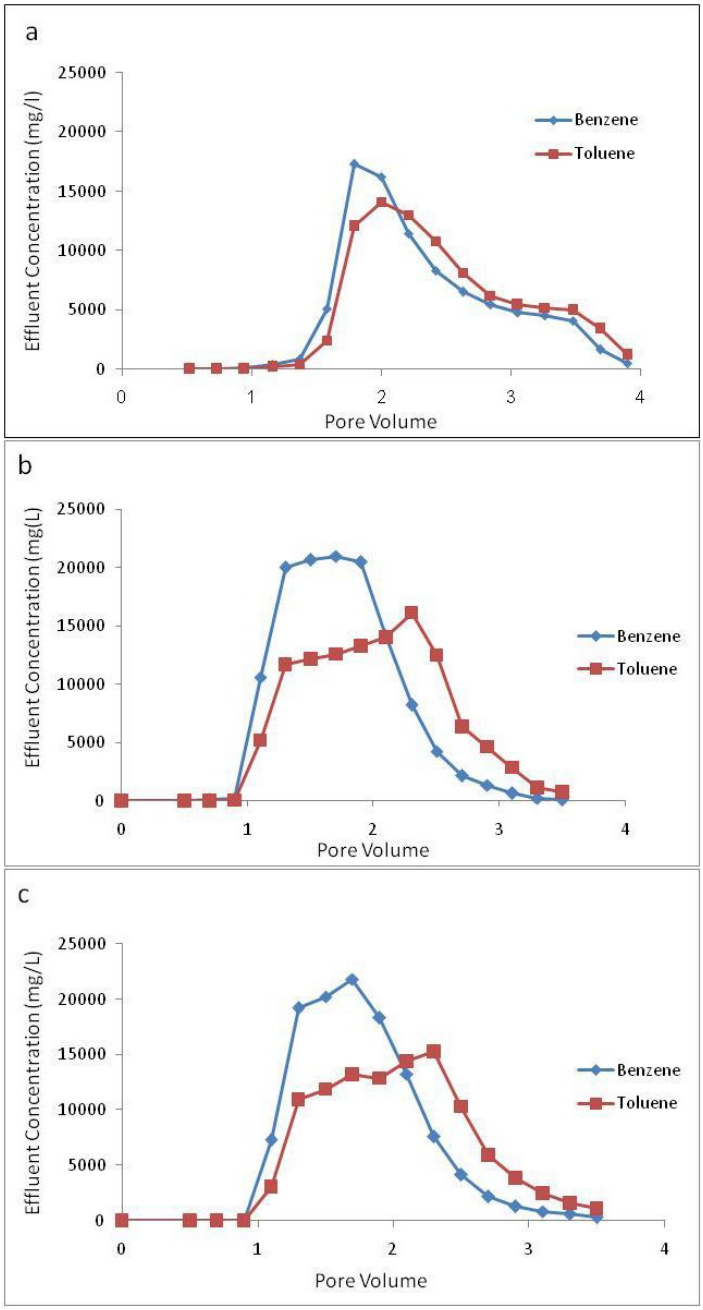

Fig.6 Effluent concentrations for the case of multi-component NAPL (benzene and toluene) with 50% ethanol content in the flushing solution at (a) high flow rate (2.85×10^{-5} m/s), (b) low flow rate (0.92×10^{-5} m/s), and (c) intermittent flow

Examination of the effluent curves of benzene and toluene at both velocities and their solubilities (Fig. 3) indicates that dissolution is the dominant recovery mechanism with the 50% ethanol solution. If NAPL mobilization was the dominant recovery mechanism, the benzene and toluene recovery (effluent concentrations) would be close to each other given that they are at equal proportions (by mass) in the injected NAPL.

The flushing experiments with a multi-component NAPL were also performed with the 50% ethanol flushing solution using an intermittent flow scheme whereby the flushing solution is injected periodically at the higher flow rate (2.8×10^{-5} m/s) for 30 minutes followed by no flow for 15 minutes. Fig. 6c shows the effluent concentration of toluene and benzene as a function of injected pore volume.

The overall NAPL recovery increased to about 90%, which is similar to that observed for the lower flow rate demonstrating the increase in recovery with increase in contact time.

Fig. 7 shows the effluent toluene and benzene concentrations when the multi-component NAPL was flushed with a 20% ethanol-water solution at the two flow rates ($2.8x10^{-5}$ and $0.92x10^{-5}$ m/s). Decreasing the ethanol content to 20% in the flushing solution resulted in no NAPL mobilization (at both flushing rates) with dissolution being the only NAPL recovery mechanism. Moreover, spreading of the NAPL inside the column was not observed unlike the case with 50% ethanol flushing. The equilibrium solubility of benzene and toluene from the mixture NAPL in 20% ethanol-water solution were measured as 3400 mg/L and 1050 mg/L respectively (Fig. 3). The observed effluent concentrations at the lower flow rate indicate that near equilibrium conditions were achieved in the column. At the higher flow rate, the effluent benzene concentrations were only a fraction of the equilibrium concentrations. Moreover, the toluene and benzene concentrations were close to each other suggesting that their mass transfer rates under non-equilibrium conditions are close to each other although the solubility of benzene is about 3.5 times higher than that of toluene. The mass transfer coefficient which in practice is very important because field conditions are often not at equilibrium is calculated as part of the modeling effort presented in the next section.

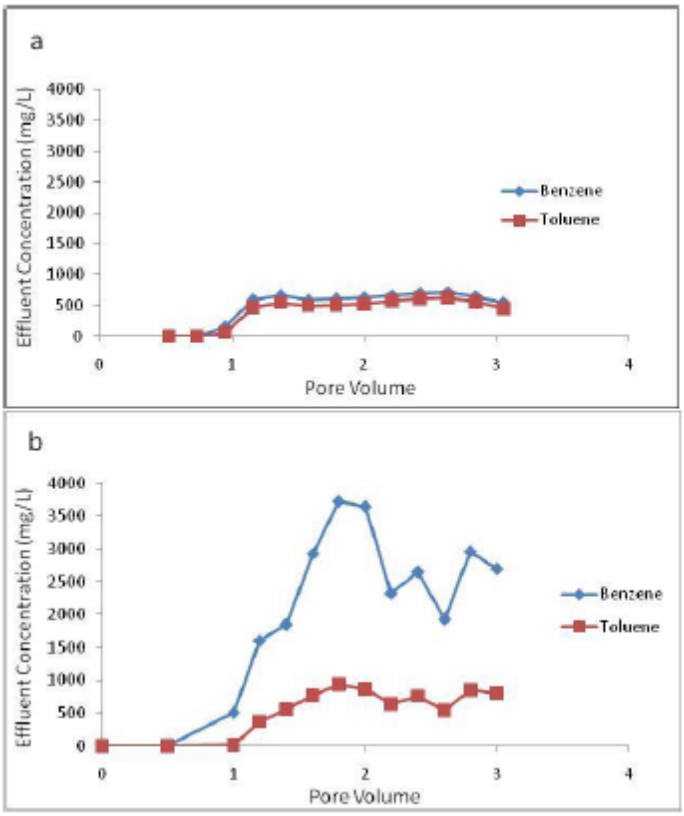

Fig.7 Effluent concentrations for the case of multi-component NAPL (benzene and toluene) with 20% ethanol content in the flushing solution at (a) high flow rate ($2.85x10^{-5}$ m/s), (b) low flow rate ($0.92x10^{-5}$ m/s), and (c) intermittent flow

4.3. Model Results

To gain further insight into the NAPL recovery mechanisms and evaluate our ability to model them, a modified version of the UTCHEM code was used to simulate the NAPL flushing experiments. An important precondition for the reliable modeling of cosolvent flushing is that the multiphase behavior of the cosolvent NAPL system is consistent with observed batch data. At 20% ethanol content

UTCHEM predicted the IFT as 12 dyne/cm whereas measured value was 10 dyne/cm. For 50% ethanol content the extrapolated IFT value from the measured values is about 3 dyne/cm whereas UTCHEM predicted this value as 4 dyne /cm. For 100% ethanol content the measured and the calculated IFT values are both zero because the fluids are fully miscible. Overall, the IFT values calculated by UTCHEM have been found consistent with measured values. The TPD's constructed by UTCHEM have been also compared to the measured TPD's. As can be seen from Fig. 8, the general shapes of the UTCHEM generated TPD and the observed TPD curves are in good agreement. In particular, the heights of the bi-nodal curves are well produced for both pure toluene and pure benzene as well as for the benzene/toluene mixture. There is a slight deviation between the observed and simulated TPD at lower ethanol contents. This is in part due to the built in Hand's model used in the UTCHEM code which assumes a symmetrical TPD. We also compared UTCHEM tie-line predictions to published data of Letcher and Siswana, 1992 for toluene-ethanol-water system and found the results consistent. It is important to note that all components of the real TPD can not be reproduced by simplified Hands model, as also noted by Liang and Falta, 2008.

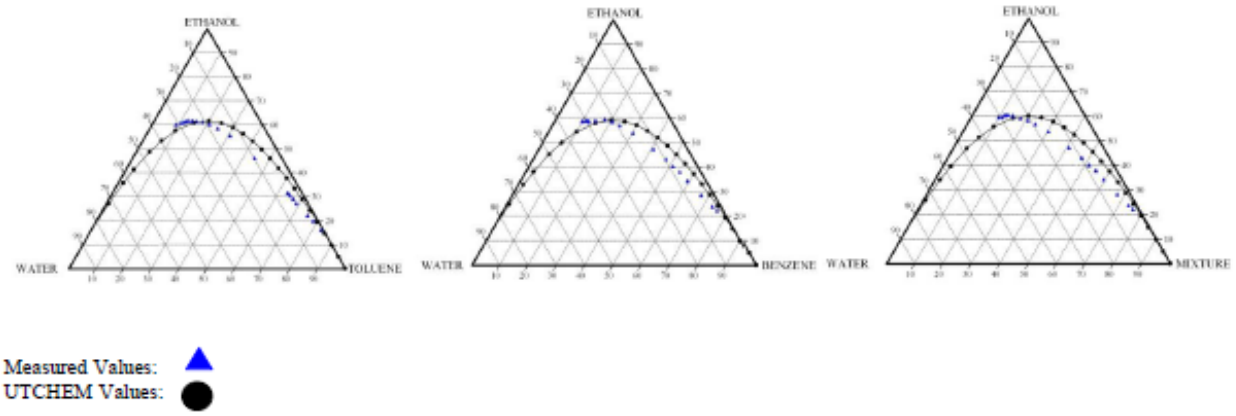

Fig.8 Measured and calculated Ternary phase diagrams for toluene-ethanol-water, benzene-ethanol-water and NAPL mixture-ethanol-water systems

The complexity of the model was gradually increased by first considering one dimensional flow and subsequently extending the model simulations to two- and three-dimensions. Compared to two-dimensional and three-dimensional simulations, the one-dimensional simulations consistently showed the greatest deviation from the experimental results, especially when the mobilization is the dominant mechanism as in pure ethanol flushing case. For demonstration we compare the one-, two- and three-dimensional simulated results for the case of pure toluene with 100% ethanol flushing (Fig. 9). A primary limitation of the one-dimensional simulations is that it unrealistically forces the contact of the NAPL with the flushing solution, resulting in higher effluent concentrations, as much as 250,000 mg/L at certain instances (Fig. 9).

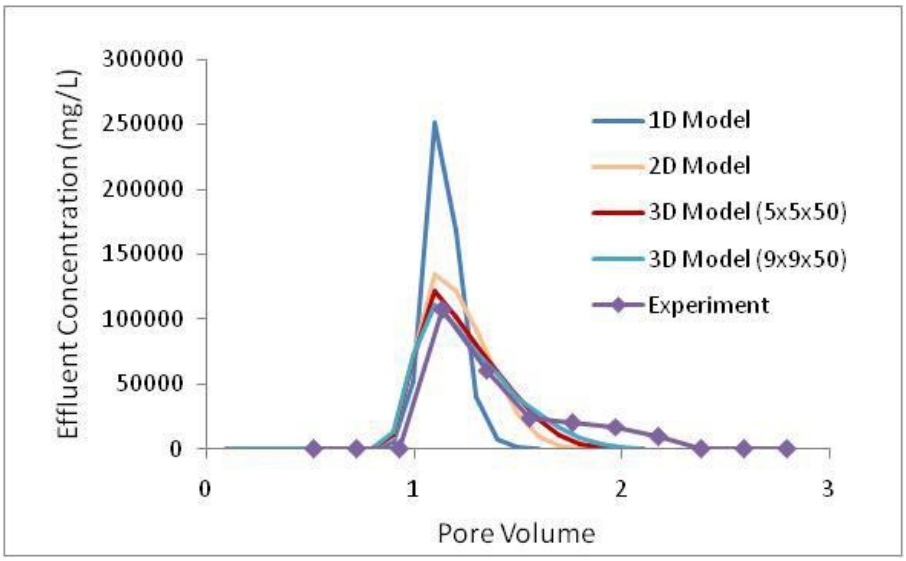

Fig.9 Simulated (1D, 2D, 3D model) and observed toluene effluent concentrations and cumulative mass recovery for the case of pre toluene NAPL and 100% ethanol content in the flushing solution.

Moreover, the three-dimensional model simulations with 5 by 5 cells and 9 by 9 cells in the horizontal plane had practically no influence on the effluent concentrations suggesting that refining the grid any finer would have limited influence on the simulated results. Therefore, subsequent modeling results will be based on the three-dimensional (5 by 5 grid) which appears to yield more realistic results than the one- and two-dimensional model. These simulations were conducted for 3 cases: "local equilibrium (LE)", "rate limited mass transfer at the higher flow (2.85×10^{-5} m/s) (RLMT)" and "rate limited mass transfer at the slow flow (0.92×10^{-5} m/s) (RLMTS)".

Photos taken during the 100% ethanol flushing of toluene experiment confirmed that (Fig. 10) mobilization is the dominant recovery mechanism. Model simulations for the case of flushing with pure ethanol flushing, also show the location of the NAPL zone moving down gradient with time. At intermediate ethanol contents (such as 50%), mobilization and dissolution are both present. Visual inspection of the experiment with 50% ethanol flushing as well as its numerical simulation indicated that the NAPL primarily spreads for the first 10 cm of the column during the first pore volume and then dissolution becomes the dominant mechanism (Fig. 10). Even after 1.5 volumes of flushing, no NAPL is predicted beyond the lower most 10 cm. The initial mobilization has a significant effect on remediation, for it influences the contact area between NAPL and the flushing solution.

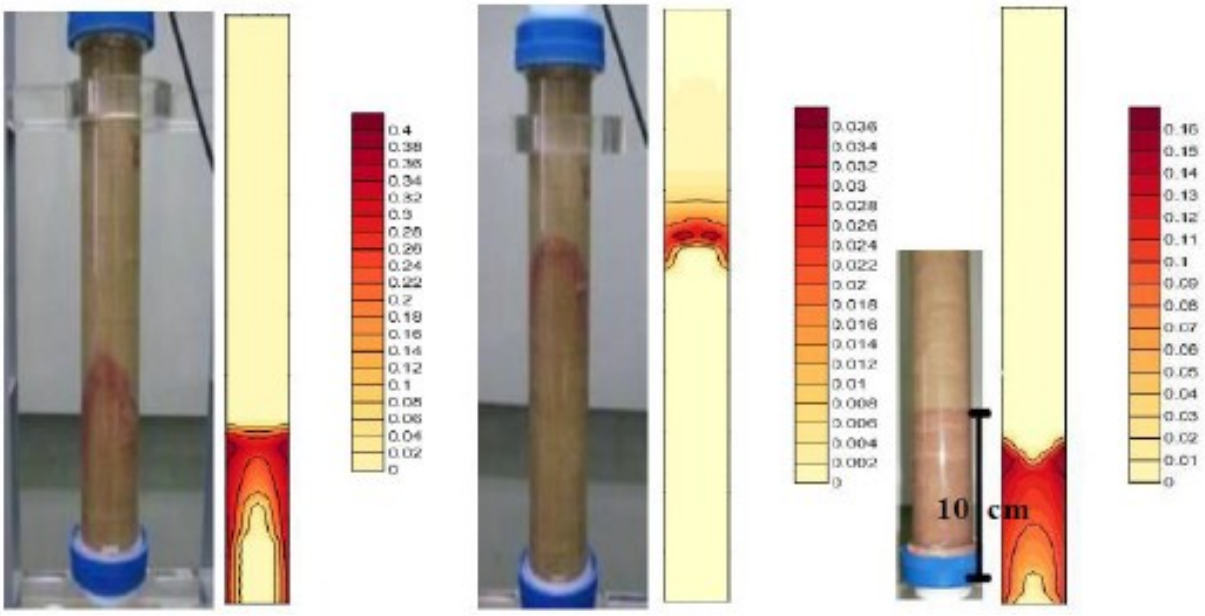

Fig.10 Saturation profiles; a) Experiment and 3D model edge cells at 0.2 pore volume for 100% ethanol flushing of toluene b) Experiment and 3D model edge cells at 0.6 pore volume for 100% ethanol flushing of toluene c) Experiment and 3D model edge cells at 1.5 pore volume for 50% ethanol flushing of toluene

Simulation of Pure NAPL Flushing

As shown in Fig. 9, the agreement between the simulated (two-dimensional model and, in particular, three–dimensional model) and observed effluent toluene concentration, including the peak NAPL concentration, is quite good. The simulated and observed effluent concentrations and NAPL mass recovery for 50% ethanol content and for the case of pure toluene and pure benzene and higher flow rate (2.85×10^{-5} m/s) are shown in Fig. 11(a and b). The simulations were performed assuming the local equilibrium (LE) or the rate limited mass transfer (RLMT) options, respectively. Better agreement between simulated and observed data was obtained using the RLMT option. The best fit mass transfer coefficients, which were determined such that the peak simulated and observed concentrations are equal to each other, were found to be 0.000197 s^{-1} and 0.000273 s^{-1} for toluene and benzene, respectively. However, because the model simulations assume the soil properties are spatially uniform, model simulations predict full NAPL recovery at the end of the simulation whereas the experiments resulted in about 60-70 % NAPL mass recovery. The decrease in NAPL recovery suggests that using a decreasing mass transfer coefficient may be more appropriate than a constant mass transfer coefficient for the entire flushing experiment. The decrease in the overall mass transfer rate would likely reflect the decrease in the contact area between the NAPL and flushing solution. Additional experimental and modeling work, which is beyond the scope of the present study, would be needed to further evaluate this hypothesis.

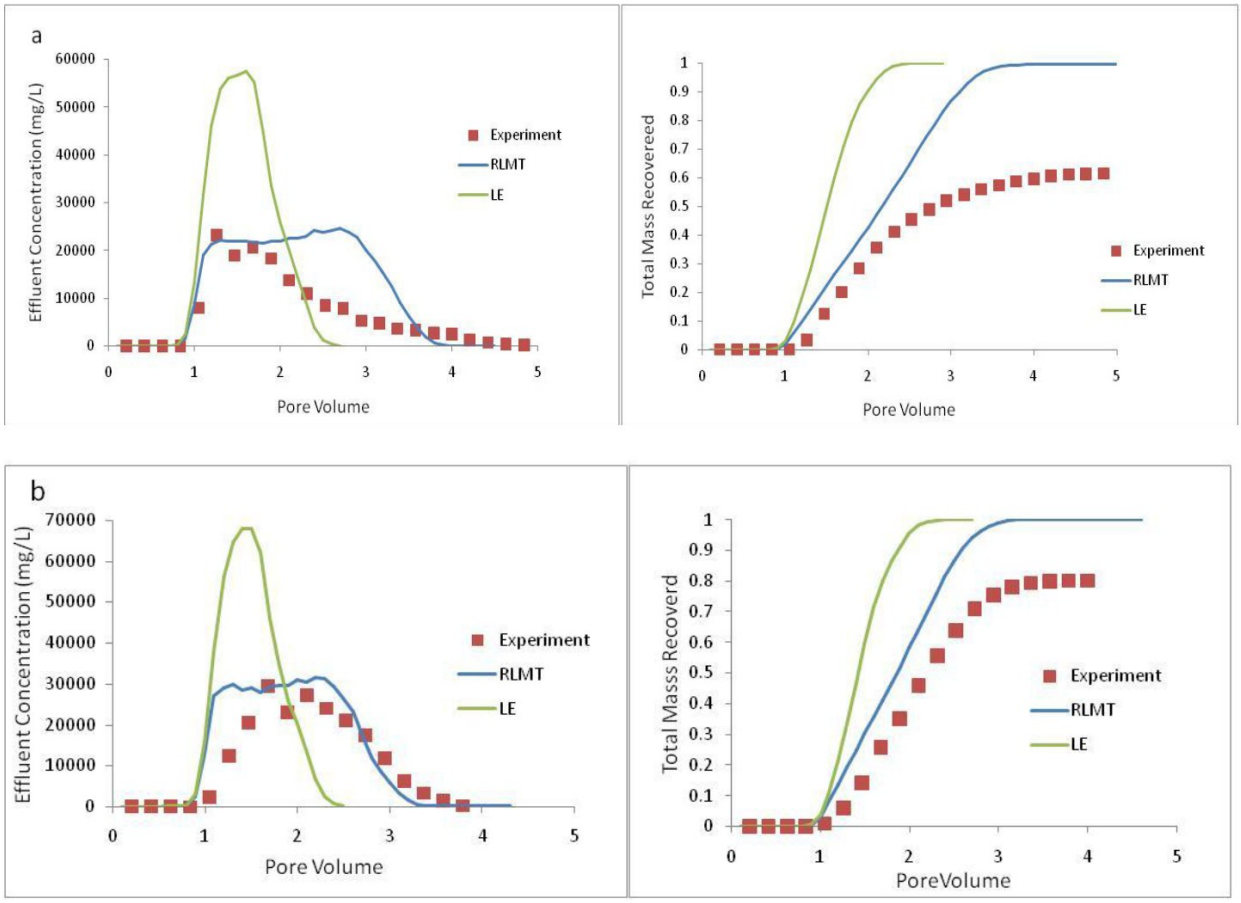

Fig.11 (a) Simulated (3D model) and observed toluene effluent concentration and cumulative mass recovery for the case of pure toluene NAPL and 50% ethanol content in the flushing solution. (b) Simulated (3D model) and observed benzene effluent concentration and cumulative mass recovery for the case of pure benzene NAPL and 50% ethanol content in the flushing solution.

The above simulations were performed using the dispersivity obtained from the tracer experiment (Table 2). The sensitivity of the numerical solution to the dispersivity was evaluated by repeating the simulations for different dispersivity values. The use of a higher dipersivity did not produce better agreement with the observed results. Increasing the dispersivity values resulted in increased dilution of the NAPL (by more mixing) and, consequently, some delay for full NAPL recovery. Yet, the agreement with observed effluent NAPL concentrations diminished suggesting that increasing the dispersion coefficient does not adequately account for the non-uniformity of the flow parameters. Batch simulations were also conducted using UTCHEM to evaluate if the calculated solubility values are consistent with the measured ones from the batch experiments. The ethanol contents considered in these simulations were 10% and 20% 30% ethanol by mass. The simulations were performed for both pure toluene NAPL and pure benzene NAPL. In particular, the purpose of these simulations was to assess whether the symmetric miscibility curve assumption made in the current version of UTCHEM leads to variations between the measured and calculated solubility values. This may be a concern for pure NAPL simulations especially when the ethanol content in the flushing solutions is low and the dissolution is the only recovery mechanism. Overall, these differences were not significant for the case of toluene and benzene flushing with ethanol. For 10% ethanol content, UTCHEM calculated the toluene and benzene solubility 400 and 300 mg/L higher than the measured values respectively. For 20% ethanol contents those values increased to 2000 and 1000 mg/L, whereas for 30% ethanol content those values reached to 9000 and 6000 mg/L.

Although some discrepancy between the measured and modeled solubility values was observed, particularly at higher ethanol contents, these differences are not the primary factor responsible for differences between experimental and simulated NAPL mass recoveries. To evaluate the impact of the differences between the measured and modeled solubility values, the simulation of the benzene flushing experiment with 50% ethanol content and high flow rate was repeated but with the solubility equal to that observed in the batch experiments. This was achieved by manipulating the Ternary Phase Diagram via raising its bi-nodal curve higher (by raising the parameter C_{3max} from 0.589 to 0.65). With this manipulation UTCHEM predicted the solubility of benzene close to that observed in the batch tests corresponding to 50% ethanol content. This sensitivity simulation predicted 100% mass recovery as in the base case simulation with the unmodified TPD, the only difference being that the complete NAPL recovery was achieved after three pore volumes instead of 2.5. Whereas the flushing experiment of benzene with 50 % ethanol content at the high flow rate resulted in 80 % NAPL recovery after 4 pore volumes.

The 100 % recovery predicted with the model for both solubility values is a direct result of the REV (Representative Elementary Volume) modeling approach used in practically all fate and transport models. Such a continuum-scale model cannot account for sub-grid pore-scale effects. Although homogeneous sand was used in the flushing experiments, variations in the pore throat size will unavoidably be present. This would lead to the development of preferential flow paths for the flushing solution and the bypassing of NAPL trapped in the smaller pores, even at the bench-scale considered in the current study. The result is a significant decrease in the NAPL recovery compared to what is predicted by continuum scale multiphase models.

Overall, UTCHEM was capable of reasonably matching the experimental results corresponding to the pure ethanol flushing where the presence of near zero IFT diminishes the impact of soil non-uniformity and the generation of preferential flow paths. However, the model over predicted NAPL recovery in the case of 50 % ethanol content in the flushing solution which induced preferential flow paths. This was true even for the case where the porous media consists of fairly uniform sand.

Simulations of multi-component NAPL Flushing

Fig. 12(a) shows the observed and simulated effluent concentrations and mass recovery for the case of 50% ethanol flushing and low flow rate. The model tends to over-estimate the toluene recovery but the agreement between the simulated and observed effluent concentrations is generally good. Moreover, when the ultimate recovery results are taken into consideration, the model simulations in this case show better agreement than those depicted in Fig. 11(a and b), which were based on the higher flow rate. The experimental results indicate that preferential flow paths and bypassing of some of the NAPL mass increases with increase in specific discharge of the flushing solution. Model predictions show that the model is incapable of simulating such flow fields when spatially uniform flow properties are assumed. The use of local equilibrium and mass transfer coefficient options did not significantly alter these results. Overall, these results suggest that accurate model predictions remain a significant challenge particularly when preferential flow paths are present. On the other hand, for lower flow rates such that preferential flow paths are less significant, the model performed reasonably well.

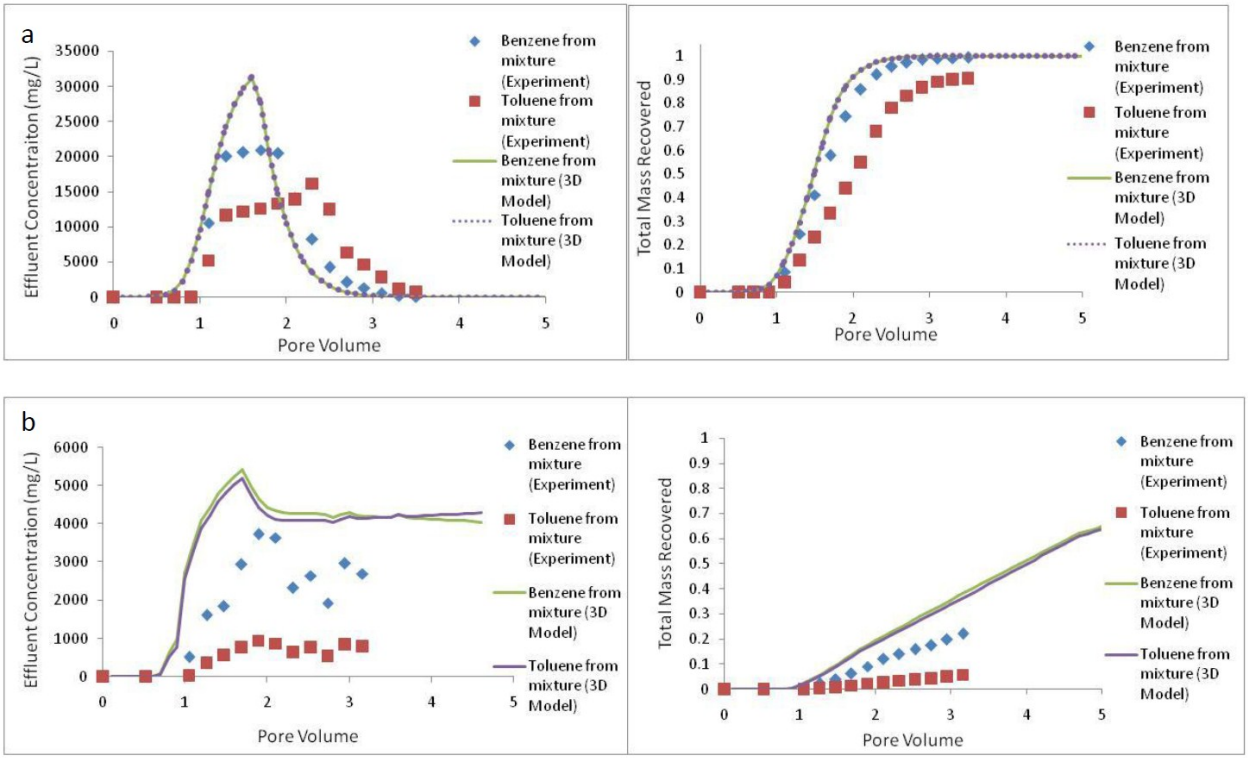

Fig.12 (a) Simulated (3D model) and observed effluent concentrations and cumulative mass recovery for the case of multi-component NAPL and 50% ethanol content in the flushing solution at the low flow rate. (b) Simulated (3D model) and observed effluent concentration and cumulative mass recovery for the case of NAPL mixture and 20% ethanol content in the flushing solution at the low flow rate.

The dissolution equation for multi-component NAPL phase incorporated in UTCHEM (Equation 20) assumes no preferential dissolution between individual NAPL components (single mass transfer coefficient) and, hence, yields almost identical effluent curves for benzene and toluene for the case of multi-component NAPL and 20% ethanol content (Fig. 12(b)). At this relatively low ethanol content, enhanced dissolution is the dominant recovery mechanism. The difference between simulated and observed effluent concentrations suggests that some preferential dissolution does occur in reality which would be dependent on compound properties, such as octanol water partition coefficient, in addition to the compounds solubility in water and its mole fraction in the NAPL phase. In non-equilibrium conditions the preferential dissolution behavior of organic compounds might also vary with respect to ethanol content in the flushing solution.

Heterogeneity

To evaluate the impact of soil non-uniformness, a series of runs were performed assuming a spatially variable permeability. Multiple realizations of the permeability were generated and used to simulate NAPL recovery for different ethanol contents in the flushing solution.

The effluent concentrations for 10 randomly selected permeability realizations and for the case of pure NAPL flushing are shown in Fig. 13. All the runs are performed with the rate limited mass transfer option. Even though all the permeability fields have the same statistical spatial structure, the results of the 100% ethanol experiments, where NAPL mobilization is the dominant recovery mechanism, exhibited the greatest variation. For the 10 randomly selected realizations with 100% ethanol content in the flushing solution, the time when NAPL recovery terminated ranged from less than 2 pore

volumes to about 4 pore volumes. The peak effluent concentrations for these simulations ranged from 25,000 to 160,000 mg/L, whereas the peak effluent concentrations for 20% ethanol content varied between 4000 to 3000 mg/L.

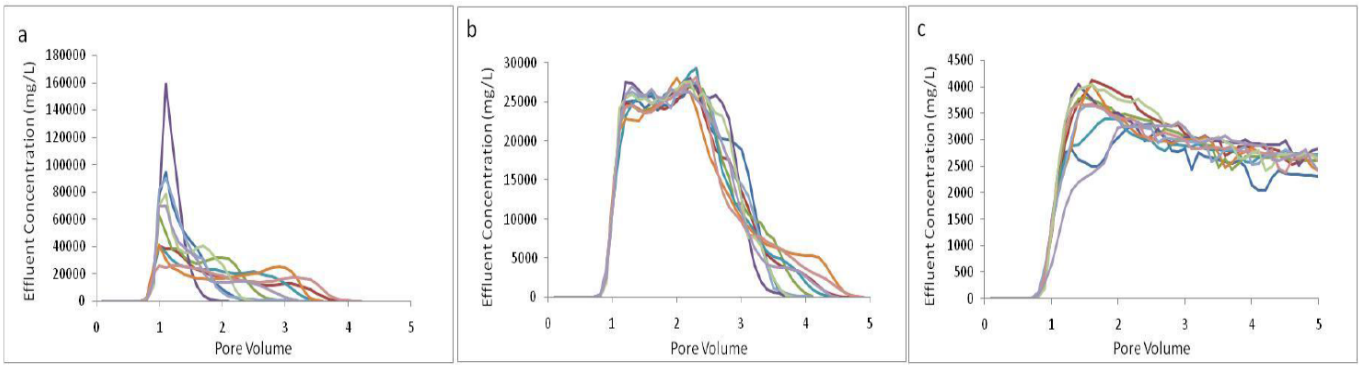

Fig.13 Simulated toluene effluent concentrations for (a) 100% (b) 50% and (c) 20% ethanol content, rate limited mass transfer and for randomly selected permeability realizations.

These simulations correspond to a moderate level of heterogeneity and simple flow geometry. It is quite possible that the level of heterogeneity, and hence model uncertainty, would be significantly higher in field applications. For lower ethanol contents where enhanced dissolution is the dominant NAPL recovery mechanism, the impact of heterogeneity is substantially less. The results of this exercise indicate that when NAPL mobility is likely to occur, soil heterogeneity and the ensuing development of preferential flow paths would have a pronounced impact on NAPL recovery. Moreover, model simulations would be most uncertain for such conditions.

5. Conclusions

A series of cosolvent flushing experiments were conducted to evaluate the factors influencing multi-component NAPL recovery mechanisms. The NAPLs considered were pure toluene, pure benzene and an idealized multi-component NAPL consisting of 50% benzene and toluene by mass. To cover situations where NAPL mobilization and/or NAPL enhanced dissolution contribute significantly to NAPL recovery, the cosolvent amount in the flushing solution ranged from 20% to 100% by mass. The flow velocity is found to be very influential on ultimate NAPL recovery, especially when the cosolvent amount in the flushing solution is kept low. Intermittent flow may be a viable option for optimization of the recovery when the optimal flushing flow rate is not known. When multi-component NAPLs are present, the dissolution rate of individual NAPL components remains a complex process depending on the mole fractions, octanol water partition coefficients and mass transfer coefficients of individual organic species.

To further analyze the experimental results and evaluate our ability to simulate cosolvent flushing experiments, a modified version of multiphase flow simulator UTCHEM was employed. Even for a relatively simple bench scale column set up, reasonable modeling requires at least two or three-dimensional geometries. Generally, the rate limited mass transfer (RLMT) option provided some flexibility to more accurately simulate NAPL dissolution. However, a single mass transfer coefficient for the entire flushing experiment was found to be inadequate for accurate modeling of the dissolution that may be attributed to the decrease in the contact area between the NAPL and flushing solution with time.

At higher velocities, preferential flow paths are more likely to occur and, therefore, modeling such flow fields becomes more challenging. The agreement between the observed and simulated (three-

dimensional) results was generally good at higher ethanol contents (such as 100 % ethanol) because the ultra low interfacial tension produce efficient sweep of the NAPL zone and minimize the development of preferential flow paths. The impact of preferential flow paths was more severe at intermediate ethanol contents, resulting in poorer agreement particularly at higher specific discharges for both pure and multi-component NAPLs.

Preferential dissolution models are needed to more accurately simulate multi-component NAPL mixture flushing. Hence, a single mass transfer coefficient for all components is not adequate. Such preferential dissolution models are particularly needed when cosolvent concentrations are relatively low and enhanced dissolution is the dominant NAPL recovery mechanism. Further research is needed to define the parameters of these models and incorporate into multiphase simulators.

Even for a simple column setup and fairly uniform soils, heterogeneity was shown to play a significant role, especially when the recovery mechanism is mobilization.

Acknowledgements
The financial support provided by the Bogazici University Research Fund (BAP), Istanbul, Turkey, Project 09HY102D is acknowledged. The authors acknowledge The University of Texas which developed the UTCHEM model and are also grateful to Dr. Ronald W. Falta for providing the modified version of UTCHEM program which includes the Li and Fu (1992) method for the calculation of the interfacial tension.

References

Akgoze Aydin G., Agaoglu B., Kocasoy G., Copty N.K., 2011. Effect of temperature on cosolvent flooding for the enhanced solubilization and mobilization of NAPLs in porous media. Journal of Hazardous Materials 186, 636-644.

Brandes D., Farley K.J., 1993. Importance of phase behavior on the removal of residual DNAPLs from porous media by alcohol flooding. Journal of Water Environment Research 65, 869–878.

Boyd G.R., Minghua L., Husserl J., Ocampa-Gomez A.M., 2006. Dip-angle influence on areal DNAPL recovery by co-solvent flooding with and without pre-flooding. Journal of Contaminant Hydrology 82, 319–337.

Brooks, R.H., Corey, A.T., 1966. Properties of porous media affecting fluid flow. Journal of the Irrigation and Drainage Division 6, 61.

Chang, Y.C.; Moulton, R.W.,1953. Quaternary liquid systems with two immiscible liquid pairs. Industrial and Engineering Chemistry 45, 2350; 1953

Corey A.T., 1994. Mechanics of immiscible fluids in porous media. Water Resources Publications, Colorado.

Dagan G., 1989. Flow and Transport in Porous Formations. 465 pp. Springer Verlag, Berlin.

Davis, E.L., 1995 Hot water enhanced remediation of hydrocarbon spills, in: V.D.W. Tedder, F.G. Pohland (Eds.), Emerging Technologies in Hazardous Waste Management, ACS, Washington, pp. 237–250.

Davis, E.L., 1997 How Heat Can Enhance In-situ Soil and Aquifer Remediation: Important Chemical Properties and Guidance on Choosing the Appropriate Technique, United States Environmental Protection Agency, Office of Solid Waste and Emergency Response Office of Research and Development, Oklahoma, EPA 540-S97-502.

Delshad, Mojdeh, G. A. Pope and K. Sepehrnoori. 1996. A Compositional Simulator for Modeling Surfactant Enhanced Aquifer Remediation. Journal of Contaminant Hydrology, 23, 303-327.

Eichel, H., Helmig, R., Neuweiler, I., Cirpka, O., 2005. Upscaling of two-phase flow processes in porous media. In Upscaling Multiphase Flow in Porous Media, (ed. Das, D. B. & Hassanizadeh, S. M.). 237–257. Springer Verlag, Berlin.

Falta R.W., 1998. Using phase diagrams to predict the performance of cosolvent floods for NAPL remediation. Ground Water Monitoring and Remediation 18, 94–102.

Falta R.W., Pruess K., Finsterle S., Battitelli A., 1995. T2VOC User's Guide, March 1995.

Fortin J., Jury W. A., Anderson M.A., 1997. Enhanced removal of trapped non-aqueous phase liquids from saturated soil using surfactant solutions. Journal of Contaminant Hydrology 24, 247-267.

Grubb D.G., Sitar N., 1999. Mobilization of trichloroethene during ethanol flooding in uniform and layered sand packs under confined conditions. Water Resources Research 3, 3275–3289.

Hand, D. B. 1939. Dineric Distribution: I. The Distribution of a Consolute Liquid Between Two Immiscible Liquids, Journal of Physics and Chemistry, 34, 1961-2000.

Henry S.M., Hardcastle C.H., Warner S.D., 2003. Chlorinated solvent and DNAPL remediation: an overview of physical, chemical, and biological processes, S.M. Henry, S.D. Warner, Editors, Chlorinated Solvent and DNAPL Remediation: Innovative Strategies for Subsurface Cleanup, ACS Symposium Series, Washington, DC, 1–20.

Hinkelmann R., 2005. Efficient numerical methods and information-processing techniques for modeling hydro- and environmental systems. Springer Verlag Berlin Heidelberg.

Imhoff P.T., Gleyzer S.N., McBride J.F., Vancho L.A., Okuda I., Miller C.T., 1995. Cosolvent enhanced remediation of residual reuse nonaqueous phase liquids: experimental investigation. Environmental Science and Technology 29, 1966–1976.

Jawitz J.W., Sillan R.K., Annable M.D., Suresh P., Rao C., Warner K., 2000. In-situ alcohol flushing of a DNAPL source zone at a dry cleaner site. Environmental Science and Technology 34, 3722-3729.

Jawitz W. J., Dai D., Rao P.S.C., Annable M.D., Rhue R. D., 2003. Rate-limited solubilization of multicomponent nonaqueous-phase liquids by flushing with cosolvents and surfactants: Modeling data from laboratory and field experiments. Environmental Science and Technology 37, 1983-1991.

Kaye A.J., Cho J., Basu N.B., Chen X., Annable M.D., Jawitz J.W., 2008. Laboratory investigation of flux reduction from dense non-aqueous phase liquid (DNAPL) partial source zone remediation by enhanced dissolution. Journal of Contaminant Hydrology 102, 17-28.

Kostarelos K., Pope G.A., Rouse B.A., Shook G.M., 1998. A new concept: the use of neutrally buoyant microemulsion for DNAPL remediation. Journal of Contaminant Hydrology 34, 383–397.

Lee K.Y., Peters C.A., 2004. UNIFAC modeling of cosolvent phase partitioning in nonaqueous phase liquid-water systems. Journal of Environmental Engineering 130, 478–483.

Letcher, T.M.; Siswana, P.M., 1992. Fluid Phase Equilib. 74, 203

Leverett, M. C., 1941. Capillary Behavior in Porous Solids, Transactions. AIME, 142, 152.

Li B., Fu J., 1992. Interfacial tensions of two-liquid-phase ternary systems. Journal of Chemical and Engineering Data 37 (2), 172–174.

Liang H, Falta R.W., 2008. Modeling field-scale cosolvent flooding for DNAPL source zone remediation. Journal of Contaminant Hydrology 96, 1-16.

Lowe D.F., Oubre C.L., Ward C.L., 1999. Surfactants and Cosolvents for NAPL Remediation: A Technology Practices Manual, Lewis Publishers, Boca Raton.

Lunn S.R.D., Kueper B.H., 1997. Removal of pooled dense, nonaqueous phase liquids from saturated porous media using upward gradient alcohol floods. Water Resources Research 33, 2207–2219.

Lunn S.R.D., Kueper B.H., 1999. Manipulation of density and viscosity for the optimization of DNAPL recovery by alcohol flooding. Journal of Contaminant Hydrology 38, 427–445.

Mantoglou A., Wilson J.L., 1982. The Turning Bands Method for simulation of random fields using line generation by a spectral method. Water Resources Research 18, 1379-1394.

Martel R., Gelinas P.J., Desnoyers J.E., 1998. Aquifer washing by micellar solutions: optimization of alcohol–surfactant–solvent solutions. Journal of Contaminant Hydrology 29, 319–346.

Mondain-Monval, P.I.; Quiquerez, J., Bull. Soc. Chim. Fr. Mem. 7, 240; 1940.

O'Carroll D. M., Sleep B.E., 2009. Role of NAPL thermal properties in the effectiveness of hot water flooding, Transport in Porous Media 79, 393–405.

Oostrom M., Dane J.H., Wietsma T.W., 2006. A review of multidimensional, multifluid intermediate-scale experiments: nonaqueous phase liquid dissolution and enhanced remediation. Vadose Zone 5, 570–596.

Pankow J.F., Cherry J.A., 1996. Dense Chlorinated Solvents and other DNAPLs in Ground Water, Waterloo Press.

Pennell K.D., Pope G.A., Abriola L.M., 1996. Influence of viscous and buoyancy forces on the mobilization of residual tetrachloroethylene during surfactant flushing. Environmental Science and Technology 30, 1328–1335.

Pennell K.D., Abriola L.M., Weber Walter J. Jr., 1993. Surfactant enhanced solubilization of residual Dodecane in soil columns. Environmental Science and Technology 27, 2332-2340.

Pope, G.A., Nelson, R.C., 1978. A chemical flooding compositional simulator. Society of Petroleum Engineers Journal 18 (5), 339–354.

Powers, S.E., L.M. Abriola and W.J. Weber, Jr., 1992. An Experimental Investigation of Nonaqueous Phase Liquid Dissolution in Saturated Subsurface System: Steady-State Mass Transfer Rates. Water Resources Research 28, 2691-2705.

Ramakrishnan V., Ogram A.V., Lindner A.S., 2005. Impacts of cosolvent, flushing on microbial populations capable of degrading trichloroethylene. Environmental Health Perspective 113, 55–61.

Ramsburg C.A., Abriola L.M., Pennell K.D., Loffler F.E., Gamache M., Amos B.K., E.A. Petrovskis E.A., 2004. Stimulated microbial reductive dechlorination following surfactant treatment at the Bachman Road site. Environmental Science and Technology 38, 5902–5914.

Reitsma S., Kueper B.H., 1998a. Non-equilibrium alcohol flooding model for immiscible phase remediation: 1. Equation development. Advances in Water Resources 21, 649-663.

Reitsma S., Kueper B.H., 1998b. Non-equilibrium alcohol flooding model for immiscible phase remediation: 2. Model development and application. Advances in Water Resources 21, 663-678.

Roeder E., Falta R.W., 2001. Modeling unstable flooding of DNAPL-contaminated columns. Advances in Water Resources 24, 803-819.

Roeder E., Falta R.W., Lee C.M., Coates J.T., 2001. DNAPL to LNAPL transitions during horizontal cosolvent flooding. Ground Water Monitoring and Remediation 4 ,77–88.

Rubin, Y. (2003), Applied Stochastic Hydrogeology. 416 p. Oxford University Press, New York.

Schlumberger, A. 2005. ECLIPSE Technical Description.

Soga K., Page J.W.E., Illangasekare T.H., 2004. A review of NAPL source zone remediation efficiency and the mass flux approach. Journal of Hazardous Materials 110, 13–27.

St-Pierre C., Martel R., Gabriel U., Lefebvre R., Robert T. Hawari J., 2004. TCE recovery mechanisms using micellar and alcohol solutions: phase diagrams and sand column experiments. Journal of Contaminant Hydrology 71, 155–192.

U.S. Environmental Protection Agency, 1997. Cleaning Up the Nation's Waste Sites: Markets and Technology Trends, 1996 Edition.

Van Valkenburg M.E., Annable M.D., 2002. Mobilization and entry of DNAPL pools into finer sand media by cosolvents: two dimensional chamber studies. Journal of Contaminant Hydrology 59, 211–230.

Wang W., Schnoor J. L., Doi J., 1996. Volatile organic compounds in the Environment, ASTM

Wood A.L., Enfield C.G., Espinoza F.P., Annable M., Brooks M.C., Rao P.S.C., Sabatini D., Knox R., 2005. Design of aquifer remediation systems: (2) Estimating site-specific performance and benefits of partial source removal. Journal of Contaminant Hydrology 81, 148-166.

5. The use of Pfannkuch Sherwood Number Correlation for the calculation of the interphase mass transfer in porous media

Berken Agaoglu[a], Traugott Scheytt[a], and Nadim K Copty[b]

[a] Institute of Applied Geosciences, Berlin Institute of Technology, Sekr. BH 3-2, Ernst-Reuter-Platz 1, 10587 Berlin, Germany

[b] Institute of Environmental Sciences, Bogazici University, 34342 Bebek, Istanbul, Turkey

Citation:
Agaoglu, B., Scheytt, T., Copty, K. N. The use of Pfannkuch Sherwood Number Correlation for the calculation of the interphase mass transfer in porous media. Submitted to Water resources research

Abstract

In this short note, we present a detailed analysis of Sherwood correlation developed by Pfannkuch [1984] which has found considerable use in different numerical models. The analysis clearly shows that the correlation involves a number of uncertainties and some fundamental errors that render it unusable in its current form. The implications of this error on the numerical models are also discussed.

1. Introduction

Interphase mass transfer in porous media is a process that occurs in numerous industrial and natural applications involving multiphase flow. A substantial number of investigations were directed in recent years to correlate this process to fluid and porous medium properties in the field of environmental engineering [Dillard and Blunt, 2000; Held and Celia, 2001; Imhoff et al., 1994; Maji and Sudicky, 2008; Miller et al., 1990; Nambi and Powers, 2000; Parker and Park, 2004; Powers et al., 1994b, 1992; Saba and Illangasekare, 2000; Schnaar and Brusseau, 2006]. The majority of these studies have expressed these correlations in terms of the non-dimensional Sherwood number. Two types of Sherwood numbers have been employed for this purpose; i) a Sherwood number that is written in terms of the mass transfer coefficient per unit area, k_f: $Sh = \frac{k_f d_m}{D}$ where D is the diffusion coefficient and d_m is representative porous medium diameter ii) a modified Sherwood number that lumps the interfacial area within the mass transfer coefficient: $Sh' = \frac{K_l {d_m}^2}{D}$ [Agaoglu et al., 2015; Miller et al., 1990; Powers et al., 1994a]. The attractive feature of the modified Sherwood number expression is that it eliminates the need for independently estimating the interfacial area between two fluids. On the other hand, lumping the interfacial area within the mass transfer coefficient limits the validity of the correlations to the specific conditions used for its development [Grant and Gerhard, 2007a].

Empirically derived expressions of the Sherwood number or modified Sherwood numbers are commonly integrated into numerical models for the prediction of interphase mass transfer in porous media. In a recent modeling approach referred to as the Thermodynamics-based model, the calculation of interphase mass transfer was achieved by combining the mass transfer coefficient, k_f that is obtained from empirically derived Sherwood correlations, with the thermodynamics-based calculation of the interfacial area [Grant and Gerhard, 2007a, 2007b; Kokkinaki et al., 2013a, 2013b]. There are only two available Sherwood number correlations in the literature which exclude the influence of interfacial area on interphase mass transfer coefficient [Pfannkuch, 1984; Powers et al., 1994a]. The Pfannkuch [1984] Sherwood model was selected in the thermodynamics-based modeling of interphase mass transfer as it was stated that the experiments to be simulated were mostly dominated by pool NAPL formations [Kokkinaki et al., 2013a]. This approach has generated substantial interest in the field because it proposes a novel way for calculating the interfacial area between two phases that has been a major limitation to prior modeling efforts. In spite of the recent attention directed to the Sherwood model of Pfannkuch [1984] in the thermodynamics-based approach, there is in fact limited validation of the Pfannkuch model. In addition to Thermodynamics-based approach there are also a number of recent studies who have used Pfankuch's models for modeling of interphase mass transfer in porous media [e.g., Powers et al., 1991; Seagren et al., 1999]. However, these latter studies have mostly used the Pfannkuch's model for comparison purposes whereas the Pfannkuch model is an integral part of the Thermodynamics-based approach. In this work we present a detailed examination of Pfannkuch's model. As we shall show, its derivation relies on highly uncertain estimates of key parameters and involves some fundamental errors that render it unusable in its published form. We also discuss the implications of this expression on the numerical models that used this correlation.

2. Calculation of Sherwood expression by Pfannkuch [1984]

The development of the Pfannkuch [1984] Sherwood correlation relies on the experimental data of Hoffmann [Hoffmann, 1969]. As these experiments were not described in detail by Pfannkuch [1984], a description of the experiments as reported in the Hoffmann [1969] is presented below.

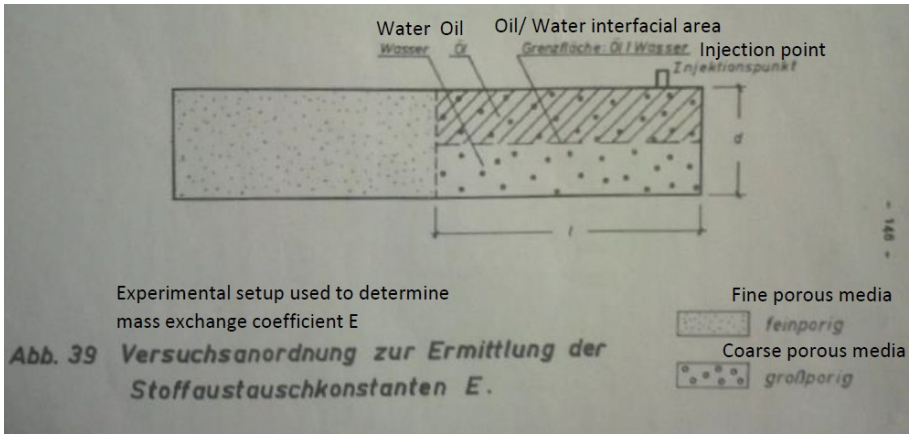

Fig. 1 Schematic of Hoffmann column from Hoffmann [1969]

Fig. 1 shows a schematic of Hoffmann's column setup. The entrance of the column is filled with fine sand to provide flow distribution whereas the rest of the column was filled with coarse glass beads. The flow was from left to right. The NAPL was injected into the column from above while the column was fully water saturated. It was observed that the injected oil entered and was retained in the upper half of the coarse medium providing a somewhat flat interfacial area between water flowing below.

Hoffmann [1969] did not explicitly report the dimensions of the column and the porosity. However, the interfacial area is given as 5.5 cm2. It was stated that this was calculated from the product of the diameter of the column (d), times the length of the column (l) and the porosity (n). Assuming a porosity of 0.36 (as Pfannkuch did) which is consistent with porosity values reported for example by Dullien [Dullien, 1979] for poured random packing, the horizontal cross sectional (dxl) area of the column is found as 15.3 cm^2. From the water velocity and flow rate reported by Hoffman [1969] it is possible to compute the vertical cross-sectional area of the column and from that the diameter and length of the column as 3 and 5 cm, respectively. Hoffmann [1969] noted however that the above estimate of the interfacial area is probably underestimated because it ignores the meniscus forming between the two fluids at the pore throats as a result of the oil volume penetrating into the aqueous phase due to the higher wettability of the aqueous phase-.

From the observed effluent concentrations, Hoffmann [1969] computed the "mass exchange exponent", *E*, by dividing the solute mass leaving the column per time, $\frac{\partial M}{\partial t}$, (i.e.; effluent concentration multiplied by the aqueous flow rate) with interfacial area, A:

$$E = \left(\frac{\partial M}{\partial t}\right)\left(\frac{1}{A}\right) \qquad (1)$$

The mass exchange exponent, *E,* represents the average mass transfer rate into the aqueous phase per unit area. *E* values reported by Hofmann [1969] for a range of velocities are presented in the Table 1.

Table 1: Estimated mass exchange coefficient as a function of velocity (from Hofmann [1969])

U (cm min^{-1})	E ($mg\ m^{-2}h^{-1}$)
0.015	0.06
0.04	0.1
0.08	0.07
0.13	0.09
0.3	0.15
0.4	0.28
0.65	0.05
1	1.1

The aqueous solubility of the fuel oil (defined in German as "*Heiz öl EL*") was not given by Hoffmann but it was reported that the solubility is between 10^{-3} mgm^{-3} and 10^{-5} mgm^{-3}. Moreover, Hoffmann [1969] did not explicitly report the diameter of the glass beads used in the experiment. However, in other sorption experiments conducted by the author it was reported that the glass beads range in diameter between 100 and 400 □m.

The above experimental results of Hoffmann [1969] were later used by Pfannkuch [1984] to compute Sherwood numbers. The second column of Table 2 (i.e., Table 1 in Pfannkuch [1984]) presents the *E* values used by Pfannkuch (which are identical to the values reported by Hoffmann [1969] with the time unit converted from hours to seconds).

Table 2: calculated Peclet and Sherwood numbers as a function of velocity (from Table 1 of Pfannkuch [1984])

U ms^{-1} 10^{-6}	E $mgm^{-2}s^{-1}$ 10^{-6}	d_m m 10^{-3}	Pe	Sh
2.6	16.66	0.5	0.65	0.42
6.66	27.77	0.5	1.67	0.7
13.33	19.44	0.5	3.33	0.49
21.66	25	0.5	5.42	0.63
50	41.66	0.5	12.5	1.08
66.67	77.77	0.5	16.67	1.95
108.33	13.88	0.5	27.08	0.35
166.67	305.55	0.5	41.67	7.65

[D =2x10^{-9} m^2s^{-1}]

From the mass exchange coefficient, *E*, Pfannkuch computed the Sherwood number as follows. The interphase mass transfer rate from an infinitesimal area dA can be defined as:

$$\left.\frac{\partial M}{\partial t}\right|_{dA} = k_f dA(C_s - C) \qquad (2)$$

where *C* is the aqueous concentration adjacent to the interfacial area and C_s is the solubility.
The interphase mass transfer rate for the entire column assuming one-dimensional flow is obtained by integrating equation (2) over the length of the column,

$$\frac{\partial M}{\partial t} = k_f \int_{x=0}^{X=L} (C_s - C)\, dA \qquad (3)$$

Rearranging terms the mass transfer coefficient k_f can be computed as:

$$k_f = \left(\frac{\partial M}{\partial t}\right)\left(\frac{1}{\int_{x=0}^{x=L}(C_s - C)dA}\right) \qquad (4)$$

Equation (4) states that the computation of k_f requires the estimate of the concentration along the column. Since this information was not available from the Hoffman [1969] data, Pfannkuch [1984] further assumed C along the column to be zero, resulting in the following expression:

$$k_f = \left(\frac{\partial M}{\partial t}\right)\left(\frac{1}{A}\right)\left(\frac{1}{C_s}\right) \qquad (5)$$

Assuming the concentration along the column to be equal to zero underestimates the mass transfer coefficient especially in low velocities where the concentration in the column may be significantly higher. Combining equation (5) with equation (1) which defined the mass exchange coefficient yields:

$$k_f = E\left(\frac{1}{C_s}\right) \qquad (6)$$

Finally, multiplying both sides by $\frac{d_m}{D}$ gives the Sherwood number:

$$Sh = \frac{E\, d_m}{C_s D} \qquad (7)$$

which is the equation given and used by Pfannkuch [1984]. The calculated Sherwood numbers are given in the 5th column of Table 2. Pfannkuch [1984] assumed the glass bead diameter to be 500 micrometers. The aqueous fuel oil solubility was assumed to be 10^{-4} mgm^{-3} (i.e., in the middle of the range suggested by Hoffman [1969]), while the diffusion coefficient of the NAPL was taken as $2\text{x}10^{-9}$ m^{2}s^{-1}. However the values obtained with Equation (7) are 1000 times smaller than the one reported by Pfannkuch possibly due to an error in unit conversion.

For example; the values of the input parameters of equation 7 for the slowest velocity (i.e.; U=$2.6\text{x}10^{-6}$ m s^{-1}) in Pfannkuch [1984] are E =$16.66\text{x}10^{-6}$ mgm^{-2}s^{-1}, d_m=$0.5\text{x}10^{-3}$ m, C_s=10^4 mgm^{-3} and D =$2\text{x}10^{-9}$ m^{2}s^{-1} which results in Sh =0.000417 whereas Pfannkuch [1984] reported it to be 0.42. The corrected Sherwood numbers are presented in Table 3. As a consequence, the Sherwood correlation proposed by Pfannkuch (i.e.; $Sh = 0.55 + 0.025Pe^{1.5}$), which is based on the erroneous Sherwood numbers, is an over-estimate by a factor of 1000.

Table 3: Corrected vs. Pfannkuch's Sherwood numbers as a function of velocity

U ms^{-1}(velocity)	Pfannkuch's Sherwood numbers	Correct Sherwood numbers
0.0000026	0.42	0.000417
0.0000066	0.70	0.000694
0.0000133	0.49	0.000486
0.00002166	0.63	0.000625
0.00005	1.08	0.00104
0.0000667	1.95	0.00194
0.00010833	0.35	0.000347
0.00016667	7.65	0.00764

3. **Reliability of corrected Sherwood numbers**

It is important to note that besides the 1000 factor error, the corrected Sherwood number correlation is associated with a number of uncertainties which make the derived Sherwood expression even after the 1000 factor correction highly unreliable. First, the non-aqueous phase solubility was not reliably determined. Hoffmann [1969] stated that oil solubility is in the range of 1-100 mgL^{-1}. Pfannkuch [1984] assumed it to be 10 mgL^{-1}. In fact, the oil used in Hoffmann's experiments is "Heiz öl EL" which is also known as domestic fuel oil and actually can have a solubility even lower than the range expressed by Hoffmann depending on the type. Secondly, assuming a diffusion coefficient of D =2x10^{-9} m^2s^{-1} is also another source of uncertainty as fuel oil is a mixture mostly of paraffins and alkylbenzenes (~90%) whose diffusion coefficients vary between 0.5x10^{-9} – 0.9x10^{-9} m^2s^{-1} [Dunlap and Beckmann, 1988; IARC, 1989; Yaws, 2009]. Third, the mass transfer coefficient, *E*, was computed by Hoffmann [1969] using an interfacial area of 5.5 cm^2 (Equation 1). The author calculated the interfacial area by multiplying length, diameter and porosity. However, the interfacial area that influences the interphase mass transfer is established at the meniscus of pores (i.e.; pore throats) which translates into a smaller area than the one assumed based on the porosity. Moreover, interfacial area might not be fully flat as assumed by Hoffmann, but may exhibit cavities with stagnant water regions. Fourth, the calculation of the mass transfer coefficient by Pfannkuch [1984] neglected the concentration along the column (Equations 4 and 5). Two of these conditions (assuming a larger diffusion coefficient and ignoring the concentration along the column) lead to the underestimation of the Sherwood numbers. The influence of solubility and the estimated interfacial area cannot be evaluated as they might lead to underestimation of Sherwood numbers if assumed greater than their real values or the opposite. In addition to the above indications, especially the low number of reported E values and the spread in the data around the best fit curve, makes the reliability of values at high velocities further questionable.

In summary, Hoffmann's experimental data and their analysis by Pfankuch [1984] involves a number of uncertainties that cast significant doubt on the Sherwood number expression developed by Pfannkuch. It is interesting to note that Hoffmann [1969] stated that his data present a positive correlation between E values and velocity; however, he also stated that no mathematical formula describing this correlation can be developed due to uncertainty in the experiments.

4. **Implications on the numerical models**

In this note we pointed to a number of errors and uncertainty in the development of the Sherwood number expression proposed by Pfannkuch [1984], and caution against its use in subsequent research work. As noted above the Sherwood correlation developed by Pfannkuch has been used by a number of studies most notably in the Thermodynamics-based models for the simulation of interphase mass

transfer [Grant and Gerhard, 2007a; Kokkinaki et al., 2013a, 2013b]. Kokkinaki et al. [2013a, 2013b] reported favorable comparison between the experimental data of Zhang et al., [2008, 2007] and predictions from the thermodynamics-based model combined with the correlation developed by Pfannkuch [1984]. We offer the following explanation to clarify why the results of thermodynamics-based approach as presented in Kokkinaki et al. [2013a, 2013b] may have offered a good match against the experimental data of Zhang et al. [2007].

The experiments of Zhang et al. [2007] involve the injection of a small amount of DNAPL (22.5 mL) into a small 3D box (14cm X 8cm X 8cm). Generally, the DNAPL mass would enter small pores (i.e., low hydraulic conductivity regions) if there is sufficient entry pressure as a result of DNAPL accumulation above the small pores. It is very likely that the small DNAPL amount used in Zhang et al.'s experiments was not enough to establish sufficient entry pressure for the DNAPL to enter into small pores. In addition, if NAPLs reside in the big pores (i.e., high conductivity regions) it is more likely that local equilibrium conditions prevail in these regions due to full contact of incoming water and NAPL. As also noted in Figure 1c and 3a of Zhang et al. [2007], the injected mass was concentrated in the high permeability regions. As a result, it is quite likely that local equilibrium conditions prevailed in these regions due to full contact of incoming water and the NAPL mass. In light of the above, the good agreement between model simulations and the experimental data presented in Kokkinaki et al. [2013a, 2013b] was most likely because the erroneous Pfannkuch correlation over-estimated the NAPL dissolution rate, rendering it closer to a local equilibrium condition which may have been consistent with the conditions of the experimental data of Zhang et al. [2007]. While the thermodynamics-based approach remains promising because of its ability to model the interfacial area between phases, further work is needed for the validation of this approach in terms of interphase mass transfer. This would require the estimation of Sherwood correlations that can reliably predict interphase mass transfer. In addition to more robust experimental work to identify and quantify the contributions of different factors on interphase mass transfer, recent developments in pore scale modeling can also serve as a valuable tool that can aid in the development of robust Sherwood correlations that can potentially be incorporated in thermodynamics-based models- as well as other models- for the accurate simulation of interphase mass transfer in porous media.

References

Agaoglu, B., Copty, K. N., Scheytt T., Hinkelmann R., (2015), Interphase mass transfer between fluids in subsurface formations: A Review. Adv. in Water Res. In press.

Dillard, L.A., and M.J. Blunt (2000), Development of a pore network simulation model to study nonaqueous phase liquid dissolution. Water Resour. Res. 36, 439–454.

Dullien, F. (1979), Porous media-fluid transport and pore structure.

Dunlap, L., and D. Beckmann (1988), Soluble hydrocarbons analysis from kerosene/diesel type hydrocarbons., in: In Proceedings of the Conference on Petroleum Hydrocarbons and Organic Chemicals in Ground Water: Prevention, Detection and Restoration.

Grant, G.P., and J.I. Gerhard (2007a), Simulating the dissolution of a complex dense nonaqueous phase liquid source zone: 2. Experimental validation of an interfacial area-based mass transfer model. Water Resour. Res. 43, n/a–n/a. doi:10.1029/2007WR006039

Grant, G.P., and J.I. Gerhard (2007b), Simulating the dissolution of a complex dense nonaqueous phase liquid source zone: 1. Model to predict interfacial area. Water Resour. Res. 43, n/a–n/a. doi:10.1029/2007WR006038

Held, R.J., and M.A. Celia (2001) Pore-scale modeling and upscaling of nonaqueous phase liquid mass transfer. Water Resour. Res. 37, 539–549.

Hoffmann, B. (1969), Über die ausbreitung gelöster kohlenwasserstoffe im grundwasserleiter. Inst. f. Wasserwirtschaft u. Landwirtschaftl. Wasserbau, Techn. Univ. Hannover

IARC (1989), IARC monographs volume 45.

Imhoff, P.T., P.R. Jaffé and G.F. Pinder (1994) An experimental study of complete dissolution of a nonaqueous phase liquid in saturated porous media. Water Resour. Res. 30, 307–320.

Kokkinaki, A., D.M. O'Carroll, C.J. Werth, and B.E. Sleep (2013a), Coupled simulation of DNAPL infiltration and dissolution in three-dimensional heterogeneous domains: Process model validation. Water Resour. Res. 49, 7023–7036. doi:10.1002/wrcr.20503

Kokkinaki, A., D.M. O'Carroll, C.J. Werth, and B.E. Sleep (2013b) An evaluation of Sherwood-Gilland models for NAPL dissolution and their relationship to soil properties. J. Contam. Hydrol. 155, 87–98. doi:10.1016/j.jconhyd.2013.09.007

Maji, R., and E.A. Sudicky (2008) Influence of mass transfer characteristics for DNAPL source depletion and contaminant flux in a highly characterized glaciofluvial aquifer. J. Contam. Hydrol. 102, 105–119. doi:10.1016/j.jconhyd.2008.08.005

Miller, C.T., M.M. Poirier-McNeill, and A.S. Mayer (1990) Dissolution of trapped nonaqueous phase liquids: Mass transfer characteristics. Water Resour. Res. 26, 2783–2796.

Nambi, I.M., and S.E. Powers (2000), NAPL dissolution in heterogeneous systems: an experimental investigation in a simple heterogeneous system. J. Contam. Hydrol. 44, 161–184. doi:10.1016/S0169-7722(00)00095-4

Parker, J.C., and E. Park (2004), Modeling field-scale dense nonaqueous phase liquid dissolution kinetics in heterogeneous aquifers. Water Resour. Res. 40, n/a–n/a. doi:10.1029/2003WR002807

Pfannkuch, H. (1984), Determination of the contaminant source strength from mass exchange processes at the petroleum-ground-water interface in shallow aquifer systems. Water Well Assoc. Am. Pet. Inst. Houston, Tex.

Powers ,S.E, C.O. Laureiro, L.M. Abriola, and W.J. Weber (1991), Theoretical study of the significance of nonequilibrium dissolution of nonaqueous phase liquids in subsurface systems. Water Resour. Res. 27:4, 463-477

Powers, S.E., L.M. Abriola, J.S. Dunkin, and W.J. Weber (1994a), Phenomenological models for transient NAPL-water mass-transfer processes. J. Contam. Hydrol. 16, 1–33.

Powers, S.E., L.M. Abriola, and W.J. Weber (1992), An experimental investigation of nonaqueous phase liquid dissolution in saturated subsurface systems: Steady state mass transfer rates. Water Resour. Res. 28, 2691–2705.

Powers, S.E., L.M. Abriola, and W.J. Weber (1994b), An experimental investigation of nonaqueous phase liquid dissolution in saturated subsurface systems: Transient mass transfer rates. Water Resour. Res. 30, 321–332.

Saba, T., and T.H. Illangasekare (2000), Effect of groundwater flow dimensionality on mass transfer from entrapped nonaqueous phase liquid contaminants. Water Resour. Res. 36, 971–979. doi:10.1029/1999WR900322

Schnaar, G., and M.L. Brusseau (2006), Characterizing pore-scale dissolution of organic immiscible liquid in natural porous media using synchrotron X-ray microtomography. Environ. Sci. Technol. 40, 6622–6629.

Seagren, E.A., B. E. Rittmann, and A. J. Valocchi (1999), A critical evaluation of the local-equilibrium assumption in modeling NAPL-pool dissolution. J. Contam. Hydrol. 39:1 109-135.

Yaws, C. (2009), Transport properties of chemicals and hydrocarbons.

Zhang, C., C.J. Werth, and A.G. Webb (2007), Characterization of NAPL Source Zone Architecture and Dissolution Kinetics in Heterogeneous Porous Media Using Magnetic Resonance Imaging. Environ. Sci. Technol. 41, 3672–3678.

Zhang, C., H. Yoon, C.J. Werth,A.J. Valocchi, N.B. Basu, and J.W. Jawitz, (2008), Evaluation of simplified mass transfer models to simulate the impacts of source zone architecture on nonaqueous phase liquid dissolution in heterogeneous porous. J. Contam. Hydrol. 102, 49–60. doi:10.1016/j.jconhyd.2008.05.007

6. Synthesis

The following content comprises an integrated summary and discussion of the manuscripts presented in the previous chapters.

6.1. Summary and the discussion of main findings

The above chapters demonstrate the level complexity involved in interphase mass transfer between fluids in porous media. In review paper (i.e., chapter 2) these factors were described in detail. The characteristic length scale of the interphase mass transfer and the flow configurations defined in Table 1 of chapter 2 were particularly considered during the review. Some of the important conclusions retrieved from this review are presented below.

The most influential parameters were shown to be interfacial area and the corresponding flow paths of the solvent phase. However, the occurrence of these parameters are dependent on many factors that relate to fluid and porous medium properties whose spatial distribution in subsurface encompass a substantial level of uncertainty. In addition to the uncertainty incorporated in the porous medium properties, the cross interactions between these properties (e.g., wettability and pore size distribution in the medium) further complicate the estimation of the interfacial area and the corresponding flow paths. In literature there has been several attempts to develop some sort of formulation that would confer the magnitude of interfacial area (e.g., functional relationships, thermodynamics approaches etc.). The thermodynamic approaches have taken considerable attention in recent years, yet there is still a need to control their validity as some of the parameters e.g., energy dissipation parameter, are fit parameters for a specific porous medium type whereas one other parameter i.e., the ratio of meniscus to film area, is developed from a single pore network model which represents a single type of porous medium.

The flow paths followed by the solvent phase were also shown to have substantial impact on the interphase mass transfer. The flow paths can be described at both pore scale and field scale. As long acknowledged, an erroneous representation of flow paths at field scale (e.g., by erroneously chosen permeability field) would lead to a completely flawed prediction of interphase mass transfer. The flow paths at pore scale are influential on the prediction of interphase mass transfer at the meso-scale and therefore a misrepresentation of flow paths at pore scale (e.g., with an erroneously chosen Sherwood formulation) would lead to flawed predictions at the meso-scale. Considering the fact that the field scale interphase mass transfer predictions make use of meso-scale interphase mass transfer rate predictions, such mistakes conducted at pore scale would also result in unrealistic dissolution predictions at the field scale.

Correct estimation of pore scale flow paths for interphase mass transfer predictions at meso-scale involve a number of factors that prove to be difficult to estimate with a fair level of reliability (e.g., the distribution of dissolving phase in the medium). In relation, the type of solvent phase blobs (singlet or multi-pore blob) occurring in different types of porous medium, which induces different types of flow paths (i.e., multi-pore blobs lead to establishment of stagnant regions of solvent phase adjacent to interfaces whereas singlets lead to distributed flow conditions without any stagnant regions of solvent phase), is very influential on the interphase mass transfer. Moreover the type of distribution of pore bodies/throats in the medium is not explicitly investigated. Even though the field scale permeability is assumed to be distributed as in normal distribution, there is very little data on the type of spatial distribution of pore bodies/throats with different sizes in a meso-scale porous medium. A further complicating issue is that the entrapment of dissolving phase in small pore bodies (of a solvent phase wetting porous medium) is related to the entry pressure exerted by the dissolving phase while it intrudes into domain. For example, in field applications, the entrapment of DNAPL blobs in layers of low permeability media is dependent on the fact that there is sufficient entry pressure built up above

such layers due to DNAPL accumulation. As entry pressure of DNAPL above low permeable layer is a function of the released DNAPL amount per time, (for example; very high amounts of DNAPL release in a small period of time will lead to high level of DNAPL accumulation above the low permeable medium hence high entry pressures) the entrapment in small permeable medium is also related to it.

In addition to above mentioned parameters there are a number of other factors which influence the interphase mass transfer as presented in the review paper in detail. Overall this review paper provided an integrated evaluation of interphase mass transfer processes in relation to multiphase flow conditions that appear in subsurface and therefore enabled clarification of some certain processes and their impacts on interphase mass transfer which was absent in the literature before.

Along with the indications of the review paper, the role of interfacial area and corresponding flow paths at pore scale was investigated with use of a two dimensional pore network model (i.e., chapter 3). In this model the dissolving phase is primarily emplaced in the selected pore bodies and the flow rate and velocities of the solvent phase was found with use of conservation of mass equation in each pore for prescribed boundary conditions. Once the flow rate is determined, the transport equation is solved explicit in time over the pore network domain where both advection and diffusion are considered. The interphase mass transfer is incorporated with use of stagnant layer assumption adjacent to meniscus interfacial area at the pore throats where molecular diffusion is the only transport mechanism. The specific focus of this paper was to investigate the impact of interfacial area and the orientation of the dissolving phase with respect to flow direction. To bracket the possible configurations that may appear in a meso-scale porous domain, extreme cases (i.e., orthogonal and parallel to flow direction) were considered during the investigation. It was demonstrated that the impact of interfacial area is not linear on interphase mass transfer coefficient and therefore explicit interphase mass transfer coefficients which are extracted by considering the impact of existing interfacial area in linear terms are still influenced by the interfacial area. This was further investigated by using the same amount of interfacial area but with different geometric allocations in the domain. The results demonstrated that even for the same amount of interfacial area, different rates of interphase mass transfer and also interphase mass transfer coefficients are possible. The reason for that was observed to be the alteration of the concentration distribution in the domain and therefore also the dissolved mass per time.

In practice the geometric allocation of dissolving phase has some sort of correspondence to fluid/medium properties (e.g., pore size distribution) since such configurations are determined either during the initial intrusion of the dissolving phase into domain or during the progress of dissolution. In relation to that in the conventional mass transfer formulations (i.e., modified Sherwood formulations) the correspondence of flow paths and relevant bypass conditions to fluid/porous medium properties are constructed with use of multiple regression analysis. However, in explicit Sherwood formulations this approach was not followed and the porous medium properties (e.g., pore size distribution, porosity) were neglected. In this work it was demonstrated that the explicit Sherwood formulations should also be developed in correlation with the fluid/porous medium properties as they are also effected by the flow bypass conditions. In addition, it was also demonstrated that the explicit Sherwood formulations are dependent on the scale of the domain that they were developed from. This was the case even for the explicitly defined flow paths.

Investigation of the impact of chemical agent use on interphase mass transfer was initially conducted through one dimensional dissolution experiments where the solvent phase comprised of water and ethanol mixtures at different ratios (i.e., chapter 4). The dissolving phase was chosen to be an LNAPL (toluene, benzene or their mixture) entrapped in the water saturated fine-medium sand filled column. The formation of the LNAPL was not residual but pool, since in practice LNAPLs mostly occur in the form of pools right below/above the water table. The column experiments showed that full ethanol

flushing lead to mobilization of NAPL and solubilization during this movement. The 50% ethanol water flushing experiments demonstrated that the LNAPL is slightly mobilized (only 5 cm) at the beginning of experiment and then became immobile altogether again. In that case, the use of high flushing velocities lead to high effluent concentrations at the early periods of experiment followed by low concentrations even though 40% of the LNAPL (in this case toluene) was still present in the column. This case was not observed when the flushing solution was injected at slower velocities. Due to substantial decrease of capillary force in the discrete pores at such ethanol contents (due to reduction of interfacial tension), LNAPL is mobilized at the beginning of experiment within the relatively larger pores at higher pressures (i.e., higher velocity) creating preferential flow paths (bypass channels) for the flushing solution. Once the bypass channels are created most of the incoming flushing solution follows these channels and leave the column without coming in direct contact with the NAPL. To control if this reduced interphase mass transfer condition can be simulated, the experiments were simulated with UTCHEM, which is the only multiphase flow program that encompass cosolvent use. It was demonstrated that the model is not capable of simulating such conditions. In literature most of the interphase mass transfer formulations are developed from the cases where chemical agents (their influence) are not present. Therefore specific interphase mass transfer formulations that consider use of chemical agents and their impact on interfacial tension reduction and increase in solubility would improve our predictive capabilities. Additional simulations were also conducted for porous medium with different spatial distribution of permabilities having the same average statistical properties (i.e., Monte Carlo simulations). It was demonstrated that the highest uncertainty in the results (the time needed to deplete LNAPL in the column) is observed when the flushing solution comprised of full ethanol content. This result is reasonable since the mobilization is the dominant recovery mechanism in such case meaning that the permeability differences would have direct influence on the results.

A detailed analysis of a well-known Sherwood formulation (i.e., Pfannkuch's Sherwood formulation, (Pfannkuch, 1984)) is also performed in the thesis (i.e., chapter 5). Even though this correlation is well-known and cited/used in different investigations there is a lack of detailed analysis to confirm its reliability. Thermodynamics model, which has taken substantial attention during the last 5 years, particularly relies on the use of this correlation. The analysis clearly shows that the correlation of Pfannkuch (1984) incorporates some fundamental mathematical errors that renders it unusable. The implication of this error is that it makes the results of the thermodynamics model which were presented in some recent publications invalid. Apart from the calculations conducted by Pfannkuch (1984) also the used data (i.e., (Hoffmann, 1969)) was analyzed. It was revealed that the data that Pfannkuch (1984) made use of incorporates a high level of uncertainty and therefore even the corrected calculation of Pfannkuch (1984) does not provide a useful formulation.

6.2. Potential areas for future research

The absence of reliable mass transfer formulations has numerous reasons as discussed above. The accurate estimation of the interfacial area is of significant importance in that sense. The thermodynamic methods used for the estimation of interfacial area can be improved to account for a range of porous medium types whereas the non-invasive imaging technologies can be used to control their validity. The pore-scale flow paths have significant impact on interphase mass transfer and their occurrence at different types of porous medium for different values of the saturation of dissolving phase may be especially helpful for prediction of interphase mass transfer rates. Pore-scale numerical models can be very helpful with that respect. The appropriateness of the pore scale domain with the real porous media can be controlled with use of non-invasive imaging techniques that incorporate sufficient resolution. A related issue is the distribution of pore bodies/throats in a certain type of porous medium. Even though the pore size distribution is helpful in terms of capillary pressure-saturation or relative permeability-saturation relationships, it does not provide information on the

spatial distribution of the pores with different sizes and in correspondence the type of the spatial distribution of entrapped blobs which can be very influential on the interphase mass transfer.

A very influential parameter that changes both the interfacial area and corresponding flow paths is wettability of the porous medium. Wettability of subsurface formations can show spatial variability. Moreover, it can be altered by interaction between the surface of the grain particles and the fluids. In terms of interphase mass transfer, wettability alteration and also variable wetting media is particularly ignored as there is only a handful investigations. To date, there is no non-invasive visualization of entrapped solvent blobs in variably wetting media. The investigation of impact of wettability and the corresponding issues may also be done with pore scale numerical models which would also enable direct determination of flow rates/velocities in discrete pores. The thickness of the film layer is of particular importance and this information can be retrieved from non-invasive methods.

Flow paths at the field scale, which is a strong function of the macro scale permeability distribution, is a very important issue not only for interphase mass transfer applications but also every other real subsurface applications (e.g. groundwater extraction). Therefore, any methodology that enhances the accuracy of the field scale flow path estimation will directly improve the interphase mass transfer predictions. With that respect, relative permeability estimates, which are function of fluid saturations, and also accurate consideration of hysteresis, are also important and their improvement will be of assistance.

7. List of figures

Fig. 2-1 Typical NAPL contamination; a)Schematic of a uniformly distributed NAPL blobs (shaded area), flow is from left to right; b) Concentration as a function of distance; for low Peclet number; c) Concentration as a function of distance; for high Peclet number 18

Fig. 2-2 Schematic of the meniscus and film area around grain particles. Electron-microscopy visualization of surface roughness can be found in [84] 22

Fig. 2-3 Shrinking of a non-wetting blob (a) and wetting blob (b) via dissolution. Numbers represent the progression of dissolution in time. L and w are the film length and width respectively [81,88] ...23

Fig. 2-4 Variation of different domains of the interfacial area with wetting phase saturation 29

Fig. 2-5 P_c-S-A_i relationship obtained from LB model; from [177] 33

Fig. 2-6 Emergence of fingering as a function capillary number and viscosity ratio based on Lenordmand et al.[179]; from [185] 34

Fig. 2-7 Schematic of NAPL formation in a chamber in pore network model of Dillard et al. [89] 45

Fig. 2-8 Schematic of pore network model with water flowing around a bubble 47

Fig. 3-1 a) The packed sphere system (light blue) and its representation as a pore network consisting of chambers (purple) and tubes (dark blue) b) Perspective and plan view of the pore network model superimposed over the pores of packed spheres for comparison 84

Fig. 3-2 NAPL distributions (in black) within the pore network model considered in this analysis. Flow direction is from left to right 86

Fig. 3-3 Impact of saturation on the modified Sherwood number 88

Fig. 3-4 Impact of saturation on the explicit Sherwood number 88

Fig. 3-5 Impact of NAPL spatial distribution on the explicit Sherwood number 89

Fig. 3-6 Impact of mean grain diameter on the interphase mass transfer coefficient 90

Fig. 3-7 Impact of domain size on the interphase mass transfer coefficient 91

Fig. 3-8 Variability of lumped mass transfer coefficient for a NAPL saturation of 0.05 (i.e., Set 1, 10) and 0.3 (i.e., Set 2, 9) 92

Fig. 3-9 Variability of explicit mass transfer coefficient for an interfacial area of 16 m^{-1} (Set 12, 13) and 32 m^{-1} (Set 10, 11) 93

Fig. 4-1 Interfacial tension as a function of ethanol mass fraction in aqueous phase 110

Fig. 4-2 Ternary phase diagrams for a) toluene-ethanol-water b) benzene-ethanol-water c) NAPL mixture-ethanol-water 110

Fig. 4-3 Solubility values attained from batch experiments as a function of ethanol mass fraction in the aqueous phase ……111

Fig. 4-4 Toluene effluent concentration for the case of pure toluene NAPL and 100% ethanol content in the flushing solution ……112

Fig. 4-5 Effluent concentration for the case of (a) pure toluene NAPL and (b) pure benzene NAPL with 50% ethanol content in the flushing solution ……113

Fig. 4-6 Effluent concentrations for the case of multi-component NAPL (benzene and toluene) with 50% ethanol content in the flushing solution at (a) high flow rate ($2.85x10^{-5}$ m/s), (b) low flow rate ($0.92x10^{-5}$ m/s), and (c) intermittent flow ……114

Fig. 4-7 Effluent concentrations for the case of multi-component NAPL (benzene and toluene) with 20% ethanol content in the flushing solution at (a) high flow rate ($2.85x10^{-5}$ m/s), (b) low flow rate ($0.92x10^{-5}$ m/s), and (c) intermittent flow ……115

Fig. 4-8 Measured and calculated Ternary phase diagrams for toluene-ethanol-water, benzene-ethanol-water and NAPL mixture-ethanol-water systems ……116

Fig. 4-9 Simulated (1D, 2D, 3D model) and observed toluene effluent concentrations and cumulative mass recovery for the case of pre toluene NAPL and 100% ethanol content in the flushing solution .117

Fig. 4-10 Saturation profiles; a) Experiment and 3D model edge cells at 0.2 pore volume for 100% ethanol flushing of toluene b) Experiment and 3D model edge cells at 0.6 pore volume for 100% ethanol flushing of toluene c) Experiment and 3D model edge cells at 1.5 pore volume for 50% ethanol flushing of toluene ……118

Fig. 4-11 (a) Simulated (3D model) and observed toluene effluent concentration and cumulative mass recovery for the case of pure toluene NAPL and 50% ethanol content in the flushing solution. (b) Simulated (3D model) and observed benzene effluent concentration and cumulative mass recovery for the case of pure benzene NAPL and 50% ethanol content in the flushing solution ……119

Fig. 4-12 (a) Simulated (3D model) and observed effluent concentrations and cumulative mass recovery for the case of multi-component NAPL and 50% ethanol content in the flushing solution at the low flow rate. (b) Simulated (3D model) and observed effluent concentration and cumulative mass recovery for the case of NAPL mixture and 20% ethanol content in the flushing solution at the low flow rate ……121

Fig. 4-13 Simulated toluene effluent concentrations for (a) 100% (b) 50% and (c) 20% ethanol content, rate limited mass transfer and for randomly selected permeability realizations ……122

Fig. 5-1 Schematic of Hoffmann column from Hoffmann [1969] ……131

8. List of tables

Tab. 2-1 Classification of two phase flow in porous media for the evaluation of interphase mass transfer……15

Tab. 3-1 List of conducted pore-network simulations ……85

Tab. 4-1 List of column experiments ……105

Tab. 4-2: List of key parameters used in the model simulations ……..109

Tab. 5-1 Estimated mass exchange coefficient as a function of velocity (from Hofmann [1969]) 132

Tab. 5-2 Calculated Peclet and Sherwood numbers as a function of velocity (from Table 1 of Pfannkuch [1984]) ……..132

Tab. 5-3 Corrected vs. Pfannkuch's Sherwood numbers as a function of velocity ……..134

9. Annexes

Annex 1 **Angaben zum Eigenanteil (The outline of the author's contributions)**

Annex 2 **Acknowledgements**

Annex 3 **Eidesstattliche Erklarung**

Annex 4 **Curriculum Vitae**

9.1 Angaben zum Eigenanteil (Outline of the author's contributions)

The thesis comprises of four manuscripts, which are presented in chapters 2, 3, 4 and 5. The author's contribution to each manuscript is described below.

Chapter 2 – first author
Interphase mass transfer between fluids in subsurface formations: A review
The concept of the study was developed by the author. The collection of literature for this study was done by the author. The interpretation of the results was done by the author, supported by the suggestions of the co-author Nadim K. Copty. The co-authors Reinhard Hinkelmann and Traugott Scheytt assisted in the writing of the manuscript. Editorial handling of the manuscript was done by the author.

Chapter 3 – first author
Impact of NAPL architecture on interphase mass transfer: A pore network study
The concept of the study was developed by the author. The pore scale numerical model was developed and coded by the author. The interpretation of the results was done by the author, supported by the suggestions of the co-author Nadim K. Copty. Co-author Traugott Scheytt assisted in the writing of the manuscript. Editorial handling of the manuscript was done by the author.

Chapter 4 – first author
Laboratory scale experiments and numerical modeling of cosolvent flushing of multicomponent NAPLs in saturated porous media
The concept of the study was developed by the author and co-authors Nadim K. Copty and Traugott Scheytt. The batch and column experiments and also analysis of the samples were done by the author. The input file for the REV-based multiphase multicomponent numerical model, UTCHEM, was developed by the author. The interpretation of the results was done by the author, supported by the suggestions of the co-authors Nadim K. Copty and Traugott Scheytt. Writing and editorial handling of the manuscript was done by the author.

Chapter 5 – first author
The use of Pfannkuch Sherwood Number Correlation for the calculation of the interphase mass transfer in porous media
The mathematical error conducted in Pfannkuch Sherwood correlation and its implication on Thermodynamics Model was recognized by the author. The concept of the technical note was developed by the author and the co-author Nadim K. Copty. Interpretation of the implications on the Thermodynamics Model was done by the author supported by the suggestions of the co-author Nadim K. Copty. Co-author Traugott Scheytt assisted in the writing of the manuscript. Editorial handling of the manuscript was done by the author.

9.2 Acknowledgements

I would like to thank …

… to Prof. Dr. Nadim K. Copty for thoughtful guidance and unlimited support. He was always there to give answers to any questions, and pose new ones. This work was continuously improved by his relentless critical perspective.

… for accepting me as a PhD candidate at TU Berlin: Dr. Traugott Scheytt.

… for arranging me a part-time job in Civil Engineering department of TU-Berlin which provided me financial support during my doctoral studies: Prof. Dr.-Ing. Reinhard Hinkelmann.

… for nice working environment: Oberholz

… for nice social environment: Berlin; Roses, Uschi Obermayer (Mozart), Hotel, Cake…

… for helpful encouragement: Dr. Tuna Eken

… for making it easier: my friends Dr. Tuna Eken, Dr. Mustafa Taşkaldıran

… for never ending impatience: my father (“so when are you finishing this PhD?” during every telephone talk)

… for the help: my brother

… for everything: my mother

9.3 Eidesstattliche Erklarung

Hiermit versichere ich, Berken Agaoglu, an Eides statt, dass die vorliegende Dissertation in vollem Umfang von mir selbst erstellt wurde. Es wurden keine weiteren als die angegebenen Quellen verwendet.

Berlin, den 29.01.2015

_____
Berken Agaoglu

9.4 Tabellarischer Lebenslauf

Persönliche Angaben

Name:	Berken Agaoglu
Geburtstag:	07.03.1981
Geburtsort:	Edirne/Türkei
Familienstand:	ledig

Berufliche Tätigkeiten

seit 2013	Wissenschaftliche Hilfskraft am Institute für Bauingenieurwesen der Technischen Universität Berlin
2010 – 2012	Studentische Hilfskraft am IABG Gmbh/Berlin
2007 – 2009	Forschungsstipendiat bei TUBITAK/Türkei

Ausbildung

Seit 2010 Technische Universität Berlin (TU Berlin), Berlin/Deutschland
- Doktorand am Fachgebiet Hydrogeologie, Institut für Angewandte Geowissenschaften

2007-2009 Bogazici Universität (BU), Istanbul/Türkei
- M.Sc. Umwelttechnologie, Institut für Umweltwissenschaften
- Abschlussdatum: September, 2009

2005-2006 Fundacion Christina Heeren (FCH), Sevilla/Spanien
- Studium der Kulturwissenschaften

2000-2005 Yildiz Technische Universität (YTU), Istanbul/Türkei
- B.Sc.Umwelttechnologie/Umweltingenieurwesen, Fakultät Bauingenieurwesen

Berlin, den 29.01.2015

_____

Berken Agaoglu